APPROVAL SHEET

Title of Dissertation: ENGINEERING OPTICAL PROPERTIES THROUGH STRONGLY CONJUGATED AND WEAKLY CONJUGATED HYDROPORPHYRIN ARRAYS

Name of Candidate: Adam Meares
Doctor of Philosophy, 2020

Dissertation and Abstract Approved: _____

Marcin Ptaszek
Associate Professor
Department of Chemistry and Biochemistry

Date Approved: 9/20/20

ABSTRACT

Title of Document: ENGINEERING NEW OPTICAL PROPERTIES THROUGH STRONGLY CONJUGATED AND WEAKLY CONJUGATED HYDROPORPHYRIN ARRAYS

Adam A. Meares, Ph.D., 2020

Directed By: Associate Professor, Dr. Marcin Ptaszek, Department of Chemistry and Biochemistry

Many classes of organic fluorophores have been developed and rigorously studied over the last century (coumarins, cyanines, porphyrins, etc.), each with their own strengths and weaknesses. When single chromophores are inadequate or underperforming for a given application, strongly conjugated or weakly conjugated multichromophore arrays can be prepared.

Strongly conjugated arrays feature two chromophores linked via sp or sp^2 hybridized atoms, allowing delocalization of π electrons over the entire system. This causes broadening and red shifting of lowest energy absorption and emission bands, increased absorptivity, the rise of new absorption features and increased non-linear

optical properties (two-photon absorption cross-section, hyperpolarizability), all of which are all sought after for solar light harvesting. In weakly conjugated arrays, chromophores are held in close proximity without sharing π electrons, allowing them to retain individual absorption and emission properties while gaining the ability to interact through excited state energy transfer. With careful molecular design, one can exploit energy transfer to create a variety of systems suitable for fluorescence sensing or *in vivo* imaging applications.

Here, we developed several series of both strongly and weakly conjugated arrays. All designs feature hydroporphyrins (chlorins and bacteriochlorins) due to their unique photophysical properties, including three absorption bands in three spectral regions (UV, green, red-NIR), narrow emission in the red-NIR window and large fluorescence quantum yield. First, we developed long wavelength absorbing and emitting chlorin monomers and dimers, in order to understand the relationship between linker type and electronic communication. Next, two chlorins were bridged by an endiynyl linker capable of photoinduced isomerization, to afford an array with both through bond and through space electronic communication. The remaining work was broken into three phases focused on the design and preparation of weakly conjugated arrays for *in vivo* imaging and fluorescence guided surgery. In the first phase we developed bright BODIPY-chlorin arrays with a large pseudo-Stokes' shift and high energy transfer efficiency. Second, amphiphilic bacteriochlorin-BODIPY arrays were prepared to facilitate solubility in aqueous media. Finally, a series of BODIPYs with tunable absorption were conjugated to a common bacteriochlorin, to enable multiplexed imaging with variable excitation and common emission.

ENGINEERING NEW OPTICAL PROPERTIES THROUGH STRONGLY CONJUGATED AND WEAKLY CONJUGATED HYDROPORPHYRIN ARRAYS

By

Adam A. Meares

Dissertation submitted to the Faculty of the Graduate School of the
University of Maryland, Baltimore County, in partial fulfillment
of the requirements for the degree of
Doctor of Philosophy,
Chemistry
2020

Dedication

Dedicated to my grandparents Jack and Corinne Meares.

Acknowledgements

I would like to thank everyone that has been a part of this long journey through graduate school. First and foremost, my advisor Dr. Marcin Ptaszek, who was my point of contact to UMBC from the beginning. He is solely responsible for introducing me to hydroporphyrin chemistry, without his tutelage none of this work would have been possible. I'd also like to thank my committee members, Drs. Marie-Christine Daniel-Onuta, Lisa Kelly, Dan Kostov and Paul Smith, for their valuable time and input. Additional thanks to Drs. Kelly and Smith for the many insightful conversations over the years and for providing feedback on my dissertation. Thank you also to the post-docs I received excellent training from both in Maryland (Dr. Zhanqian Yu) and in Connecticut (Dr. Albert DeBerardinis).

On a more personal level, I must thank my close friends Scott Riley and Andy Satraitis for their contributions. Andy for his synthetic skills and humor, and Scott for helping me commit to a regimented gym schedule (as well as his willingness to help me move). I would also like to thank both sets of parents (Pam and Joe, Tony and Sophie) for their support from back north, without their collective influence I wouldn't be where I am today. Also, thank you to Aunt Colleen for being a great listener and prevailing source of reason during my more frustrating days. Last but not least, I want to thank my growing Maryland family; Lisa for your endless patience and uplifting me when I needed it most, and both Sarge and Pickles for being the best rescues we could ask for.

Table of Contents

Chapter 1: Introduction

Optical properties dictate how the world perceives materials, both physically and in terms of application. The application of a given material, will be driven by which of the three basic interactions of light and matter (absorbance, reflectance, transmittance) it favors. Absorbance is particularly interesting because it leads to higher energy molecules that want to release their excess energy. For most organic molecules, this energy is dissipated as heat through internal conversion but with the proper molecular structure, a stepwise de-excitation becomes more difficult and the molecule releases the energy as light of a slightly longer wavelength. This emitted light is what we know as fluorescence.

Fluorophores have several fundamental properties including: molar absorptivity (or extinction coefficient, ε) maximum wavelengths of absorption and emission (λ_{abs} and λ_{emi}), the Stokes' shift (difference between λ_{emi} and λ_{abs}), band broadness (defined as full-width at half-maximum, FWHM), fluorescence quantum yield (Φ_F), fluorescence lifetime (τ_F) and where intersystem crossing is allowed, triplet quantum yield (Φ_T) and triplet lifetime (τ_T).[1,2] Collectively, these properties translate into a wide variety of uses. In biology and biochemistry, fluorophores are utilized for both *in vitro* and *in vivo* techniques. This includes but is not limited to flow cytometry,[3–5] fluorescence assays (e.g. enzyme activity assays or molecular binding studies)[6–8] and fluorescence imaging.[9–11] Furthermore, fluorophores are applied as photosensitizing agents in photodynamic therapy (PDT),[10–13] which can treat cancers (esophageal and lung),[14–17] skin conditions (acne, rosacea, psoriasis)[18–21] and eye diseases (macular degeneration).[22–24] Additionally, materials scientists and chemists are collectively

interested in fluorophores for the development of novel photoelectronic devices. The most prominent examples are perhaps photovoltaics for solar light harvesting to address the world's growing energy needs,[25–28] and organic light emitting diodes (OLEDS) to meet the public demand for high resolution screens in smart watches, phones and televisions.[29–32] With such broad uses, fluorophores are not universal and require proper tailoring.

Two ways to modulate the properties of fluorophores include the construction of strongly and weakly conjugated arrays. Both approaches generate multichromophore arrays, but they have very different behavior. In strongly conjugated arrays two or more fluorophores are covalently bridged through either sp or sp^2 hybridized linkers (such as ethynyl or butadiynyl for sp, or aryl for sp^2). Such linkers, with π electrons of their own, permit delocalization of the two chromophore π systems merging them into one.[17,33–46] In general, strongly conjugated arrays undergo significant broadening and bathochromic shifting of the lowest energy absorption band (between the two parent chromophores), large increase to ε, as well as the rise of new broad/structureless absorption features.[17,33–48] In addition, strongly conjugated arrays have improved non-linear optical properties, such as hyperpolarizability[49] and increased two-photon absorption cross section.[42,46,47] Large two-photon absorption cross-sections in particular are sought after for solar energy harvesting.[39,50] Some limited examples of strongly conjugated arrays include BODIPY,[51] and squaraine[52] homodimers and BODIPY-squaraine,[53] BODIPY-pyrene[46] heterodimers, but the vast majority of examples incorporate porphyrin or hydroporphyrins. This includes a variety of both homo-[35,35,36,36,37,54–58] and heterodimers,[59–64] oligomers (such as porphyrin tapes), [40,41]

as well as extraordinarily π-expanded porphyrin-perylene systems.[44,45,65] The cited examples are by no means exhaustive, and the relevant porphyrin and hydroporphyrin based systems are discussed later as necessary.

Weakly conjugated arrays behave nearly in contrast to strongly conjugated arrays. In weakly conjugated arrays component chromophores retain all of their individual fluorescence properties, and gain the ability to interact through excited state energy.[1,2] This is achieved by utilizing linkers that prohibit electronic communication (such as aliphatic chains)[66,67] or by forcing close spatial interaction (usually under 10 nm) without a linker.[68–79] Where no linkers are present, the dyes can be held together closely through a molecular scaffold such as proteins (seen in photosynthetic reaction centers)[68–73] or DNA (artificial systems).[74–79] When sufficiently close (and properly aligned) the component chromophores can interact through either energy transfer or electron transfer.[80,81] The most commonly invoked model for energy transfer is the Förster resonance energy transfer (FRET) model. In FRET, the donor chromophore is first excited, then it transfers energy to the ground state acceptor chromophore via dipole-dipole interaction.[1,2] Although the process is nonradiative, it is highly dependent upon the overlap of the donor's emission spectrum and the acceptor's absorption spectrum (overlap integral, *J*), meaning the components must be energetically compatible. FRET is also dependent upon the mutual orientation of the individual transition dipole moments (orientation factor, κ^2) and decreases with respect to intermolecular distance (*r*, measured center-to-center between dipole moments) to the sixth power.[1,2,8,82] For our purposes, we are primarily interested in maximization of FRET.

There are numerous examples of FRET based systems in the literature, featuring a wide variety of constituent chromophores such as: BODIPY-BODIPY,[83,84] BODIPY-corrole,[85,86] BODIPY-porphyrins,[87] fluorescein-rhodamine,[88] cyanine-rhodamine,[89] perylene-perylene[90] and so on. The literature is rich with examples of systems which utilize FRET, and the chromophore pairings are dictated by the application. Some of the more interesting applications of FRET are for activatable probes which either become fluorescent or have a change to fluorescence properties upon molecular recognition. In many cases, these arrays possess a chromophore and a quencher molecule (strongly absorbing but non-emissive) which cause the arrays to remain dark until the target interaction occurs.[10] There is extensive literature on this topic but some of the more notable examples include molecular beacons which consist of a chromophore and quencher covalently linked to opposite ends of single stranded DNA,[78,79,91–93] peptides bearing large fluorophore payloads that separate and unquench upon enzymatic cleavage[94,95] and molecular logic gates which require multiple stimuli to turn on fluorescence.[96,97]

In addition to the construction of multichromophore arrays, fluorophore properties can be more finely tuned through the installation of auxochromes. Auxochromes modulate the electronic properties of the fluorophore through either induction (alkyl substituents or halides) or resonance (vinyl, aryl, etc.). The most effective tuning of electronic properties occurs when the auxochromes possess π electrons that contribute directly to the π system of the chromophore via resonance, and are installed where the HOMO coefficients are greatest (usually this is on the axis of the dye's transition dipole moment).[98,99] Regardless of the auxochrome, they typically

lower the band gap between the HOMO and LUMO, resulting in a red (bathochromic) shift of absorption and emission maxima.[100] The extent of the apparent red shift can be controlled further through the use of electron donating or withdrawing groups on the auxochrome itself. For example, the absorption maximum of a 10-tolyl chlorin with two phenylethynyl substituents is shorter than the same chlorin with (4-aminophenyl)ethynyl (674 nm and 679 nm, respectively).[101] An important consideration with regard to increasing the overall π system is the mutual orientation of the chromophore and its auxochrome because significant deviation from co-planarity limits electronic interaction.[54,102] Auxochromes can also reliably alter the redox properties of a given fluorophore, in order to prevent (or promote) the quenching of fluorescence by photoinduced electron transfer.[103–105] Both Φ_F and τ_F are influenced by auxochromes as well but should be carefully considered on a case by case basis, as the ability of bonds to freely rotate can lead to significantly faster internal conversion. A prime example of this is the dramatically reduced Φ_F of 8-aryl boron-dipyrromethene, when replacing sterically hindered mesityl substituent ($\Phi_F = 0.93$) with a freely rotating phenyl group ($\Phi_F = 0.06$).[106]

The work presented herein focuses on the construction of both strongly conjugated (Chapters 2-3) and weakly conjugated (Chapters 4-6) arrays utilizing hydroporphyrins. Due to the slight variation in topics and goals, each chapter features an introduction, but all presented arrays utilized at least one hydroporphyrin, due in combination to their excellent photophysical properties and their recent synthetic availability via the Lindsey method.[107,108] Hydroporphyrins are based on the tetrapyrrolic scaffold and feature reduction of one (for chlorin) or two (for

bacteriochlorin) double bonds (indicated by dashed ellipses, Figure 1.1) relative to porphine. Hydroporphyrins possess several absorption bands, the *B* bands, Q_x and Q_y bands which absorb in the near UV/violet, green, and the deep-red/NIR, respectively.[109–112] The *B* and Q_y absorption bands are very intense (ε ~100,000-200,000 $M^{-1}\cdot cm^{-1}$ and 50,000-100,000 $M^{-1}\cdot cm^{-1}$, respectively) while the Q_x band is moderately intense (ε = 15,000-40,000 $M^{-1}\cdot cm^{-1}$).[107,113] When progressing from porphyrin to chlorin to bacteriochlorin, the relative intensity of the *B* bands decreases while the Q_y band intensity increases. Hydroporphyrins also have narrow emission bands in the deep-red/NIR (FWHM below 25 nm), with a small Stokes' shift, and large Φ_F (< 0.20) for the spectral region.[99,107,109,111,113] The Q_y absorption and emission maxima can be tuned through auxochromes, with the greatest effect occurring at the 3- and 13- positions.[109–111,114] This is where the Lindsey method for chlorin synthesis becomes so important, as it is the only reliable way of preparing chlorin starting materials with bromine in the 3- and/or 13- positions.[115–118] These bromine synthetic handles enable relatively facile derivatization of the parent macrocycle through palladium catalyzed coupling reactions.[99,108,119,120] The Lindsey method of chlorin synthesis also allows for installation of various aryl substituents at the 10-position, through the combination of various eastern with one of two common western halves.[107,117,121,122] Lindsey's group later developed a similar synthesis of 3,13-dibromo bacteriochlorins, that we also routinely employ.[113,116,123]

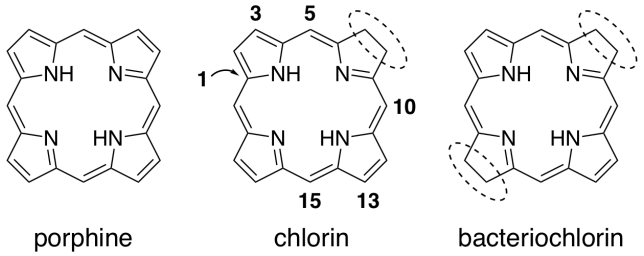

Figure 1.1: Porphine and simple hydroporphyrins

The relevant hydroporphyrin properties will be revisited and elaborated upon on a chapter by chapter basis, and the aims of each chapter are as follows. Chapter 2 focuses on the development of a series of long wavelength absorbing and emitting hydroporphyrin monomers and dimers, with emphasis on understanding the relationship between linker type (containing sp or sp^2 hybridized carbon atoms) and the influence of steric interactions on electronic communication. As part of this work we developed microwave assisted olefin metathesis reaction for synthesis of symmetrical, ethenyl linked chlorin dyads. The work of Chapter 2 is published in the *Journal of Organic Chemistry.*[124] Chapter 3 builds upon the strongly conjugated arrays discussed in Chapter 2, where we prepared symmetrical dyads linked by 3-hexen-1,5-diyne, in order to prepare an array which features extensive electronic coupling both through space and through bond. This is of particular interest in modelling the photosynthetic reaction center without need for complex scaffolding. The work presented in Chapter 3 is also published in the *Journal of Organic Chemistry.*[125]

The weakly conjugated arrays discussed in chapters 4-6 revolve around a central theme of preparing bright fluorophores with a large pseudo-Stokes' shift that are useful for imaging in biological media. The work on weakly conjugated arrays was broken down in three stages 1) achieving bright arrays with efficient energy transfer, minimal fluorescence quenching and emission in the deep-red to NIR spectral windows 2) attaining arrays with sufficient water solubility to be utilized in the biological setting and 3) achieving arrays with long wavelength absorption maxima and NIR emission. Each of the goals was met and is reviewed on a chapter by chapter basis. Chapter 4 discusses the series of chlorin-BODIPY arrays that were prepared in order to

understand the relationship between linker type, and its influence on both energy transfer and quenching in our systems. This work is published in the *Journal of Organic Chemistry* as well.[126] Chapter 5 discusses novel hydrophilic BODIPYs that were incorporated into hydroporphyrin-BODIPY arrays, to attain arrays that are functional (do not aggregate) in the biological setting. The synthesis and photophysical characterization of these compounds is published in in the *Journal of Organic Chemistry*[127] while the *in vitro* and *in vivo* testing performed by our collaborators is published in *Bioconjugate Chemistry*.[128] Chapter 6 discusses novel long-wavelength absorbing and emitting styryl BODIPYs, and their incorporation into arrays alongside bacteriochlorin. The emphasis here was two-fold. First, we wanted a system capable of multiplexed imaging with variable excitation and common emission. And second, to acquire arrays with absorption and emission maxima that are both within the biological window, to optimize the tissue depth at which they can be imaged. The work presented in Chapter 6 is similarly published in the *Journal of Organic Chemistry.*[129]

Chapter 2: Achieving Long-Wavelength Absorbing and Emitting Chlorin Monomers and Dimers

Section 2.1: Introduction

Expansion of the π-systems in porphyrins and hydroporphyrins can be performed to generate new arrays with significantly different photophysical, photochemical and electrochemical properties. This expansion is done either through the addition of auxochromes to the macrocycle periphery[33,34,49,54,114,130–134] or by linking multiple macrocycles together such that the two (or more) chromophores possess excellent electronic communication.[35–38,41,47,135–144] Depending upon the substituents or method of linking, the expanded systems can have various properties such as increased near-infrared (NIR) fluorescence quantum yields,[141] increased two-photon absorption cross-section,[47] and hyperpolarizability,[49] as well as panchromatic absorption.[33,34] These advanced properties are desirable in applications such as NIR fluorescence imaging,[33–36,41,49,54,114,130–138] two-photon excitable fluorescence imaging and photodynamic therapy, [47,144] modeling of the photosynthetic reaction center,[142] and light-harvesting/electron transfer in dye-sensitized solar cells.[39,50] The ability of an auxochrome (or linker between two macrocycles) to alter properties of the parent chromophore depends on the strength of their electronic communication (i.e., the relative ease of sharing π electrons). One of the major factors determining the strength of electronic interaction is the mutual orientation of the macrocycle(s) and substituent. For example, *meso*- aryl substituents (commonly tolyl or mesityl for synthetic chlorins and porphyrins)[145,146] have a small influence on the macrocycle properties because they adopt a nearly perpendicular orientation in order to minimize steric interactions. When this occurs, the orthogonal π-orbitals are unable to interact, and remain non-conjugated.

In the most sterically hindered cases, like *meso-meso* directly linked chlorins, free rotation is no longer observed, and such dimers exist as a racemate of atropisomers.[147] Conversely, installation of substituents onto a tetrapyrrolic macrocycle that permit coplanarity red shifts the longest wavelength (Q_y) band and increases fluorescence quantum yield.[41,54,130,135] Such is observed in the case of hydroporphyrin dimers with ethynyl or butadiynyl linkers[35–38] and monomers with arylethynyl substituents, although to a lesser degree.[33,34,37,114,133,134,148] There are similar ethenyl linked dimers[51,56,136] and monomers with styryl[49,132,148,149] or chalcone[131] auxochromes.

At first glance, the sp^2-hybridized carbon atoms of an ethenyl linker (opposed to sp hybridized ethynyl linker) should better match the sp^2 hybridized carbon atoms of the macrocycle. However, arrays possessing ethenyl linkers are inherently less planar than those with an ethynyl one, due to the presence of vinylic protons prohibiting the linker and macrocycle(s) from achieving co-planarity. Such steric interactions prevent optimal π-orbital overlap and electronic conjugation is decreased, whereas an ethynyl linker readily permits co-planarity. *The net effect of orbital energy matching and orbital overlap, observed as the extent of bathochromic shift of λ_{max} relative to parent fluorophore, is dependent upon the dihedral angle between the macrocycle and the linker.* From this point forward, the mention of "dihedral angle" in Chapter 2 refers to the dihedral angle between the macrocycle mean plane and the linker mean plane, unless clearly stated otherwise.

For our purposes, porphyrinic systems offer a starting point, the most relevant being those prepared by Anderson *et al*. Anderson prepared and studied several *meso-meso* linked porphyrinato zinc (II) dimers that utilized ethenyl (**D1**), ethynyl (**D2**) or

iminyl (**D3**) linkers (Chart 2.1).[54] The ethenyl (**D1**) and iminyl (**D3**), showed

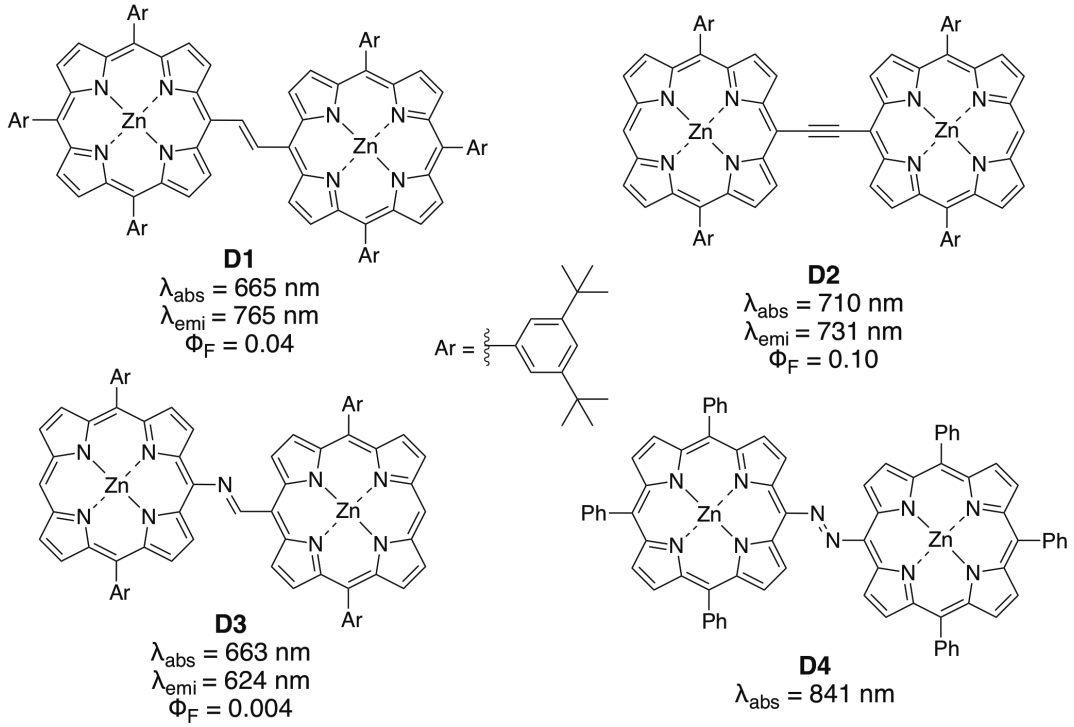

Chart 2.1: Porphyrin dimers with ethenyl (D1), ethynyl (D2), iminyl (D3) and azo (D4) linkers.

comparable absorption maxima where only **D1** showed appreciable emission. The reported emission of dimer **D3** is likely due to the presence of an impurity and should not be considered (emission is reported at shorter wavelength than lowest energy absorption band). Ethenyl linked **D1** exhibited inferior electronic conjugation in the ground state relative to **D2** (absorption maxima at 665 and 710 nm, respectively) while **D1** showed superior conjugation in the excited state (emission maxima of 765 nm for **D2**, 710 nm for **D3**). At a later time this was reinforced through electrochemical measurements (cyclic voltammetry) that indicated the smaller HOMO-LUMO energy gap for **D1**.[136] The less extensive conjugation of **D1** in the ground state can be explained by its large dihedral angle of 45º (solid state, determined by X-ray diffraction), affording less efficient orbital overlap relative to **D2**.[136] Conversely, it appears that in

the excited state, the linker of **D1** adopts a more co-planar geometry allowing for greater electronic conjugation. Following Anderson's publication, Arnold reported a similar *meso-meso* linked porphyrin dimer (**D4**)[102] featuring an azo bridge. Dimer **D4** possessed an absorption maximum (841 nm) well beyond that of either **D1** or **D2**, and it's nickel complex congener was shown to have a dihedral angle of 37º (Chart 2.1).[102] The lone pairs of the **D4** linker appear to also prevent planarity, but to a lesser extent than with an ethenyl linker. **D4** is expectedly non-emissive, as this azo-linked motif is well known to promote non-radiative relaxation through *trans-cis* isomerization.[78,92,150] From this work it becomes clear that there is a relationship between the linker type and electronic properties, but the above examples neglect to also address the importance of substituent/linker location.

There are many other examples of porphyrin[151–155] and chlorin[56,156–159] dimers that are bridged through *meso-meso*, *meso-β,* and *β-β* positions, but they are not suitable for direct comparison due to significant structural variation in terms of metal coordination, auxochromes and the presence of substituents near the linker site (Chart 2.2). Much like the porphyrin dimer **D1**, *meso-meso* ethenyl linked chlorin dimers exhibit large dihedral angles.[51,56,136] Similar large angles can be seen for *β-β* ethenyl linked chlorin dimers that possess one or more substituents at the neighboring positions. One such dimer, **D5** (prepared by Wasielewski *et al.*), was determined to have a dihedral angle between 49-53º.[156,157] Wasielewski's dimer (and likely dimers **D6**,[56] **D8**[56] and **D9**[159]) exhibits a large angle due to steric clash with the nearby 12-alkyl substituent. In dimer **D7**, Smith rigidified the ethenyl linker via a five-member

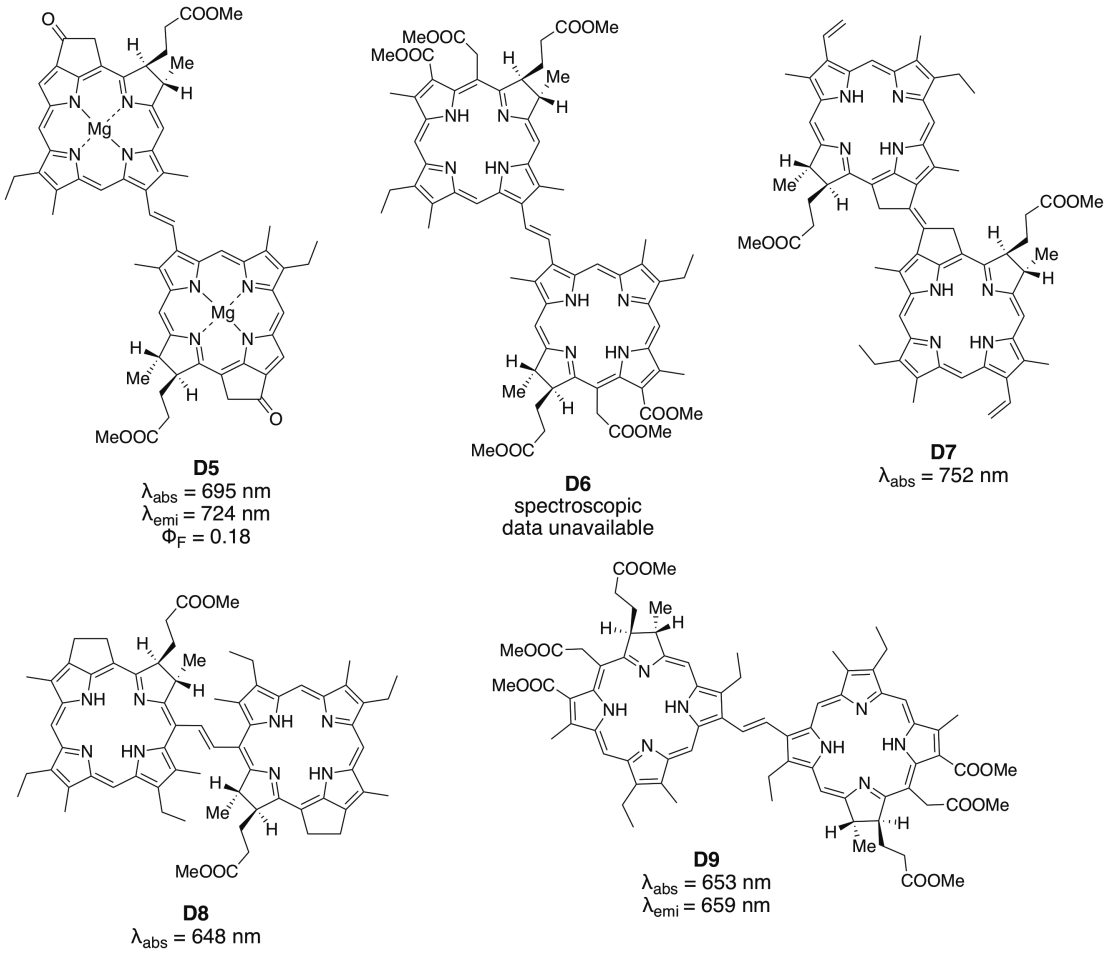

Chart 2.2: Select ethenyl linked chlorin dimers.

exocyclic ring, forcing the two macrocycles into a nearly coplanar orientation (dihedral angle < 2º).[158] As a consequence, the Q_y-like absorption band of **D7** is red-shifted nearly 100 nm relative to its parent monomer (656 nm).[160] A similar study by Bröring on *β*-*β* (2-2) ethenyl linked boron-dipyrromethene (BODIPY) derivatives indicates that the strength of conjugation in such systems is highly dependent upon the presence of substituents neighboring the linker site.[51]

The results from these various groups imply that with proper molecular design, ethenyl linked dimers can afford superior electronic conjugation between chromophores in multi-unit arrays. Because chlorins are inherently better than

porphyrins for NIR imaging applications (larger Φ_F, longer λ_{max} and larger ε of Q_y band) we reasoned that carefully tailored ethenyl linked dimers could provide stronger electronic communication than observed in analogous ethynyl or butadiynyl linked dyads, *provided there are no substituents adjacent to the linker*. Until recently, such compounds would have been inaccessible due to the difficulty in preparing synthetic chlorins. Over the late 90s and early 2000s Lindsey and co-workers developed (and optimized) new methodology that serves as the foundation for many modern synthetic chlorin containing scaffolds.[108,115,118,146,161,162] The main features of such chlorins are an 18-position geminal dimethyl group to prevent oxidation of chlorin to porphyrin,[117] a 10-aryl substituent and bromine at the 3- and/or 13- positions to enable palladium catalyzed cross coupling reactions.[108] All other positions are occupied only by hydrogen, thus, such chlorins are ideal for controlled, systematic study of linker effects.

Beginning from Lindsey's "sparsely substituted" chlorins, we sought to prepare a series of ethenyl and ethynyl substituted/bridged chlorin monomers and dimers to determine how the nature of the linker impacts the strength of electronic conjugation between macrocycles, for both the *meso* and *β* positions. Including both positions for linkage was important as both sites provide different degrees of inherent steric strain. Herein we report the synthesis and characterization of those compounds (Chart 2.1).

The *β*-*β* linked series of compounds features 13-mono- and 3,13-distyryl-substituted chlorins **C1-S** and **C2-2S**, with analogous phenylethynyl substituted **C1-P** and **C2-2P**, ethenyl linked dimers **SC1**, **ZnSC1** and **SC2** with corresponding ethynyl dimer **SC3**. Similarly, the *meso-meso* linked series features 15-styryl chlorin **C1-S15** with counterpart 15-phenylethynyl chlorin **C1-P15**. Attempts were made to prepare a

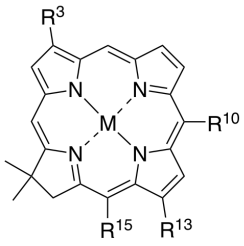

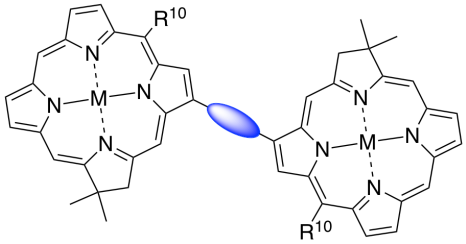

Monomers					
	R^3	**R^{10}**	**R^{13}**	**R^{15}**	**M**
C1-S	-H	-Mes	Ph	-H	-H, H
C2-2S	Ph	-C_6H_4-COOMe	Ph	-H	-H, H
C1-S15	-H	-Mes	-H	Ph	-H, H
C1-P	-H	-Mes	Ph	-H	-H, H
C2-2P	Ph	-C_6H_4-COOMe	Ph	-H	-H, H
C1-P15	-H	-Mes	-H	Ph	-H, H
Dimers					
	R^3	**R^{10}**		**R^{15}**	**M**
SC1	-H	-Mes		-H	-H, H
ZnSC1	-H	-Mes		-H	-Zn
SC2	-H	-C_6F_5		-H	-H, H
SC3	-H	-Mes		-H	-H, H

Chart 2.1: Novel styryl substituted chlorin monomers and ethenyl linked chlorin dimers prepared herein.

15-15 ethenyl linked chlorin dimer, however, we were unable to obtain this compound and were only able to study the relevant monomers. **ZnSC1** was introduced in order to determine if zinc (II) complexed dimers behave similarly to zinc coordinated monomers, and **SC2** was introduced later in the study to address the stability of ethenyl linked dimers (Section 2.3.3). Also note that distyryl and di(phenylethynyl) monomers **C2-2S** and **C2-2P** possess methyl benzoate moieties at the 10-position, as opposed to 10-mesityl seen in all other chlorins seen in this chapter. The maxima of the lowest

energy Q_y absorption bands for 10-mesityl-18,18-dimethyl[163] (638 nm) and 10-(4-methoxycarbonylphenyl)-18,18-dimethyl[126] (636 nm) chlorins vary only by 1-2 nm, making this exchange permissible. Our choice of 10-position substituent is due to **C2-2P** simultaneously being utilized for hydrophobic chlorin-BODIPY energy transfer arrays (Chapter 4), making **C2-2S** more cost-effective. All prepared target compounds are found in Chart 2.1, the originally proposed *meso-meso* linked dimers are omitted.

Section 2.2: Synthesis of Ethenyl Chlorin Monomers and Dimers

Section 2.2.1: Synthesis of β-β Linked Monomers and Dimers

First we prepared 13-13/*β-β* linked chlorin monomers and dimers. Earlier methods for installation of styryl substituents on chlorins featured Heck reaction[131] or Knoevenagel condensation when derivatizing naturally occurring chlorophylls.[148,149] We adopted the Heck reaction route due to the availability of 13-bromo-10-mesityl and 3,13-dibromo-10-methyl benzoate chlorins **C1-Br**[108,161] and **C2-2Br**,[126] respectively. From **C2-2Br** we were able to prepare 3,13-distyryl chlorin **C2-2S** by Heck reaction under conventional heating, however, we were unhappy with the long reaction time (> 60 hours). By treating **C2-2Br** with styrene (**1**), PPh_3, Et_3N and $Pd(OAc)_2$, in

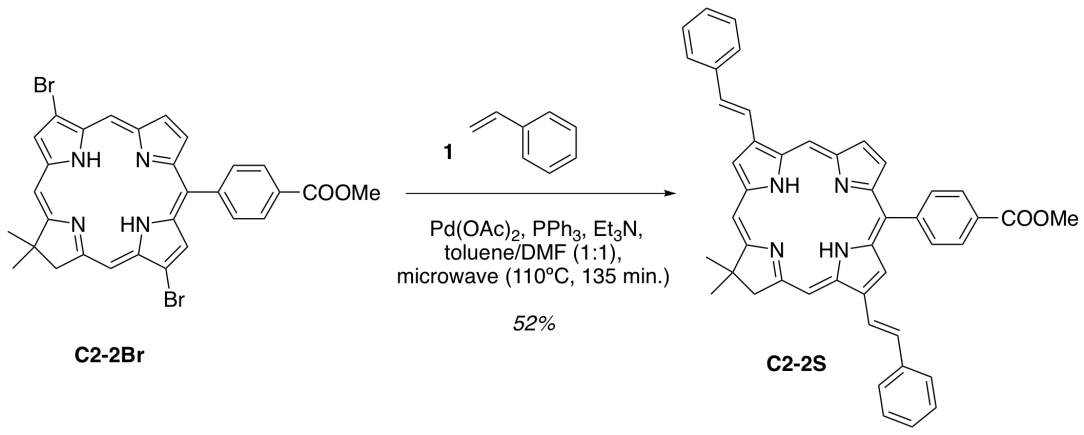

Scheme 2.1: Synthesis of distyryl chlorin C2-2S via microwave assisted Heck reaction

toluene/DMF, and heating to 110°C under microwave irradiation for 135 minutes, **C2-2S** was obtained in comparable yield (52%, Scheme 2.1). We attempted to prepare mono-styryl chlorin **C1-S** by the same conditions, but it decomposed during column chromatography, presumably due to the large excess of styrene (100 molar equivalents). We then changed our approach to Stille coupling[161] with subsequent olefin metathesis (Scheme 2.2).[164–171] Stille coupling of **C1-Br** with tributyl(vinyl)tin (**2**) yielded intermediate **C1-V** (87%). 13-vinyl chlorin **C1-V** was then subjected to olefin cross-metathesis under the conditions optimized for dimer synthesis (discussed below), yielding **C1-S** (39%). The 13-phenylethynyl chlorin monomer **C1-P**[33] was prepared following known procedure, and the synthesis of 3,13-di(phenylethynyl) chlorin monomer **C2-2P** is described later (Section 4.2.1).

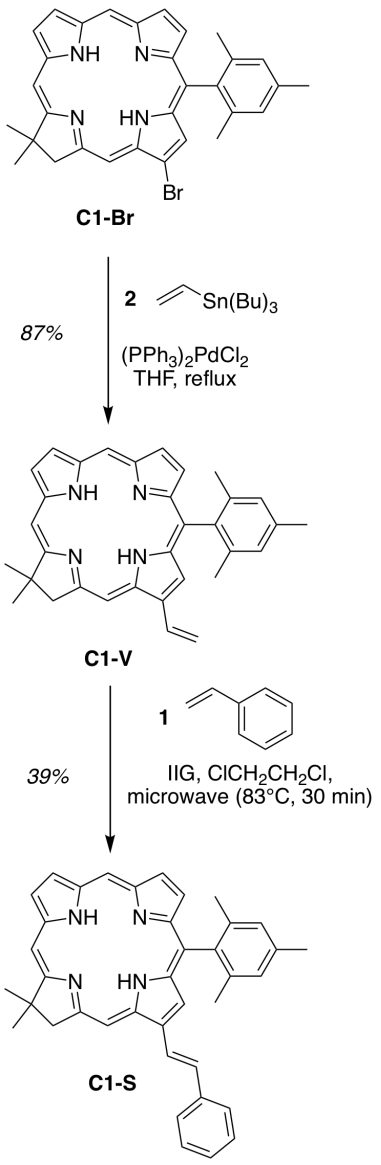

Scheme 2.2: Synthesis of 13-styryl chlorin, C1-S

Initially, we attempted the synthesis of the β-β linked dimer **SC1** directly from 13-bromochlorin **C1-Br**, through double Stille coupling with *trans*-1,2-bis(tributylstannyl)-ethene.[136] We screened several conditions and all attempts yielded only trace amount of product. Because the starting material was fully consumed in all cases (based upon TLC and absorption spectrum) we hypothesized that after the

intermediate 13-(1-(tributylstannyl)-ethen-2-yl) chlorin was formed, the second Stille coupling was extraordinarily slow due to significant steric hindrance limiting the Pd catalyst's ability to undergo transmetallation. We next attempted the Baldwin protocol[172] to expedite the reaction, which calls for the use of cesium fluoride and copper iodide in addition to the catalyst and organostannane. The presence of copper can be quite problematic (copper (II) can readily insert into chlorins, rendering them non-emissive,[163,173] and copper removal leads to significant decomposition)[174] so copper insertion was prevented by using the zinc (II) analog[108] of **C1-Br**. However, this approach also failed to produce a dimer, and lead to our use of the olefin metathesis reaction.

There are previous examples of olefin metathesis performed on porphyrins and hydroporphyrins[164–170] however, this is the first instance where olefin metathesis was utilized for direct formation of hydroporphyrin dimers. The earlier examples of ethenyl linked dimers were all prepared from natural chlorophyll analogues through either Wittig reaction[156] or McMurry Coupling[56,158] Thus, we began screening conditions for dimer formation using those previously reported for installing auxochromes on chlorin monomers.[169,170] We began by treating **C1-V** with second generation Grubbs' Catalyst (IIG) in refluxing THF. After an overnight reaction we saw only trace amounts of product, so we instead used higher boiling 1,2-dichloroethane as solvent, and also changed from conventional to microwave heating.[171] The combination of changes lead to a dramatically improved yield of **SC1**(46%), after a single 30-minute microwave exposure (provided that purification is performed in darkness to avoid "decomposition," Scheme 2.3). Also note that some amount of styryl chlorin monomer

(**C1-S**, for this reaction) is always observed as a byproduct due to IIG possessing a

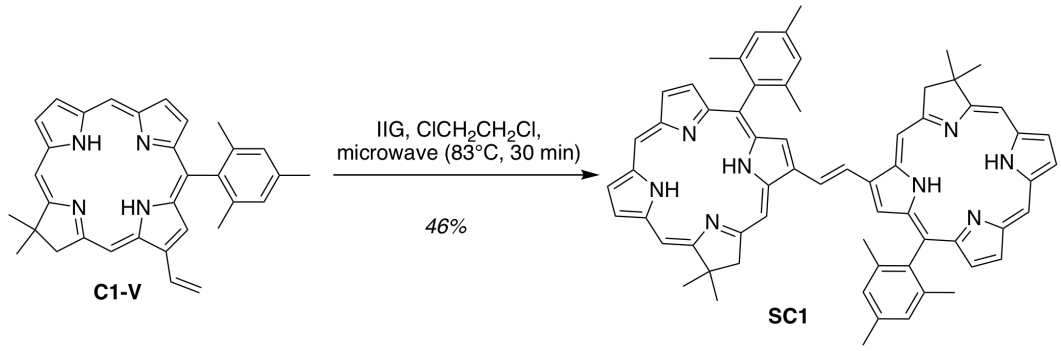

Scheme 2.3: Synthesis of freebase ethenyl linked chlorin dimer, SC1

benzylidene ligand, and the need for handling in the absence of light is discussed in Section 2.3.3. In order to understand the apparent decomposition, we next prepared target dimers **ZnSC1** and **SC2**, which feature a lower and greater oxidation potential than **SC1**, respectively. The synthesis of **ZnSC1** was attempted two ways. First, **ZnC1-V** was prepared by common zinc insertion conditions[110] where chlorin monomer **C1-V**, was treated with $Zn(OAc)_2$ in chloroform/methanol (Scheme 2.4). **ZnC1-V** was obtained in 78% yield and subsequently subjected to olefin metathesis; however, we were unable to purify what appeared to be dimer **ZnSC1** due to the presence of a highly red fluorescent impurity. Therefore, we treated ethenyl linked dimer **SC1** with $Zn(OAc)_2$ in chloroform/methanol, yielding **ZnSC1** (34%, Scheme 2.5). We attribute the low yield to decomposition during column chromatography despite careful handling in darkness.

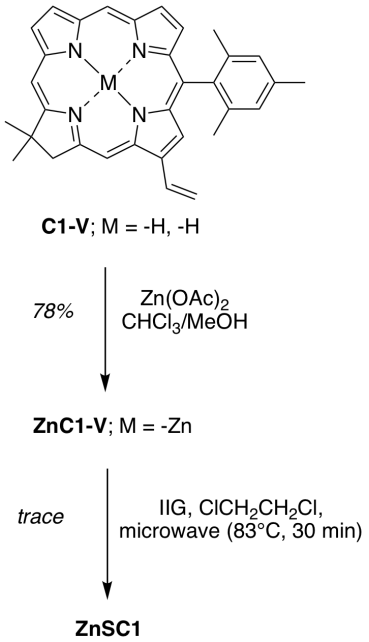

Scheme 2.4: Synthesis of ZnSC1 via zinc (II) complexation and subsequent olefin metathesis

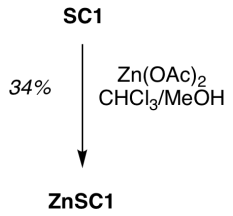

Scheme 2.5: Synthesis of zinc complexed ethenyl linked dimer ZnSC1.

For the more electron deficient dyad, **SC2**, we required a novel 13-bromo-10-pentafluorophenyl chlorin (**C3-Br**). **C3-Br** was prepared following the standard 3 step, 2 pot chlorin synthesis.[108,161] The steps include 1) an initial combination of eastern and western halves through condensation, forming deeply red colored bilene intermediate, 2) coordination with zinc to afford macrocycle-like orientation of bilene followed by cyclization via nucleophilic aromatic substitution and oxidation to give zinc chlorin, and finally 3) acid mediated demetallation to remove zinc. Here, we utilized tetrahydrodipyrrin **WH**[115] and 8,9-dibromo-1-formyl-5-pentafluorophenyl dipyrromethane **EH3-2Br**[121] obtaining chlorin **C3-Br** in 6% yield after the 3 steps. **C3-Br** was converted by Stille coupling to **C3-V** (71%) then olefin metathesis yielded target dyad **SC2** (36%, Scheme 2.6).

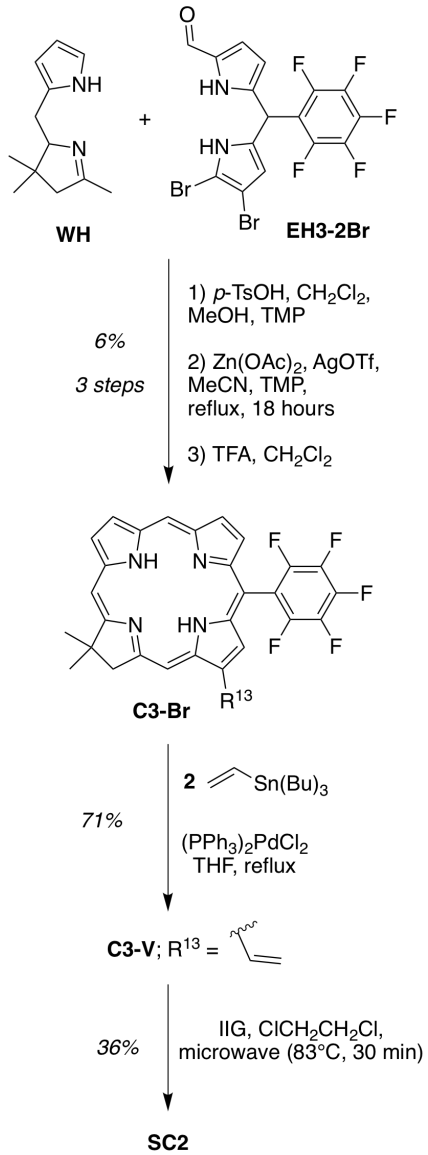

Scheme 2.6: Synthesis of ethenyl linked chlorin dyad SC2.

Ethynyl linked dyad **SC3** was prepared following the approach used to synthesize a similar dimer (Scheme 2.7).[35] First, 13-(trimethylsilyl)ethynyl chlorin **C1-ETMS** was prepared by Sonogashira cross coupling of **C1-Br**

and ethynyltrimethylsilane (3) in 68% yield following the known procedure.[108] Next, desilylation of **C1-ETMS** was performed with K_2CO_3 in THF/MeOH, yielding 13-ethynyl chlorin **C1-EH** (86%). Finally, Sonogashira cross coupling of **C1-EH** and **C1-Br** gave **SC3** that could be readily separated from butadiynyl linked chlorin dimer byproduct through column chromatography in 53% yield.

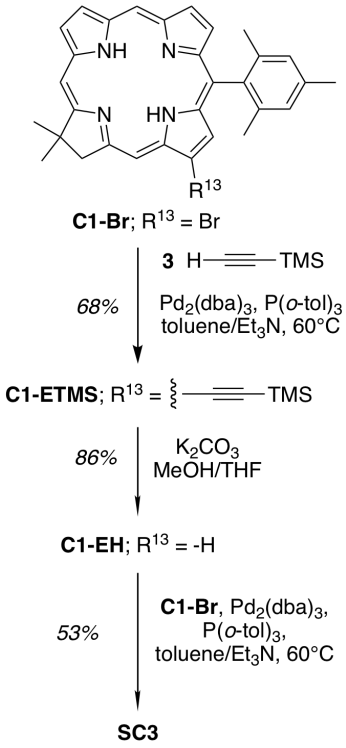

Scheme 2.7: Synthesis of ethynyl linked chlorin dyad SC3

Section 2.2.1: Synthesis of meso-meso Substituted Monomers

The corresponding *meso-meso* substituted chlorin compounds were prepared in similar fashion to the *β-β* linked compounds (Scheme 2.8). Beginning from 15-bromo-10-mesityl chlorin **C1-Br15**,[175] 15-styryl chlorin **C1-S15** was prepared by the same Heck reaction conditions employed for *β*-styryl chlorins in 23% yield. This low yield was resultant from a significant portion of **C1-Br15** undergoing des-bromination (61%). Next, **C1-P15** was prepared by Sonogashira cross coupling of **C1-Br15** and phenylacetylene (**4**) in 57% yield. Again des-bromination was observed, but to a much lesser degree.

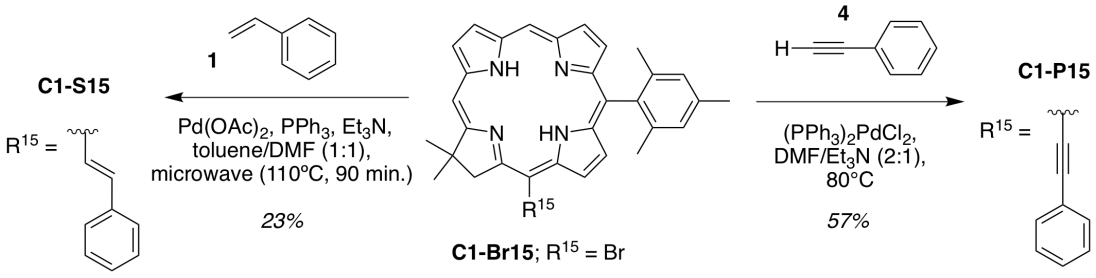

Scheme 2.8: Synthesis of 15-substituted chlorin monomers C1-S15 and C1-P15

Finally, we approached the synthesis of the vinyl and ethynyl 15-15 linked chlorin dyads. Beginning from 15-bromo chlorin **C1-Br15**, Stille coupling was performed with tributyl(vinyl)stannane (**2**) giving vinyl chlorin **C1-V15** (60%). Monomer **C1-V15** was subjected to olefin metathesis in an attempt to obtain *meso-meso* linked dimer **SC1-*meso***, but only starting material and trace **C1-S15** byproduct were recovered (Scheme 2.9). Because the failure was so pronounced, and the syntheses of both **C1-S15** and **C1-P15** resulted in poor yield, we reasoned that the high steric hindrance at the 15 position prohibits dimerization via olefin metathesis.

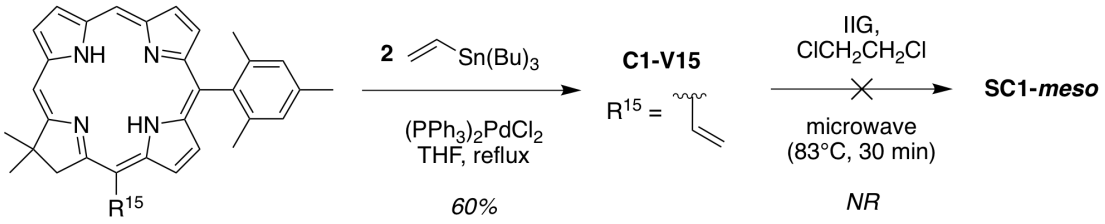

C1-15Br; R^{15} = -Br

Scheme 2.9: Attempted synthesis of meso-meso ethenyl linked chlorin dyad SC1-*meso*.

Considering that the Wittig reaction[156] or McMurry Coupling[56,158] (both of which feature congested intermediates) were previously used for similar constructs, the increased steric demand of the Ru catalyst requires too much energy to overcome. Furthermore, utilizing the more reactive Schrock catalyst[176–178] was not an option for us due to its high air sensitivity, and our lack of access to an oxygen free glove box. Ultimately, we determined that the relationship between **SC1-*meso*** and its ethynyl analog would be the same as for **C1-P** and **C1-S**, ending our pursuit of dimer **SC1-*meso***.

Section 2.3: Characterization of Chlorin Monomers & Dimers

Section 2.3.1: Structure Determination

All new compounds were characterized by ^{1}H NMR, ^{13}C NMR and HRMS (either ESI-HRMS or MALDI-HRMS). All of the data are consistent with that expected for the given compounds. All compounds prepared by a known procedure were characterized by ^{1}H NMR to confirm identity against literature. For all novel styryl monomers, from ^{1}H NMR we determined that 1) the large coupling constants (*J* between 16.0-16.2 Hz) indicate only *trans*/*E* configuration and 2) no axial chirality is observed (no diastereotopic signals) despite the likelihood of different conformers (rotamers) depending upon mutual orientation of linker and macrocycle (i.e., ethenyl linker of dimers could face "inward" toward chlorin 15 position or "outward" toward 12 position). The lack of observed chirality has been attributed to free rotation of the bond between the first carbon atom of the linker and the macrocycle. Through DFT energy minimized structures, the energy of rotation has been approximated, and in the most sterically demanding case **C1-S15** (where chlorin and styryl substituent are planar), the energy barrier is predicted not to exceed 18 kJ/mol (Section 2.5.6, Table 2.5), well below the 23 kJ/mol threshold for free rotation at room temperature.[179] Similarly, from ^{1}H NMR, all dimers display high symmetry with two equivalent chlorin macrocycles, based upon the total number of signals and relative integration (mass obtained by HRMS confirms that relative integration is correct). We attempted to obtain large single crystals for X-ray crystallography (XRC) for quite some time, however, we were unsuccessful. In lieu of XRC, and lacking coupling constants due to symmetry, 2D NOESY was obtained for **C1-V**, **SC1** and **SC3**, in order to confirm the

configuration of the ethenyl linker in dimers. Both *cis* or *trans* linker conformations allow for the high symmetry observed in ^{1}H NMR, but in the case of *cis* linker we anticipate a significant upfield shift of resonances corresponding to protons in the southwest portion of macrocycle. This is due to the proximity of the macrocycles and their respective shielding cones (structures shown in Figure 2.1). Such a shielding effect has been previously reported for *cis* ethenyl linked porphyrin[180] and chlorophyll dimers.[56] Assigning all signals of **C1-V**, **SC1** and **SC3** through 2D NOESY (Section, 2.6.1, Table 2.6), it is evident that the majority of signals in both dimers are comparable to those of **C1-V**. No shielding was observed for any resonances. The only significant deviations of chemical shift from **C1-V** resonances were observed for H-12, H-15 and V1 (first vinylic proton of linker, relative to macrocycle) resonances, all of which showed deshielding of ~0.5-1 ppm (Figure 2.2, below). To rule out the possibility of molecular motions averaging the ^{1}H NMR signals and preventing observation of distinct conformers, we acquired ^{1}H NMR spectrum for **SC1** at 5°C. No significant changes relative to the room temperature spectrum were observed (Section 2.6.2, Figure 2.12). Finally, the results of the styryl

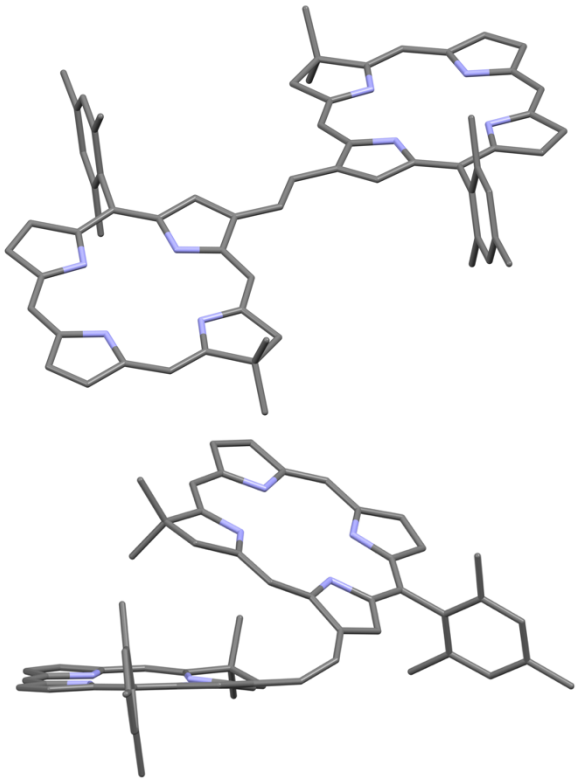

Figure 2.1: DFT energy-minimized structures of SC1 (top) and imaginary cis ethenyl linked chlorin dyad (cis-SC1, bottom). Hydrogen atoms omitted for clarity.

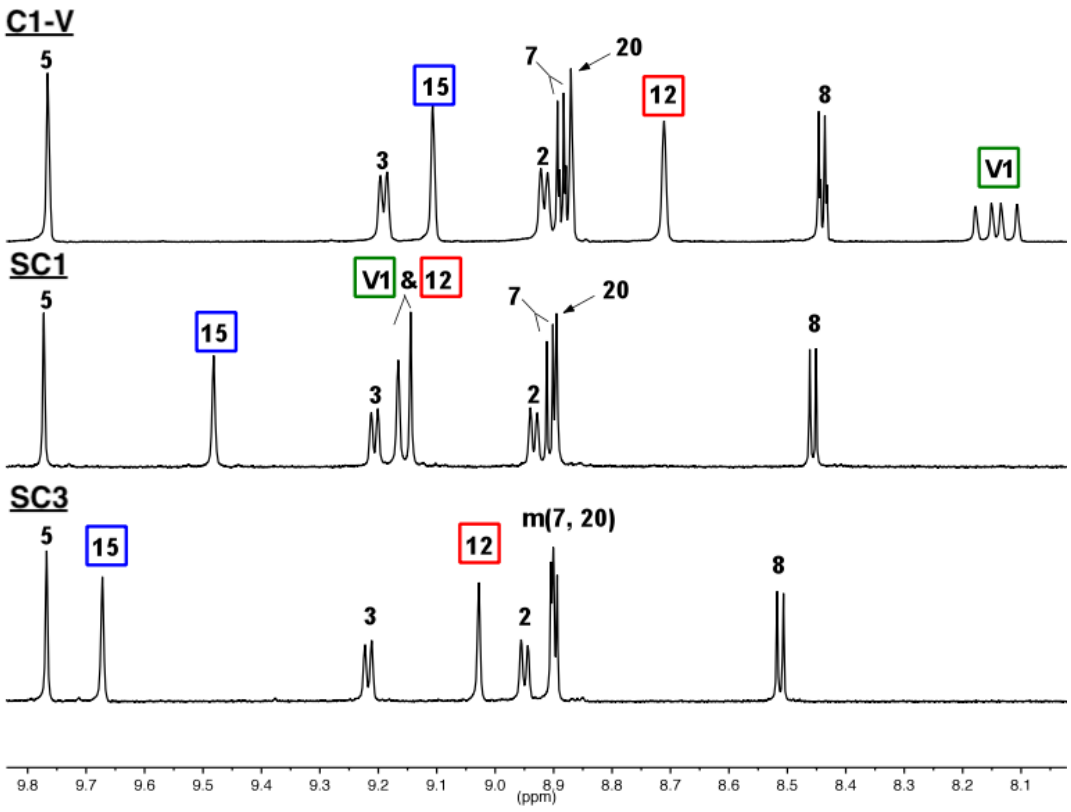

Figure 2.2: Aromatic region of ^{1}H NMR for C1-V, SC1 and SC3, with resonances labeled according to position on chlorin. Signals with notable difference in shift (δ_{ppm}) between monomer C1-V and dimers indicated by colored box; position 15 (blue), position 12 (red) and linker V1 (green).

chlorin syntheses provide another indirect piece of evidence for *trans* conformer dyads. Whether prepared by olefin metathesis or by Heck reaction, only the *trans* styryl monomers were observed, suggesting that the *cis* isomers are too energetically disfavored to form by our approach. Considering the *cis* dimers would exhibit greater crowding than *cis* styryl monomers, they are even less feasible to form. Thus, from the confirmation of high symmetry, along with the lack of shielded ^{1}H NMR resonances and the close agreement of chemical shifts for **C1-V**, **SC1** and **SC3** we have concluded that the vinyl linkers of all novel dimers are *trans*/*E*.

Section 2.3.2: Photophysical Characterization

The absorption and emission spectra of all new compounds were acquired in air equilibrated toluene and DMF. No significant solvatochromism was observed, thus all

data discussed in this section were acquired in toluene, unless stated otherwise. All absorption spectra were acquired at a concentration of ~10 μM and emission spectra at a concentration of ~ 1.0 μM. Concentrations were roughly estimated based on the absorbance values in the range of A = 0.1-1.0, under the assumption that ε of the chlorin *B* band is in the average range of 100,000-150,000 $M^{-1} \cdot cm^{-1}$.[107,118] The absorption and emission spectra of target monomers are shown in Figure 2.3, and spectra of dyads are shown in Figure 2.4. The absorption and emission spectra of all novel intermediate chlorin monomers are also included in Figure 2.5. Stokes' shift and full width at half maximum (FWHM) were determined manually from absorption and emission spectra.

Fluorescence quantum yields (Φ_F) for all new compounds and fluorescence lifetime (τ_F) for nearly all compounds were determined. Compounds **C2-2S** and **C2-2P** are the exceptions due to lack of sample availability when time-correlated single photon counting (TCSPC) became available to us. Details of how data were acquired and reported for Φ_F and τ_F can be found in Sections 2.5.4 and 2.5.5. A summary of all absorption and emission data can be found in Table 2.1.

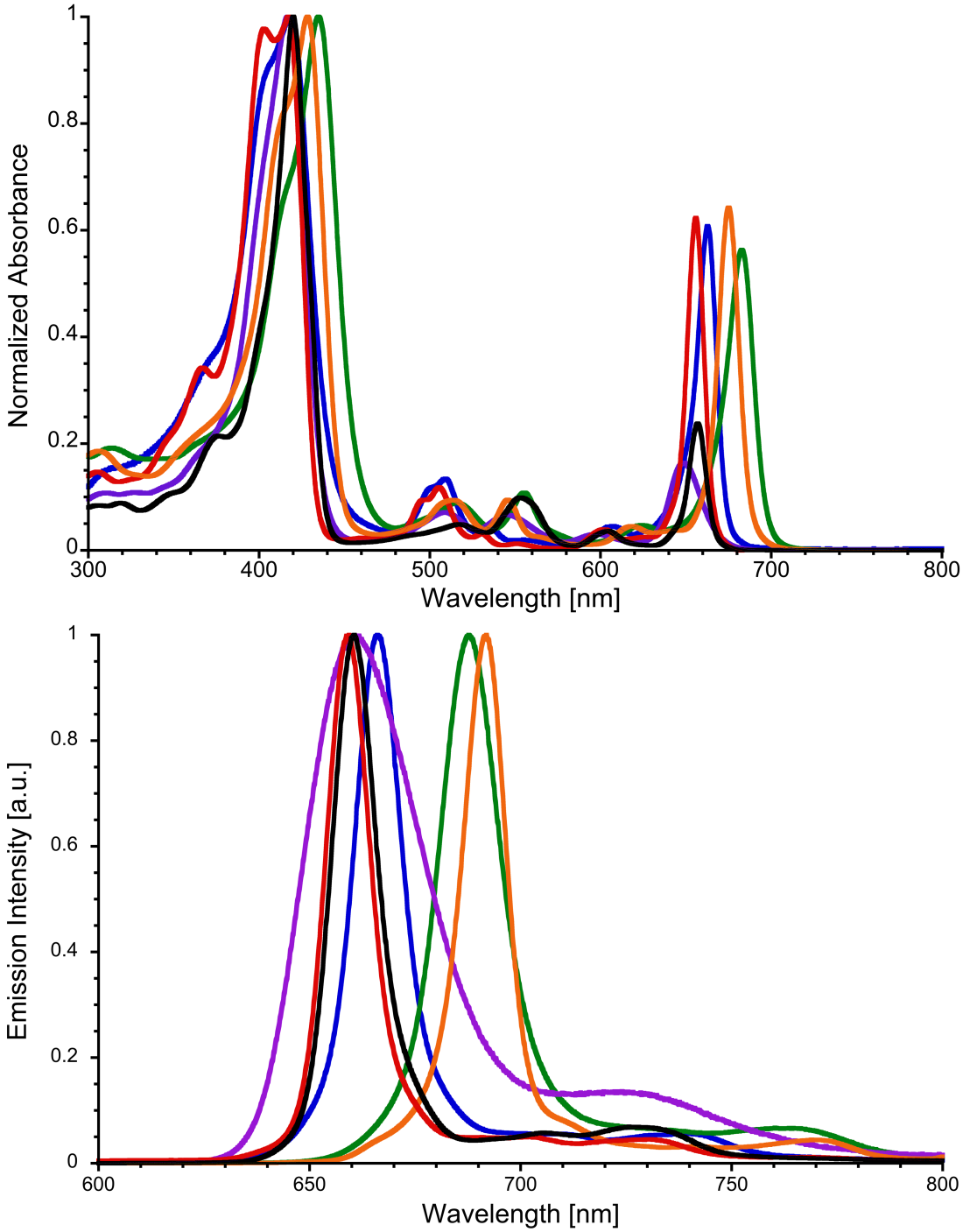

Figure 2.3: Normalized absorption (top) and emission (bottom) spectra of target styryl and phenylethynyl substituted chlorin monomers C1-S (blue), C1-P (red), C2-2S (green), C2-2P (orange), C1-S15 (purple) and C1-P15 (black). All data shown acquired in toluene, for emission spectra, excitation at maximum of *B* band. Absorption spectra acquired at ~10μM concentration and emission spectra at ~ 1.0 μM.

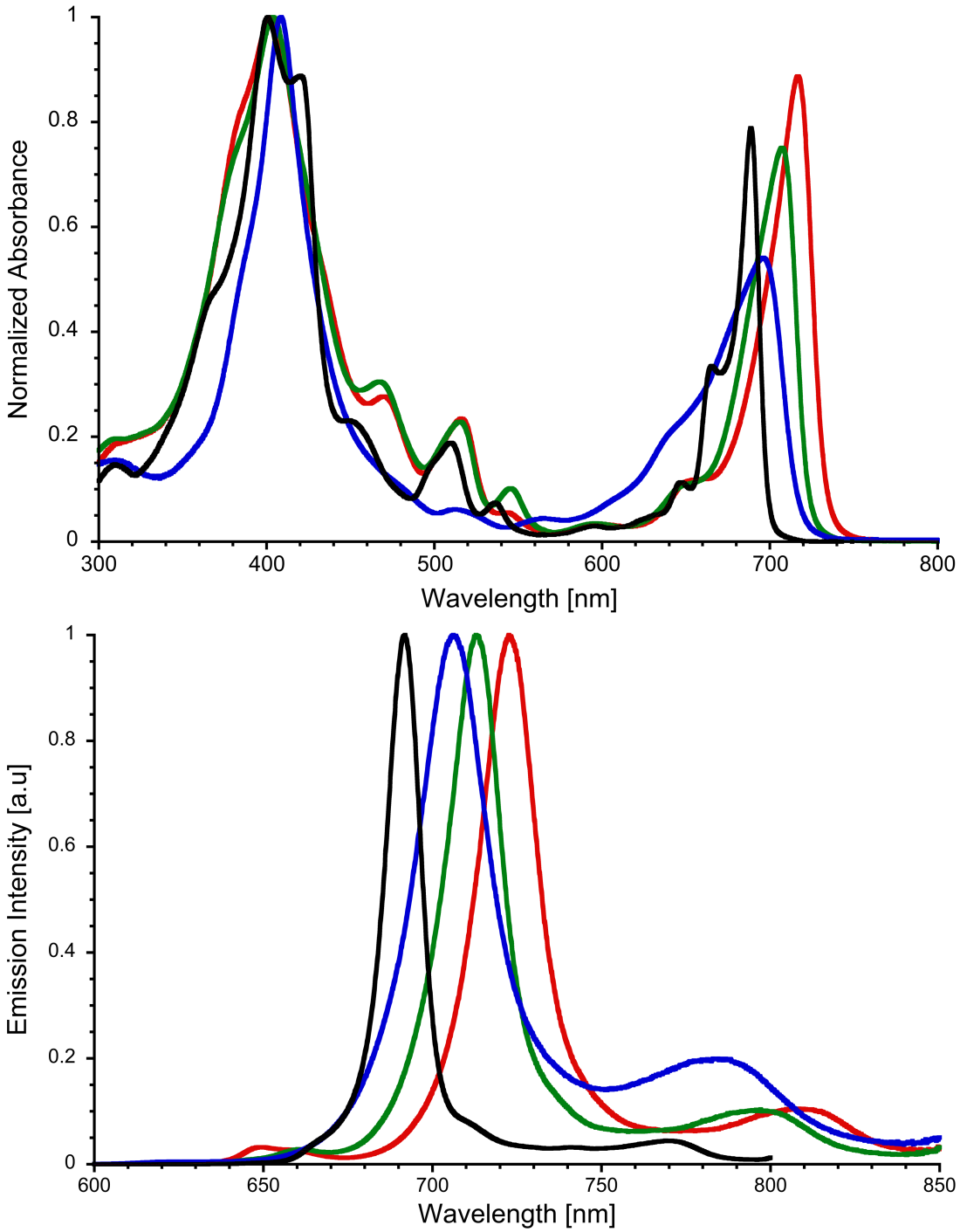

Figure 2.4: Normalized absorption (top) and emission (bottom) spectra of ethenyl and ethynyl linked chlorin dyads ZnSC1 (blue), SC1 (green), SC2 (red) and SC3 (black). All data shown acquired in toluene, for emission spectra, excitation at maximum of *B* band. Absorption spectra acquired at ~10μM concentration and emission spectra at ~ 1.0 μM.

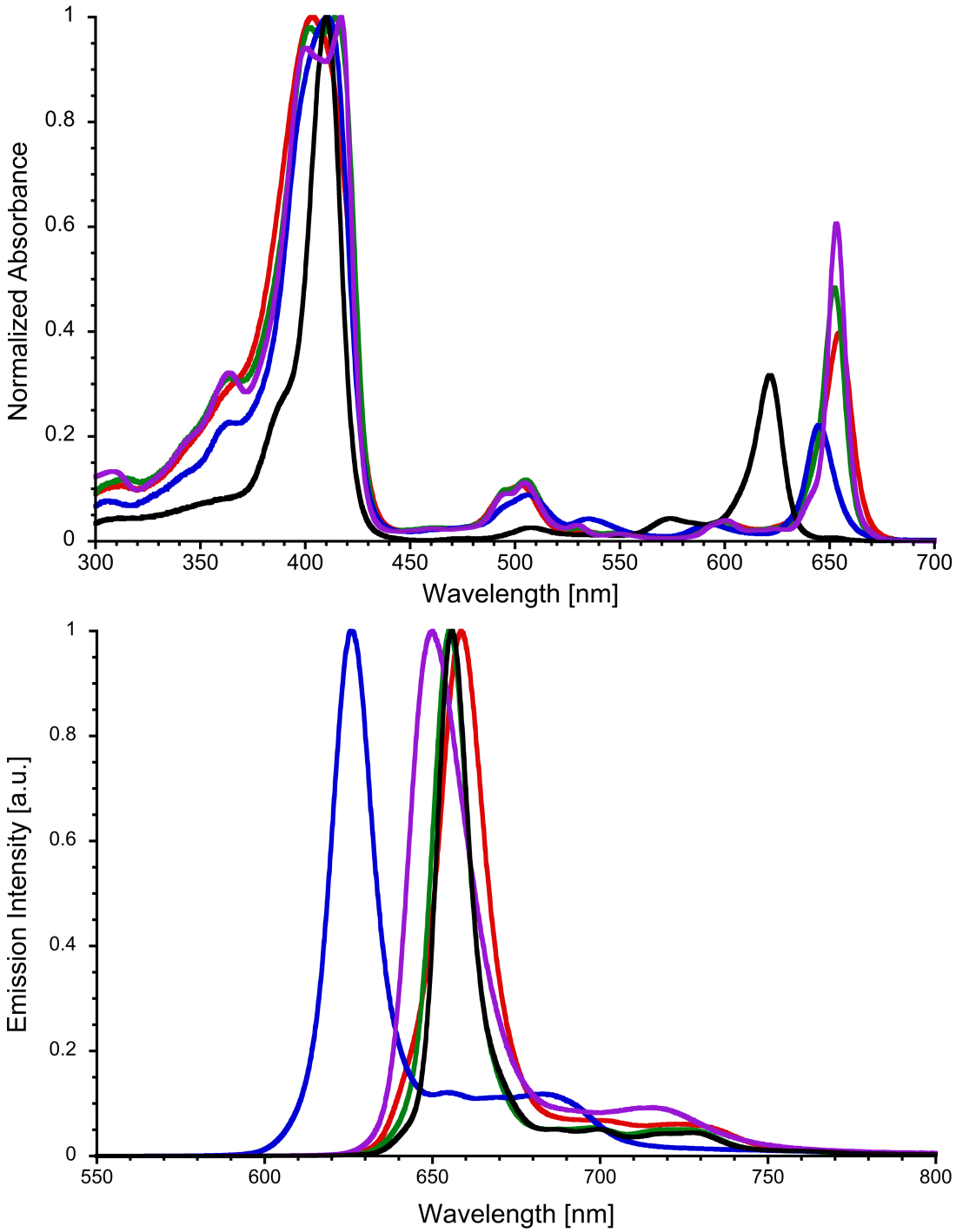

Figure 2.5: Normalized absorption (top) and emission (bottom) spectra of ethenyl and ethynyl substituted chlorin monomers ZnC1-V (blue), C1-V (green), C3-V (red), C1-V15 (purple) and C1-ETMS (black). All data shown acquired in toluene, for emission spectra, excitation at maximum of *B* band. Absorption spectra acquired at ~10μM concentration and emission spectra at ~ 1.0 μM.

Compound	Absorption λ_{max} [nm]			λ_{emi} [nm]	Stokes Shift [nm] (cm^{-1})	Emission FWHM [nm] (cm^{-1})	Φ_F tol. (Φ_F DMF)
	$\lambda_{B\ bands}$	λ_{Qx}	λ_{Qy}				
Vinyl & ethynyl substituted monomers (chlorin intermediates)							
C1-V	414	505	652	655	3 (70)	13 (303)	0.29 (0.29)
C1-ETMS	400, 417	505	653	656	3 (70)	11 (255)	0.31 (0.30)
ZnC1-V	410	508	622	626	4 (103)	15 (382)	0.14 (0.16)
C3-V	404	503	655	659	4 (93)	16 (369)	0.26 (0.26)
C1-V15	411	506	645	650	5 (120)	21 (493)	0.26 (0.25)
Styryl & phenylethynyl substituted monomers							
C1-S	419	509	663	666	3 (68)	13 (293)	0.34 (0.32)
C1-P[a)]	402, 417	506	656	659	3 (69)	14 (304)	0.33 (0.34)
C2-2S	435	515, 555	683	688	5 (106)	18 (380)	0.38 (0.38)
C2-2P	431	514, 546	675	679	4 (87)	13 (298)	0.37 (0.36)
C1-S15	417	509, 546	649	660	11 (257)	32 (728)	0.28 (0.28)
C1-P15	420	553	657	661	4 (92)	13 (298)	0.31 (0.32)
Ethenyl and ethynyl linked dimers							
SC1	403	514	707	712	5 (99)	20 (395)	0.48 (0.39)
SC3	401, 417	510	689	692	3 (63)	13 (272)	0.46 (0.38)
ZnSC1	409	512	696	706	10 (204)	26 (522)	0.30 (0.12)
SC2	403	516	717	723	6 (116)	20 (384)	0.45 (0.33)

Table 2.1: Summary of absorption and emission properties of all compounds prepared and discussed in Chapter 2. Presented data acquired in toluene except where solvent indicated as DMF. Table organized such that all freebase 10-mesityl ethenyl and ethynyl substituted/linked chlorin counterparts are presented adjacent to one another. a) Original values reported in ref.[33] For consistency, all data presented above were obtained in our laboratory. Error for quantum yield measurements estimated at ± 5% (see section 2.5.4 for details).

The absorption spectra of all new monomers feature the typical chlorin bands. These include the deep blue (nearly overlapping) *B* bands, green spectral window Q_x band and deep red Q_y band. In the monomers presented here, the bands spanned the regions of 401-435 nm, 500-555 nm, and 622-683 nm. The range of values on Q_y bands is quite large due to inclusion of hypsochromically shifted Q_y band of **ZnC1-V**. The chlorin dimers feature *B* bands in the range of 401-417 nm, Q_x bands in the range of 510-516 nm, and Q_y bands between 689-717 nm. From this point forward, discussion of spectra will focus primarily on the Q_y bands as they correspond to the lowest energy ($S_0 \rightarrow S_1$) transition, and more accurately demonstrate the extent to which electronic conjugation occurs. The greater the electronic conjugation, the lower the energy required for the $S_0 \rightarrow S_1$ transition, which is seen as bathochromic shifting of the Q_y band. For *β-β* linked monomers, the styryl substituents of **C1-S** (λ_{max} = 663 nm) and **C2-2S** (λ_{max} = 683 nm) afford larger bathochromic shift than corresponding phenylethynyl substituents in **C1-P** (λ_{max} = 656 nm) and **C2-2P** (λ_{max} = 675 nm). The difference between **C1-S** and **C1-P** being 7 nm (160.9 cm^{-1}), while the difference for **C2-2S** and **C2-2P** is comparable at 8 nm (173.5 cm^{-1}). In the case of *meso-meso* linked monomers, the opposite trend was observed. The 15-phenylethynyl chlorin **C1-P15** (λ_{max} = 657 nm) exhibited a more significant bathochromic shift than 15-styryl chlorin **C1-S15** (λ_{max} = 649 nm). The difference here is similar at 8 nm (187.6 cm^{-1}). In all cases discussed for Q_y bands, the same relationships between relative bathochromic shifts were observed for *B* bands (Table 2.1). It is also worth noting that 13-ethenyl (**C1-V**) and 13-(trimethylsilyl)ethynyl (**C1-ETMS**) chlorins exhibit nearly identical

absorption spectra with Q_y band maxima at 652 nm and 653 nm, respectively (Figure 2.5).

The Q_y-like absorption bands for all dimers are highly red shifted, more intense and broader (FWHM) than the Q_y bands of styryl and ethynyl monomers. Replacing benzene with chlorin results in a 44 nm (938.7 cm^{-1}) red shift (**C1-S** vs **SC1**) where ethene is present and 33 nm (730.1 cm^{-1}) red shift where ethyne is present (**C1-P** vs **SC3**). Band broadening (greater FWHM) is observed with *B* bands of all ethenyl linked dyads as well (Figure 2.4). The absorption profile of ethynyl linked dimer **SC3** is slightly different in that it appears to have a more discrete vibronic transition (0-1) associated with the Q_y-like band. Similar observation was made for an analogous ethynyl chlorin dimer derived from the Sonogashira reaction of 13-bromo-10-tolyl chlorin and 13-ethnynyl-10-tolyl chlorin.[35,36] Direct comparison of the λ_{max} of the Q_y-like band of freebase ethenyl dimer **SC1** (707 nm) vs ethynyl dimer **SC3** (689 nm) shows that the prior has a superior bathochromic shift by 18 nm (369.5 cm^{-1}), double the difference that was observed between the styryl vs ethynyl monomers. Ethenyl linked zinc chlorin dimer **ZnSC1** exhibited a hypsochromically shifted Q_y-like band (696 nm) relative to its parent dimer **SC1**. This behavior is consistent with that of chlorin monomers (**C1-V** to **ZnC1-V**, results in blue shift of 30 nm, 739.7 cm^{-1}), despite occurring to a lesser degree (11 nm, 223.5 cm^{-1}). Conversely, replacing 10-mesityl substituent with pentafluorophenyl results in a bathochromic shift of Q_y-like band by 10 nm (197.3 cm^{-1}) to 717 nm in dimer **SC2**.

The emission spectra for all chlorin monomers (Figures 2.3 and 2.5) and dimers (Figure 2.4) exhibit the characteristic 0-0 emission band with weak vibronic tail. Like

most hydroporphyrins, these emission bands are quite narrow, with FWHM ranging from 13 to 21 nm (255.2 to 493.4 cm^{-1}) for β substituted chlorins, and from 13 to 32 nm (298.0 to 728.4 cm^{-1}, Table 2.1) for *meso* substituted chlorins. The wider emission bands for meso substituted chlorins (particularly **C1-S15**) is the result of extensive steric hindrance leading to more conformational variability. Mono-substituted chlorins **C1-S** and **C1-P** show emission maxima at 666 nm and 659 nm, respectively, a difference of 7 nm (159.5 cm^{-1}). Similarly, disubstituted chlorins **C2-2S** and **C2-2P** emission maxima are at 688 nm and 679, respectively, a difference of 9 nm (192.7 cm^{-1}). Thus, for β substituted monomers, the styryl substituted chlorins exhibit a superior bathochromic shift relative to the phenylethynyl substituted ones. For the *meso* substituted monomers, **C1-S15** and **C1-P15**, the emission maxima occur at 660 nm and 661 nm, respectively. Interestingly, this coincides with a Stokes' shift for **C1-S15** (11 nm, 256.8 cm^{-1}) more than double that observed with the other chlorin monomers (67.9 - 106.4 cm^{-1}, Table 2.1). We have attributed this larger Stokes' shift to the compound having greater structural flexibility in the excited state than in the ground state, enabling the styryl moiety of **C1-S15** to reach a more planar configuration before undergoing fluorescence.

Emission spectra of the dimers show an intense 0-0 emission band as well as a weaker band at longer wavelength. Because the secondary emission bands observed in the emission spectra of dimers are more discrete than in the monomers, we have rationalized their presence as 0-1 vibronic transitions. The 0-0 emission bands are narrow, with FWHM ranging from 13-26 nm (271.9-521.8 cm^{-1}) and have a small Stokes' shift of 3-10 nm (62.9-203.5 cm^{-1}). The emission maxima parallel the

absorption maxima in order of least to most red shifted dimer; **SC3** (692 nm) < **ZnSC1** (706 nm) < **SC1** (712 nm) < **SC2** (723 nm).

Fluorescence quantum yields of the monomers are comparable to their counterparts (*e.g.*, Φ_F **C1-S** ≈ Φ_F **C1-P**), and in all cases increase as the total number of conjugated π bonds in the system increases (Table 2.1). Zinc monomer **ZnC1-V** has a much lower Φ_F (0.14) than the others, as is often the case for metallated hydroporphyrins. This phenomenon is well characterized by Lindsey and Holten, who demonstrated that for a large series of chlorins, their corresponding zinc chelates possess both diminished Φ_F and a significantly shorter fluorescence lifetime.[110] At a later time they reported rate constants (k_f and k_{nr}) for many of these compounds, indicating that the lowered Φ_F is due to increased intersystem crossing.[181] This demonstration of the heavy atom effect is certainly at work in **ZnC1-V** as well. Fluorescence quantum yields of the freebase chlorin dimers are significantly larger than those of the chlorin monomers, from 0.45-0.48. Within experimental error (±5%, see section 2.5.4 for details), all three freebase dimers have identical Φ_F. Zinc dimer, **ZnSC1**, exhibits Φ_F (0.30) decreased by roughly one third compared to freebase **SC1** (0.48). To establish the extent of fluorescence quenching in polar solvents, we determined Φ_F of all new compounds in DMF and compared to values found in toluene. Chlorin monomers exhibited no quenching, with nearly identical values of Φ_F in both toluene and DMF, while the dimers showed partial quenching in DMF, ranging from 19% decrease in the case of **SC1** up to 60% in the case of **ZnSC1**. The more dramatic quenching in **ZnSC1** is likely due to the presence of zinc lowering the oxidation potential of the individual chlorin components, making the system more prone to

oxidative photoinduced electron transfer. The general trend of larger Φ_F for the dimers relative to the monomers is likely due, in part, to faster rate of fluorescence. This is based off of preliminary TCSPC data that indicates the fluorescence lifetime (τ_F) of dimers is approximately half that of monomers. We can infer from the shorter τ_F in tandem with the increased Φ_F, that k_r is increasing, however, individual rate constants (k_r, k_{ic}, k_{isc}) remain unknown, so any discussion would be speculative. This has been one of the primary interests in our ongoing collaboration with Dr. Dewey Holten (Washington University in St. Louis), we anticipate publication of such results in the near future.

The overall absorption and emission data can be compared to determine the relative strength of electronic communication. In the case of β substituted monomers, or β linked dimers, the ethenyl linker provides superior conjugation in both the ground and excited states. This is apparent because when considering only the freebase chlorins (**C1-S** v. **C1-P**, **C2-2S** v. **C2-2P**, and dimers **SC1** v. **SC3**), the greatest bathochromic shift is observed for ethenyl linkers, in both the absorption and emission spectra. In the case of *meso* substituted monomers, the absorption of **C1-P15** exhibits superior bathochromic shift relative to **C1-S15**, but the two have nearly identical emission spectra. This indicates that for the *meso* linked monomers, ethynyl linker provides greater electronic conjugation in the ground state, while in the excited state both linkers afford the same degree of communication.

With the aid of DFT-optimized structures, we are able to justify the observed trends. As mentioned earlier, we attempted at great length to acquire crystals suitable for X-ray diffraction, yet we were unable to do so, and utilized DFT energy-minimized

structures in lieu of such data. Dihedral angles were determined using Spartan '10 software to select appropriate atoms. For mean macrocycle planes in 13- substituted chlorins, C12, C13 and first linker carbon are selected, in 15- substituted chlorins C14, C15 and first linker carbon are selected, and linker planes were determined by both linker carbons and linker site at chlorin. These values were shown to have excellent agreement with the mean planes that were calculated by Mercury software, without need for the additional steps in data processing. The predicted dihedral angles agree with the observed absorption and emission data. *β*- substituted monomers **C1-V** and **C1-S** were predicted to have dihedral angles at or near 0º, while the *meso*-substituted **C1-V15** and **C1-S15** were predicted to be closer to 45º (Table 2.3).

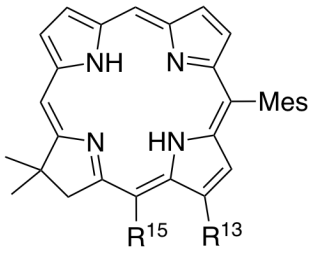

Monomer	R^{13}	R^{15}	Angle (deg.)
C1-V		-H	0.13
C1-S	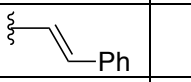	-H	0.07
C1-V15	-H		47.79
C1-S15	-H	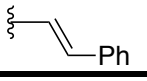	43.82

Table 2.3: Dihedral angles for select compounds predicted by DFT energy-minimized structures.

For *β*-*β* linked dimer **SC1**, the dihedral angle between linker and chlorin was determined separately for each component macrocycle, giving an average value of 7.5º. The average dihedral angle for imaginary dimer **SC1-i** (with 12-methyl substituent present) was significantly larger at ~34º. To ensure that the large increase in predicted dihedral angel was not a result of 10-mesityl and 12-methyl steric interaction, a second imaginary dimer **SC1-ii** was modeled in which the bulky 10-Mes was removed. This final DFT energy-minimized structure predicted an average dihedral angle of ~23º, still

significantly larger than that predicted for **SC1** (Table 2.4). The small dihedral angles predicted for **C1-S** and **SC1** are in agreement with their superior bathochromic shift to respective ethynyl analogues **C1-P** and **SC3**. Likewise, the large predicted dihedral angle of **C1-S15** supports its shorter absorption maxima relative to **C1-P15**, indicating **C1-S15** has less effective electronic conjugation than **C1-P15** (in the ground state). The large Stokes' shift observed with **C1-S15** can also be justified by this ground state deviation in planarity. In the excited state bonds elongate,[182] and the auxochrome of **C1-S15** can reach a more co-planar configuration with the macrocycle, improving its electronic communication.

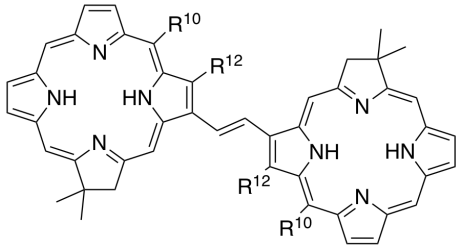

Dimer	R^{10}	R^{12}	Average Angle (deg.)
SC1	-Mes	-H	7.5
SC1-i	-Mes	-Me	33.6
SC1-ii	-H	-Me	22.9

Table 2.4: Average dihedral angle for dyad SC1 and imaginary dyads SC1-i and SC1-ii.

Section 2.3.3: Reactivity of Ethenyl Linked Dimers with Singlet Oxygen

The reaction of dimer **SC1** with singlet oxygen was apparent as early as its synthesis but was challenging to properly identify. Initially, synthesis and purification of dimer **SC1** led to very low yields. TLC suggested rapid decomposition accompanying purification, as a bright red fluorescent impurity was always observed (where **SC1** emits at a wavelength beyond the visible window). Noting this fluorescence was very important because it indicated that the dimer was cleaving in some fashion, and at least one of the constituent chlorins remained intact. A sample of **SC1** containing the impurity was analyzed by absorption spectroscopy, HRMS and ^{1}H NMR. Absorption spectrum of the mixture showed a band at 657 nm (in toluene) in

addition to the Q_y-*like* band of **SC1** at 707 nm. This band was close to, but not identical to that of **C1-V**. In addition, we were confident that **C1-V** was fully removed during purification due to the lack of this absorption band immediately following chromatography. Next, HRMS showed a peak with *m/z* of 487.2492, close yet too large to be **C1-V** (*m/z* = 485.2701 for $[M+H]^+ = C_{33}H_{33}N_4$). Finally, ^{1}H NMR of the mixture

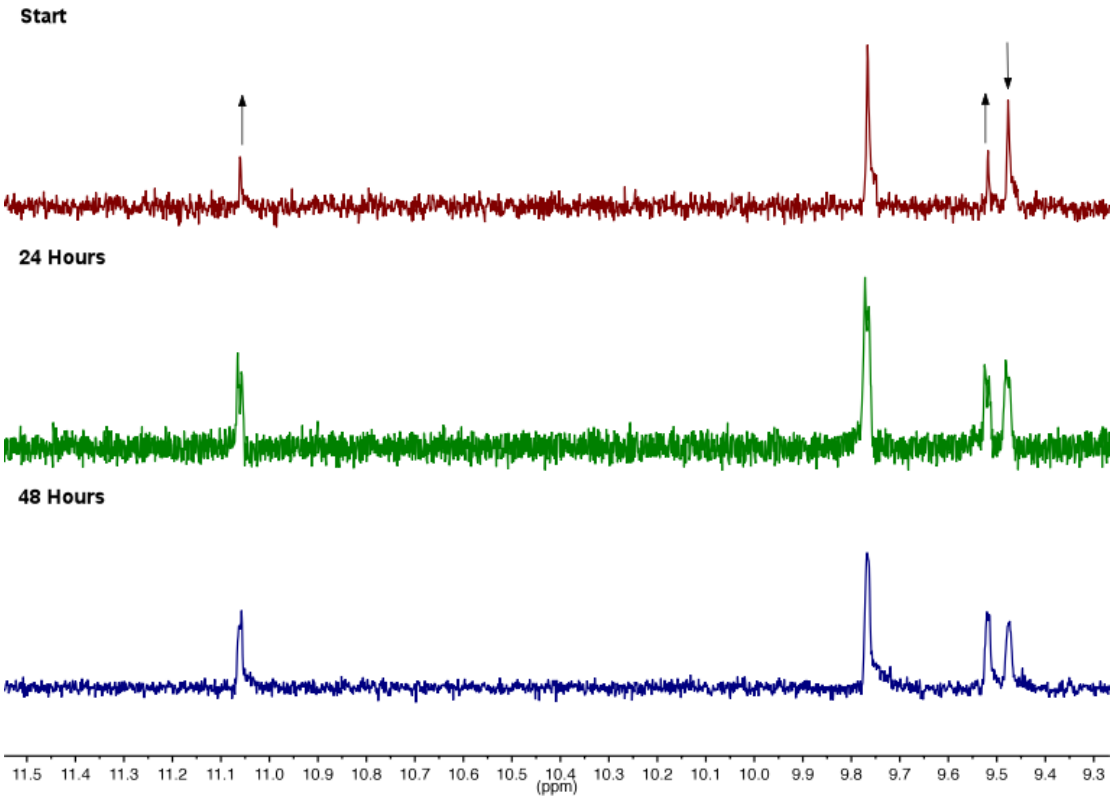

Figure 2.7: Increasing intensity of aldehyde ^{1}H NMR resonance of C1-CHO after ambient light irradiation of SC1 in chloroform-d. Observed signals from left to right: aldehyde (C1-CHO), chlorin 5 position (C1-CHO & SC1, overlapping), chlorin 15 position (C1-CHO), and chlorin 15 position (SC1). Note, SC1 sample was partially converted at the start of this experiment.

showed a new resonance at 11.07 ppm, that increases in relative intensity upon additional light exposure (Figure 2.7). A resonance in this region is highly suggestive of an aldehydic proton, thus we hypothesized that the observed impurity was 13-formylchlorin (**C1-CHO**). Fortunately, **C1-CHO** had been previously reported, and the data was consistent with our own: λ_{max} Q_y of 657 nm, HRMS (reported *m/z* = 486.2422 for $[M]^+ = C_{32}H_{30}N_4O$, ours found for $[M+H]^+ = C_{32}H_{31}N_4O$), and ^{1}H NMR

resonance of formyl proton at 11.06 ppm.[162] In addition, the dimer **ZnSC1** underwent analogous changes and showed the appearance of a new emission band with λ_{max} at 637 nm (toluene), matching that reported for the zinc (II) complex of **C1-CHO**.[183] Thus, we were satisfied that the identity of the impurity in the **SC1** sample was **C1-CHO**.

It is well established that alkenes undergo [2+2] cycloaddition with singlet oxygen,[184] so the ability of our dimers to react in such a fashion is reasonable. Singlet oxygen ($^1O_2$) is a highly reactive form of oxygen generated by the interaction of a triplet excited state chromophore with ground state molecular oxygen ($^3O_2$).[185,186] Hydroporphyrins are well established in their ability to generate $^1O_2$,[187] so we proposed that **SC1** is first reacting with $^3O_2$ (and light) then rapidly participating in cycloaddition, with cleavage of 1,2-dioxetane intermediate to form **C1-CHO** (Scheme 2.10). In retrospect, such a conversion is almost expected; however, we were surprised because earlier literature involving similar porphyrin or chlorophyll dimers made no mention of dimer properties and/or integrity quickly changing upon exposure to light.

To confirm that **C1-CHO** was produced from reaction with $^1O_2$, we sought to verify that first that ethenyl linked dimers are capable of generating singlet oxygen and second, that light is required for the transformation. The generation of $^1O_2$ was verified by a photobleaching experiment in which a singlet oxygen scavenger, 1,3-diphenylisobenzofuran (DPBF), was mixed with dyad **SC1** and subjected to light irradiation. DPBF is frequently used

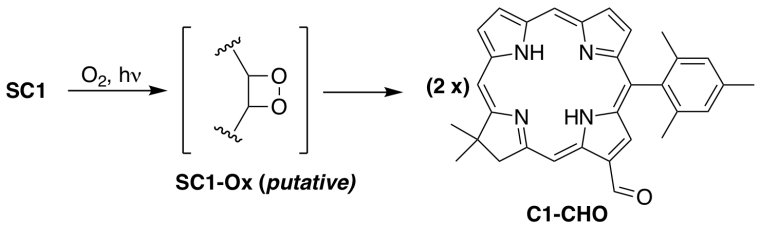

Scheme 2.10: Reaction of dyad SC1 with photosensitized oxygen to yield 13-formyl chlorin C1-CHO.

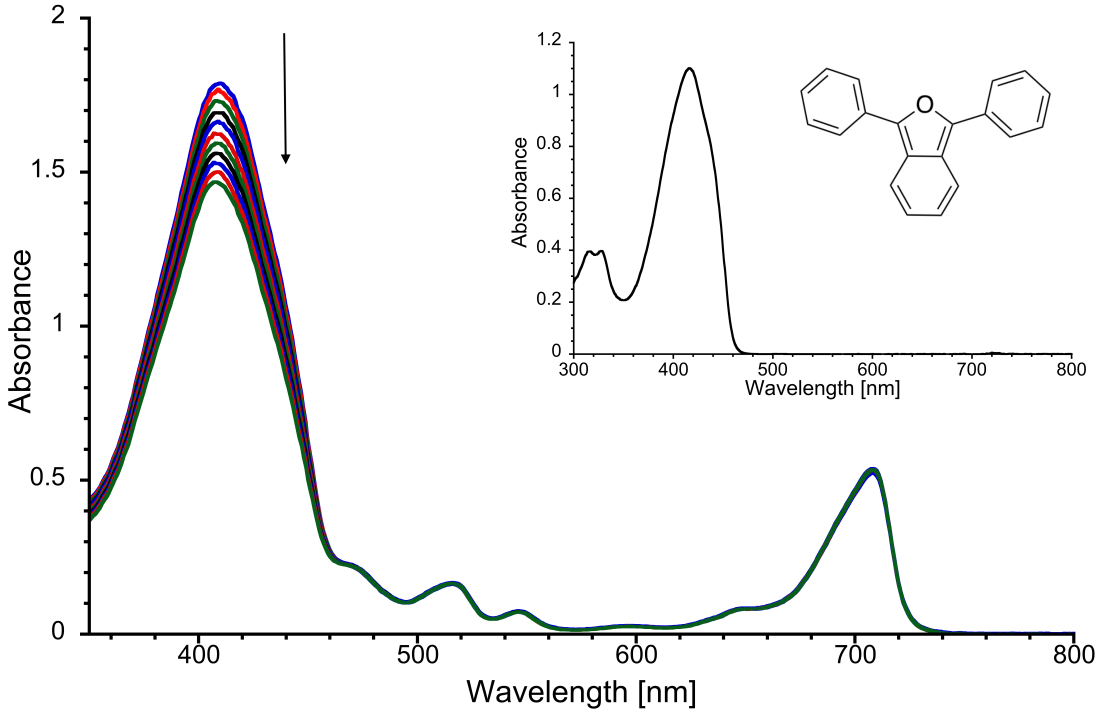

Figure 2.8: Absorption spectra of DPBF mixture with dyad SC1 in toluene, over time. Absorption spectra acquired immediately following two-minute cycles of irradiation at dyad *Q_y-like* band, for total of 20 minutes (10 exposures). Shown on inset are structure of DPBF and absorption spectrum of DPBF stock solution (toluene).

to detect the presence of $^1O_2$ as it rapidly undergoes cycloaddition at furan, forming a peroxide intermediate that decomposes to 1,2-dibenzoylbenzene.[188] This change is monitored by a decrease in the DPBF absorption band at 417 nm, thus, one must simply irradiate the photosensitizer and measure DPBF absorption over time. It is important to note that DPBF will generate $^1O_2$ if directly excited, therefore the photosensitizer must be selectively excited, (e.g. **SC1** was excited at the maximum of the Q_y-like band at 707 nm). Taking a mixture of both **SC1** and DPBF in toluene, upon excitation of **SC1**, the DPBF signal diminished in proportion to the duration of light exposure (Figure 2.8). Meanwhile there was no change to the absorbance intensity of **SC1** at 707 nm, indicating the high concentration of DPBF protected **SC1** from conversion to **C1-CHO**. The control experiment with DPBF alone and irradiation at 707 nm resulted in no change of the DPBF absorption spectrum. At a later time, we also acquired a detector

with near-infrared capability, enabling direct measurement of singlet oxygen luminescence at 1270 nm, upon excitation of dyad (Figure 2.9). In all cases, the signal from singlet oxygen was observed, but overlapped heavily with weak dyad

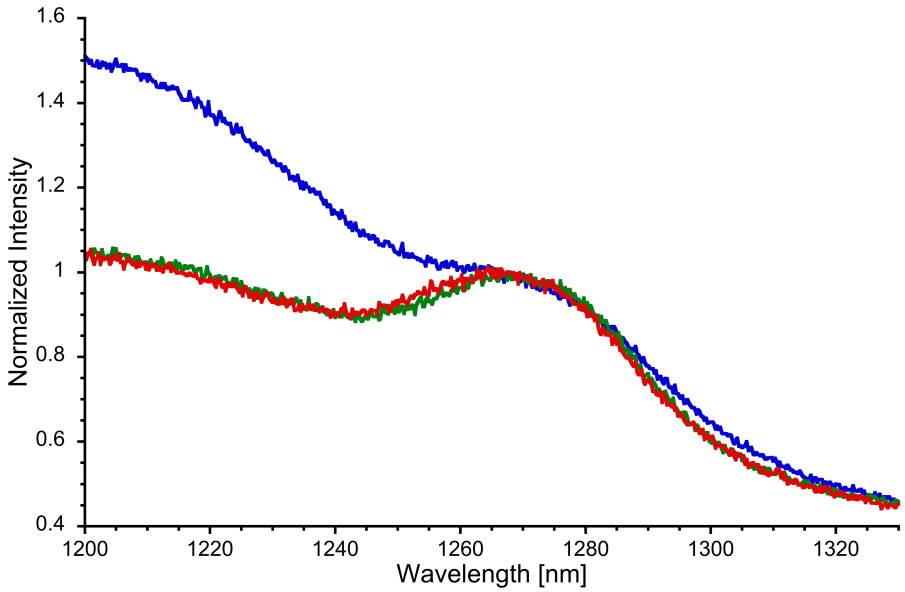

Figure 2.9: Normalized singlet oxygen luminescence generated by irradiation of ZnSC1 (blue), SC1 (green) and SC2 (red) in toluene, at the maximum of the *B* band with sample concentration of ~ 10 µM.

luminescence. Finally, we attempted several control experiments where **SC1** was exposed to light in deoxygenated solvent (toluene or chloroform, degassed by freeze-pump-thaw method), however, we were unable to stop or slow the rate of conversion to **C1-CHO** by this method. We attribute incomplete deoxygenation to the continued changes, as opposed to the reaction being independent on the presence of oxygen. The deoxygenation could have been improved by using argon instead of nitrogen.

The necessity of light for the conversion of **SC1** to **C1-CHO** was confirmed by creating a single solution of **SC1** in toluene, partitioning into two equal aliquots and subjecting one to ambient light exposure overnight, while the other was stored under darkness. Only the irradiated sample showed the appearance of the **C1-CHO** absorption band. The requirement of light, along with the unchanging absorbance of

SC1 in the presence of excess singlet oxygen scavenger DPBF, confirms that singlet oxygen is responsible for the appearance of **C1-CHO**.

Once we were satisfied with the cause of **C1-CHO** formation, we sought to better understand the process, specifically, 1) can we control the rate of cycloaddition reaction at ethenyl linker 2) is there a dependence on chromophore concentration on the rate of reaction and 3) is there a predictable solvent dependence on the rate of reaction?

To address the first point, we required additional compounds. It is known that the more electron rich the olefin, the more readily it can react with $^1O_2$.[189–191] Therefore, we developed the electron deficient **SC2**, and electron rich **ZnSC1**, with the intent to slow down and speed up singlet oxygen cycloaddition, respectively. It is worth noting that we revisited the synthesis and purification of **SC1** at this time and performed all operations and handling under darkness, vastly improving the yield. In turn, these precautions were applied to the preparation of **ZnSC1** and **SC2**. Next, we probed the relative reactivity of the three dimers. We prepared samples of pure dimer in toluene and chloroform and exposed them to ambient artificial lighting while in a sealed test tube. After one week of light exposure, the absorption spectrum of **SC2** was unchanged in both solvents. Dyad **SC1** showed little to no change in toluene, with a gradual decrease in signal in $CHCl_3$ (75% intensity at λ_{max} after 24 hours), and for **ZnSC1** Q_y-like band was no longer present after 24 hours in either solvent. Qualitatively, the relative reactivity of the dimers follows the trend of most to least reactive **ZnSC1** >> **SC1** > **SC2**, when compared in the same environment. We attempted to illicit similar

conversion of distyryl substituted monomer **C2-2S** to **C1-CHO**, but no reaction was observed, nor was reaction with singlet oxygen apparent for ethynyl dimer **SC3**.

Because the rate of the cycloaddition reaction is dependent upon singlet oxygen concentration, we next determined if the dyads have a comparable singlet oxygen quantum yield (Φ_Δ). To do so we performed the same DPBF quenching experiment as described for dyad **SC1** (Figure 2.8) for dyad **SC2** (Section 2.5.7, Figure 2.13), and compared the remaining signal of DPBF. In both cases, 65-70% of DPBF was retained, with no change to the integrity of chromophore (based upon Q_y-like absorption band), suggesting that the two are similarly potent photosensitizers. We also attempted to do the same for **ZnSC1**, however, in the time it took to prepare the mixed sample, the absorption spectrum indicated partial conversion of **ZnSC1** to corresponding formyl chlorin (see Section 2.5.7 for experimental details). We were also unable to attempt determination of Φ_Δ based upon singlet oxygen luminescence, due to the high overlap of dimer luminescent tail with singlet oxygen signal (Figure 2.9). Therefore, Φ_Δ for dyads **SC1** and **SC2** are similar enough that we can assume their relative reactivity towards singlet oxygen depends only on their structural differences/electrophilicity. We cannot be certain of the relative Φ_Δ in the case of **ZnSC1** as it is much more challenging to handle than the other samples. Also, dimers **SC1** and **SC2** have similar fluorescence lifetimes at 3.38 and 3.11 ns, respectively, while **ZnSC1** has a shorter lifetime of 2.11 ns. It is possible that **ZnSC1**, due to the heavy atom effect, has a faster rate of intersystem crossing than either of the freebase dimers, causing it to have greater singlet oxygen production. Because of this it is challenging to state that **ZnSC1**

undergoes cycloaddition significantly faster than the other two dimers due to electronic factors, or increased singlet oxygen generation, or both.

Next, we wanted to determine if the rate of reactivity for our dimers varied with concentration over the range of absorbance from 0.1-1.5. This was important for us as we were uncertain of the concentration of our samples, and we are unable to determine molar absorptivity (ε) accurately. This is due to the inherent inaccuracy when weighing small quantities (final quantities often range from 5-20 mg) and cost ineffectiveness of sacrificing an entire sample to determine *ε*. At this time, we encountered significant issues with reproducibility of the data, as some samples of dyad **SC1** in toluene did not change, while others resulted in significant change in 24 hours. This behavior was independent of concentration as it was even observed in samples with approximately the same concentration (A ≈ 0.3). Data was similarly inconsistent for **ZnSC1**, however, decrease of the Q_y*-like* band was always observed. Unfortunately, we were unable make any conclusions regarding rate and dimer concentration.

Probing the reactivity rates in different solvents was equally problematic, and no meaningful trend was established with respect to solvent polarity (solvents included toluene, dichloromethane, chloroform, THF and acetonitrile). For select solvents, in addition to the appearance of **C1-CHO** absorption and emission bands, we observed new hypsochromically shifted bands (abs. λ_{max} ≈ 641 nm., emi. λ_{max} ≈ 650 nm.) that have been tentatively assigned to the 1,2-dioxetane intermediate (**SC1-Ox**, Scheme 2.10, Figure 2.10). We acknowledge that it is possible these new signals could belong to the *ciz/Z* isomer of dyad **SC1**, formed due to photochemical *E-Z* isomerization. Such photochromism is well documented for hexa-3-en-1,5-yne or “enediyne” containing

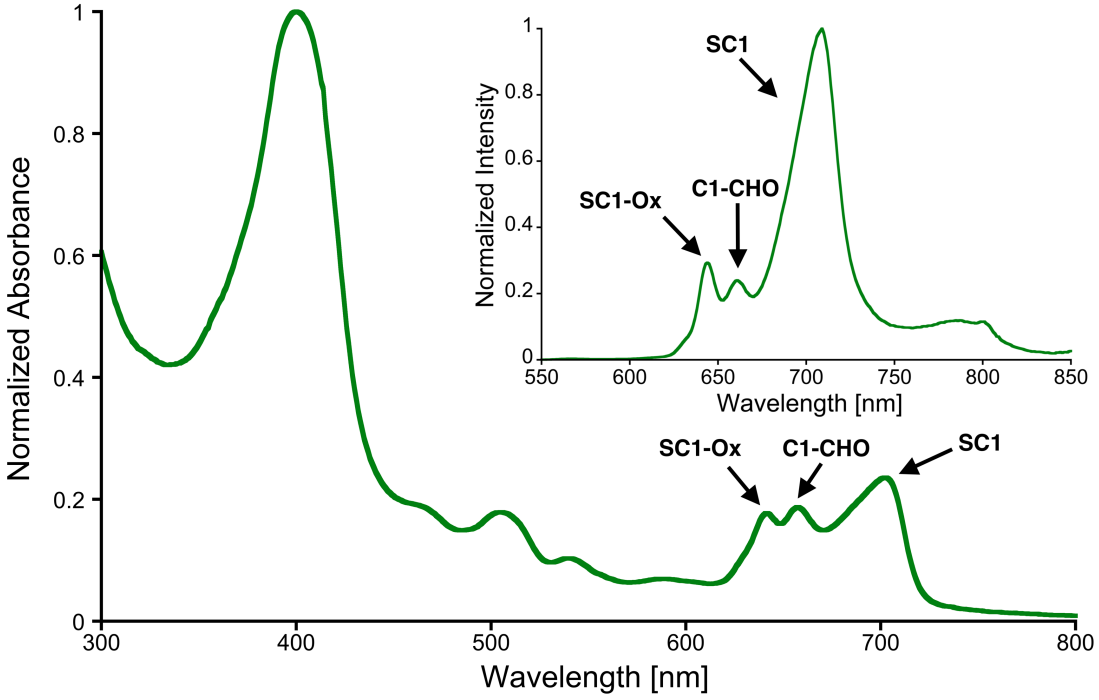

Figure 2.10: Normalized absorption and emission (inset) spectra of SC1 upon ambient light exposure in TX-100. Absorption acquired in neat TX-100 after 2-hour exposure, emission acquired upon excitation at *B* band in TX-100 (0.1% in PBS) after 5-hour light exposure. Samples were diluted from the stock to acquire spectra. Absorption spectrum acquired with sample concentration ~10 µM and emission spectrum acquired at ~1.0 µM.

systems[192,193] and also observed with select alkene bridged bisporphyrins.[180,194] Due to the inconsistent appearance of these higher energy signals, we did not attempt to elucidate anything further. We also observed that the reaction appears to occur exceptionally fast when in the solid state (as thin film deposited on microscope slide) and in viscous solvents (Triton X-100). While unclear without further investigation, it is possible that the rigidification of the dimer, and/or a lowered oxygen diffusion coefficient may play a role. In the case of the prior, rigidification may impart steric constraints on the dyad that enables $^1O_2$ to readily interact with the ethenyl linker, while for the latter, a slower rate of diffusion for $^1O_2$ would allow more time for interaction with dyad linker. Overall, the reactivity of the new dyads with $^1O_2$ has a complex relationship with the solvent (properties such as viscosity, O_2 concentration, and

possibly polarity) but the stability of dyads can be controlled by tuning their electronic properties.

Section 2.4: Conclusions

We prepared a short series of 13-13 ethenyl linked chlorin dimers through microwave assisted olefin metathesis, as well as styryl substituted chlorin monomers through either microwave assisted olefin metathesis or Heck reactions. For β substituted chlorin monomers and β linked dimers, the ethenyl linker results in a superior bathochromic shift of lowest energy Q_y or Q_y-like absorption band and the emission band, relative to the corresponding ethynyl linker. Thus, an ethenyl linker at the 13- (3 and 13- in the case of **C2-2S**) position affords greater electronic communication than an ethynyl one, in both the ground and excited states. This feature of the β substituted/linked chlorin monomers and dimers results from the ability of the central ethene to attain nearly co-planar geometry with the macrocycle(s).

In the case of 15- substituted chlorin monomers, nearly the opposite trend is observed, a phenylacetylene substituent provides greater bathochromic shift of Q_y band than a styryl substituent in the ground state, and the two auxochromes result in identical emission maxima. This, in addition to supporting evidence by DFT generated models, indicates that the higher steric interactions of the *meso* position prevent the styryl group from achieving co-planarity with the macrocycle, limiting electronic coupling. Combined, the observations for the β and *meso* linked compounds prepared here indicates the ethenyl linker can be useful for facilitating stronger electronic communication, provided that steric requirements are given careful consideration.

The fluorescence quantum yields for all ethenyl monomers were comparable to their ethynyl counterparts, and overall, Φ_F increased as the π-system increased. All mono- and di- styryl substituted monomers exhibited red to deep-red emission, comparable to or at longer wavelength than corresponding phenylethynyl monomers. For the *β* linked dimers, absorption and emission maxima were significantly red shifted to beyond 700 nm, and Φ_F increased roughly 1.5-fold compared to relevant parent monomer. These ≥ 0.45 Φ_F values are over two-fold larger than for hydroporphyrin monomers (bacteriochlorins and purpurinimides) that absorb in the same spectral region.[109,195] These results provide a blueprint for hydroporphyrin based arrays with significantly improved Φ_F for the deep red to near-infrared spectral windows.

In addition to the improved properties noted above, ethenyl linked dimers possess the interesting feature of self-cleavage upon exposure to light. We have demonstrated that the rate at which the dimers convert to aldehydes can be controlled through modulation of electronic properties, and we hypothesize that further tuning can make these compounds viable for real applications. For example, the self-cleavage is disfavored for *in vivo* imaging, because absorption maxima are blue shifted to the edge of the biological window (650-900 nm). By sufficiently slowing the dimer reaction with $^1O_2$, these dyes would be useful as bright NIR imaging agents. On the other hand, it is possible to take advantage of the dimers' rapid reactivity through use as a ratiometric probe for singlet oxygen detection. The large hypsochromic shift of both absorption and emission maxima that accompanies the formation of aldehyde allows easy distinction between the two signals.

Section 2.5: Experimental Procedures

Section 2.5.1: General Synthetic & Spectroscopic Procedures

All non-solvent chemicals were used as received from supplier. For Stille couplings, fresh THF was distilled from Na/benzophenone immediately prior to use. For olefin metathesis and palladium coupling reactions, commercially available anhydrous dichloroethane and toluene were used respectively. Tetrahydrodipyrrin **WH**,[115] dibromodipyrromethane **EH3-2Br**,[121] and the chlorins **C1-Br**,[161] **C1-P**,[33] and **C1-Br15**[175] were all synthesized following reported procedures. The syntheses of **C2-2Br** and **C2-2P**,[126] are discussed in Section 4.2.1, with procedures included in Section 4.5. All column chromatography was performed using silica gel (60Å pore size, 32-63 μm particle distance), purchased from either Scientific Adsorbents, Inc. or Silicycle.

General Procedure for Palladium Catalyzed Cross-Couplings (Conventional Heating)

For Sonogashira and Stille couplings, all solvents and reagents except catalyst and highly volatile liquids (such as trimethylsilylacetylene or phenylacetylene) were placed in a dried Schlenk flash then degassed by two cycles of freeze-pump-thaw. While under positive pressure of N_2, catalyst was added to the flask, and subjected to a third and final cycle of freeze-pump-thaw. If necessary, volatile liquids were added following third cycle of freeze-pump-thaw, with flask under positive pressure of N_2. Exterior of flask was then cleaned of any ice that formed during degassing and placed in an oil bath at the designated temperature.

General Procedure for Microwave Assisted Reactions

Microwave-assisted reactions were performed using a CEM Discover (CEM, Mathew, NC) microwave instrument. All reactions were performed in a 10 mL closed

tube with continuous monitoring of pressure and temperature. Temperature was monitored using a built-in IR sensor. Each microwave cycle involves three stages: (1) “run time”, approximately 1−4 min, in which the reaction mixture was irradiated at indicated power level (W) until it reaches the indicated temperature; (2) “hold time”, where the reaction mixture was maintained at set temperature for 30-45 min., as indicated, (3) “cooling time”, approximately 10 min, in which the reaction vessel was allowed to cool to 50 °C, before automated release from the instrument.

General Procedure for Microwave Assisted Heck Reaction

For Heck reactions, solid reagents (bromo chlorin, catalyst and ligand) are first flushed with nitrogen in a dried, capped microwave test tube, for 20 minutes. Simultaneously, all liquid chemicals (solvents, base and styrene) are degassed in a dried Schlenk flash by three cycles of freeze-pump-thaw and filled with N_2. Once thoroughly degassed, styrene solution was transferred to the test tube containing solid reagents, via N_2 purged syringe. The microwave tube was then subjected to three irradiation cycles with 30-45 minute hold time (total time irradiated of 90-135 mins.) at 250W and 110°C. While it is unclear why such an elaborate degassing technique is required, simply performing freeze-pump-thaw under typical procedure (as described for Sonogashira and Stille coupling) failed to yield product. Three irradiation cycles of 45 min. were performed because the instrument will not perform reactions longer than 45 mins, and in order to drive reaction to completion three microwave exposure cycles were necessary.

General Procedure for Microwave Assisted Olefin Metathesis

For olefin metathesis, vinyl chlorin **C1-V** or **C3-V**, was placed in microwave test tube with second-generation Grubbs' catalyst (IIG) and microscale stir-bar. The tube was capped then purged with N_2 for 15-20 mins before anhydrous 1,2-dichloroethane was added. Reaction mixture then subjected to a single microwave exposure with 30-minute hold time at 300 W and 83°C. Additional catalyst, and/or prolonged reaction times did not favor further product formation, based upon analysis from TLC and absorption spectroscopy.

Characterization of New Compounds

For all new compounds ^{1}H NMR and HRMS were collected, wherever possible ^{13}C NMR was also collected. ^{1}H NMR (400 or 500 MHz) and ^{13}C NMR (100 or 125 MHz) spectra were collected at room temperature in $CDCl_3$ unless noted otherwise. Chemical shifts (δ) were calibrated using solvent peaks (^{1}H signals, residual proton signal at 7.26 ppm for chloroform and 2.50 ppm for DMSO; ^{13}C signals, 77.16 ppm for $CDCl_3$ and 39.5 ppm for DMSO-d_6).[196] For 2D NOESY NMR experiments, sample mixing time was set to 0.8 s. HRMS was acquired through Fourier transform ion-cyclotron resonance (FT-ICR) or time-of-flight (TOF) analysis, where indicated. Sample ionization was most often achieved by electrospray ionization (ESI) and in the cases where that failed, matrix assisted laser desorption/ionization (MALDI) was successful.

Absorption and Emission Spectra

All absorption and emission spectra were acquired in air equilibrated HPLC grade solvents unless otherwise indicated. Absorption spectra acquired using Beckman-Coulter Spectrophotometer, emission spectra acquired on PTI QuantaMaster

8000 Fluorometer. When acquiring emission beyond 850 nm, PTI modular NIR detector was utilized. Published absorption spectra acquired at sample absorbance of ~1.0 for hydroporphyrin *B* band, emission spectra acquired at sample absorbance of ≤0.1 for hydroporphyrin *B* band.

Section 2.5.2: Synthesis of Novel Chlorin & Intermediate Chlorin Monomers

13-Bromo-10-pentafluorophenyl-18,18-dimethylchlorin (***C3-Br***)

Following the established chlorin synthesis procedure,[121,161] a mixture of **WH** (1.00 g, 2.01 mmol) and **EH3-2Br** (382.0 mg, 2.01 mmol) in CH_2Cl_2 (60 mL) was treated with a solution of *p*-toluenesulfonic acid monohydrate (1.91 g, 10.05 mmol) in MeOH (20 mL). After 30 mins. the reaction mixture was treated with 2,2,6,6-tetramethylpiperidine (10.0 mL, 60.0 mmol) and concentrated. The residue was suspended in CH_3CN (200 mL) and treated with additional 2,2,6,6-tetramethylpiperidine (10.0 mL, 60.0 mmol), $Zn(OAc)_2$ (5.50g, 30.1 mmol), and AgOTf (1.54 g, 6.00 mmol). The mixture was refluxed for 18 hours, while covered with aluminum foil and fume hood lights turned off. The crude reaction was then cooled to room temperature and concentrated. The residue was filtered through a short silica column using CH_2Cl_2, collecting all blue-green fractions. Note that these fractions are also red fluorescent, which is visible with the assistance of a UV-lamp. The filtrate was concentrated, leaving a dark blue-green (nearly black) residue. The residue was then dissolved in CH_2Cl_2 (20 mL), treated dropwise with TFA (1.90 mL, 25.0 mmol), and stirred for 1 hour. The reaction mixture was quenched with Na_2CO_3 (saturated, aq.), washed (water and brine), dried (Na_2SO_4), and concentrated. Column chromatography [silica, hexanes/CH_2Cl_2 (5:1)] afforded a **C3-Br** as a green powder (70.2 mg, 6%). Product is the major green colored, red fluorescent band, minor red fluorescent

impurity was apparent following product. ^{1}H NMR ($CDCl_3$, 500 MHz): δ −2.53 (bs, 1H), −2.15, (bs, 1H), 2.02 (s, 6H), 4.64 (s, 2H), 8.60 (d, J = 4.3 Hz, 1H), 8.86 (s, 1H), 8.96 (d, J = 4.5 Hz, 1H), 8.97 (s, 1H), 9.01 (d, J = 4.3 Hz, 1H), 9.28 (d, J = 4.5 Hz, 1H), 9.27 (s, 1H), 9.81 (s, 1H); ^{13}C{^{1}H}NMR ($CDCl_3$, 126 MHz): δ 31.3, 46.7, 52.4, 77.4, 94.8, 96.2, 96.4, 107.9, 114.4, 124.5, 126.5, 129.0, 130.5, 133.0, 134.2, 135.2, 136.4, 141.2, 151.8, 152.1, 164.2, 176.0; HRMS (ESI-FT-ICR) m/z Calcd for $[M]^+$ $C_{28}H_{18}BrF_5N_4$ 586.0613; Found 586.0620.

*10-Mesityl-18,18-dimethyl-13-trimethylsilylethynyl-13-vinylchlorin (**C1-V**)*

Following the reported procedure,[108] samples of **C1-Br** (60.0 mg, 0.112 mmol) and $(PPh_3)PdCl_2$ (11.7 mg, 0.0167 mg) and tributyl(vinyl) tin (65.5 μL, 0.224 mmol) were dissolved in THF (7 mL) in a Schlenk flask (degassed as described under general procedure for Stille reaction) and the reaction was stirred at reflux for 4 h. Column chromatography [silica, hexanes/CH_2Cl_2 (3:1)] provided **C1-V** as a dark green powder (47.3 mg, 87%). Product has smaller R_f compared to starting material. Gravity column chromatography results in decomposition of the product and significantly diminished yields. Decomposition is readily visible as extensive streaking on silica, it is possible that **C1-CHO** is forming in a fashion similar to that observed for ethenyl linked dimers, however, this new material was not removed from the column. ^{1}H NMR ($CDCl_3$, 400 MHz): δ −1.96 (bs, 1H), −1.84 (bs, 1H), 1.89 (s, 6H), 2.07 (s, 6H), St5 (s, 3H), 4.66 (s, 2H), 5.83 (d, J = 10.9 Hz, 1H), 6.39 (d, J = 17.6, 1H), 7.29 (s, 2H), 8.15 (dd, J_1 = 10.9 Hz, J_2 = 17.4 Hz, 1H), 8.46 (d, J = 4.3, 1H), 8.73 (s, 1H), 8.88 (s, 1H), 8.90 (d, J = 4.3, 1H), 8.92 (d, J = 4.6, 1H), 9.12 (s, 1H), 9.29 (d, J = 4.5, 1H), 9.77 (s, 1H); ^{13}C{^{1}H}NMR ($CDCl_3$, 100 MHz): δ 21.4, 21.5, 31.1, 46.3, 52.2, 93.4, 94.3, 106.9, 117.7, 119.8,

121.6, 123.2, 127.7, 128.0, 128.8, 131.2, 132.8, 133.3, 133.5, 134.4, 137.4, 137.5, 137.9, 139.2, 140.9, 151.4, 152.9, 162.7, 175.3; HRMS (ESI-FT-ICR) *m/z* Calcd for $[M+H]^+$ $C_{33}H_{33}N_4$ 485.2670; Found 485.2701.

*10-Mesityl-18,18-dimethyl-13-vinylchlorinato zinc(II) (**ZnC1-V**)*

A sample of **C1-V** (20.0 mg, 41.0 μmol) was dissolved in chloroform/MeOH (5:1, 3 mL), treated with anhydrous zinc acetate (15.1 mg, 82.0 μmol), and stirred at 40 °C in the dark for 30 min. The reaction was quenched with saturated $NaHCO_3$ (aq), extracted with CH_2Cl_2 washed (water and brine), dried (Na_2SO_4), and concentrated. Flash column chromatography [silica, hexanes/CH_2Cl_2 (2:1)] afforded **ZnC1-V** as a blue powder (17.7 mg, 78%). Product is easily distinguished from starting material on TLC as it is much more polar (smaller R_f) and appears as a bright blue at low concentration. Both product and starting material are red fluorescent under UV exposure. ^{1}H NMR ($CDCl_3$, 400 MHz): δ 1.86 (bs, 6H), 2.03 (bs, 6H), 2.61 (s, 3H), 4.53 (s, 2H), 5.70 (dd, J_1 = 1.5 Hz, J_2 = 10.9 Hz, 1H), 6.23 (dd, J_1 = 1.5 Hz, J_2 = 17.5 Hz, 1H), 7.23 (s, 2H), 7.99 (dd, J_1 =10.9Hz, J_2 =17.5Hz, 1H), 8.33 (d, J = 4.2Hz, 1H), 8.57−8.59 (m, 2H), 8.74 (d, J = 4.3 Hz, 1H), 8.79−8.81 (m, 2H), 9.05 (d, J = 4.3 Hz, 1H), 9.55 (s, 1H). Aromatic signal (s, 2H) from mesityl group is masked by chloroform at 7.26 ppm; ^{13}C{^{1}H}NMR ($CDCl_3$, 126 MHz): δ 21.43, 21.59, 31.05, 45.37, 50.76, 93.65, 94.55, 109.42, 116.97, 122.37, 126.59, 127.41, 127.77, 128.18, 128.81, 129.60, 133.04, 137.18, 137.34, 138.76, 139.01, 144.58, 146.29, 146.94, 147.56, 151.26, 154.35, 159.21, 171.21; HRMS (ESI-FT-ICR) *m/z* $[M+H]^+$ Calcd for $C_{33}H_{31}N_4Zn$ 546.1756; Found 546.1758.

*10-Pentafluorophenyl-18,18-dimethyl-13-vinylchlorin (**C3-V**)*

Following the reported procedure,[108] with degassing as described by general procedure for Stille reaction above, a mixture of **C3-Br** (35.0 mg, 59.8 μmol) and $(PPh_3)PdCl_2$ (6.3 mg, 8.97 μmol) in freshly distilled THF (4 mL) was treated with tributyl(vinyl)tin (35.0 μL, 120.0 μmol) and subjected to reflux. After 4 hours the reaction was incomplete based upon TLC; thus, additional batches of tributyl(vinyl)tin (35.0 μL, 120.0 μmol) and $(PPh_3)PdCl_2$ (6.3 mg, 8.97 μmol) were added. After a total reaction time of 6 h, the reaction mixture was concentrated. Flash column chromatography [silica, hexanes/CH_2Cl_2 (5:1)] afforded a green solid (22.6 mg, 71%). Similar to **C1-V**, flash column chromatography is necessary, and the product has smaller R_f than starting material. ^{1}H NMR ($CDCl_3$, 500 MHz): δ −2.33(bs, 1H), −2.14 (bs, 1H), 2.04 (s, 6H), 4.64 (s, 2H), 5.96 (dd, J_1 = 0.7 Hz, J_2 = 11.0 Hz, 1H), 6.51 (dd, J_1 = 0.8 Hz, J_2 = 17.4 Hz, 1H), 8.20 (dd, J_1 = 10.9 Hz, J_2 = 17.2 Hz, 1H), 8.59 (d, J = 4.2 Hz, 1H), 8.84 (s, 1H), 8.94−8.99 (m, 2H), 9.04 (d, J = 4.3 Hz, 1H), 9.20 (d, J = 4.6 Hz, 1H), 9.22 (s, 1H), 9.84 (s, 1H); ^{13}C{^{1}H}NMR ($CDCl_3$, 126 MHz): δ 31.3, 46.5, 52.6, 94.8, 95.9, 101.8, 107.8, 119.0, 120.7, 123.8, 128.5, 128.6, 130.2, 133.8, 134.0, 134.8, 134.9, 140.9, 151.8, 152.0, 163.9, 175.6; HRMS (ESI-FT-ICR) *m/z* Calcd for $[M+H]^+$ $C_{30}H_{22}F_5N_4$ 533.1759; Found 533.1768.

*10-Mesityl-18,18-dimethyl-15-vinylchlorin (**C1-V15**)*

Following the reported procedure,[108] with degassing as described by general procedure for Stille reaction above, a solution of **C1-Br15** (41.5 mg, 77.0 μmol) in freshly distilled THF (5 mL) was treated with tributyl(vinyl)tin (45.0 μL, 154.0 μmol) and $(PPh_3)PdCl_2$ (8.1 mg, 11.6 μmol) and refluxed. After 5 hours the reaction was incomplete based upon TLC; thus, the mixture was treated with additional

tributyl(vinyl)tin (45.0 μL, 154.0 μmol) and $(PPh_3)PdCl_2$ (8.1 mg, 11.6 μmol). After a total reaction time of 7 hours, the contents were concentrated down. Column chromatography [silica, hexanes/CH_2Cl_2 (2:1)] afforded a purple powder (22.6 mg, 60%). Product has smaller R_f than parent **C1-Br15**. ^{1}H NMR ($CDCl_3$, 400 MHz): δ −1.98 (s, 2H), 1.86 (s, 6H), 2.06 (s, 6H), 2.63 (s, 3H), 4.52 (s, 2H), 5.94 (dd, J_1 = 1.9 Hz, J_2 = 17.5 Hz, 1H), 6.26 (dd, J_1 = 1.9 Hz, J_2 = 11.0 Hz, 1H), 8.27 (dd, J_1 = 11.0 Hz, J_2 =17.3 Hz, 1H), 8.45 (d, J = 4.3 Hz, 1H), 8.62 (d, J = 4.9Hz, 1H), 8.88 (d, J = 4.3 Hz, 1H), 8.90 (s, 1H), 8.93 (d, J = 4.6 Hz, 1H), 9.06 (d, J = 4.8 Hz, 1H), 9.18 (d, J = 4.6 Hz, 1H), 9.74 (s, 1H). Note that the aromatic signal (s, 2H) from the 10-mesityl group is masked by chloroform at 7.26 ppm; $^{13}C\{^1H\}$NMR ($CDCl_3$, 126 MHz): δ 21.4, 21.6, 31.8, 46.1, 51.9, 94.7, 106.6, 109.2, 120.4, 123.3, 123.7, 123.8, 127.1, 127.7, 127.8, 131.6, 132.6, 134.4, 135.0, 137.6, 138.2, 138.6, 139.3, 139.5, 140.3, 151.9, 152.4, 162.0, 174.4; HRMS (ESI-FT-ICR) *m/z* Calcd for $[M+H]^+$ $C_{33}H_{33}N_4$ 485.2670; Found 485.2706.

*10-Mesityl-18,18- dimethyl-13-trimethylsilylethynylchlorin (**C1-ETMS**)*

Following the reported procedure,[108] as described by general procedure for Sonogashira reaction, a solution of **C1-Br** (70.0 mg, 0.13 mmol), P(o-tol)$_3$ (47.5 mg, 0.16 mmol), $Pd_2(dba)_3$ (36.0 mg, 0.039 mmol), and trimethylsilylacetylene (20 μL, 0.14 mmol) in toluene/Et_3N (60 mL, 5:1) was stirred at 60 °C in a Schlenk flask. The progress of the reaction was monitored by absorption spectroscopy by observing the disappearance of the Q_y band of the starting chlorin, **C1-Br**, as the product and starting material have similar R_f, and the presence of Et_3N makes distinguishing the two difficult. After 2 hours, further trimethylsilylacetylene (20 μL, 0.14 mmol), $Pd_2(dba)_3$

(36.0 mg, 0.039 mmol), and P(o-tol)$_3$ (47.5 mg, 0.16 mmol) were added, and the stirring was continued at 60 °C overnight. After 18 hours of total reaction time, the reaction mixture was concentrated under reduced pressure and purified by column chromatography [hexanes/CH_2Cl_2 (2:1)] to afford a dark green solid (49.0 mg, 68%). Product has smaller R_f than the starting chlorin. ^{1}H NMR (400 MHz, $CDCl_3$): δ −1.97 (bs, 1H), −1.69 (bs, 1H), 0.49 (s, 9H), 1.83 (s, 6H), 2.06 (s, 6H), 2.60 (s, 3H), 4.67 (s, 2H), 7.23 (s, 2H), 8.44 (d, J = 4.3 Hz, 1H), 8.69 (s, 1H), 8.83 (s, 1H), 8.85 (d, J = 4.3 Hz, 1H), 8.91 (d, J = 4.6 Hz, 1H), 9.18 (d, J = 4.7 Hz, 1H), 9.19 (s, 1H), 9.72 (s, 1H); ^{13}C{^{1}H}NMR (100 MHz, $CDCl_3$): δ 0.43, 21.5, 21.6, 31.2, 46.7, 52.0, 94.6, 95.1, 100.1, 101.9, 106.87, 106.90, 116.9, 121.0, 124.0, 127.9, 128.8, 129.2, 131.7, 132.8, 133.0, 135.2, 137.6, 137.8, 139.2, 140.1, 141.7, 152.1, 152.7, 163.3, 176.2; HRMS (ESI-FT-ICR) *m/z* $[M+H]^+$ Calcd for $C_{36}H_{39}N_4Si$, 555.2939; Found 555.2946.

*13-Ethynyl-10-mesityl-18,18-dimethylchlorin (**C1-EH**)*

A solution of **C1-ETMS** (48.0 mg, 0.087 mmol) in THF/MeOH (20 mL, 1:1) was treated with K_2CO_3 (17.0 mg, 0.12 mmol) and stirred at room temperature for 30 min. The reaction mixture was diluted with CH_2Cl_2, washed (water then brine), dried (Na_2SO_4), and concentrated. Column chromatography [silica, hexanes/CH_2Cl_2 (2:1)] afforded the deprotected chlorin **C1-EH** as a dark green solid (36.0 mg, 86%). Product has very slightly smaller R_f than starting material, it will not be visible if TLC spots are too concentrated. ^{1}H NMR (400 MHz, $CDCl_3$): δ −1.97 (bs, 1H), −1.62 (bs, 1H), 1.85 (s, 6H), 1.99 (s, 6H), 2.58 (s, 3H), 3.83 (s, 1H), 4.58 (s, 2H), 7.17 (s, 2H), 8.45 (d, J = 4.1 Hz, 1H), 8.79 (s, 1H), 8.81 (d, J = 4.1 Hz, 1H), 8.84 (d, J = 4.6 Hz, 1H), 9.09 (d, J = 4.6 Hz, 1H), 9.22 (s, 1H), 9.66 (s, 1H); ^{13}C{^{1}H}NMR (100 MHz, $CDCl_3$): δ 21.5,

31.2, 46.7, 51.9, 79.1, 84.2, 94.6, 95.0, 106.9, 115.6, 121.2, 124.2, 127.9, 128.9, 129.5, 131.8, 132.7, 133.0, 135.3, 137.5, 137.9, 139.2, 140.0, 141.8, 152.3, 152.8, 163.2, 176.3; HRMS (ESI-FT-ICR) *m/z* $[M+H]^+$ Calcd for $C_{33}H_{31}N_4$, 483.2543; Found 483.2532.

Section 2.5.3: Synthesis of Styryl and Phenylethynyl Chlorin Monomers

*10-Mesityl-18,18-dimethyl-13-styrylchlorin (**C1-S**)*

Synthesis via Olefin Metathesis. Following the general procedure, a mixture of **C1-V** (20.0 mg, 41.0 μmol), styrene (24.0 μL, 206.0 μmol), and IIG (8.7 mg, 10.3 μmol) in 1,2-dichloroethane (2 mL) was reacted under microwave irradiation for a total of four 30 min cycles. Between the first and the second exposures little progress (monitored via TLC based upon consumption of **C1-V**) was observed; thus, another portion of styrene (24.0 μL, 206.0 μmol) was added for the third exposure. Again, little progress was observed, and for the fourth and final exposure, an additional batch of IIG (8.7 mg, 10.3 μmol) was placed in the reaction vessel. No further progress was observed from this fourth exposure; at this time the reaction was concentrated. Column chromatography [silica, hexanes/CH_2Cl_2 (4:1)] yielded a **C1-S** as a green powder (8.9 mg, 39%). Product has lower R_f than parent **C1-V**. ^{1}H NMR ($CDCl_3$, 400 MHz): δ −1.91 (bs, 1H), −1.76 (bs, 1H), 1.91 (s, 6H), 2.08 (s, 6H), 2.66 (s, 3H), 4.69 (s, 2H), 7.31 (s, 2H), 7.38 (t, J = 7.3 Hz, 1H), 7.49−7.54 (m, 2H), 7.76 (d, J = 16.1 Hz, 1H), 7.86 (d, J = 7.5 Hz, 2H), 8.44 (d, J = 4.2 Hz, 1H), 8.55 (d, J = 16.1 Hz, 1H), 8.80 (s, 1H), 8.87 (s, 1H), 8.89 (d, J = 4.3 Hz, 1H), 8.92 (d, J = 4.5 Hz, 1H), 9.19 (d, J = 4.5 Hz, 1H), 9.20 (s, 1H), 9.75 (s, 1H); ^{13}C{^{1}H}NMR ($CDCl_3$, 126 MHz): δ 21.55, 21.64, 31.3, 46.5, 52.5, 93.4, 94.5, 107.1, 119.9, 120.4, 120.9, 123.4, 126.9, 127.9, 128.1, 128.2, 129.0, 131.4, 132.3, 133.1, 133.3, 134.0, 134.7, 137.7, 137.9, 138.0, 138.2, 139.4,

141.1, 151.7, 153.2, 163.0, 175.5; HRMS (ESI-FT-ICR) *m/z* Calcd for $[M+H]^+$ $C_{39}H_{37}N_4$, 561.3013; Found 561.3022.

Synthesis via Heck Reaction. Following the general procedure, a mixture of **C1-V** (30.0 mg, 55.8 μmol), $Pd(OAc)_2$ (3.8 mg, 16.7 μmol), PPh_3 (73.2 mg, 279.0 μmol), styrene (320 μL, 2.79 mmol), and Et_3N (78.0 μL, 558.0 μmol) in toluene/DMF (6 mL, 1:1) was subjected to three 45 minute microwave irradiation cycles. After third cycle, upon TLC analysis, the reaction showed nearly complete conversion to product with minor impurity determined to be des-brominated starting material. Reaction mixture was concentrated and flash column chromatography [silica, hexanes/CH_2Cl_2 (3:1)] yielded **C1-S** as a green powder (4.0 mg, 13%). Analysis matched that reported for olefin metathesis procedure above.

*10-(4-Methoxycarbonylphenyl)-18,18-dimethyl-3,13-distyrylchlorin (**C2-2S**)*

Following the general procedure for Heck reaction, a mixture of **C2-2Br** (20.4 mg, 0.032 mmol), PPh_3 (44.5 mg, 0.158 mmol), and $Pd(OAc)_2$ (1.6 mg, (0.0071 mmol), styrene (365 μL, 3.16 mmol) and Et_3N (50 μL, 0.34 mmol) in DMF/toluene (5 mL, 1:1) was subjected to three 45 minute microwave exposure cycles. The resulting solution was diluted with CH_2Cl_2, washed (water and brine), dried (Na_2SO_4), and concentrated. Column chromatography [silica, hexanes/CH_2Cl_2 (1:2)] afforded a dark brown powder (11.3 mg, 52%). Product has significantly smaller R_f than starting material and is easily distinguished by change of color from green to brown. ^1H NMR ($CDCl_3$, 400 MHz): δ −1.86 (bs, 1H), −1.58 (bs, 1H), 2.07 (s, 6H), 4.12 (s, 3H), 4.66 (s, 2H), 7.36−7.45 (m, 2H), 7.49− 7.58 (m, 4H), 7.73 (d, J = 16.2 Hz, 1H), 7.83 (d, J = 7.4 Hz, 2H), 7.93 (d, J = 7.4 Hz, 2H), 8.00 (d, J = 16.2 Hz ,1H), 8.24 (d, J = 8.1 Hz, 2H), 8.46 (d, J = 8.1 Hz,

2H), 8.51 (d, J = 15.6 Hz, 1H), 8.52 (d, J = 4.3 Hz, 1H), 8.68 (d, J = 16.1 Hz, 1H), 8.82 (s, 1H), 8.86 (s, 1H), 8.97 (d, J = 4.4 Hz, 1H), 9.09 (s, 1H), 9.17 (s, 1H), 9.97 (s, 1H); $^{13}C\{^{1}H\}$NMR (100 MHz) δ 14.2, 21.5, 22.9, 29.8, 31.4, 32.0, 46.4, 77.1, 93.8, 94.9, 104.1, 117.2, 120.0, 121.7, 125.4, 126.8, 127.1, 128.2, 129.1, 131.9, 132.6, 133.0, 134.2, 146.8, 152.8, 163.8, 175.9; HRMS (ESI-FT-ICR) *m/z* Calcd for $[M+H]^+$ $C_{46}H_{39}N_4O_2$, 679.3068; Found 679.3067.

*10-Mesityl-18,18-dimethyl-15-styrylchlorin (**C1-S15**)*

Following the general procedure for Heck reaction, a mixture of **C1-Br15** (20.0 mg, 0.037 mmol), $Pd(OAc)_2$ (1.7 mg, 7.4 μmol), and PPh_3 (48.8 mg, 0.186 mmol), styrene (213 μL, 1.85 mmol) and Et_3N (52 μL, 0.37 mmol) was dissolved in toluene/DMF (4 mL, 1:1) and subjected to three 30 minute microwave irradiation cycles, at which time TLC indicated that all starting material was consumed. Column chromatography [silica, hexanes/CH_2Cl_2 (3:1)] yielded the desired product as a purple film (4.8 mg, 23%) with the major fraction consisting of des-brominated starting material (10.5 mg, 61%). Residual starting material elutes first, followed by des-bromo chlorin and finally by product (purple-green band in solution). ^{1}H NMR ($CDCl_3$, 500 MHz): δ −1.85 (bs, 2H), 1.87 (bs, 6H), 2.06 (s, 6H), 2.62 (s, 3H), 4.59 (s, 2H), 7.24 (d, J = 16.1 Hz, 1H), 7.43 (t, J = 7.5 Hz, 1H), 7.53−7.57 (m, 2H), 7.86 (d, J = 7.3 Hz), 8.44 (d, J = 4.3Hz, 1H), 8.61 (d, J = 4.8Hz, 1H), 8.69 (d, J = 16.0 Hz, 1H), 8.87 (d, J = 4.3 Hz, 1H), 8.90 (s, 1H), 8.92 (d J = 4.5 Hz, 1H), 9.08 (d, J = 4.8 Hz, 1H), 9.17 (d, J = 4.5 Hz, 1H), 9.73 (s, 1H). Aromatic signal (s, 2H) from 10-mesityl group is masked by chloroform at 7.26 ppm; $^{13}C\{^{1}H\}$NMR ($CDCl_3$, 126 MHz): δ 21.4, 21.6, 31.8, 46.0, 52.0, 77.2, 94.9, 106.7, 108.6, 120.6, 123.3, 126.8, 127.1, 127.7, 127.8, 128.0, 129.1,

130.1, 131.6, 132.7, 134.4, 135.1, 137.6, 138.3, 138.6, 139.2, 139.3, 139.6, 140.3, 152.0, 152.4, 162.6, 174.3; HRMS (ESI-FT-ICR) *m/z* Calcd for $[M]^+$ $C_{39}H_{36}N_4$, 560.2934; Found 560.2940.

*10-Mesityl-18,18-dimethyl-15-phenylethynylchlorin (**C1-P15**)*

Following the general procedure for Sonogashira reaction, a solution of **C1-Br15** (30.0 mg, 55.8 μmol), phenylacetylene (12.3 μL, 112.0 μmol), and $(PPh_3)_2PdCl_2$ (7.8 mg, 11.0 μmol) in DMF/Et_3N (6 mL, 2:1) was stirred at 80 °C for 20 hours, at which time reaction mixture was concentrated. Gravity column chromatography [silica, hexanes/CH_2Cl_2 (4:1) → (3:1)] yielded **C1-P15** as a purple powder (17.7 mg, 57%). Product has a smaller R_f than parent **C1-Br15**. ^{1}H NMR ($CDCl_3$, 500 MHz): δ −1.53 (bs, 1H), −1.35 (bs, 1H), 1.87 (s, 6H), 2.08 (s, 6H), 2.62 (s, 3H), 4.81 (s, 2H), 7.26 (s, 2H), 7.44−7.48 (m, 1H), 7.51−7.56 (m, 2H), 7.90−7.95 (m, 2H), 8.39 (d, J = 4.2 Hz, 1H), 8.61 (d, J = 4.7 Hz, 1H), 8.81−8.83 (m, 2H), 8.86 (d, J = 4.5 Hz, 1H), 9.13 (d, J = 4.5 Hz, 1H), 9.26 (d, J = 4.7 Hz, 1H), 9.68 (s, 1H); ^{13}C{^{1}H}NMR ($CDCl_3$, 126 MHz): δ 21.4, 21.6, 31.7, 46.0, 52.8, 92.1, 92.9, 95.2, 95.4, 108.0, 122.1, 123.0, 123.7, 124.6, 127.5, 127.9, 128.2, 128.5, 128.8, 131.6, 131.6, 132.9, 134.5, 135.0, 137.8, 138.0, 139.2, 141.3, 152.0, 152.7, 166.8, 175.9; HRMS (ESI-FT-ICR) *m/z* Calcd for $[M+H]^+$ $C_{39}H_{35}N_4$ 559.2856; Found 559.2863.

Section 2.5.3: Synthesis of Ethenyl and Ethynyl Chlorin Dimers

All operations performed with ethenyl-linked dyads (synthesis, purification, drying, handling, and storage) were done in darkness; otherwise 13-formylchlorin **C1-CHO** is formed, which can only be removed by column chromatography. Precautions include, turning off all light sources, closing all window blinds to prevent sunlight (*or* performing operations after nightfall), and covering all vessels containing sample in

aluminum foil. For experimenter to see in this dark environment, Energizer brand LED headlamp with red light capabilities was used– this was particularly helpful during column chromatography to locate bands, but sample exposure even to this low light was always kept to a minimum. Pure samples of dyads were stored in nitrogen-flushed vials, covered with aluminum foil, and stored in the freezer. When protected properly, samples are stable for several weeks without appearance of **C1-CHO**.

SC1

Following the general procedure for Olefin Metathesis, samples of **C1-V** (20.0 mg, 0.0412 mmol), IIG (8.0 mg, 0.0103 mmol) were dissolved in 1,2-dichloroethane (2 mL) and subjected to a microwave irradiation cycle. The resulting brown crude reaction mixture was concentrated, and column chromatography [silica, hexanes/CH_2Cl_2 (2:1)] afforded a brown powder (8.9 mg, 46%). Two bands were observed during column chromatography; the first consisted of both unreacted starting material and **C1-S** [based upon LRMS (MALDI-TOF) and absorption spectra], while the second band contained the desired product. Due to the nature of IIG containing a benzylidene ligand, **C1-S** is an unavoidable byproduct. ^{1}H NMR ($CDCl_3$, 400 MHz): δ −1.80 (bs, 2H), −1.59 (bs, 2H), 2.01 (s, 12H), 2.12 (s, 12H), 2.74 (s, 6H), 4.80 (s, 4H), 7.40 (s, 4H), 8.46 (d, J = 4.3 Hz, 2H), 8.90 (s, 2H), 8.91 (d, J = 4.3 Hz, 2H), 8.94 (d, J = 4.5 Hz, 2H), 9.15 (s, 2H), 9.17 (s, 2H), 9.21 (d, J = 4.5 Hz, 2H), 9.48 (s, 2H), 9.77 (s, 2H); ^{13}C{^{1}H}NMR ($CDCl_3$, 100 MHz): δ 21.5, 21.6, 31.2, 46.4, 52.4, 93.6, 94.4, 106.9, 119.8, 120.8, 123.3, 123.7, 127.9, 128.1, 131.30, 132.9, 133.6, 134.00, 134.6, 137.6, 138.1, 138.2, 139.4, 141.0, 151.7, 153.1, 163.1, 175.6; HRMS (ESI-FT-ICR) *m/z* Calcd for $[M+H]^+$ $C_{64}H_{61}N_8$, 941.5013; Found 941.4979.

2ZnC-V

A sample of **SC1** (6.2 mg, 6.6 μmol) was dissolved in chloroform/MeOH (5:1, 6 mL), treated with zinc acetate dihydrate (72.2 mg, 329.0 μmol), and allowed to stir at room temperature in the dark for 4 hours. The reaction was quenched with saturated $NaHCO_3$ (aq.), extracted with CH_2Cl_2, washed (water and brine), dried (Na_2SO_4), and concentrated. Flash column chromatography [silica, hexanes/CH_2Cl_2 (2:1)] afforded a green film (2.4 mg, 34%). Product can be easily identified based upon color change (brown to green) and smaller R_f. ^{1}H NMR ($CDCl_3$, 400 MHz): 2.00 (bs, 12H), 2.08 (bs, 12H), 2.71 (s, 6H), 4.67 (s, 4H), 7.36 (s, 4H), 8.35 (d, J = 4.2 Hz, 2H), 8.61 (s, 2H), 8.77 (d, J = 4.3 Hz), 8.82 (d, J = 4.2 Hz, 2H), 8.88 (s, 2H), 9.01 (s, 2H), 9.08 (d, J = 4.3 Hz, 2H), 9.15 (s, 2H), 9.57 (s, 2H); HRMS (MALDI-TOF) m/z Calcd for $[M]^+$ $C_{64}H_{56}N_8Zn$, 1064.3205; Found 1064.3204. The ^{13}C spectrum was not acquired due to the poor solubility and stability of the compound.

SC2

Following the general procedure for Olefin Metathesis, samples of **C3-V** (22.3 mg, 42.0 μmol) and IIG (9.3 mg, 110.0 μmol) in 1,2-dichloroethane (2 mL) subjected to one microwave exposure cycle. Upon removal from the microwave instrument the reaction mixture appeared brown. Flash column chromatography [silica, hexanes/CH_2Cl_2 (3:1)] yielded a brown powder that was washed with MeOH and then with hexanes (HPLC grade) for a final yield of 7.8 mg (36%). Product can be identified by smaller R_f and color change from green to brown, similar to with the synthesis of **SC1**, the first band to elute from column contained residual starting material and what was presumed to be a styryl substituted chlorin derivative (based upon absorption

spectra). ^{1}H NMR ($CDCl_3$, 500 MHz): δ −2.12 (bs, 2H), −1.87 (bs, 2H), 1.53 (s, 6H), 2.14 (s, 12H), 4.85 (s, 4H), 8.61 (d, J = 4.2 Hz, 2H), 9.01−9.05 (m, 4H), 9.08 (d, J = 4.3 Hz, 2H), 9.25−9.31 (m, 6H), 9.62 (s, 2H), 9.90 (s, 2H); ^{19}F NMR ($CDCl_3$, 376 MHz): δ −161.93 (s, 4F), −153.05 (s, 2F), −136.45 (s, 4F); ^{13}C{^{1}H}NMR ($CDCl_3$, 126 MHz): δ 31.4, 46.7, 52.8, 95.0, 96.1, 102.0, 107.8, 120.0, 124.2, 124.3, 124.4, 128.8, 130.5, 134.1, 134.2, 138.3, 141.2, 145.9, 152.2, 152.3, 164.2, 176.1; HRMS (ESI-FT-ICR) *m/z* Calcd for $[M]^+$ $C_{58}H_{38}F_{10}N_8$, 1036.3054; Found 1036.3059.

SC3

Following the reported procedure,[35] with degassing as described by general procedure for Sonogashira coupling, a solution of **Ch-E** (10 mg, 0.021 mmol), **C1-Br** (12 mg, 0.023 mmol), $P(o\text{-}tol)_3$ (7.7 mg, 0.025 mmol) and $Pd_2(dba)_3$ (6.0 mg, 6.6 μmol) were dissolved in toluene/Et_3N (9.6 mL, 5:1) and stirred at 60 °C. After 1 hour, the reaction was determined to be complete based on disappearance of the Q_y absorption band of **C1-Br**. The reaction mixture was concentrated and purified by column chromatography [silica, hexanes/CH_2Cl_2 (2:1 → 1:1)]. The first band (green) was tentatively identified as the homo-coupled, butadiynyl linked chlorin dimer (2 mg, 10%).[35] The second band (green) was the target cross-coupled dyad **SC3**, isolated as a brownish-green solid (10 mg, 53%). ^{1}H NMR (400 MHz, $CDCl_3$): δ −1.82 (bs, 2H), −1.45 (bs, 2H), 1.96 (s, 12H), 2.13 (s, 12H), 2.66 (s, 6H), 4.82 (s, 4H), 7.32 (s, 4H), 8.51 (d, J = 4.6 Hz, 2H), 8.96−8.89 (m, 4H), 8.95 (d, J = 4.6 Hz, 2H), 9.02 (s, 2H), 9.21 (d, J = 4.6 Hz, 2H), 9.67 (s, 2H), 9.76 (s, 2H); ^{13}C{^{1}H}NMR (100 MHz, $CDCl_3$): δ 21.55, 21.64, 31.3, 46.8, 52.1, 94.6, 95.4, 107.0, 117.3, 120.9, 124.1, 128.0, 128.7, 131.7, 133.0, 133.4, 135.3, 137.6, 137.9, 139.4, 140.0, 141.8, 152.2, 152.9, 163.5,

176.3; HRMS (ESI-FT-ICR) *m/z* Calcd for $[M+H]^+$ $C_{64}H_{59}N_8$, 939.4857; Found 939.4872.

Section 2.5.4: Determination of Fluorescence Quantum Yields Φ_F

We determine the fluorescence quantum yield of all compounds by comparison to standard using the following equation:

$$\Phi_{\mathrm{F,compound}} = \left(\frac{\mathrm{N_{cmpd}}}{\mathrm{N_{std}}}\right) \mathrm{x} \left(\Phi_{\mathrm{F,std}}\right) \mathrm{x} \left(\frac{\eta_{\mathrm{cmpd\ solvent}}}{\eta_{\mathrm{std\ solvent}}}\right)^2$$

Where N is the normalized emission intensity for compound of interest (cmpd) or standard (std), and η is the solvent refractive index corresponding solution of compound of interest or standard. N is calculated from the integrated emission (I) that using the equation: $\mathrm{N} = \left(\frac{\mathrm{I}}{1-10^{-A}}\right)$. Integrated emission is determined from the full emission spectra (including the luminescent tail of hydroporphyrins) that are acquired on PTI-QuantaMaster Spectrofluorometer with FelixGX operating software/suite. Note that sample absorbance is set to ~0.1 at the maximum of the excitation wavelength, for all initial trials/emission spectra acquisition, then diluted for a second trial. We then measure all compounds of interest (as well as TPP) in the same fashion, in all solvents of interest. It is critical that all compounds of interest are measured in the same session, because parameters will vary between sessions. The most commonly used values for solvents we utilize are toluene (η = 1.496) and DMF (η = 1.430).

When determining Φ_F by method of integration the primary sources of error that we encounter are instrumental error, systematic error and measurement error. The instrumental error can be apparent on both the Beckman-Coulter UV-vis and the PTI spectrofluorometer but can be properly accounted for. Both instruments require sufficient time for the respective lamps to "warm-up" and reach a constant light output.

The UV-vis requires approximately 2 hours to warm up while the spectrofluorometer is stable after 30 minutes. For the UV-vis, if any significant deviation from 0 (greater than ± 5 x 10^{-4}) is seen across the blanked spectral window (typically 300-900 nm), the lamp requires more time until light output is constant. To assess the spectrofluorometer, measure the emission spectrum of given sample, then measure again after ~15 minutes, there should be no difference of intensity between the two emission spectra (spectra should superimpose). Another form of instrumental error found in the spectrofluorometer, assuming the lamp is already stable, is due to the spectral response of the detector. The PTI spectrofluorometer comes standard with a photomultiplier tube (PMT) detector, which will have a variable response depending upon the frequency of the incident light. Thus, the initially acquired emission spectrum is incorrect and requires correction. In our case, the spectral response is calibrated by the PTI technicians, and saved as the correction file "emcorr" for the visible detector and "NIRemcorr" for the NIR detector. To determine the accuracy of the correction factors, we measure Φ_F of a standard reported elsewhere against tetraphenyl porphyrin ($\Phi_{F,TPP}$ = 0.070).[197] During each experiment, the correction factors can be more quickly assessed by comparing the relative intensity of the two emission bands of the TPP standard. The two TPP bands (0-0 and 0-1), have a relative intensity of 3:2 at their respective maxima. In an uncorrected spectrum the intensity of the 0-1 band appears less than its true value, increasing the ratio in favor of the 0-0 band.

There are two places for significant measurement error when determining Φ_F. The first is in acquiring the true sample absorbance. When working with hydroporphyrins, solubility of the chromophores can become problematic. To

determine if the sample concentration is accurate, one should measure the absorption spectrum, then wait ~10 minutes and measure again. If intensity changes between the two measurements, it may require filtration (through 20 μm filter). The second measurement error comes from fitting the wavelength range when determining the integrated emission. Hydroporphyrin emission spectra feature a weak luminescent tail that should be factored into the overall integration; however, the detector has significant noise beyond 830 nm, and integration must be truncated at that point. We have determined that, on average, truncation of the entire luminescent tail (for those hydroporphyrins whose emission returns to zero below 830 nm) diminishes the total integration by less than two percent.

Because these errors are collectively small, we have found that the simplest method for assessing error is the margin of error at 95% confidence interval (CI). For a single Φ_F determination, the emission spectrum should be measured four or more times. At a minimum, it should be measured as part of two separate experiments, such that the second measurement in a given experiment can come from a diluted sample. After having determined many Φ_F, we have found that, on average, four measurements should result in a maximum margin of error of ± 5% at the 95% CI. There are some examples where the margin of error for Φ_F is much smaller such as the case of **ET3** (Chapter 4) which came to only ± 0.54% at 95% CI. This is atypical, however, and the margin of error tends to fall closer to the 4-5% range. We have chosen this threshold because we generally care about the trends with Φ_F as opposed to absolute value, and comparisons made with ± 5% margin of error should not influence the conclusions we

can draw from the trends. In the event that ± 5% margin of error at 95% CI is exceeded, the sample purity is reassessed and Φ_F measurements are repeated.

Finally, between different laboratories utilizing TPP as a standard there is significant systematic error. Over the last 50+ years, there are conflicting reports to the true value of $\Phi_{F,TPP}$ ranging anywhere between 0.04 and 0.13. The most commonly utilized value is $\Phi_{F,TPP} = 0.11$ in deoxygenated benzene (determined by Gouterman).[198] However, to be consistent with our collaborators and other current porphyrin chemists we utilize $\Phi_{F,TPP} = 0.070$ in non-deoxygenated toluene.[197]

Section 2.5.5: Determination of Fluorescence Lifetimes τ_F

Fluorescence lifetimes were determined by time-correlated single photon counting (TCSPC) using PTI-QuantaMaster 400 Spectrofluorometer (FelixGX operating software/suite) with PTI's PicoMaster TCSPC addon (375 nm femtosecond pulsed laser diode). The instrument response factor (IRF) was determined before each set of measurements, using the light scattered by colloidal silica (LUDOX) solution in de-ionized water. For compounds of interest, the concentration was set to ~1.0 μM (A ~ 0.1) and each lifetime trace was acquired such that ~10,000 photon counting events were accumulated at the peak channel. Lifetime traces were acquired in triplicate, then non-linear regression was performed using the FelixGX software suite using the "Powerfit 1-4 exponential" operation. To assess the fit, we consider χ^2 (chi-squared), Durbin-Watson parameter and visual interpretation of the residuals plot. The χ^2 value should fall close to 1 (below 1.2 is acceptable) implying a single decay component. If the sample appears to have multiple components (>1.2), then there is most likely a second hydroporphyrin species emitting at the wavelength of detection, and sample must be purified further. The Durbin-Watson parameter assesses the autocorrelation of

the data, and the ideal value is 2 (acceptable range is within 2 ± 0.25). Values significantly above or below 2 indicate that a trend is present in the residuals and there is most likely an additional component to fit, again suggesting sample is not pure. Similarly, the residuals plot can be inspected to assess the randomness of data. The residuals plot shows the difference between the measured value relative to the fitted mean, over time. It should appear as data points alternating randomly above and below 0. For each acquired dataset, the regression line was found with several different ranges of channels selected, and considered only when the χ^2, and Durbin-Watson parameter values fell within acceptable range. From there several other truncated or exaggerated ranges were also used to generate τ_F, and collectively the margin of error was found to be ± 0.03 ns, well below 1% on a 95% CI. This was similar for all tested compounds where margin of error with respect to fitting was below 1%.

Section 2.5.6: DFT-Calculations (Spartan Model)

All DFT calculations were performed using Spartan '10 Software (Wavefunction, Inc.) using the B3LYP functional with the 6-31G* basis set (B3LYP/6-31G*). Prior to submitting calculations, the proposed structures have strain energy minimized via "Minimizer" function, and the fixed dihedral angles are subsequently input and locked. Dihedral angles are defined by the program using four points that are not identical to, but closely match the planes defined by four pyrrolic N atoms (mean macrocycle plane) and the linker atoms as well as the C at which they attach to macrocycle(s) and/or auxiliary aromatic ring (mean linker plane).

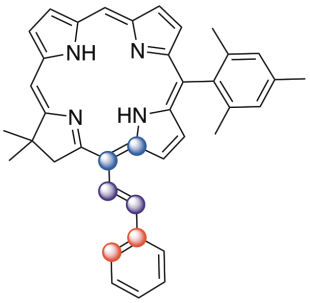

Description	Angle 1	Angle 2	E_{rel} (kJ/mol)	Energy Difference (kJ/mol)
Dihedral Angle 1 fixed	-180.00	12.04	-4533829.99	16.77
	-150.00	18.57	-4533837.96	8.80
	-120.00	13.53	-4533838.32	8.44
	-90.00	2.32	-4533836.50	10.26
	-60.00	11.42	-4533844.07	2.69
	-30.00	15.50	-4533844.75	2.01
	0.00	14.44	-4533829.26	17.50
	30.00	15.47	-4533844.74	2.02
	60.00	15.89	-4533846.68	0.08
	90.00	2.19	-4533836.54	10.22
	120.00	12.86	-4533838.39	8.37
	150.00	17.02	-4533837.78	8.98
	180.00	12.04	-4533829.99	16.77
Max. E	0.00	0.00	-4533828.71	18.05
Min. E	43.80	15.51	-4533846.76	0.0

Table 2.5: Summary of DFT Calculated Energies for C1-S15. Angle 1 defined by C14, C15, and ethene linker carbons, shown in blue. Angle 2 defined by first and second benzene carbons (where second C is that twisted closest to planarity with C15) and ethene linker carbons, shown in red. Purple spheres indicate linker carbon atoms, utilized in defining both angles. For all entries but min and max, dihedral angle 1 (red) is fixed, while angle 2 is free. For max, both angles are constrained to 0°, for min both angles are free.

Section 2.5.7: Reactivity of Dimers with Singlet Oxygen

General Procedure for Dyad Light Exposure Experiments

The relative reactivity of dyads **SC1**, **SC2** and **ZnSC1** was probed against ambient light exposure. First, a dyad solution was prepared in darkness such that absorbance (A) at dimer B band λ_{max} was in the range of 0.1-2.0. Once in desired range, the most recent absorption spectrum (where A was in the range of 0.1-2.0) was treated as the starting point, and the sample was transferred to a test tube. The test tube was then capped with rubber septum and sealed with parafilm to prevent solvent loss. Next, the test tube was placed inside a test tube rack with exposed sides. The test tube rack was then transferred to a fume hood and exposed to the fume hood's fluorescent lighting. The sample was exposed to the ambient lighting at all times, except when acquiring absorption measurements. Absorption spectrum was acquired periodically (hourly for first 6 hours, then daily for one week) until the Q_y-like band of the dyad was no longer present. This process was then repeated for each dyad.

Singlet Oxygen Production/Quenching of 1,3-diphenylisobenzofuran (DPBF)

Solutions containing both DPBF and dyad for the data shown in Figures 2.8 and 2.11 were prepared directly in quartz cuvette by combining 1.5 mL of DPBF solution (toluene, A ≈ 2.2) and 1.5 mL of dyad solution (toluene, A ≈ 1.0) and mixing using micro stirbar and stirring function of PTI spectrofluorometer. Samples were irradiated by PTI spectrofluorometer at the maximum of dyad Q_y*-like* band for two minutes, while the solution was stirring at maximum setting. After two minutes, the cuvette was immediately transferred to spectrophotometer to obtain absorption spectrum, once obtained the cuvette was again irradiated. The cycle of irradiation and absorption data

acquisition was repeated for a total of twenty minutes exposure time. Note that once solutions of DPBF or dyad were prepared they were covered in foil to prevent ambient light exposure. Due to the challenge of reaching initial dyad sample absorbance of 1.0 without change of the absorption spectrum shape (light exposure of measuring absorption spectrum results in small change of sample after several measurements), dyad **ZnSC1** was omitted from this experiment. Dyads **SC1** and **SC2** did not change during sample preparation, nor during the course of the experiment.

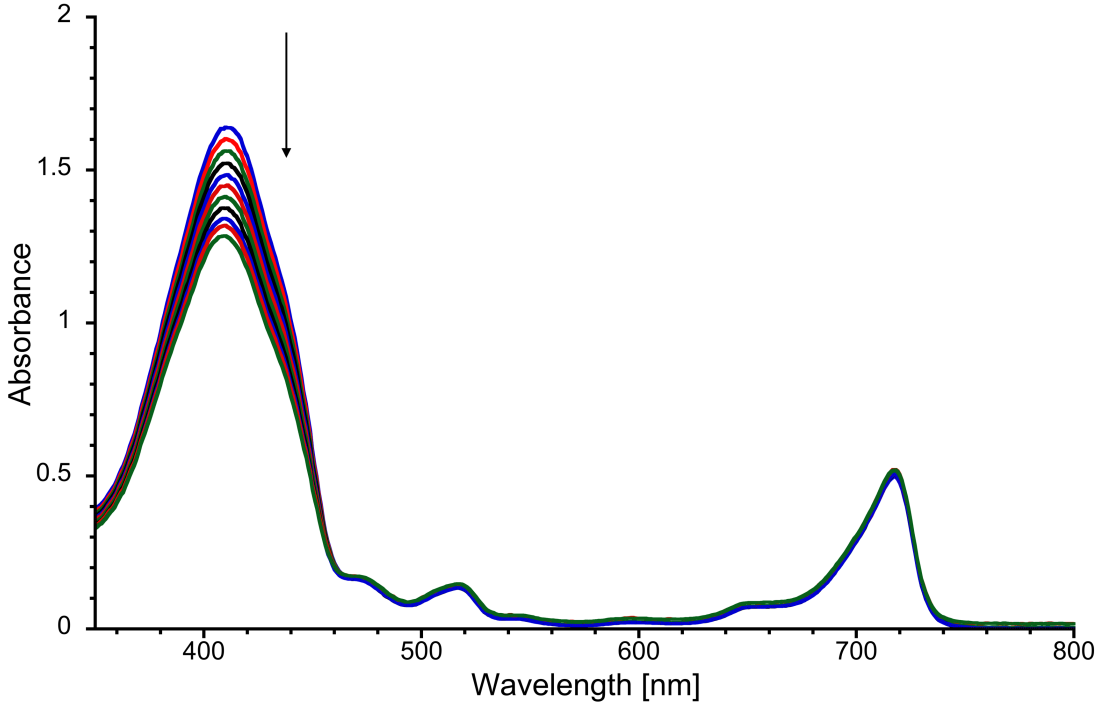

Figure 2.13: Absorption spectra of DPBF mixture with dyad SC2, in toluene, over time. Absorption spectra acquired immediately following two-minute cycles of irradiation at dyad *Q_y-like* band, for total of 10 exposures.

Section 2.6: Supplemental Data

Section 2.6.1: 2D NOESY Summary of Chemical Shifts for Select Dyads

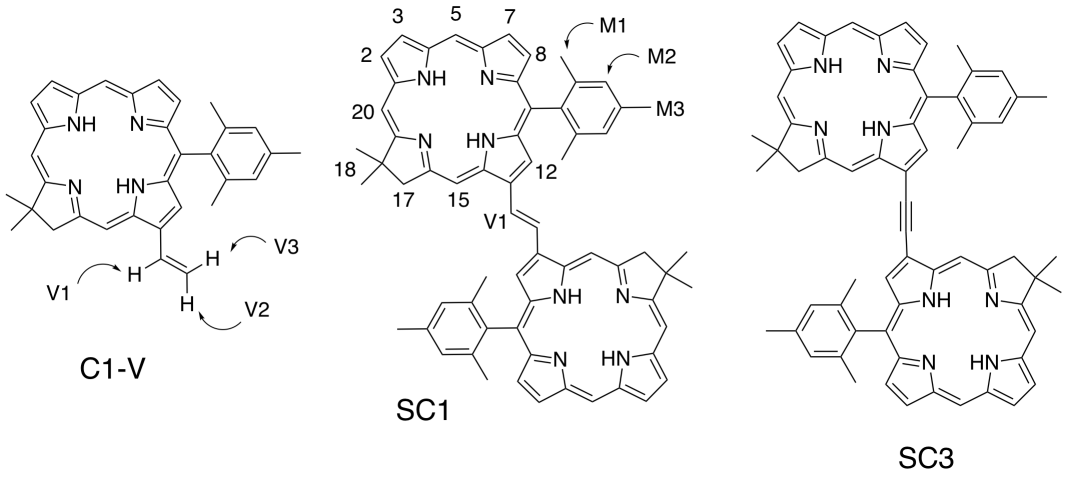

Position	C1-V	SC1	SC3
2	8.92 (d, 1H)	8.93 (d, 2H)	8.96 (d, 2H)
3	9.20 (d, 1H)	9.20 (d, 2H)	9.22 (d, 2H)
5	9.77 (s, 1H)	9.77 (s, 2H)	9.77 (s, 2H)
7	8.90 (d, 1H)	8.92 (d, 2H)	8.92-8.89 (m, 2H)†
8	8.46 (d, 1H)	8.46 (d, 2H)	8.52 (d, 2H)
M1	1.89 (s, 6H)	2.01(s, 12H)	1.96 (s, 12H)
M2	7.26 (s, 2H)	7.40 (s, 4H)	7.33 (s, 4H)
M3	2.65 (s, 3H)	2.74 (s, 6H)	2.66 (s, 6H)
12	***8.73 (s, 1H)***	***9.17 (s, 2H)***	***9.03 (s, 2H)***
V1	***8.16 (dd, 1H)***	***9.14 (d, 2H)***	
V2	6.39 (d, 1H)		
V3	5.84 (d, 1H)		
15	***9.10 (s, 1H)***	***9.48 (s, 2H)***	***9.68 (s, 2H)***
17	4.66 (s, 2H)	4.80 (s, 4H)	4.83 (s, 4H)
18	2.07 (s, 2H)	2.12 (s, 4H)	2.13 (s, 4H)
20	8.88 (s, 1H)	8.90 (s, 1H)	8.92-8.89 (m, 2H)†

Table 2.6: Summary of chemical shift (δ ppm) for C1-V, SC1 and SC3 as determined by 2D NOESY. Data in each cell displayed as follows: chemical shift (multiplicity, integration). Coupling constants can be found in Section 2.5.2 for C1-EH and Section 2.5.3 for dimers. Signals which show considerable shift upon dimerization indicated in bold italics, chlorin sites lacking proton and internal N-H resonances are not indicated. †) signals mixed within multiplet of total integration 4H, displayed at predicted values. Where cells are blank, no proton at designated site.

Section 2.6.2: Temperature Dependent 1H NMR of Dyad SC1

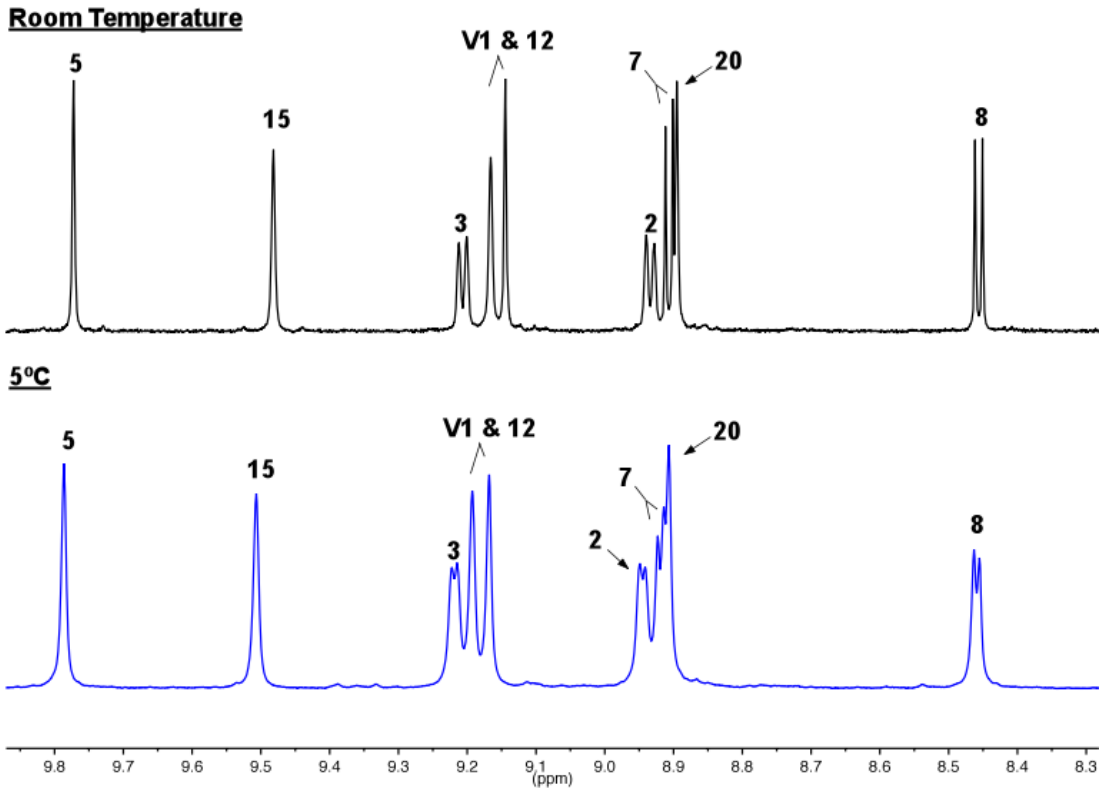

Figure 2.12: Temperature dependent ^{1}H NMR (400 MHz) spectra of dyad SC1 in chloroform-*d*. Top spectrum (black) acquired at room temperature, bottom spectrum (blue) acquired at 5°C, only aromatic region is shown. Numbers correspond to H atom at designated chlorin site, see table 2.6 for numbering system.

Chapter 3: Enediyne Hydroporphyrin Dimers for Arrays with Strong Electronic Coupling

Section 3.1: Introduction

Solar light harvesting is a key topic as scientists attempt to address the increasing global need for energy. Nature provides an excellent guideline through plants and bacteria that are reliant upon photosynthesis to meet their energy demands. The first steps of photosynthesis involve light absorption and charge separation,[68] both of which are made possible through the use of strongly coupled hydroporphyrins. The systems found in nature differ significantly from those presented in Chapter 2, because they achieve new properties through excitonic coupling as opposed to exclusively through bond interactions. Excitonic coupling is currently understood to occur in two ways, either long-range or short-range coupling. Long-range excitonic coupling is described by Kasha[199] as an electrostatic (Coulombic) interaction between the transition dipole moments (μ) of two chromophores.[200] Short-range excitonic coupling is the consequence of direct π-orbital overlap between chromophores, due to their close proximity.[200] Short-range excitonic coupling in particular, appears to play a large role in natural light-harvesting arrays, such as chlorosomes,[68,201,202] and the more universal photosynthetic reaction centers which are found in both plant life[68,69] and light-harvesting bacteria.[70–73]

Photosynthetic reaction centers feature two closely positioned chlorophylls or bacteriochlorophylls, known as the special pair, with additional peripheral chlorophylls or bacteriochlorophylls to facilitate the subsequent electron transfer.[68] Like the strongly conjugated arrays featured in Chapter 2, special pairs feature extensively red-shifted Q_y absorption maxima, but it is due to the excitonic coupling of the closely held

chromophores. Depending upon the derivatives used, and their relative orientations, different Q_y absorption maxima are achieved. For example, P867 (special pair found in *Rhodobacter sphaeroides*) features excitonically coupled bacteriochlorophyll *a* molecules to shift Q_y band from ~800 nm to 867 nm.[203] Closely related P960 (of *Rhodopseudomonas viridis*), utilizes bacteriochlorophyll *b* to achieve an even greater red shift from ~830 nm to 960 nm.[71] The strength of excitonic coupling V (measured as half of the energy difference between the split Q_y-like bands) is ~550 cm^{-1} for P867,[73] and ~900 cm^{-1} for P960.[71] The larger the value of V, the stronger the coupling, which leads to greater bathochromic shifting of absorption maxima and changes to excited state energies. These interconnected properties, through subtle changes to mutual orientation of chlorophylls and bacteriochlorophylls, have been optimized by plants and bacteria to allow for efficient photosynthesis.

Numerous groups have prepared a variety of porphyrin based systems trying to reproduce the properties achieved by the photosynthetic arrays, these approaches include: directly linked,[204,205] cofacial[206–208] (and slipped-cofacial),[209] ethynyl and butadiynyl[41] linked arrays. However, these examples are not the most accurate models for naturally occurring photosynthetic arrays due to their lack of hydroporphyrins. Not only do hydroporphyrins possess more intensive and longer wavelength Q_y bands compared to porphyrins,[118,119,210] but they are also easier to oxidize ($E_{1/2}^{0/+}$ bacteriochlorin < chlorin < porphyrin) and more difficult to reduce ($E_{1/2}^{-/0}$ bacteriochlorin < chlorin < porphyrin).[211] Because of this, others have attempted to prepare constructs with strong excitonic coupling utilizing semi-synthetic hydroporphyrins. There are limited examples of directly linked hydroporphyrin

arrays[212,213] and numerous examples of covalently and non-covalently linked co-facial arrays.[55,56,214–230] Covalently linked arrays can be further categorized as having a flexible or rigid linker. The number of rigidly linked arrays are more limited (Smith's *cis* ethenyl linked chlorin dimer,[56] and Montforts' 4,5-diethynylbiphenylene spaced dimer)[229] but are of interest to us because of our familiarity with strongly coupled hydroporphyrin arrays.

Recently, our lab has published several papers on strongly conjugated hydroporphyrin arrays featuring ethynyl or vinyl linkers[35,124] (Chapter 2) and *meso-meso* directly linked dyads,[147,231] that possess properties reminiscent of the photosynthetic reaction center. One linker motif that was yet to be explored in hydroporphyrins, was the series of alternating carbon-carbon triple, double and triple bonds provided by 3-hexen-1,5-diyne. Such a linker is interesting for several reasons. First, where the central alkene is *trans*, excellent through-bond electronic communication should be achieved.[232,233] A *trans* enediyne may provide superior bathochromic shift compared to previous arrays due to introduction of addition delocalized electrons or may reach the limit where increased distance between arrays leads to less extensive electronic communication. Here, we sought to determine the limitations of the through bond coupling in our dimeric arrays. Second, where the central alkene is *cis*, the dimer's constituent macrocycles should be forced into close proximity, facilitating interaction of π-orbitals and excitonic coupling. Finally, the enediyne motif itself has interesting photophysical properties that could lead to a unique hydroporphyrin dimer. Hexa-3-en-1,5-diyne linked chromophores have been explored by Diederich[234–238] (included a porphyrin dimer)[239] as well as others.[232,233]

Depending upon the components properties may include increased two-photon absorption cross section, increased emission intensity, significant solvatochromism, multiple emission bands or the ability to undergo photoinduced *trans-cis* isomerization.[232–238] Photoisomerization is well established for conjugated enediyne containing systems, and it has been utilized for photochromism or altering redox properties of a molecule.[192,193,232,240–242] Thus, photoisomerization would provide a facile route to studying both the *cis* and *trans* forms of a hydroporphyrin dimer, which are anticipated to have very different properties due to varying degrees of excitonic coupling.

In this chapter we report the synthesis and photophysical properties of a series of symmetrical hydroporphyrin dimers that are linked through the 13- position, by a 3,4-dimethoxycarbonyl-hexa-3-en-1,5-diyne linker. From 13-bromo-10-mesityl chlorin we prepared both the *cis* and *trans* forms of enediyne dimer (***cis*-SC4** and ***trans*-SC4**), as well as the *cis* zinc (II) complex ***cis*-ZnSC4**. 3,4-dimethoxycarbonyl-hexa-3-en-1,5-diyne was the linker of choice, as opposed to the simpler 3-hexen-1,5-diyne, because such substituted enediynes are established as photochromic switches.[192,193,240] In addition, we predicted that the linker could be readily prepared from dimethyl dibromofumarate,[243,244] enabling synthesis of dimers directly from bromo-chlorins (Scheme 3.1, Section 3.2). We also synthesized dyad **SC5**, featuring a 1,2-diethynylbenzene linker, as a more easily studied reference incapable of photoinduced isomerization. To relate dimer properties against a comparable monomer, we utilized

13-phenylethynyl chlorin **C1-P** (synthesis found in Chapter 2). The structures of target dimers, and the benchmark monomer can be found in Chart 3.1.

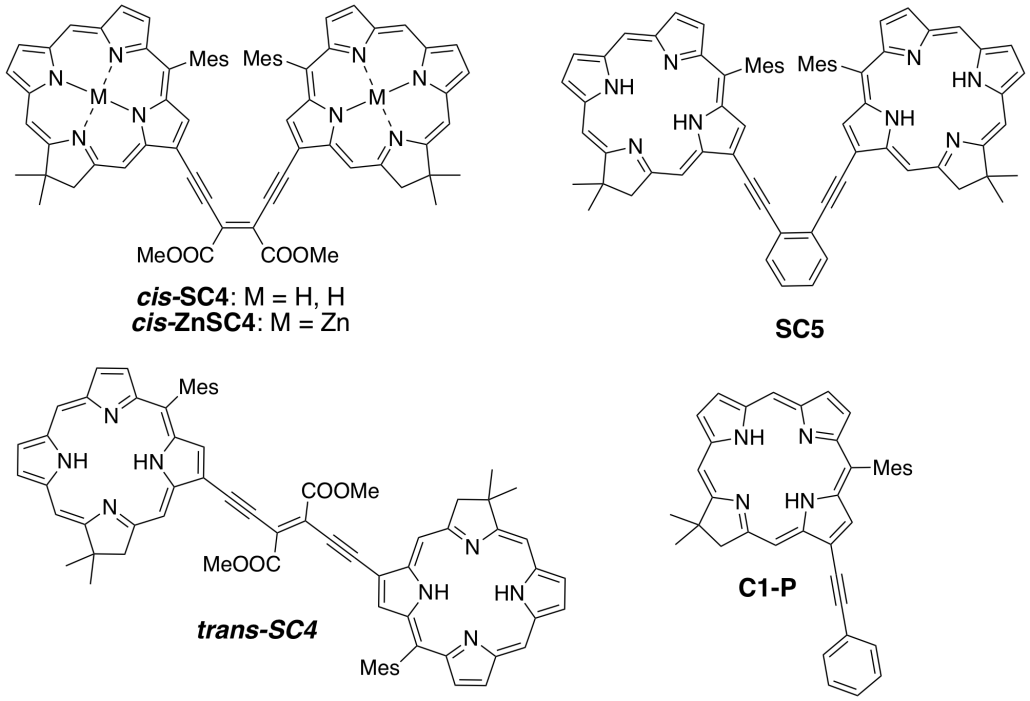

Chart 3.1: Enediyne linked chlorin dyads, *o*-diethynylphenylene linked dyad and benchmark monomer discussed in this chapter.

Section 3.2: Synthesis of Enediyne Linked Dimers

Due to the nature of our 3,13-dibromochlorin starting materials, the preferred reaction for installing a 3,4-dimethoxycarbonyl-hexa-3-en-1,5-diyne was the Sonogashira cross coupling. We could approach this from one of two ways, by either 1) preparing the completed linker then coupling it to two chlorins or 2) installing ethynyl substituents on chlorin with subsequent coupling to dimethyl dibromofumarate. As part of his work on a related project, Dr. Zhanqian Yu attempted the synthesis of the completed linker, however, it underwent rapid decomposition prior to purification of the final product. This behavior agreed with other reports of enediynes decomposing

at low/room temperature,[245] so I opted instead to couple ethynyl substituted chlorin **C1-EH** to the (Scheme 2.7).

The altered route again proceeded through Sonogashira coupling, now using dimethyl dibromofumarate **5** along with **C1-EH** catalyzed by $Pd_2(dba)_3$, in toluene/Et_3N at 60ºC (Scheme 3.2). Ethynyl chlorin **C1-EH** was fully consumed after two hours, and column chromatography yielded both ***cis*-SC4** (28%) and ***trans*-SC4** (~5%), along with the homo-coupled, butadiynyl linked dimer **2C1-b** (~30%, with unidentified impurities present). We suspected that the high yield of *cis* dimer was due to ambient light exposure promoting *trans-cis* isomerization of product and repeated the reaction in total darkness. With proper protection from light at all stages (synthesis, purification, characterization), we obtained ***trans*-SC4** (21%) as the primary enediyne with trace ***cis*-SC4** and a large amount of byproduct **2C1-b** (based on TLC only) that was not

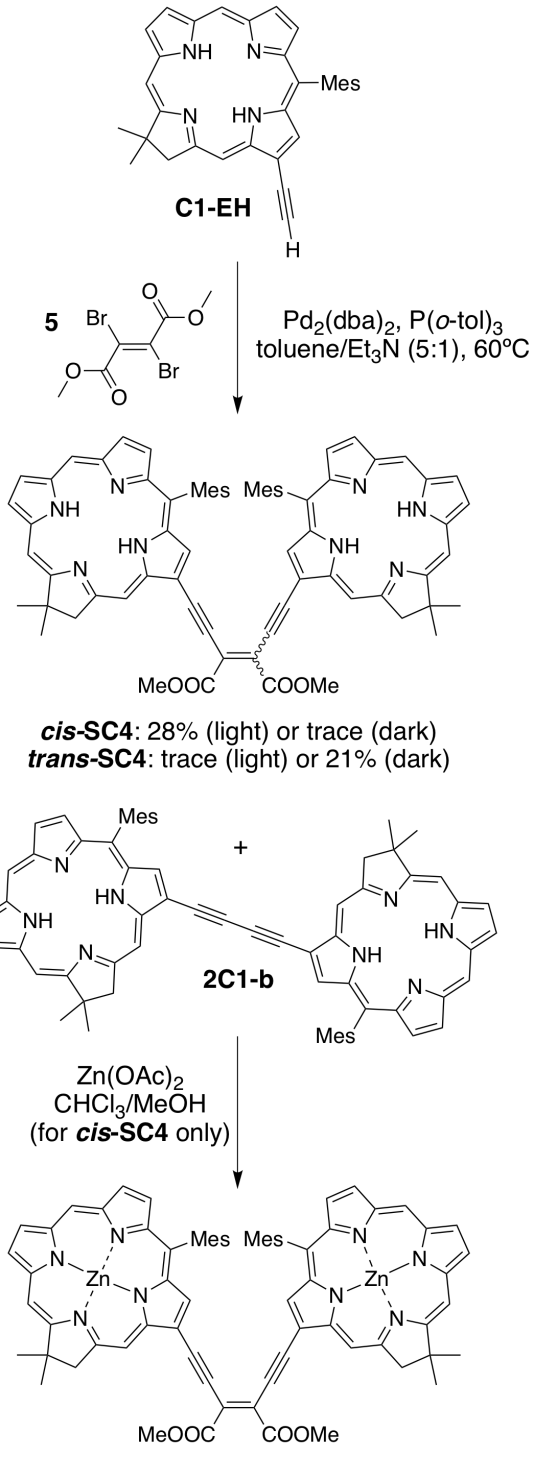

Scheme 3.2: Synthesis of enediyne linked chlorin dyads, *cis*/*trans*-SC4 and *cis*-ZnSC4.

purified. The bis-zinc(II) complex ***cis*-ZnSC4** was prepared in 67% yield by treating ***cis*-SC4** with zinc (II) acetate in chloroform/methanol solution (Scheme 3.2).

The analogous Sonogashira reaction between **C1-EH** and 1,2-dibromobenzene **8** yielded *o*-phenylene linked dyad **SC5** in 38% yield (Scheme 3.3). There is no need for light protection in the case of **SC5**, and again a large quantity of **2C1-b** was observed.

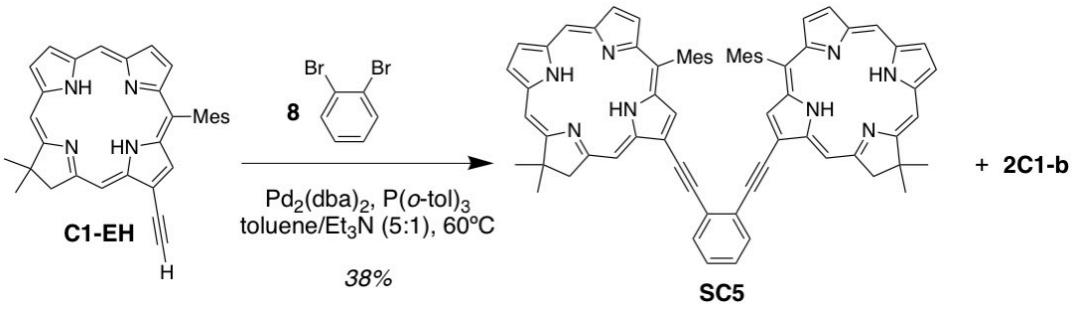

Scheme 3.3: Synthesis of *o*-diethynylphenylene linked chlorin dyad, SC5.

Section 3.3: Characterization of Enediyne Linked Dimers

Section 3.3.1: Structure Determination

The structures of all new compounds were determined by careful analysis of NMR spectra. We utilized 2D NOESY NMR to first assign all ^{1}H resonances of dimers ***cis*-SC4, *trans*-SC4, SC5** and monomer **C1-EH**. The aliphatic portions of the ^{1}H NMR spectra for compounds ***cis*-SC4, *trans*-SC4, SC5** and **C1-EH** are shown in Figure 3.1, a complete summary of chemical shift assignments can be found in Section 3.6.1, Table 3.3.All resonances of ***trans*-SC4** closely match those of **C1-EH** (except the non-equivalent L1 "linker" protons, Figure 3.1), providing strong evidence in lieu of a coupling constant that this was indeed the trans isomer. For ***cis*-SC4** we anticipated the observation of significant anisotropic shielding effects. In other words, in the *cis* orientation, the proximity of the first macrocycle would shield protons of the second

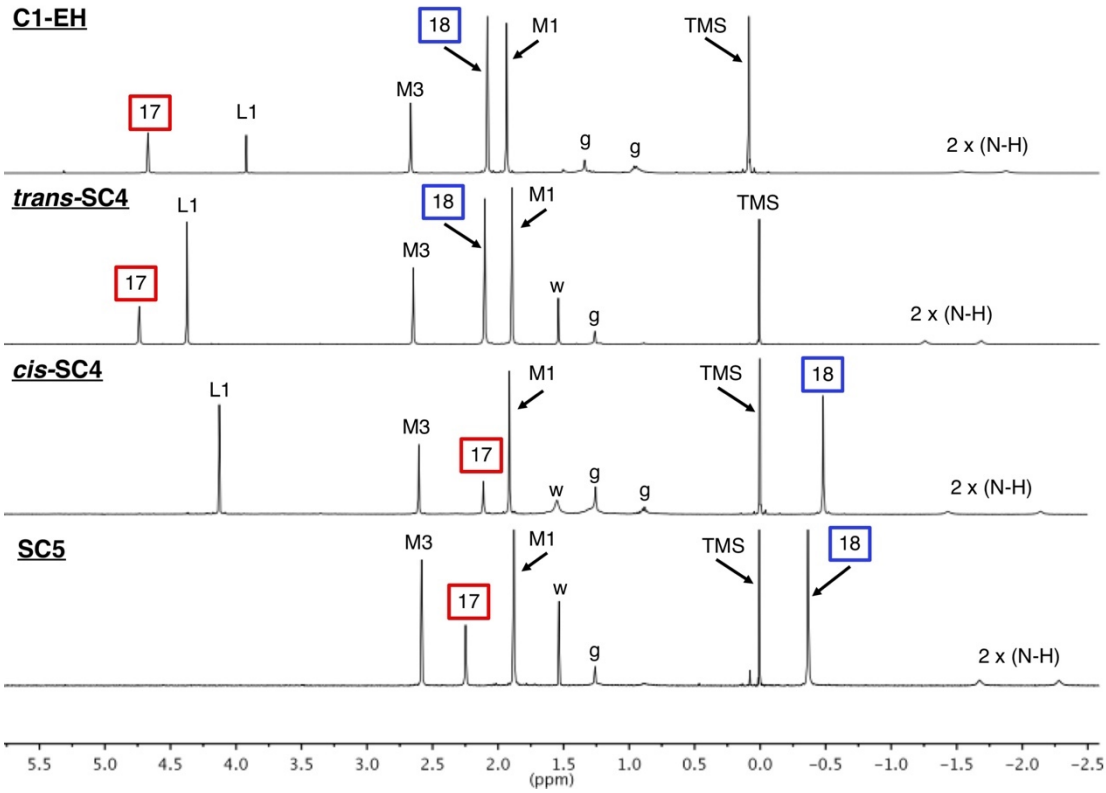

Figure 3.1: Aliphatic region of ^{1}H NMR (chloroform-*d*) for *cis/trans*-SC4, SC5 and reference monomer C1-EH. Chlorin 17-methylene protons highlighted by red box, chlorin 18-geminal dimethyl protons highlighted by blue box. L1 corresponds to methoxy protons of linker for SC4 dimers and terminal acetylene for C1-EH, M1 corresponds to 1,5-dimethyl protons of chlorin mesityl substituent, M3 corresponds to 3-methyl protons of chlorin 10 mesityl substituent. All non-chlorin signals are attributable to residual water (w), grease (g) or reference tetramethylsilane

and vice versa. Furthermore, we hypothesized that *o*-diethynylphenylene linked **SC5** would have similar spatial arrangement to ***cis*-SC4** and should exhibit similar chemical shifts without possibility for isomerization. Indeed, dyads ***cis*-SC4** and **SC5** have very similar ^{1}H NMR spectra relative to one another, and a few key resonances that differ from **C1-EH**. First, the methylene protons at chlorin 17-position show a 2.53 ppm shielding in ***cis*-SC4** and 2.39 ppm shielding in **SC5** relative to **C1-EH** ($\delta = 4.64$ ppm). Next, the 18-position geminal methyl groups of ***cis*-SC4** and **SC5** are shielded by 2.56 ppm and 2.45 ppm, respectively, in comparison to $\delta = 2.06$ ppm for **C1-EH**. The large change to chemical shift in this 18-position resonance is immediately obvious from

standard ^{1}H NMR, because the signal appears below 0 ppm. Finally, a less significant shielding is observed for the aromatic proton at the chlorin 20-position, it is shielded by 1.17 ppm for ***cis*-SC4** and 1.07 ppm for **SC5**, relative to $\delta = 8.84$ ppm for **C1-EH**. Thus, with the strong anisotropic shielding of ***cis*-SC4** relative to **C1-EH**, and strong similarity to **SC5**, we were confident in our assignments of *cis* and *trans* to the isomers of dyad SC4.

Satisfied with confirmation of the *cis* linker orientation, we wanted to probe further to determine how the macrocycles were arranged relative to one another, either in parallel, or anti-parallel. We generated models for ***cis*-SC4, *cis*-ZnSC4** and **SC5** through DFT energy-minimized structures, all of which showed that the lowest energy for the *cis* linker was achieved when the macrocycles adopted an anti-parallel slipped cofacial conformation. In other words, for *cis* and *o*-phenylene linked chlorin dimers the 10-meso positions are oriented away from one another (Figure 3.2 shows ***cis*-SC4**, for remaining dyads see Section 3.6.2, Figure 3.9). Furthermore, the average center-to-center distance between freebase hydroporphyrins was 7.20Å and

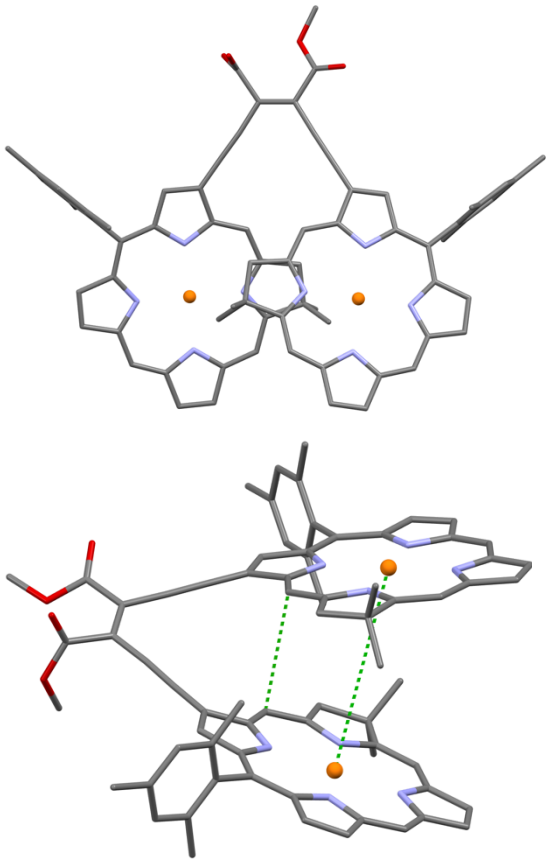

Figure 3.2: DFT energy-minimized structure of *cis*-SC4. Calculations performed using Spartan, processed image generated from Mercury. Orange spheres are centroids defined by macrocycle N atoms, H atoms omitted for clarity.

the average edge-to-edge distance (carbon to carbon distance between 15 positions) was 3.62Å (measurements demonstrated by dashed line in Figure 3.2, bottom; see Section 3.6.2, Table 3.4 for individual data). These short distances agree with the strong shielding at the hydroporphyrin 17, 18 and 20 positions. The slipped cofacial geometry is excellently supported by the chemical shifts of all relevant dimers, as the models show the chlorin 17-methylene 18-geminal dimethyl and 20-hydrogen positions within the shielding cone of the neighboring macrocycle. Furthermore, the lack of anisotropic effects (δ ppm nearly identical to monomer, Figure 3.1) on chlorin 10-mesityl substituent supports the anti-planar mutual orientation.

Based upon the slipped-cofacial mutual orientation, we anticipated the dimers to show axial chirality, and exist as a pair of atropisomers. Such a feature should manifest on ^{1}H NMR by the appearance of additional resonances,[246] for both the "inner" and "outer" 17-methylene and 18-methyl. We did not observe additional resonances, indicating that the atropisomers of our *cis* dimers are capable of rapid interconversion. Utilizing DFT calculated energy-minimized structures, we began from the lowest energy model and carefully rotated one macrocycle about the C13-ethynyl bond while keeping the other macrocycle constant, to generate a series of higher energy structures. We used the increase in energy to predict the barrier of rotation and found that while a full rotation of one macrocycle over the other is energetically unfavorable, a simultaneous partial rotation of both macrocycles appears quite facile. Similarly, there should be nearly free rotation of each macrocycle about the ethynyl linker in the direction its neighbor is not occupying. We performed low temperature (-10ºC) ^{1}H

NMR with **SC5** to slow the interconversion, but the acquired spectrum matched data for room temperature, further demonstrating how facile the conformational change is.

Section 3.3.2: Photophysical Characterization

The absorption and emission spectra of all new compounds were acquired in toluene (and DMF for select compounds), and it should be assumed that all data discussed in this chapter was acquired in air equilibrated toluene, unless stated otherwise. The absorption spectra of ***cis*-SC4**, ***cis*-*Zn*SC4**, ***trans*-SC4**, and **SC5** are shown in Figure 3.3, corresponding emission spectra in Figure 3.4. Stokes' shift and full width at half maximum (FWHM) were determined manually from absorption and emission spectra. In order to determine the value for coupling strength (*V)*, the two appropriate λ_{max} must be identified. To do so, peak fitting was performed using MagicPlot software, where integrals of two overlapping Gaussian curves are made to match the observed Q_y absorption features. Note that MagicPlot allows first provides a crude fit automatically, that can then be optimized by the user shifting both the maximum wavelength and maximum intensity of the individual Gaussian curves. Fluorescence quantum yields (Φ_F) were determined by method of comparison against the standard TPP.[109] Details of how data were acquired and reported for Φ_F can be found in Section 2.5.4. A summary of all absorption and emission data discussed in this chapter can be found in Table 3.1.

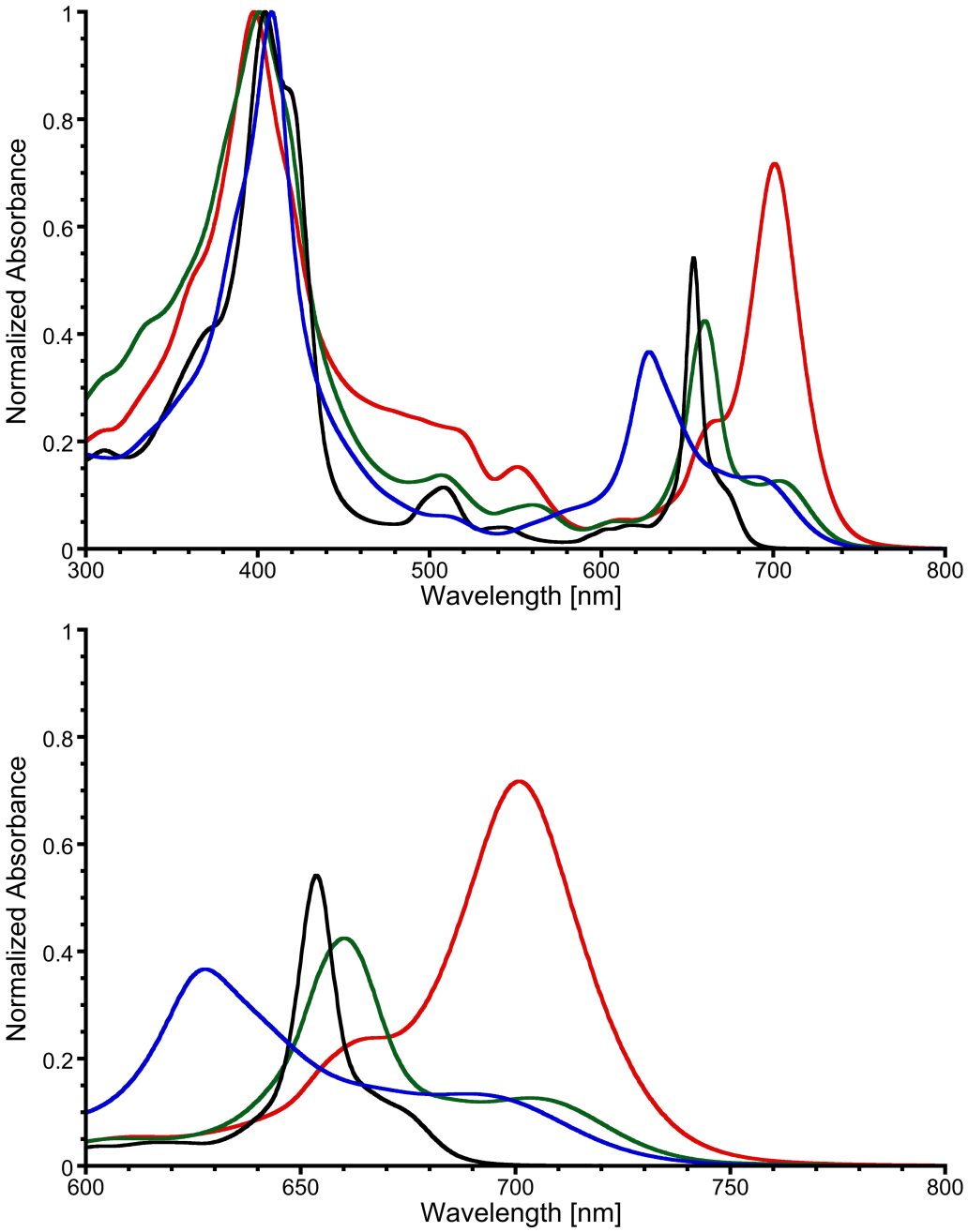

Figure 3.3: Full absorption spectra (top) and close-up of red-NIR band (bottom) of dyads *cis*-SC4 (green), *cis*-*Zn*SC4 (blue), *trans*-SC4 (red), and SC5 (black). All spectra acquired in toluene. At concentration of ~10 µM, and normalized at maximum of the *B* band.

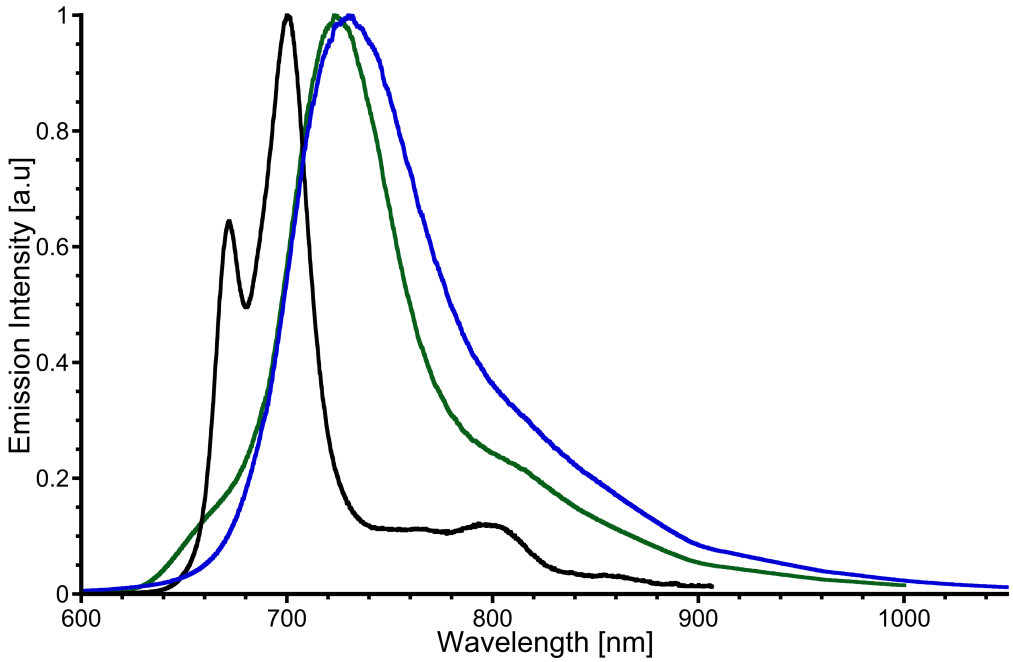

Figure 3.4: Emission spectra of dyads *cis*-SC4 (green), *cis-Zn*SC4 (blue) and SC5 (black). All spectra acquired in toluene, upon excitation at maximum of dyad *B* band, at sample concentration of ~1.0 μM. Note that *cis*-SC4 and *trans*-SC4 have identical emission profiles.

Compound	Absorption λ_{max} [nm]			λ_{emi} [nm]	Stokes Shift [nm] (cm^{-1})	Emission FWHM [nm] (cm^{-1})	$\frac{B}{Q_y}$ a)	Φ_F tol. (Φ_F DMF)
	$\lambda_{B\ bands}$	λ_{Qx}	λ_{Qy}					
Dyads								
***cis*-SC4**	401	507	660, 704	727	23 (449)	63 (1008)	2.36	0.082 (<0.01)
***trans*-SC4**	398	551	701	727	26 (510)	63 (1008)	1.40	0.092
***cis*-ZnSC4**	408		628, 690	732	42 (832)	82 (1475)	2.73	n.d.
SC5	404	508	653	657, 678			1.85	0.21 (0.20)
Monomer Standard								
C1-P[b)]	402, 417	506	656	659	3 (69)	14 (304)	1.61	0.33 (0.34)

Table 3.1: Absorption and emission properties of all compounds presented in Chapter 3, as well as model monomer. All data acquired in air equilibrated toluene unless otherwise noted. TPP used as standard (Φ_F = 0.070 in air equilibrated toluene).[197] The Φ_F values in parentheses were acquired in air equilibrated DMF. a) B/Q_y is ratio of absorption at λ_{max} for respective bands, used in lieu of molar absorptivity coefficient, ε. b) Data taken from Chapter 2, Table 2.1. c) Data taken from reference,[35] determined in Ar-purged toluene. Error for quantum yield measurements estimated at ± 5% (see section 2.5.4 for details).

The absorption spectra of all dimers feature the typical hydroporphyrin *B* bands and Q_x band, however the longest wavelength Q_y-like band is more complex in the case of *cis* dimers. Compound ***trans*-SC4** has an absorption spectrum similar to ethenyl linked dimer **SC1** (single Q_y-like band) with a less bathochromically shifted λ_{max} (701 nm). Interestingly, the Q_y-like maxima of ***trans*-SC4** falls nearly perfectly between that of **SC1** (707 nm) and ethynyl linker dimer **SC3** (689 nm). This is surprising because the introduction of additional π electrons typically results in a further bathochromic shift as seen with the absorption maxima of *trans*-stilbene (297 nm)[247] and *trans*-1,6-diphenylhexa-3-en-1,5-diyne (352 nm).[232] This comparison neglects to account for the influence of the two electron withdrawing esters, however, *trans*-3,4-dimethoxycarbonyl-1,6-diphenylhexa-3-en-1,5-diyne is known only as a synthetic intermediate and its electronic spectra are not reported.[248] Structurally similar *trans*-3,4-dimethoxycarbonyl-1,6-bis(*p*-toluoyl)hexa-3-en-1,5-diyne possesses absorption maxima at ~390 nm suggesting that the presence of the fumarate moiety in linker should also result in a significant bathochromic shift.[192,240]

All cofacial dimers feature a split Q_y-like band, in all cases the shorter wavelength band exhibits a greater oscillator strength than the longer wavelength band. For ***cis*-SC4** the maxima of the longer wavelength Q_y-like band (704 nm) overlaps the Q_y-like band of ***trans*-SC4**, and it is possible that even after careful purification in the absence of light that samples of ***cis*-SC4** contain trace quantities of ***trans*-SC4**. The splitting of the lowest energy Q_y-like band is consistent with excitonic coupling

occurring within the dyads.[249] In excitonically coupled chromophores the lowest energy excited state (S_1) is split into two new states, one with lower and one with higher energy, denoted as P_- and P_+, respectively. The mutual orientation of the chromophores' transition dipole moments dictates which transitions ($S_0 \rightarrow P_-$ or $S_0 \rightarrow P_+$) are allowed. When in parallel, the $S_0 \rightarrow P_+$ transition is permitted, and when head-to-tail, the $S_0 \rightarrow P_-$ transition is allowed (Figure 3.5).[199] The anti-parallel slipped cofacial orientation of the macrocycles in *cis* enediyne dyads is consistent with both transitions being permitted, as it is somewhere between the head-to-head and head-to-tail mutual orientations (commonly referred to as "oblique.") To quantify the strength of electronic coupling, we calculated V [half of the energy difference between the split Q_y-like bands, i.e., $V = 0.5[E(P_+) - E(P_-)]$, in cm^{-1}], for both *cis* enediyne dyads, and *o*-diethynylphenylene linked **SC5**. The freebase dimer ***cis*-SC4** has high coupling strength (V = 474 cm^{-1}) while zinc coordinated ***cis*-ZnSC4** has further increased coupling strength (V = 724 cm^{-1}). The strong coupling observed with both *cis* enediyne dyads is within the range seen in naturally occurring special pairs.

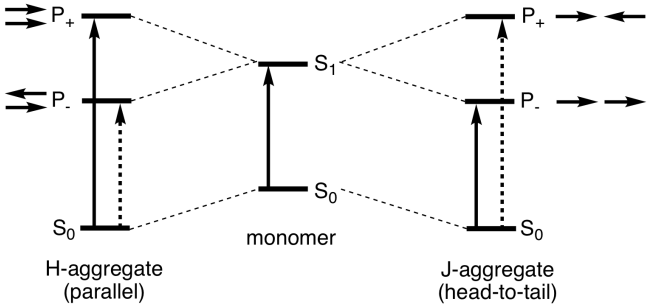

Figure 3.5: Splitting of excited state in H- and J- type aggregates.

Dyad **SC5** shows much lower coupling strength (V = 205 cm^{-1}) than the other dimers after deconvolution of its closely overlapping bands (maxima of 653 and 671 nm), despite the close agreement of its geometry with ***cis*-SC4**. This indicates that the choice of linker contributes significantly to the coupling strength, and through-bond coupling is non-trivial.

The emission spectra of *cis* enediyne dyads ***cis*-SC4** and ***cis*-ZnSC4** feature a single, broad (FWHM > 900 cm^{-1}) band with large Stokes' shifts of 449 cm^{-1} and 832 cm^{-1}, respectively. These values are significantly larger than is typically observed for chlorin monomers, butadiynyl linked hydroporphyrin dimers,[35] and dimers **SC1-3** (Chapter 2) which featured narrow emission bands (FWHM < 400 cm^{-1}) and small Stokes shifts (below 200 cm^{-1}). The fluorescence quantum yields of the *cis* and *trans* **SC4** dimers (Φ_F = 0.082-0.092) are significantly reduced (4-fold) relative to **C1-P** (Φ_F = 0.33). This behavior is in contrast to previously discussed dimers **SC1** and **SC3** that had increased (nearly doubled) Φ_F relative to their analogous styryl and phenylethynyl substituted monomers. The combination of features (large FWHM, large Stokes shift and broad/structureless emission band) are suggestive of excimer formation.[250–255] Formally, excimers result from the mixing of excited states localized on the chromophore subunits with charge-transfer states.[254,256] Excimer formation also coincides with geometrical relaxation of the molecule that is responsible for its lower excited-state energy.[257,258] The size of the Stokes' shift, as well as emission FWHM are directly proportional to the coupling strength, *V*, a trend that is apparent for both ***cis*-SC4** and ***cis*-ZnSC4**. For ***cis*-SC4**, a weak emission band is present on the blue edge of the primary emission band, it is unclear if this is due to the presence of a trace amount of a highly fluorescent monomer, or emission from a localized excited state that closely resembles that of a monomer. Excitation spectra centered on the weak, blue edge bands did not provide meaning full data, and further work is necessary to determine the origin of these bands.

The emission spectrum of ***trans*-SC4** (not shown) is identical to that of ***cis*-SC4** (Figure 3.4) and the excitation spectrum of ***trans*-SC4** closely matches the absorption of ***cis*-SC4** (Figure 3.6). This suggests that the excited ***trans*-SC4*** rapidly isomerizes to ***cis*-SC4***, which then undergoes emission. This is further supported by the weak Φ_F found for both ***cis*** and ***trans*** forms of **SC4** (Table 3.1).

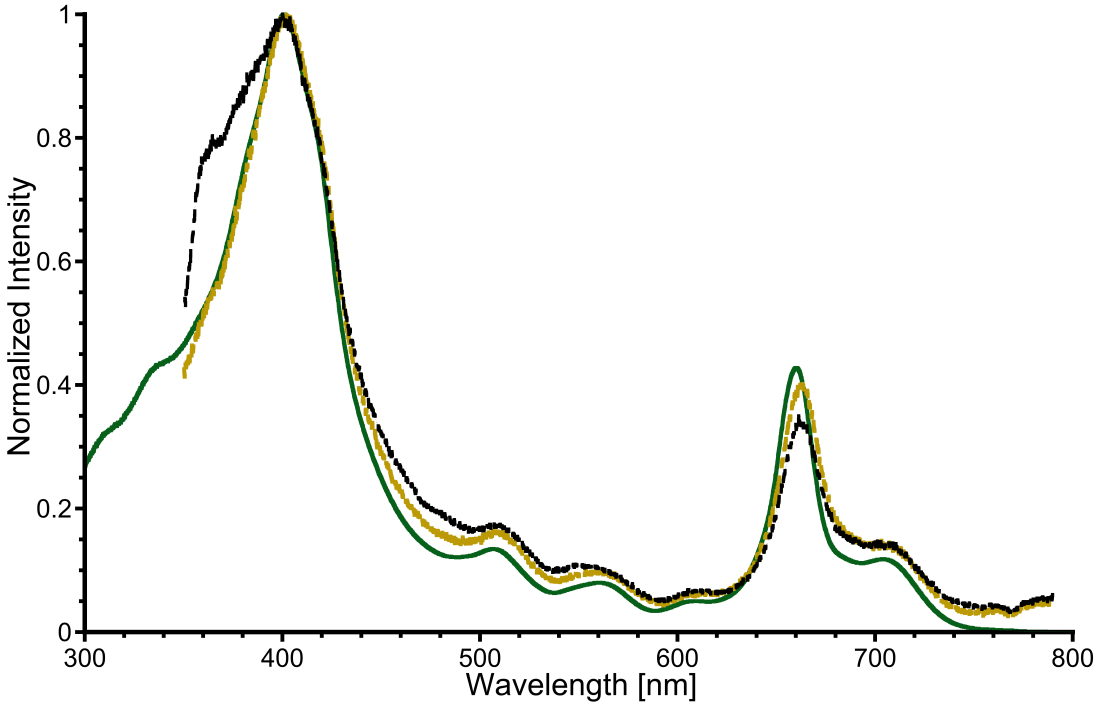

Figure 3.6: Absorption spectrum of *cis*-SC4 (green), with excitation spectra of *cis*-SC4 (gold, dashed) and *trans*-SC4 (black, dashed). Absorption acquired at ~10 µM concentration and excitation spectra at ~1.0 µM. Excitation spectra acquired while monitoring emission at 800 nm, all shown spectra acquired in toluene and normalized to the *B* band.

The emission spectra of *o*-diethynylphenylene dyad **SC5** is unique from all dyads discussed up until this point. It features two monomer-like emission bands, with a small Stokes shift. The Φ_F of **SC5** is diminished relative to phenylethynyl **C1-P** but is still large relative to the enediyne linked dyads. The two bands here do not appear to be the result of strong coupling (small *V*) but due to multiple excited state conformers that emission may occur from. This type of dual emission band was previously reported

by Montforts for his cofacial chlorin dimer containing a 4,5-diethynylbiphenylene spacer.[229]

Section 3.3.2: Isomerization of Enediyne-Linked Dyad SC4

As noted earlier, the synthesis of dyad **SC4**, as well as the identical emission spectra for ***cis*-SC4** and ***trans*-SC4** suggests rapid *trans-cis* photoisomerization. When solutions of pure ***cis*-SC4** and pure ***trans*-SC4** were exposed to ambient light, both isomers reached the same equilibrium ratio of *cis* to *trans* 10:1, within a few hours. We then took samples of pure ***cis*-SC4** and pure ***trans*-SC4** in toluene and subjected them to irradiation at the *B* band maxima. After 23 minutes of selective irradiation of either sample, the same equilibrium endpoint of 10:1, *cis* to *trans* was achieved (Figure 3.7). We repeated the experiment for ***trans*-SC4**, with irradiation centered at the maxima of Q_y-like band, and the same ratio was achieved after the same irradiation period (not shown). In a similar experiment we dissolved pure ***cis*-SC4** in $CDCl_3$ and monitored the appearance of ***trans*-SC4** resonances (17-methylene and 18-dimethyl resonances that are not highly shielded) by ^{1}H NMR, upon ambient light exposure over several days. Again, the endpoint of 10:1, *cis* to *trans* was apparent, this time taking days to reach due to the high sample concentration and limited surface area of the NMR tube. When left in solution, in darkness, neither ***cis*-SC4** nor ***trans*-SC4** undergoes isomerization, and both isomers can be stored at room temperature for several months in solid form, in the absence of light.

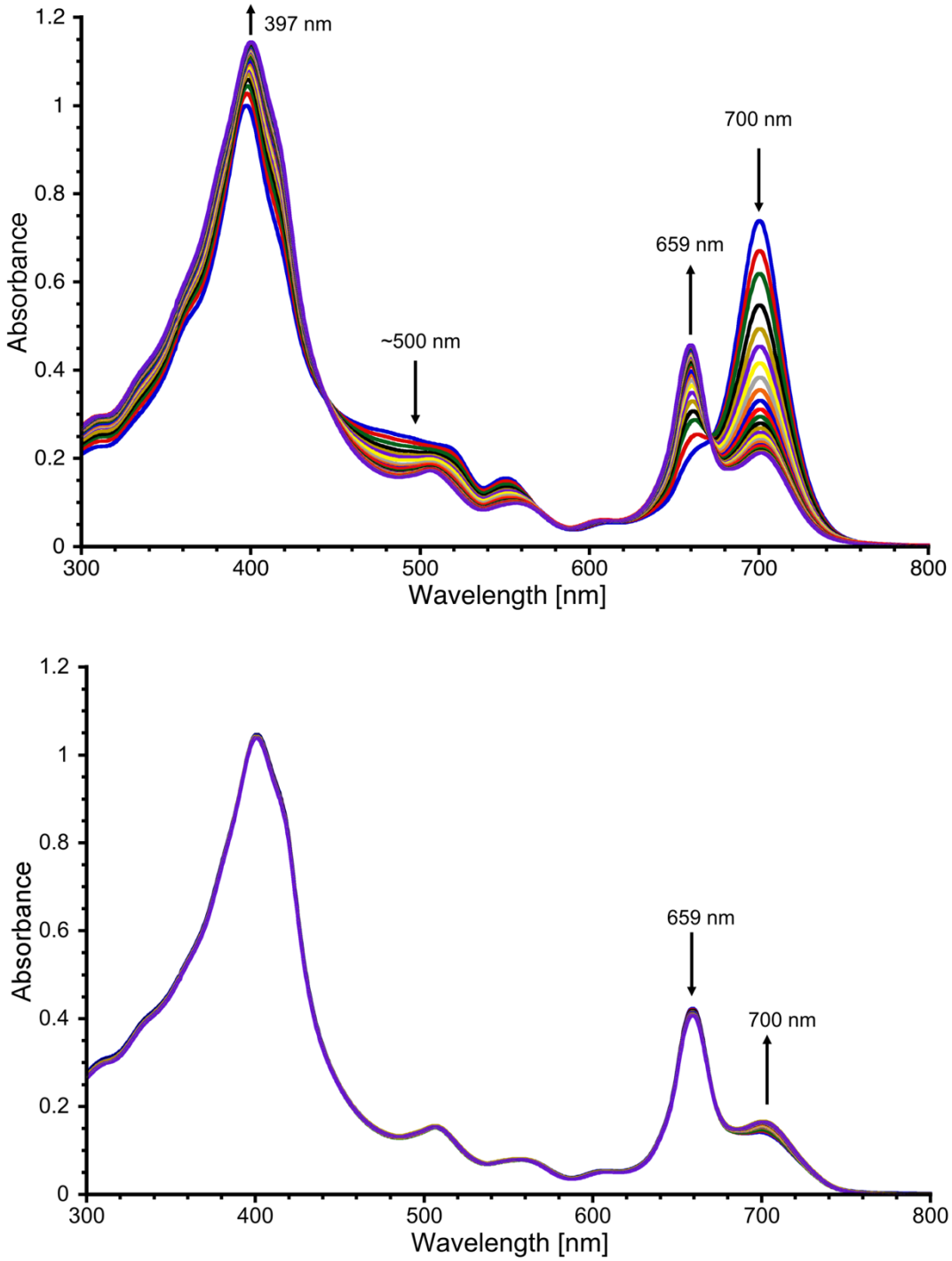

Figure 3.7: Photoisomerization of *trans*-SC4 (top) and *cis*-SC4 (bottom) in toluene, upon irradiation at maximum of *B* band, at ~ 10 µM concentration.

To further test the stability of ***cis*-SC4** and ***trans*-SC4** we performed a similar series of experiments probing thermal isomerization. Samples of both pure ***cis*-SC4** and pure ***trans*-SC4**, were refluxed in toluene, in darkness and after one day, approximately the same equilibrium of 10:1, *cis* to *trans* was again reached (Figure 3.8).

While *trans*-*cis* photoisomerization is well characterized in enediyne containing systems,[192,193,240–242] this was a bit surprising because we anticipated the *trans* form to be more thermally stable than *cis*, due to less extensive steric interactions. DFT calculations show that this should be the case, because ***trans*-SC4** is more stable than ***cis*-SC4** by 13.8 kJ/mol. We suspect that the large π-π interactions between adjacent macrocycles can account for additional stabilization,[259] however, the simple method we are able to use (due to hardware limitations) does not account for π-π interactions, a more sophisticated dispersion-corrected DFT method is required for better assessment of relative stabilities.[250]

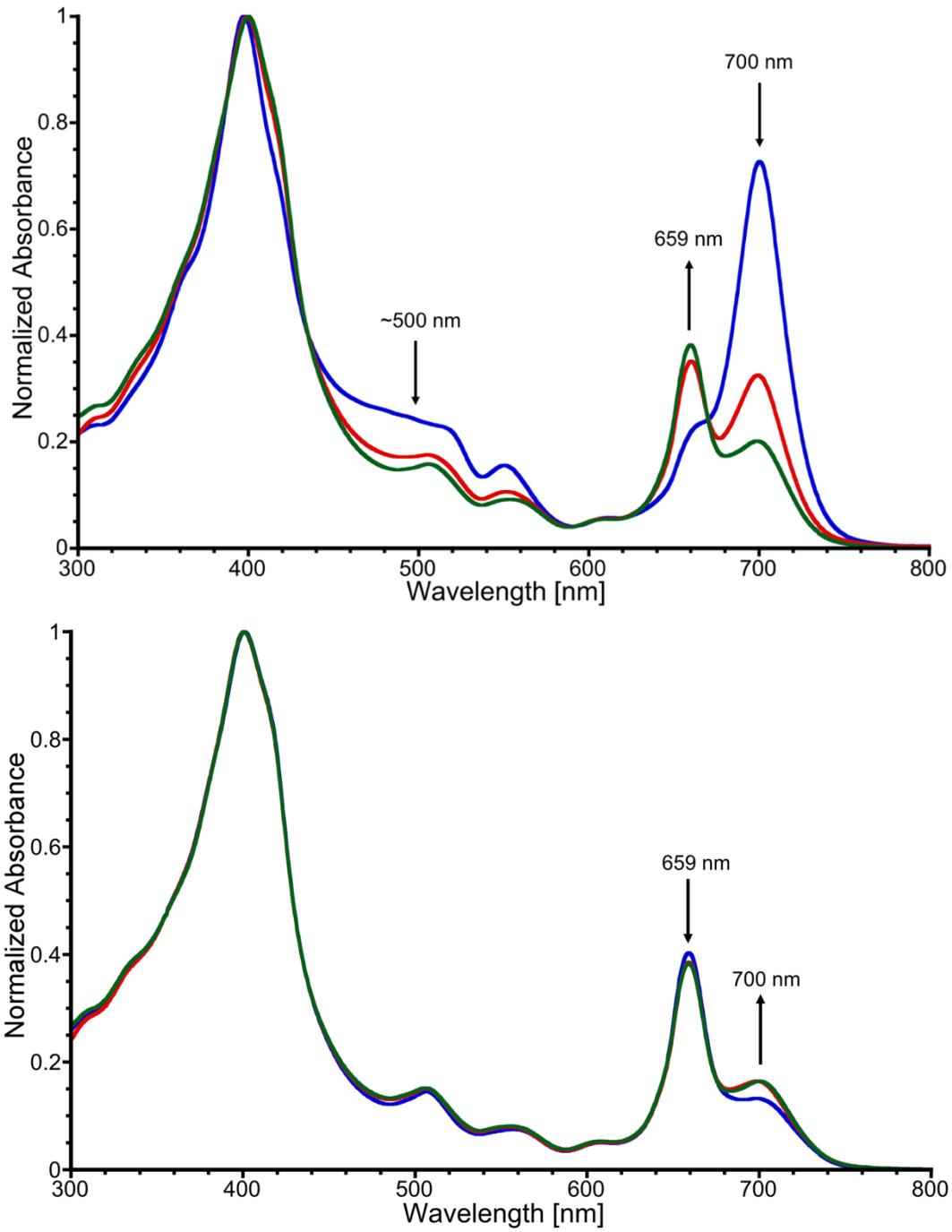

Figure 3.8: Thermal isomerization of *trans*-SC4 (top) and *cis*-SC4 (bottom) in refluxing toluene, in darkness. Trace colors correspond to time refluxed: Initial (blue), 6 hours (red), and 24 hours (green). Shown spectra were acquired in toluene after dilution to ~10 µM concentration, then normalized at the maximum of the *B* band.

Section 3.3.3: DFT Calculations

The absorption and emission properties of dimers ***cis*-SC4** and ***cis*-ZnSC4** demonstrate significant interactions between component macrocycles. The observed properties differ from simpler systems, such as the linearly arranged arrays seen in Chapter 2. In the slipped-cofacial arrays we must consider that three types of interactions are involved including 1) dipole-dipole coupling (long-rang coupling)[199] 2) through-space interactions due to the proximity of macrocycles causing orbital overlap (short-range coupling)[200] and 3) through-bond coupling (conjugated linker, the primary interest of Chapter 2).[41] Certainly all three interactions are at play, however, precisely distinguishing the extent each of these contributes to the absorption and emission properties of *cis* enediyne dyads is well beyond the scope of our work. Here, we utilized DFT calculations to determine the presence of through-space interactions and role of the linker in delocalization.

The first property we looked for was orbital splitting, which is the immediate indicator for strong electronic interactions. Because there are four orbitals responsible for the absorption and emission properties of hydroporphyrins (Gouterman's Four-Orbital Model)[260] we anticipate the splitting of the HOMO-1, HOMO, LUMO and LUMO+1 orbitals. Orbital splitting is well known in model systems for photosynthetic special pairs that feature bacteriochlorins held in close proximity noncovalently.[261] We observed orbital splitting for all dimers prepared in Chapter 3, the energies of the split orbitals are reported as two values for each standard frontier MO (e.g., we report two values for HOMO), and energy difference was used to calculate splitting energies (ΔE, Table 3.2).

Compound	HOMO-1 (eV) [ΔE]	HOMO (eV) [ΔE]	LUMO (eV) [ΔE]	LUMO+1 (eV) [ΔE]
***cis*-SC4**	-5.30, -5.19 [0.11]	-5.13, -4.89 [0.24]	-2.78, -2.38 [0.40]	-1.98, -1.92 [0.06]
***cis*-SC4** *disconnected*	-5.14, -5.07 [0.07]	-4.96, -4.87 [0.09]	-2.38, -2.32 [0.06]	-1.78, -1.74 [0.04]
***trans*-SC4**	-5.10, -5.08 [0.02]	-5.00, -4.76 [0.24]	-2.79, -2.28 [0.51]	-1.95, -1.75 [0.20]
***trans*-SC4** *disconnected* [a)]	-5.12, -5.12 [0.00]	-4.95, -4.94 [0.01]	-2.36, -2.36 [0.00]	-1.77, -1.77 [0.00]
***trans*-SC4** *twisted* [b)]	-5.08, -5.09 [0.01]	-4.77, -4.99 [0.22]	-2.76, -2.27 [0.49]	-1.96, -1.75 [0.19]
***cis*-ZnSC4**	-5.40, -5.27 [0.13]	-5.07, -4.84 [0.23]	-2.71, -2.35 [0.36]	-1.90, -1.80 [0.10]
***cis*-ZnSC4** *disconnected* [a)]	-5.24, -5.12 [0.12]	-4.85, -4.80 [0.05]	-2.30, -2.27 [0.03]	-1.64, -1.63 [0.01]
SC5	-5.13, -5.05 [0.08]	-4.96, -4.78 [0.18]	-2.44, -2.27 [0.17]	-1.76, -1.73 [0.03]
SC5 *disconnected* [a)]	-5.14, -5.07 [0.07]	-4.96, -4.88 [0.08]	-2.38, -2.31 [0.07]	-1.78, -1.74 [0.04]

Table 3.2: DFT-calculated molecular orbital energies for dyads discussed in Chapter 3, and their model compounds. All calculations were performed using the DFT B3LYP/6-31G* method. a) Molecular orbitals were calculated from the energy-minimized structures of corresponding dyads, having removed linker atoms (fumarate or benzene) and replacing empty valence with hydrogen, leaving two 13-ethynyl chlorins with the identical mutual orientation as the macrocycles of linked dyad they were taken from. b) Molecular orbitals were calculated from the modified structure of *trans*-SC4, where the dihedral angle between mean macrocycle plane and linker was increased to 27º.

The splitting energies for dimers ***cis*-SC4**, ***cis*-ZnSC4** and ***trans*-SC4** are comparable to those calculated for ethynyl- and butadiynyl- linked hydroporphyrin dimers,[36] while ΔE for **SC5** was lower, suggesting weaker electronic interactions. The split Frontier MOs can be seen in Section 3.6.2, Figures 3.10-3.15. Dimers with *cis* enediyne show significant distribution of electron density throughout a single hydroporphyrin and linker, with smaller orbital coefficients on the second hydroporphyrin, for both HOMO and LUMO. Split orbitals show close agreement with

the most common difference being the extent of electron density present on the linker. In the case of dyad **SC5** both the HOMO and LUMO show nearly identical electron distribution over both chlorins, indicating the lack of delocalization.

Next, we examined the through-space electronic interactions by performing DFT calculations for imaginary dimers in which direct conjugation was removed, but spatial orientation was unchanged. When performing calculations for the disconnected dimers we began with the energy-minimized structure for given enediyne linked dyad, then removed the fumarate component (for **SC5** benzene was remove), leaving a pair of 13-ethynyl substituted hydroporphyrins with identical spatial coordinates to the originals. The data for these dyads can also be found in Table 3.2, with the descriptor "*disconnected*." Removal of the linker predictably results in a negligible splitting energy for the planar ***trans*-SC4** (ΔE = 0.01 eV) while disconnected ***cis*-SC4**, ***cis*-ZnSC4** and **SC5** had nonzero values (ΔE ranged from 0.05-0.09 eV), indicating continued interaction through-space rather than exclusively through-bond. The large difference in ΔE between the **SC4** dimers and their respective disconnected counterparts is likely due to the small deviation from planarity. The dihedral angle between the mean macrocycle plane and the linker plane is close to 27º for all dimers sharing the slipped-cofacial geometry (Section 3.6.2, Table 3.4). To gauge the impact of this small angle, we performed a final DFT calculation of ***trans*-SC4 *twisted*,** where the dihedral angles between linker and mean macrocycle planes were both set to 27º. The resulting data show the twisting of ***trans*-SC4** resulted in a negligible change to the splitting energy.

Overall, these calculations demonstrate that there are large contributions of through-space and through-bond electronic interactions to the dipole-dipole coupling. Only with the combined effect of all three, do we see the extensive splitting of *cis* enediyne dyads Q_y-like absorption band and emission properties significantly different from hydroporphyrin monomers. This is reinforced when comparing **SC5** against ***cis*-SC4**, both of which showed similar splitting energies, and geometries, when disconnected (ΔE = 0.08 and 0.09 eV, respectively). The ΔE for ***cis*-SC4** (0.24 eV) relative to **SC5** (0.18 eV) is significantly larger, and that can only be attributed to the choice of linker. Thus, the 3,4-dimethylcarbonyl-hexa-3-en-1,5-diyne linker provides superior through-bond conjugation than the 1,2-diethynylphenyl linker. This relationship was inferred by the more extensive coupling strength *V* observed in ***cis*-SC4** versus **SC5** and reinforced by the calculations. In addition, more extensive through-bond conjugation was observed for similar compounds featuring terminal phenyl substituents rather than chlorin macrocycles. The counterpart to ***cis*-SC4**, *cis*-1,6-diphenylhexa-3-en-1,5-diyne, features more extensive bathochromic shift in its absorption (λ_{max} = 387 nm)[232] compared to the **SC5**-like 1,2-bis(phenylethynyl)benzene (λ_{max} = 346 nm).[262]

Section 3.4: Conclusions

We have successfully prepared hydroporphyrin dimers linked by the 3,4-methoxycarbonyl-hexa-3-en-1,5-diyne moiety, and isolated both the *cis* and *trans* forms of dyad **SC4** comprised of enediyne linked 10-mesityl chlorin. The *trans* isomer, ***trans*-SC4**, possesses absorption maxima of the Q_y-like band between that of analogous ethenyl (**SC1)** and ethynyl (**SC3)** linked chlorin dyads. Compound ***trans*-SC4**

undergoes rapid photoisomerization to reach a state of equilibrium featuring *cis:trans*, 10:1. Both the *cis* and *trans* isomers are stable at room temperature in the absence of light, but can be forced to the equilibrium mixture under heating in solution. Dyad ***cis*-SC4** exists in a slipped-cofacial mutual orientation of the component macrocycles that closely resembles the photosynthetic special pair and features extensive electronic coupling. The strong coupling results in a splitting of the lowest energy (Q_y-like) absorption band of the dimer and splitting of molecular orbitals. The large electronic coupling has been determined to be the result of short range excitonic coupling (close proximity of macrocycles) and through-bond conjugation (small twisting of macrocycles relative to central alkene) enhancing the long-range excitonic coupling responsible for initial splitting of the Q_y-like band. The emission properties (broad and featureless emission band, and large Stokes shift) are suggestive of excimer formation. Due to the closely matching geometry and spectral features, we anticipate that the enediyne linked hydroporphyrin motif can be used for modeling of the photosynthetic reaction center and could be viable for solar-energy harvesting applications. Furthermore, our method of *cis* enediyne preparation requires only a single synthetic step performed on ethynyl substituted chromophore, done in the presence of light. This approach could be used to explore other similar systems, for example, chlorins linked via enediyne through *meso* (rather than β) position, or arrays with the same hydroporphyrins linked via different positions to achieve unique geometries.

Section 3.5: Experimental Procedures

Section 3.5.1: General Synthetic & Spectroscopic Procedures

For general procedures involving palladium catalyzed (Sonogashira) reactions and characterization of new compounds by NMR and HRMS, see section 2.5.1. For determination of fluorescence quantum yields see section 2.5.4.

The known compound **C1-EH** was prepared as described in Chapter 2. The synthesis of dimethyl 2,3-dibromofumarate **5** has been reported by several methods, we prepared it following a modified procedure[244] but required other literature[263,264] to compare characterization data.

Section 3.5.1: Synthesis of dibromofumarate and dyads (order of appearance)

*Dimethyl 2,3-dibromofumarate (**5**)*

Following the reported procedure,[244] dimethyl acetylene dicarboxylate (2.86g, 20.0 mmol) in anhydrous CH_2Cl_2 (20 mL) was treated with pyridinium tribromide (2.47g, 28.1 mmol) under argon, and stirred for 6 days. The reaction was quenched by treatment with excess sodium thiosulfate (10%, aq.), and extracted using diethyl ether. The ether was then washed (water then brine), dried ($MgSO_4$) and concentrated. The crude oil was purified by column chromatography [silica, CH_2Cl_2/hexanes (1:1) $\rightarrow$ (1:0)] yielding isomerically pure (2.31g, 38%) as a white solid. Both ^1H and ^{13}C NMR are consistent with that reported for *E* isomer of dimethyl 2,3-dibromofumarate.[264]

***cis-SC4:** Sonogashira reaction of **C1-EH** and **5** with exposure to ambient light*

Following the general procedure for Sonogashira reaction, a mixture of **C1-EH** (26.0 mg, 0.054 mmol), dimethyl 2,3-dibromofumarate **5** (8.2 mg, 27.0 μmol), $Pd_2(dba)_3$ (7.4 mg, 8.1 μmol) and $P(o\text{-}tol)_3$ (4.1 mg, 0.014 mmol) in anhydrous

toluene/Et_3N (5:1, 12.0 mL) was stirred at 60 ºC overnight, with fume hood lights turned on. After 16 hours, the reaction mixture was concentrated under reduced pressure. Column chromatography [silica gel, hexanes/CH_2Cl_2 (3:7)] afforded butadiynyl linked chlorin dimer (**2C1-b**) as a red-brown solid (yield not determined) followed by ***cis-SC4*** (8.2 mg, 28%) as a dark green solid, the last compound to elute was identified as ***trans-SC4*** (trace).

Data for byproduct **2C1-b**: ^{1}H NMR (400 MHz, $CDCl_3$): δ −1.79 (bs, 2H), −1.41 (bs, 2H), 1.90 (s, 12H), 2.09 (s, 12H), 2.64 (s, 6H), 4.71 (s, 4H), 7.29 (s, 4H), 8.48 (d, J = 4.1 Hz, 2H), 8.86−8.84 (m, 6H), 8.92 (d, J = 4.6 Hz, 2H), 9.19 (d, J = 4.6 Hz, 2H), 9.37 (s, 2H), 9.71 (s, 2H); $^{13}C\{^1H\}$NMR (100 MHz, $CDCl_3$): δ 21.4, 29.8, 31.2, 46.8, 51.8, 94.7, 95.2, 106.8, 108.9, 115.1, 121.5, 124.5, 127.9, 129.1, 129.8, 132.1, 132.8, 133.0, 135.7, 137.4, 138.0, 139.2, 140.8, 142.1, 152.7, 152.8, 163.5, 176.8; HRMS (ESI-FT-ICR): m/z $[M+H]^+$ Calcd for $C_{66}H_{58}N_8$, 963.4857; Found 963.4890.

Data for ***cis*-SC4**: ^{1}H NMR (400 MHz, $CDCl_3$): δ -2.14 (bs, 2H), -1.43 (bs, 2H), -0.48 (s, 12H), 1.91 (s, 12H), 2.11 (s, 4H), 2.60 (s, 6H), 4.13 (s, 6H), 7.25 (s, 4H), 7.67 (s, 2H), 8.43 (d, *J* = 4.7 Hz, 2H), 8.45 (d, *J* = 4.4 Hz, 2H), 8.80 (d, *J* = 4.4 Hz, 2H), 8.93 (s, 2H), 8.95 (d, *J* = 4.7 Hz, 2H), 9.23 (s, 2H), 9.54 (s, 2H); $^{13}C\{^1H\}$NMR (100 MHz, $CDCl_3$): δ 21.4, 21.6, 28.8, 29.6, 29.9, 44.8, 49.3, 53.7, 93.0, 93.9, 96.1, 100.2, 106.3, 114.9, 121.6, 124.3, 127.0, 128.0, 128.8, 129.1, 132.1, 132.8, 133.0, 135.7, 137.5, 138.0, 139.1, 139.7, 141.6, 152.6, 152.8, 163.3, 164.9, 176.2; HRMS (ESI-FT-ICR) *m/z* $[M+H]^+$ Calcd for $C_{72}H_{65}N_8O_4$, 1105.5123; Found 1105.5175.

trans-SC4: *Sonogashira reaction of* ***C1-EH*** *and* ***5*** *in darkness*

The reaction mixture was rigorously protected from light using aluminum foil and minimization of ambient light during the reaction, purification and any other handling. In particular, purification was done in darkness with the use of an LED headlamp (on red light setting) in order to visualize separation of bands while still on the column. Following the general procedure for Sonogashira reaction, a mixture of ethynyl chlorin **C1-EH** (37.9 mg, 0.079 mmol), dibromofumarate **5** (11.9 mg, 0.039 mmol), $Pd_2(dba)_3$ (10.1 mg, 0.011 mmol) and $P(o\text{-}tol)_3$ (10.8 mg, 0.035 mmol) in anhydrous toluene/Et_3N (5:1, 18.0 mL) was stirred at 60ºC. After 21 hours, the reaction mixture was concentrated down. Column chromatography [silica, hexanes/dichloromethane (2:1)] yielded the ***trans-SC4*** (9.3 mg, 21%) as a brown solid. ***cis-SC4*** was also observed on TLC as a minor product (greater R_f than ***trans-SC4***) but was not isolated cleanly following this procedure. ^{1}H NMR (400 MHz, $CDCl_3$): δ -1.69 (bs, 2H), -1.26 (bs, 2H), 1.89 (s, 12H), 2.10 (s, 12H), 2.65 (s, 6H), 4.37 (s, 6H), 4.74 (s, 4H), 7.29 (s, 4H), 8.46 (d, *J* = 4.3 Hz, 2H), 8.81 (s, 2H), 8.83 (s, 2H), 8.83 (d, *J* = 4.3 Hz, 2H), 8.92 (d, *J* = 4.6 Hz, 2H), 9.17 (d, *J* = 4.6 Hz, 2H), 9.57 (s, 2H), 9.68 (s, 2H); HRMS (ESI-FT-ICR) *m/z* $[M+H]^+$ Calcd for $C_{72}H_{65}N_8O_4$,1105.5123; Found 1105.5136.

***cis*-ZnSC4**

A solution of ***cis*-SC4** (at equilibrium containing ~10% *trans* isomer, 8.0 mg, 7.2 μmol) in chloroform/methanol (6 mL, 5:1) was treated with zinc acetate dihydrate (79.0 mg, 0.36 mmol) and stirred at room temperature. TLC analysis after 3 h showed the presence of unreacted ***cis*-SC4**. At that time another portion of zinc acetate dihydrate (79.0 mg, 0.36 mmol) was added and stirring was continued for another 4

hours (total reaction time 7 hours). The reaction mixture was quenched $NaHCO_3$ (sat'd, aq.) and extracted with dichloromethane. The organic layer was washed (water then brine), dried (Na_2SO_4), and concentrated. Column chromatography [silica, dichloromethane] yielded the zinc complex *cis* enediyne dyad ***cis*-ZnSC4** as a dark green solid (6.0 mg, 67%). Product zinc complex elutes following residual unreacted ***cis*-SC4**. ^{1}H NMR (400 MHz, $CDCl_3$): δ -0.08 (s, 12H), 1.91 (s, 12H), 2.44 (s, 4H), 2.56 (s, 6H), 4.10 (s, 6H), 7.19 (s, 2H), 7.60 (s, 2H), 8.32 (d, J = 4.3 Hz, 2H), 8.39 (d, J = 4.3 Hz, 2H), 8.75 (d, J = 4.3 Hz, 2H), 8.85 (d, J = 4.4 Hz, 2H), 8.88 (s, 2H), 9.06 (s, 2H), 9.39 (s, 2H); HRMS (ESI-FT-ICR) *m/z* $[M+H]^+$ Calcd for $C_{72}H_{61}N_8O_4Zn_2$, 1229.3393; Found 1229.3453.

SC5

Following the general procedure for Sonogashira reaction a mixture of ethynyl chlorin **C1-EH** (30.0 mg, 0.062 mmol), *o*-dibromobenzene **8** (7.3 mg, 0.031 mmol), $Pd_2(dba)_3$ (8.6 mg, 9.3 μmol) and P(o-tol)$_3$ (8.5 mg, 0.028 mmol) in anhydrous toluene/Et_3N (5:1, 6.0 mL) was stirred at 60ºC. After 16 hours, the reaction mixture was concentrated down. Column chromatography [silica, hexanes/dichloromethane (2:1)] yielded a green solid (12.3 mg, 38%). Product was the primary band to elute, following a trace amount of unreacted **C1-EH.** Also note that an unidentified red fluorescent impurity nearly co-eluted with desired product, and early fractions of product were discarded. ^{1}H NMR (400 MHz, $CDCl_3$): δ -2.28 (bs, 2H), -1.68 (bs, 2H), -0.36 (s, 12H), 1.88 (s, 12H), 2.25 (s, 4H), 2.58 (s, 6H), 7.22 (s, 4H), 7.56 (dd, J_1 = 3.3 Hz, J_2 = 5.8 Hz, 2H), 7.78 (s, 2H), 7.99 (dd, J_1 = 3.3 Hz, J_2 = 5.8 Hz, 2H), 8.46 (d, J = 4.3 Hz, 2H), 8.48 (d, J = 4.6 Hz, 2H), 8.83 (d, J = 4.3 Hz, 2H),8.94 (s, 2H), 8.99 (d, J

= 4.6 Hz, 2H), 9.41 (s, 2H), 9.61 (s, 2H); $^{13}C\{^{1}H\}$NMR (100 MHz, $CDCl_3$): δ 21.7, 21.8, 29.1, 44.9, 49.8, 77.6, 89.7, 94.1, 96.0, 96.2, 106.7, 117.2, 120.8, 123.9, 126.4, 128.1, 128.5, 128.8, 128.9 131.8, 132.8, 133.1, 133.2, 135.2, 137.9, 138.0, 139.3, 139.9, 141.2, 152.2, 152.8, 163.5, 175.7; HRMS (ESI-FT-ICR) *m/z* $[M+H]^+$ Calcd for $C_{72}H_{63}N_8$, 1039.5170; Found 1039.514.

Section 3.5.3: DFT-Calculations (Spartan Model)

DFT calculations were all performed using Spartan 10 for Windows (Wavefunction., Inc., Irvine, CA, USA) and subsequent visualization was done using both Spartan 10, and Mercury for Mac (Cambridge Crystallographic Data Centre, Cambridge, UK). For each calculation the, the B3LYP functional with the 6-31G* basis set (B3LYP/6-31G*) in vacuum was used. We examined numerous different geometries of each studied dyad to identify global energy minimum, following full-structure optimization/energy minimization. When performing calculations on imaginary "disconnected" dyads (Table 3.2) we began from the corresponding connected dyad, after identification of its global minimum, and removed the linker moiety (fumarate or benzene) and added hydrogen to the open ethynyl fragments, without any change of geometry to the macrocycles. Split MO energies noted in Table 3.2 are generated in Spartan under traditional numbering and those orbitals most closely agreeing in energy were grouped as follows, split MO:(calculated MO of lower absolute energy, calculated MO of higher absolute energy) such that HOMO-1:(HOMO-3, HOMO-2), HOMO:(HOMO-1, HOMO), LUMO:(LUMO, LUMO+1), LUMO+1:(LUMO+2, LUMO+3).

Section 3.6: Supplemental Information

Section 3.6.1: 2D NOESY Summary of Chemical Shifts

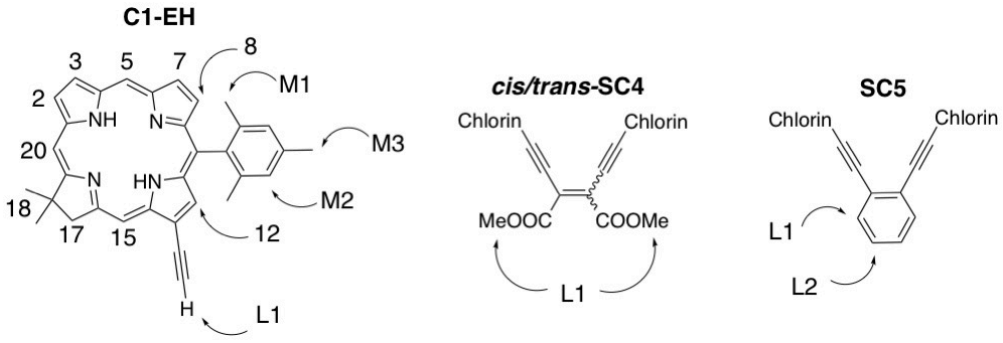

Position	C1-EH	*trans*-SC4	*cis*-SC4	SC5
2	8.92 (d, 1H)	8.91 (d, 2H)	8.43 (d, 2H)	8.47 (d, 2H)
3	9.18 (d, 1H)	9.17 (d, 2H)	8.95 (d, 2H)	8.99 (d, 2H)
5	9.72 (s, 1H)	9.68 (s, 2H)	9.54 (s, 2H)	9.61 (s, 2H)
7	8.85 (d, 1H)	8.83 (d, 2H)	8.79 (d, 2H)	8.83 (d, 2H)
8	8.45 (d, 1H)	8.46 (d, 2H)	8.45 (d, 2H)	8.45 (d, 2H)
M1	1.84 (s, 6H)	1.90 (s, 12H)	1.92 (s, 12H)	1.88 (s, 12H)
M2	7.24 (s, 2H)	7.29 (s, 4H)	7.25 (s, 4H)	7.22 (s, 4H)
M3	2.60 (s, 3H)	2.65 (s, 6H)	2.61 (s, 6H)	2.58 (s, 6H)
12	8.72 (s, 1H)	8.81 (s, 2H)	8.94 (s, 2H)	8.94 (s, 2H)
15	9.23 (s, 1H)	9.57 (s, 2H)	9.24 (s, 2H)	9.41 (s, 2H)
17	4.64 (s, 2H)	4.74 (s, 4H)	***2.11 (s, 4H)***	***2.25 (s, 4H)***
18	2.06 (s, 6H)	2.10 (s, 12H)	***-0.48 (s, 12H)***	***-0.37 (s, 12H)***
20	8.84 (s, 1H)	8.83 (s, 2H)	***7.67 (s, 2H)***	***7.78 (s, 2H)***
L1	3.86 (s, 1H)	4.37 (s, 6H)	4.13 (s, 6H)	7.98-8.01 (m, 2H)
L2	---	---	---	7.55-7.57 (m, 2H)

Table 3.3: Summary of chemical shift (δ ppm) for C1-EH, *cis*-SC4, *trans*-SC4 and SC5 as determined by 2D NOESY NMR. Data in each cell displayed as follows: chemical shift (multiplicity, integration). Coupling constants (*J,* Hz) can be found in Section 3.5.1. Dyad signals which show considerable upfield shift relative to C1-EH are indicated by bold italics, chlorin sites lacking proton and internal N-H resonances are not indicated here.

Section 3.6.2: DFT-calculated structures and related data

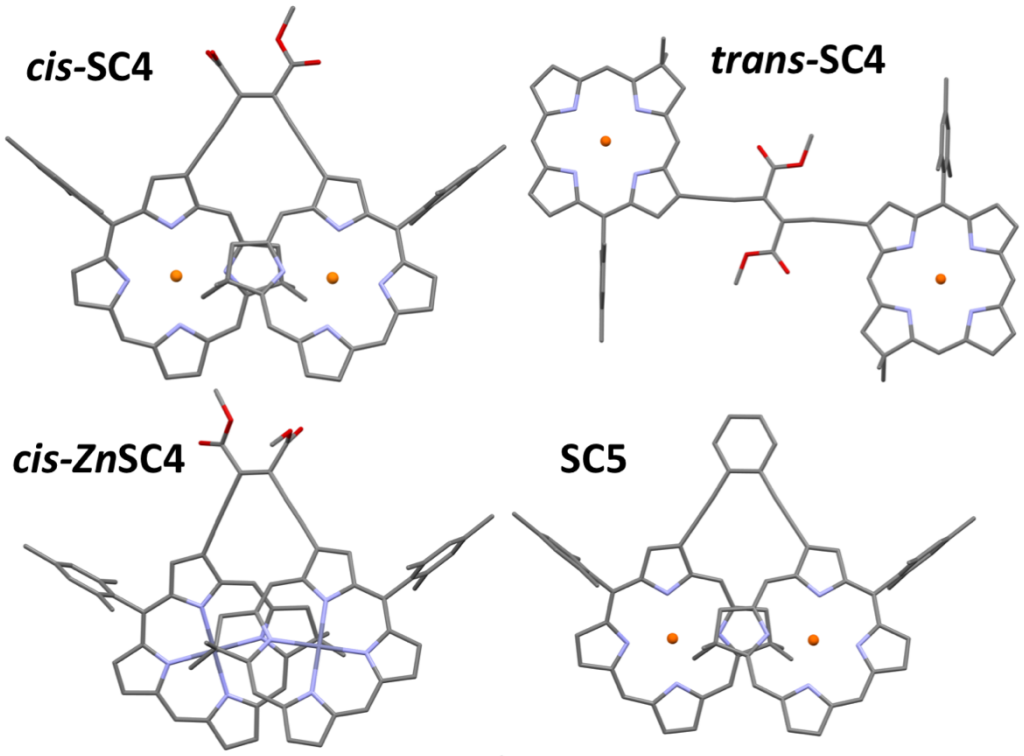

Figure 3.9: DFT energy-minimized structures of dyads presented in Chapter 3. Calculations performed using Spartan, processed images generated from Mercury. Orange spheres are centroids defined by macrocycle N atoms, H atoms omitted for clarity

Dyad	Angle 1	Angle 2	Mean Angle	Center-to-center distance (Å)	15-15 distance (Å)
***cis*-SC4**	27.99	26.48	27.2	7.166	3.641
***trans*-SC4**	2.4†	--	--	17.030	11.047
***cis*-ZnSC4**	30.63	31.11	30.9	6.593	3.556
SC5	27.79	28.07	27.9	7.153	3.645

Table 3.4: Dihedral angles and select distances for dyads presented in Chapter 3. All data acquired from DFT calculated energy-minimized structures performed in Spartan, then processed in Mercury. Dihedral angles 1 & 2 are arbitrarily assigned angles between one hydroporphyrin mean plane (calculated from the four pyrrolic nitrogen atoms) and the mean linker plane (calculated from the two central sp^2 hybridized carbon atoms and connected sp hybridized carbon atoms), mean angle is the average of angles 1 & 2. Dihedral angle marked by † is measured between the two chlorin mean planes of *trans*-SC4. Center-to-center distances are measured from centroid to centroid, where centroids are calculated from the coordinates of the four pyrrolic nitrogen atoms of given macrocycle. 15 to 15 distance is measured directly from carbon atoms.

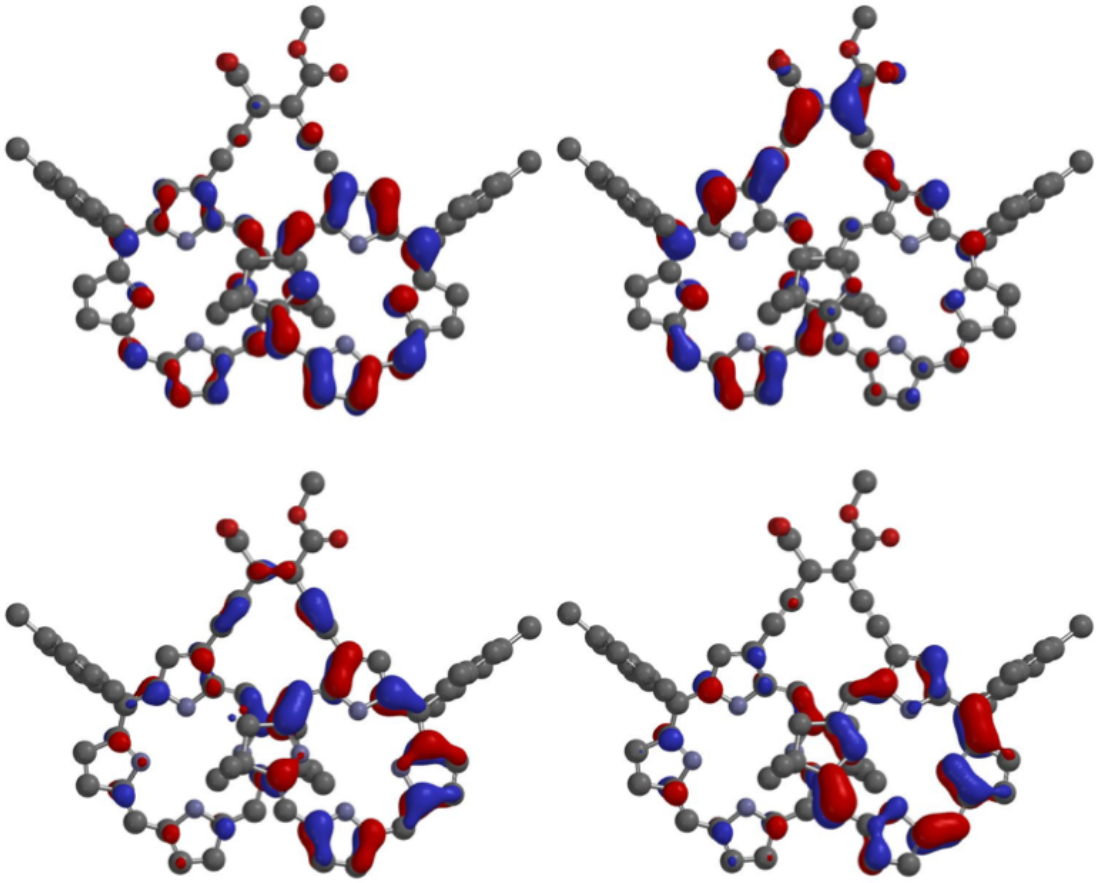

Figure 3.10: DFT calculated frontier MOs of dyad *cis*-SC4, split LUMO on top (LUMO+1 and LUMO, left and right, respectively), split HOMO on bottom (HOMO and HOMO-1, left and right, respectively). H atoms omitted for clarity.

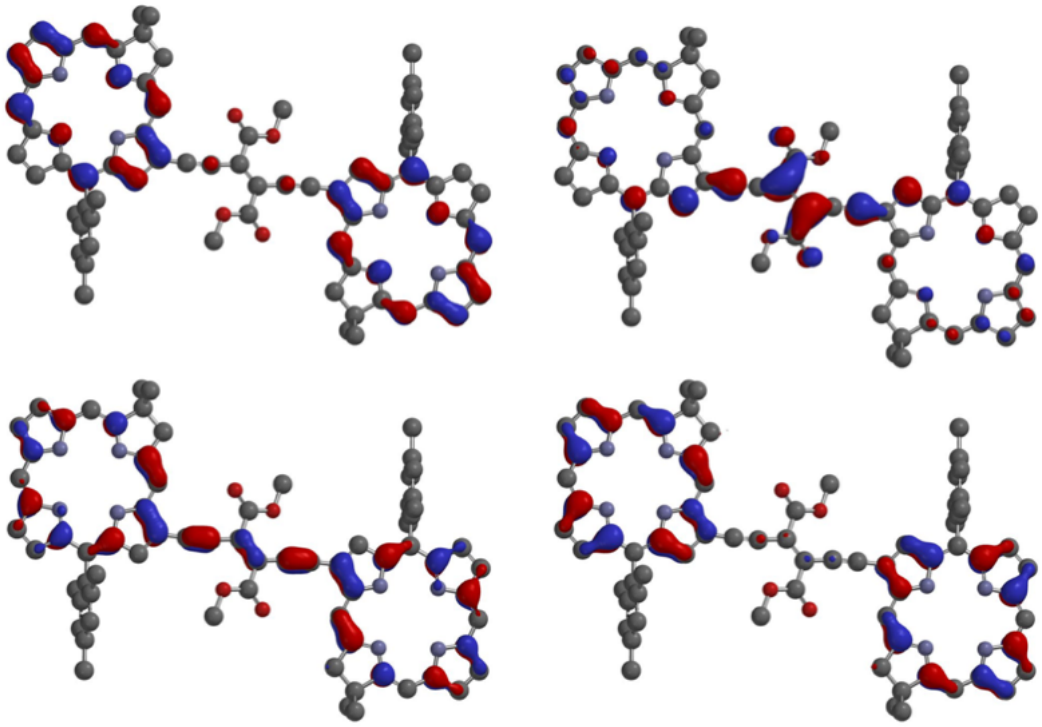

Figure 3.11: DFT calculated frontier MOs of dyad *trans*-SC4, split LUMO on top (LUMO+1 and LUMO, left and right, respectively), split HOMO on bottom (HOMO and HOMO-1, left and right, respectively). H atoms omitted for clarity.

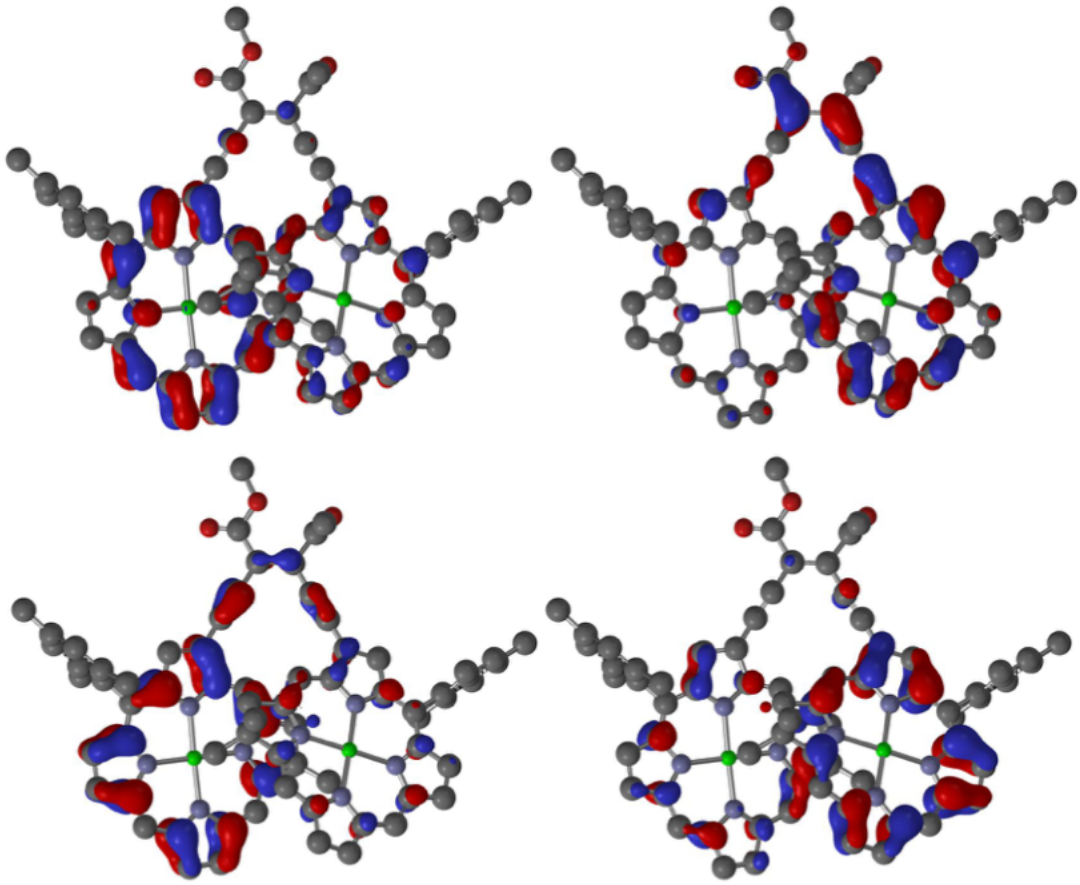

Figure 3.12: DFT calculated frontier MOs of dyad *cis*-ZnSC4, split LUMO on top (LUMO+1 and LUMO, left and right, respectively), split HOMO on bottom (HOMO and HOMO-1, left and right, respectively). H atoms omitted for clarity.

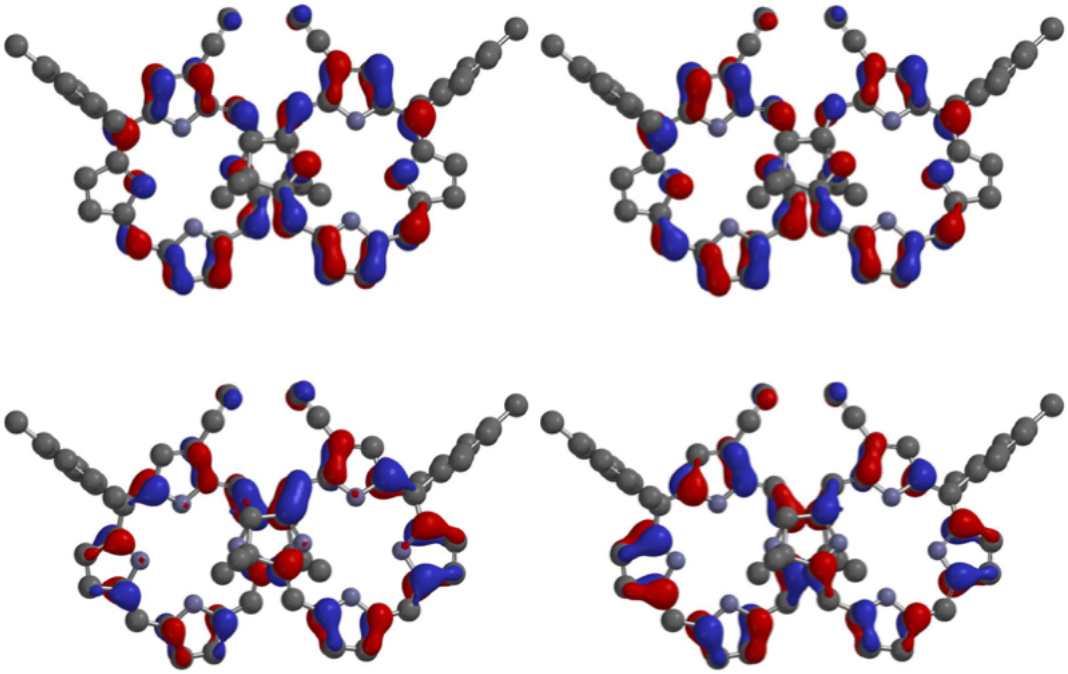

Figure 3.13: DFT calculated frontier MOs of dyad *cis*-SC4 *disconnected*, split LUMO on top (LUMO+1 and LUMO, left and right, respectively), split HOMO on bottom (HOMO and HOMO-1, left and right, respectively). H atoms omitted for clarity.

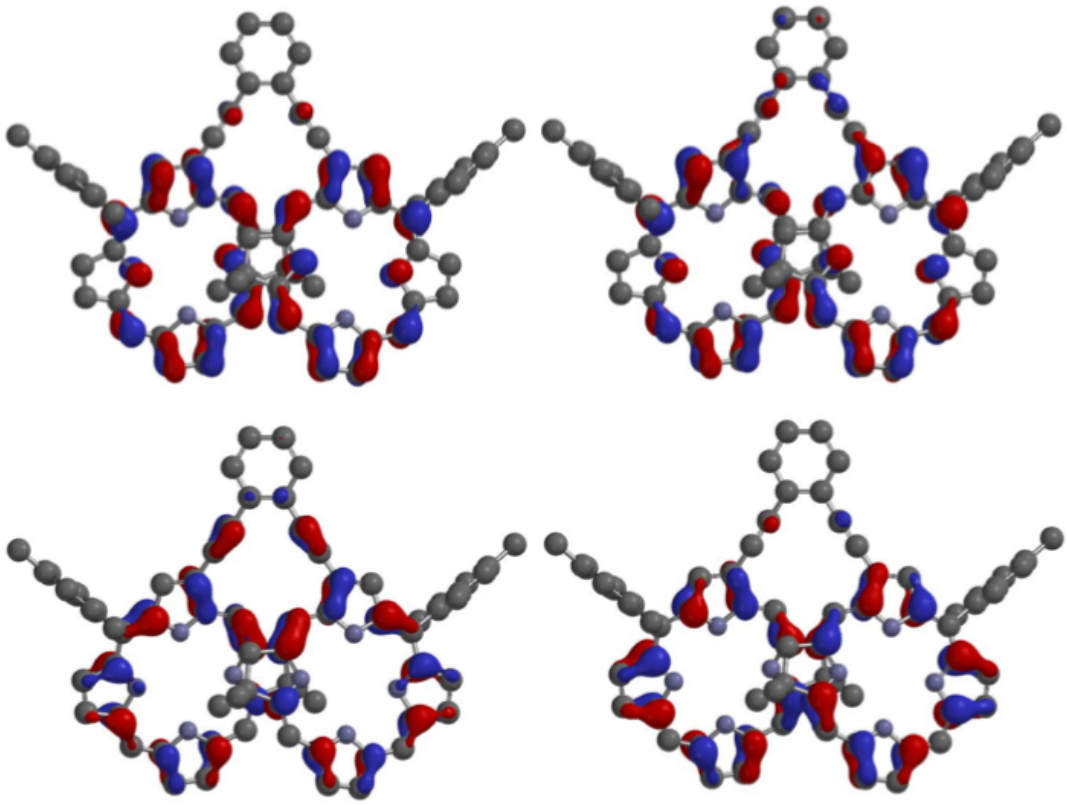

Figure 3.14: DFT calculated frontier MOs of dyad SC5, split LUMO on top (LUMO+1 and LUMO, left and right, respectively), split HOMO on bottom (HOMO and HOMO-1, left and right, respectively). H atoms omitted for clarity.

Chapter 4: Optimizing Energy Transfer and Minimizing Quenching in BODIPY-Chlorin Energy Transfer Arrays

Section 4.1: Introduction

Hydroporphyrins are uniquely suited chromophores for biomedical imaging. They possess several absorption bands that operate in three spectral windows: the *B* bands in the near UV (bacteriochlorins, 360-380 nm) or violet (chlorins, 400-430 nm), the Q_x band in the green region (500-520 nm), and the Q_y band in the deep-red (chlorins, 630-700 nm) to near-infrared (bacteriochlorins, 720-800 nm).[109–112] They possess a small Stokes' shift, emission in either the deep-red (chlorins, 640-710 nm) or NIR (bacteriochlorins, 730-810 nm). Both the Q_y absorption and emission maxima can be readily tuned by installing auxochromes around the macrocycle, with the greatest affect occurring upon substitution at 3- and 13- positions.[109–111,114] Furthermore, the emission bands of hydroporphyrins are exceptionally narrow (full-width at half-of-maximum, < 25 nm) in comparison to other common organic chromophores (e.g., cyanine and BODIPY emission FWHM are typically > 40 nm).[265,266] Through collaboration, our lab has demonstrated that these properties of hydroporphyrins can be exploited to create visual aids for fluorescence guided surgery.[267,268] First, our collaborators demonstrated that a lectin targeting probe, consisting of a human galactosyl serum albumin (hGSA) bound bacteriochlorin, can be used to visualize both surface and deeper tissue tumors. Selective excitation in the green window (~510 nm) with emission detection at 760 nm provides a large pseudo-Stokes' shift (250 nm) allows for high resolution images (large signal-to-background ratio) of surface tumors.[268] The excellent image quality was due to the large pseudo-Stokes' shift, which limited the noise in two ways, 1) the light scattered from the excitation source was at a significantly different wavelength than

light being detected and 2) tissue autofluorescence (greatest in the green spectral window) similarly goes undetected.[269] The decreased noise is not without cost, however, as green light only affords shallow tissue penetration. To improve tissue penetration with the same bacteriochlorin probe, the Q_y band was excited directly (750 nm). Unlike with green excitation, this afforded blurred images due to the small Stokes shift of only 10 nm. Despite the (relatively) blurry images, deeper tumors can be readily recognized, providing surgeons with a region of interest.[270–272] The surgeon can then cut into the tissue and excite with green light to properly determine the tumor margins. This dual-excitation technique is only possible with chromophores possessing multiple absorption bands, where at least one is in the deep red-NIR. Such features are rare among the current catalog of fluorophores.

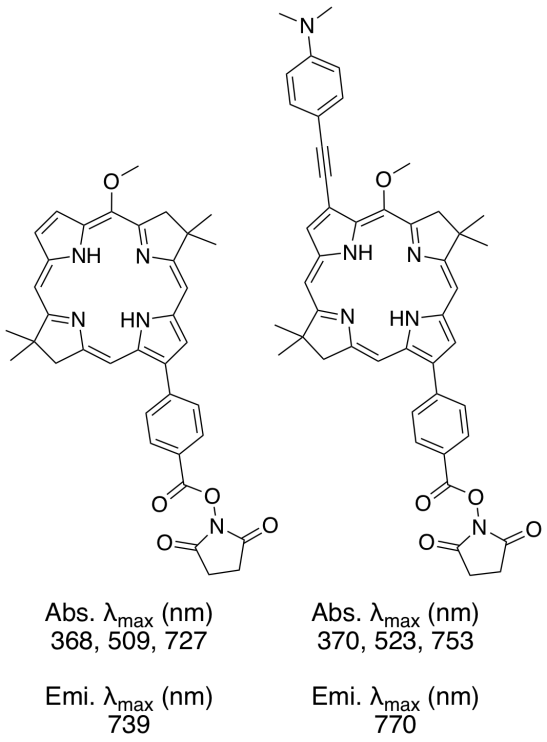

Figure 4.1: Bacteriochlorin analogs that were utilized for dual emission multiplexed imaging of tumor xenograft in mouse. Maxima were reported in DMSO.

For example, cyanines are commonly used for *in vivo* imaging and they possess an S_0-S_1 absorption band in the NIR, but their S_0-S_2 absorption band falls in the near UV.[273,274] Excitation in the ultraviolet region is avoided for *in vivo* imaging because UV light both fails to deeply penetrate tissue,[275] and kills surface cells by damaging DNA.[276] Building on the initial study, we have demonstrated (through the same collaboration) that two different bacteriochlorin-antibody conjugates can be utilized *in*

vivo, with clear resolution between chromophores.[267] This was made possible due to the narrow emission bands of the chosen bacteriochlorins (structure and maxima are shown in Figure 4.1).

Perhaps the greatest limitation of hydroporphyrins for dual-excitation fluorescence guided surgery is their weak absorbance in the green spectral window. The molar absorptivity coefficient *(ε)* at the maxima of the Q_x band (500-520 nm) is typically small for bacteriochlorins (35,000-40,000 $M^{-1}cm^{-1}$),[113] and weaker still for chlorins (8,000-13,000 $M^{-1}cm^{-1}$).[107] These ε values are significantly lower than that of chromophores sought after for fluorescence imaging (where ε >100,000 $M^{-1}cm^{-1}$), which in turn leads to lower fluorescence brightness (*B*). Brightness is the product of ε and Φ_F, therefore when one parameter is low, the imaging effectiveness of the chromophore declines. There does not appear to be a general consensus as to what the lower limit for a functionally bright fluorophore is, but there are several examples of red and NIR emitting dyes where *B* exceeds 50,000 $M^{-1}cm^{-1}$.[274,277]

To improve upon the low brightness of hydroporphyrins when excited in the green spectral window, we envisioned tethering an intensely green absorbing (and emitting) chromophore to the hydroporphyrin core, such that it acts as an energy donor to the hydroporphyrin. In the majority of cases, it is assumed that energy transfer occurs through-space (Förster Resonance Energy Transfer) which is dependent upon spectral overlap of the donor emission and acceptor absorption. Thus, for an energy donor to interact with the chlorin Q_x band it must interact strongly with green light.

At the time, there were already several examples of energy transfer arrays where the hydroporphyrin acted as either energy donor or acceptor.[122,278–285] One array in

particular interested us, in which a green absorbing rhodamine dye (energy donor) was tethered to a derivative of chlorophyll *a* (energy acceptor).[278] Rhodamine, being positively charged, can potentially act as an electron acceptor from a photoexcited hydroporphyrin, something unaddressed by Zheng et al.[278] Other literature suggested that in porphyrin-rhodamine arrays this photoinduced electron transfer (PET) occurs readily, so we chose not to pursue rhodamine as our energy donor.[286,287] Surveying the literature for a more suitable chromophore, 4,4-difluoro-4-bora-3a,4a-diaza-*s*-indacene (more commonly referred to as boron-dipyrromethene or BODIPY) stood out.[87,265,288–307] BODIPYs are neutral, have large molar absorptivity (up to 100,000 $M^{-1}cm^{-1}$),[265] have large Φ_F (up to 1)[265,308] and have been extensively studied as fluorescent probes.[309] In many examples the BODIPYs are acting as energy donor,[87,265,288–300,302,305] in some cases this is alongside deep red or NIR absorbing acceptor molecules,[301–307] including porphyrin containing systems.[87] When we began this work, only one example of a hydroporphyrin-BODIPY array was reported, but it incorporated an aza-BODIPY as the energy acceptor tethered to a semi-synthetic chlorophyll energy donor.[285] Therefore our work features the first examples of BODIPY-hydroporphyrin arrays, particularly those prepared from fully synthetic hydroporphyrins.

In this chapter we focus on the synthesis and characterization of the photophysical properties of novel BODIPY-chlorin energy transfer arrays. In designing the arrays, we considered that to be applicable in a real setting, they must have both high energy transfer efficiency (ETE) and resistance to any competitive processes that would decrease fluorescence intensity of the acceptor chlorin. The most problematic process for us would be photoinduced electron transfer (PET), as seen for rhodamine-

porphyrin arrays.[286,287] Our concern for this originated from the fact that 1) chlorins are well documented to undergo PET[282,310–312] and 2) reports show that BODIPY fluorescence is also subject to quenching by PET depending on peripheral substituents.[313] Furthermore, the fluorescence of Tamiaki's aza-BODIPY-chlorophyll *a* dyad was highly quenched in polar solvent.[285]

In addition to optimizing ETE and minimizing PET, we sought the ability to tune the chlorin's absorption and emission maxima, making the arrays suitable for multiplexed imaging. For example, taking two arrays with the same donor BODIPY and different acceptor chlorins, one could perform imaging using a single excitation wavelength (BODIPY absorption maxima) and distinguish arrays from one other by simply changing the detection wavelength. In order to work towards this, we needed only to tune the absorption and emission maxima of the chlorins by installing auxochromes at the 3- and 13- positions.[110,111]

To attain dyads with efficient energy transfer, minimal quenching and various emission maxima we explored two general types of arrays. The first set of arrays feature one or two BODIPYs connected to the chlorin macrocycle through 3- and 3-,13- positions via phenylethynyl linker. In these dyads (**ET1** and **ET2**) the phenylethynyl moiety also tunes the absorption and emission maxima of the chlorin, as emphasized in Chapter 2. In the second set of arrays we linked the two chromophores through the chlorin 10- position and BODIPY 8- position via N-phenyl benzamide. For the 10-linked dyads (**ET3** and **ET4**) we were able to place auxochromes independently of the BODIPY installation. By placing the BODIPYs on different positions of the chlorin periphery, we were able to probe the relationships between mutual orientation (κ^2) and

ETE. We also prepared two chlorin zinc (II) complexes (one from each set, **ZnET2** and **ZnET4**) to determine how the metal complexation impacts dyad properties. In particular, we anticipated that zinc containing arrays would more readily undergo PET, due to a higher (less negative) chlorin oxidation potential.[282] In the event that freebase chlorins showed minimal quenching, the zinc complexes would help us understand the relationship between linker type and PET. It is worth noting, that for this first stage of our research, we opted to utilize only chlorins (as opposed to bacteriochlorins) because they are slightly easier to prepare, and current methodology does not allow one to easily prepare 10-substituted bacteriochlorins.[113,314] Overall, our array designs gave a wide array of chlorin photochemical and redox properties, while keeping BODIPY properties constant. In addition to the target energy transfer arrays, we prepared model compounds for both donor and acceptor roles. For energy donor benchmarks, two BODIPY derivatives (**B1-TMS** and **B2-A**) were synthesized. A total of four energy acceptor benchmarks were prepared, including three freebase chlorins featuring no (**C2**), one (**C2-P**) or two (**C2-2P**) phenylethynyl substituents, and one zinc (II) chlorin complex (**ZnC2-2P**). Such benchmark compounds are necessary to properly characterize the separate components of energy transfer arrays, because arrays are expected to behave as a sum of their parts. The structures of all energy transfer arrays and model compounds can be seen in Table 4.1.

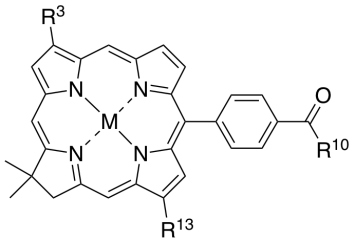

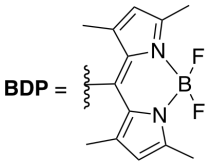

Compound	R^3	R^{10}	R^{13}	M
chlorin-BODIPY dyads				
ET1	-H	-OMe	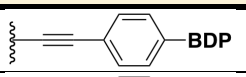	-H, -H
ET2	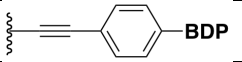	-OMe	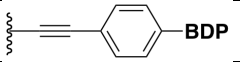	-H, -H
ZnET2	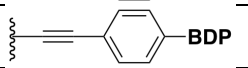	-OMe	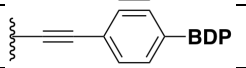	-Zn
ET3	-H	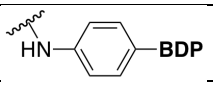	-H	-H, -H
ET4	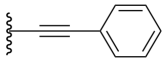	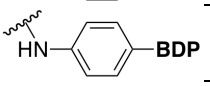	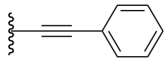	-H, -H
ZnET4	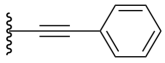	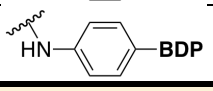	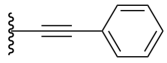	-Zn
chlorin monomers				
C2	-H	-OMe	-H	-H, -H
C2-P	-H	-OMe	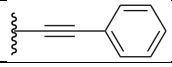	-H, -H
C2-2P	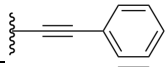	-OMe	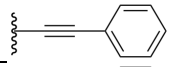	-H, -H
ZnC2-2P	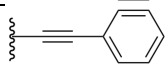	-OMe	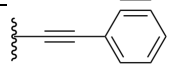	-Zn

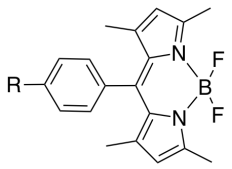

BODIPY	R
B1-TMS	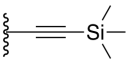
B2-A	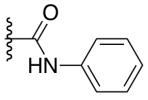

Chart 4.1: Target chlorin-BODIPY energy transfer arrays and benchmark monomers discussed in Chapter 4.

Section 4.2: Synthesis

Our general approach to dyad synthesis focuses on a few key themes 1) hydroporphyrin component should be manipulated as few times as possible to minimize loss of the most valuable/difficult to prepare component 2) energy transfer array should be prepared in the final reaction with no need for further tuning of optical properties 3) final reaction must feature mild conditions to retain chromophore integrity. To address point 1, we utilized our auxochrome of choice (phenylethynyl) as the linker when applicable. Point 3 becomes much more apparent in chapters 5 and 6, where modification (such as water solubilization) of the chromophore is extensively focused toward the BODIPY component. Keeping to points 2 and 3, we focused on EDC mediated amide synthesis and Sonogashira cross coupling as our methods of linking BODIPYs to chlorin.

The critical reactions then, are the Sonogashira coupling required to prepare dyads **ET1** and **ET2**, as well as the synthesis of dyads **ET3** and **ET4** through amide coupling. For **ET1** and **ET2**, we prepared a known BODIPY featuring a *meso* phenylethynyl substituent (**B1**)[43,315–317] that could be conjugated to a bromo-chlorin. Our preparation of **B1** followed a popular three step, one pot synthesis that was not described for this particular BODIPY (Scheme 4.1). Of the requisite 3-bromo and 3,13-dibromo chlorins, only **C2-Br** was known.[122] We prepared dibromo-chlorin **C2-2Br**, via an analogous route, details of which are described below. For dyads **ET3** and **ET4** we required chlorins possessing 4-(carboxy)phenyl substituents at the chlorin 10-position, and BODIPY with terminal amine. A suitable BODIPY, 8-(4-amino)phenyl BODIPY (**B2**)[318] was already known, and the ester of **C2-2Br** could be hydrolyzed for

preparation of **ET4**, however, we required another chlorin lacking 3,13- substituents to prepare **ET3**. The synthesis of this chlorin, **C2**, and its new precursors are also described below. In addition, dyads **ZnET2** and **ZnET4** were prepared directly from **ET2** and **ET4**, and model compounds were prepared in analogous fashion to the dyads via either Sonogashira coupling (**C2-P**, **C2-2P**) or EDC mediated amide coupling (**B2-A**).

Section 4.2.1: Synthesis of Parent Chromophores & Model Compounds

As noted above, **B1** and its precursor (**B1-TMS**) have been reported several times before, but we prepared them by a slightly different method.[43,315–317] First, **B1-TMS** was prepared by treating a mixture of 4-[(trimethylsilyl)ethynyl]benzaldehyde **9** and 2,4-dimethylpyrrole **10** with TFA, generating intermediate dipyrromethane, which was then oxidized to dipyrrin by the addition of DDQ. Next, dipyrrin was converted to BODIPY by treatment with Et_3N and $BF_3{\cdot}OEt_2$ (Scheme 4.1). After the three steps, **B1-TMS** was acquired in 23% yield. Subsequent desilylation was performed using K_2CO_3 in THF/MeOH following a reported procedure,[43,315–317] yielding target ethynyl terminated BODIPY, **B1** in 60% yield (Scheme 4.1).

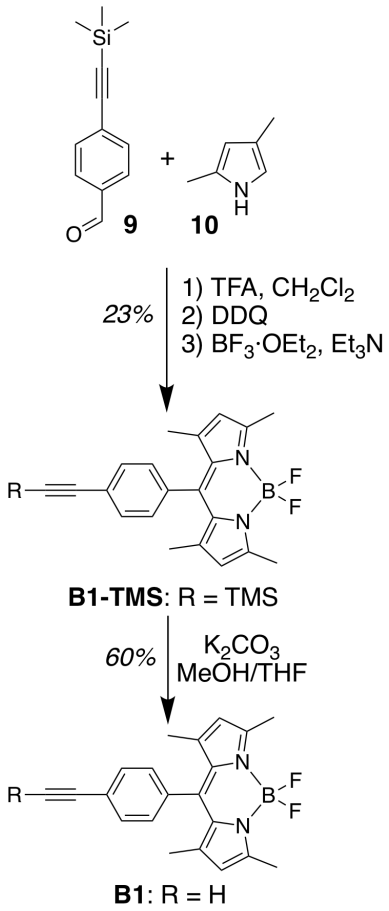

Scheme 4.1: Synthesis of BODIPY benchmark B1-TMS and silyl-deprotected B1.

BODIPY **B1-TMS** was utilized as our first benchmark, for phenylethynyl linked dyads, and required no further modification. For our amide linked arrays we prepared a second BODIPY benchmark. This was done by coupling 8-(4-amino)phenyl substituted **B2** with benzoic acid in the presence of EDC·HCl, to yield **B2-A** (80%, Scheme 4.2).

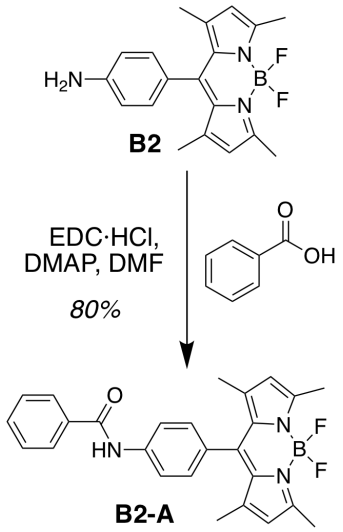

Scheme 4.2: Synthesis of benchmark BODIPY B2-A.

Chlorins **C2** and **C2-2Br** were prepared beginning from the known, shared precursor formyldipyrromethane **11**.[122] The bromination of **11**, with either 1 or 2 equivalents of N-bromosuccinimide, provides 1-bromo-9-formyldipyrromethane **EH2-Br** (94%) or 1,2-dibromo-9-formyldipyrromethane **EH2-2Br** (67%), respectively (Scheme 4.3). Following the usual process for chlorin synthesis we then prepared the two new chlorins by the two-pot procedure involving condensation of eastern half with western half (for **C2**, **EH2-Br** with tetrahydrodipyrrin **WH**,[115] and for **C2-2Br**, **EH2-2Br** with 8-bromotetrahydrodipyrrin **WH-Br**[116]) in the presence of *p*-toluenesulfonic acid, followed by zinc-templated oxidative cyclization with subsequent removal of zinc. After three steps, **C2** was isolated in 25% yield, and **C2-2Br** in 17% yield (Scheme 4.3).

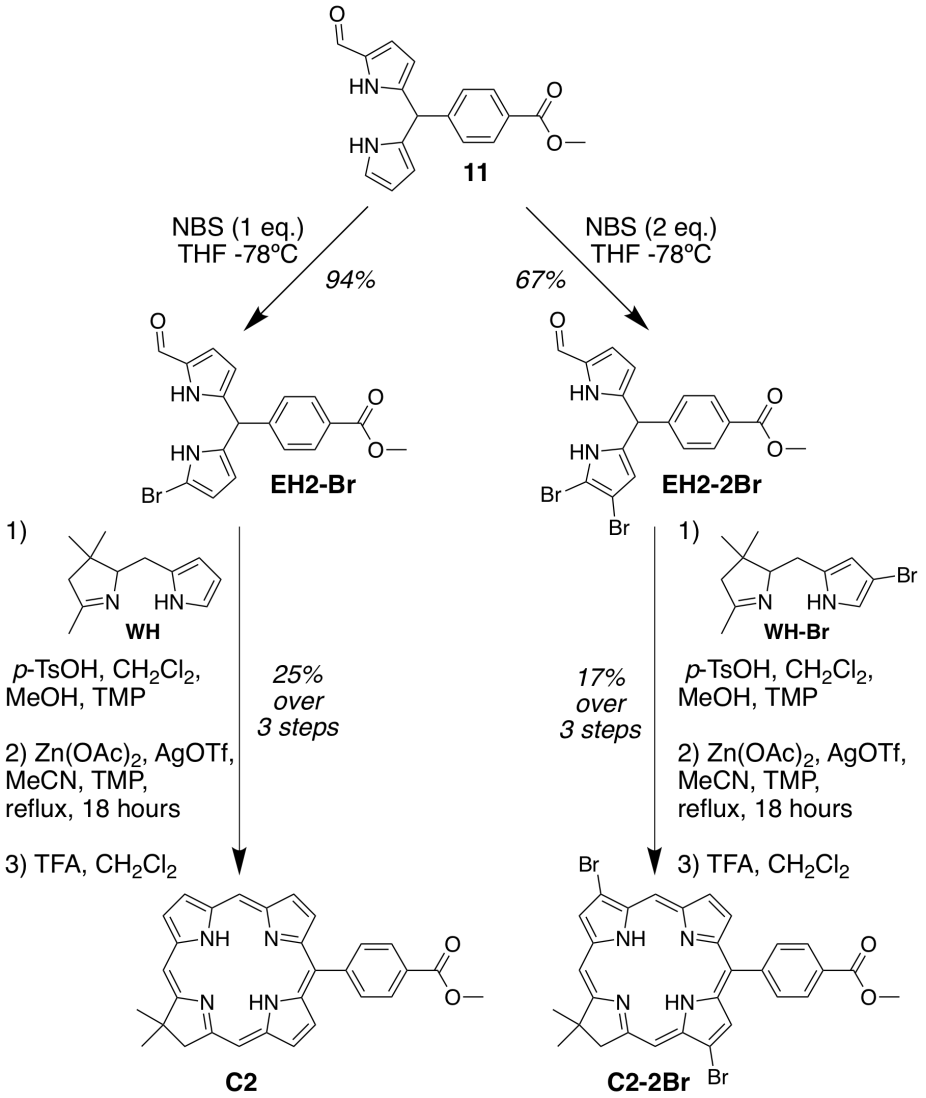

Scheme 4.3: Synthesis of novel chlorins C2 and C2-2Br, and their respective precursors EH2-Br and EH2-2Br.

Chlorin **C2** was utilized as the first benchmark monomer, due to its lack of auxochromes, and the remaining benchmark chlorins were prepared from either **C2-Br** or **C2-2Br**. Both substituted benchmarks were prepared via Sonogashira cross coupling with phenylacetylene **2** catalyzed by $(PPh_3)_2PdCl_2$ in DMF/Et_3N (conditions previously optimized for bacteriochlorins).[120] **C2-P** was synthesized from **C2-Br** in 84% yield, while **C2-2P** was prepared from **C2-2Br** in 60% yield (Scheme 4.4). The final chlorin

benchmark, **ZnC2-2P** was prepared by treatment of **C2-2P** with zinc (II) acetate in $CHCl_3$/MeOH (5:1), giving the chlorin zinc chelate in 71% yield (Scheme 4.4.).

Section 4.2.2: Synthesis of 3- and 3,13- position linked arrays

Phenylethynyl linked energy transfer arrays were prepared by Sonogashira cross coupling analogous to their benchmark monomers. We screened two sets of previously reported conditions [$Pd_2(dba)_2$ and tris(*o*-tolyl)phosphine in toluene/Et_3N,[108] or $(PPh_3)_2PdCl_2$ in DMF/Et_3N][120] that were utilized to install auxochromes on hydroporphyrins, both of which avoid the use of copper. When we reacted **B1** with either **C2-Br** or **C2-2Br** catalyzed by $(PPh_3)_2PdCl_2$ we noted both improved yields and less difficulty with purification due to lack of tris(*o*-tolyl)phosphine (based upon ^1H NMR analysis). Following the better set of conditions, we were able to prepare **ET1** and **ET2** in 52% and 47% yields, respectively (Scheme 4.5).

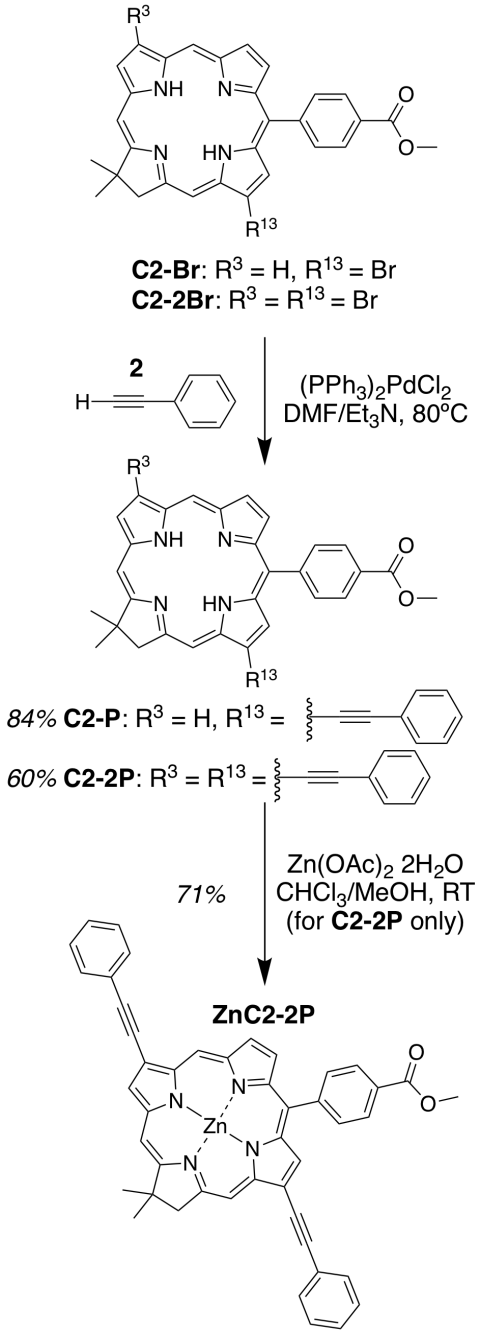

Scheme 4.4: Synthesis of benchmark chlorin monomers C2-P, C2-2P and ZnC2-2P.

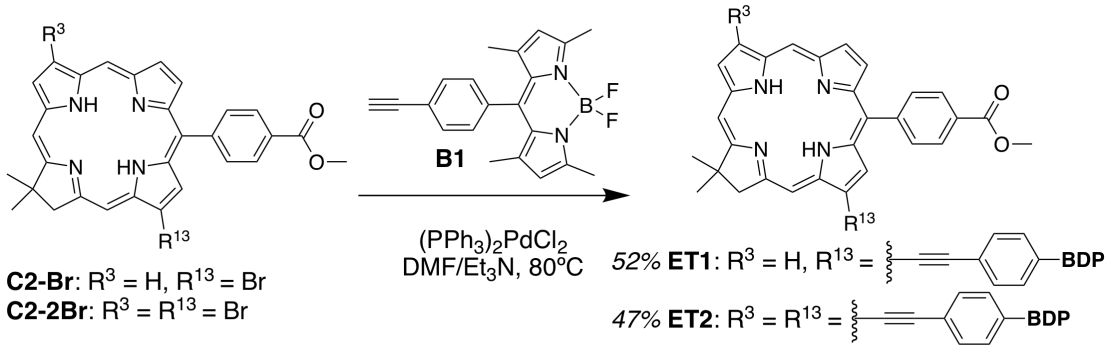

Scheme 4.5: Synthesis of chlorin-BODIPY arrays ET1 and ET2 by Sonogashira cross coupling

Subsequently, **ET2** was converted to the zinc (II) complex by treatment with zinc (II) acetate in $CHCl_3$/MeOH (5:1), yielding **ZnET2** (50%, Scheme 4.6). Such zinc insertions on chlorin monomers are typically high yielding, the same was not true here as we required excessive washing with methanol to remove all fluorescent impurities.

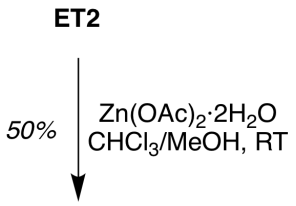

Scheme 4.6: Zinc metalation of dyad ET2

Section 4.2.3: Synthesis of 10-position linked arrays

Energy transfer arrays **ET3** and **ET4** were prepared by EDC mediated amide synthesis of amino BODIPY **B2** with carboxylic acid functionalized chlorins. The ester functionalized chlorins **C2** and **C2-2P** were first dissolved in a solution of THF/methanol, then hydrolyzed by treatment with NaOH (1M, aq.), quantitatively yielding the acid chlorins **C2-COOH** and **C2-2P-COOH** (not shown). The integrity of these intermediates was confirmed by both ^{1}H NMR and absorption spectroscopy before being reacted with BODIPY **B2** in the presence of EDC·HCl and DMAP (Scheme 4.7). This pair of reactions yielded arrays **ET3** and **ET4** in 53% and 25%

yield, respectively. The yield of **ET4** is noticeably lower than that of **ET3**, we attribute this to the difficulty of removing fluorescent impurities, requiring numerous solvent washes. From **ET4**, the zinc complex **ZnET4** was prepared in analogous fashion as **ZnET2**, in 57% yield (Scheme 4.7).

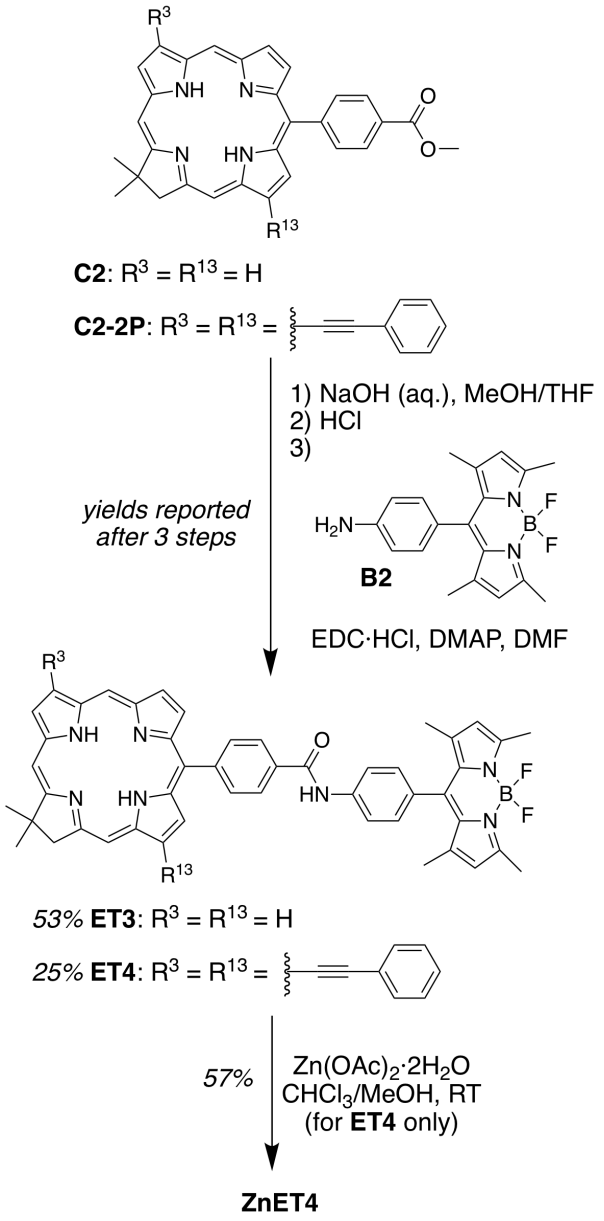

Scheme 4.7: Synthesis of arrays ET3 and ET4 by amidation and ZnET4 by zinc insertion.

Section 4.3: Characterization of Compounds

Section 4.3.1: Structure Determination

All novel compounds were characterized by ^{1}H and ^{13}C NMR, and HRMS. Arrays were also characterized by ^{19}F NMR to confirm integrity of BODIPY upon dyad preparation. We were unable to acquire ^{13}C or ^{19}F NMR of appreciable quality for dyad **ET2**, due to its poor solubility. All NMR and HRMS data are consistent with those expected for the given compound. Specifically, ^{1}H NMR resonances integrate such that BODIPY and chlorin are clearly in a 1-to-1 ratio for all arrays, except **ET2** and **ZnET2**. Instead, **ET2** and **ZnET2** correctly show a BODIPY to chlorin ratio of 2:1 where the two BODIPYs are chemically non-equivalent. For

these arrays we observed nearly identical but unique chemical shifts for all expected BODIPY resonances, and the individual BODIPYs retain symmetry due to free rotation where ethynyl linker meets chlorin macrocycle (e.g., we observe two nearly overlapping singlets at δ ~6.05-6.06 ppm, each with integration of two, corresponding to two sets of BODIPY pyrrolic hydrogen). It is worth noting that, in the case of **ZnET2**, ^{1}H NMR was acquired from the crude sample. This is because after purification the compound becomes insoluble in common organic solvents, preventing us from recording any meaningful ^{1}H NMR spectrum.

Section 4.3.2: Photophysical Characterization

For all novel arrays, we acquired absorption and emission spectra, fluorescence quantum yields and determined the energy transfer efficiency. Both Φ_F and ETE were determined in toluene and DMF to determine how solvent polarity affects the properties, particularly with regard to quenching. For all novel monomers we also acquired absorption and emission spectra and determined Φ_F in the case of benchmark chlorins. At this time, we did not determine the fluorescence quantum yields for benchmark BODIPYs, as we were primarily interested in identifying their absorption and emission maxima to compare against those observed in the dyads. The normalized absorption spectra of dyads can be found in Figure 4.2. Figure 4.3 features a closer view of the Q_y absorption bands for clarity, as well as the emission spectra of dyads. The electronic spectra of benchmark monomers can be found in Figure 4.4. A summary of all absorption and emission properties can be found in Table 4.1.

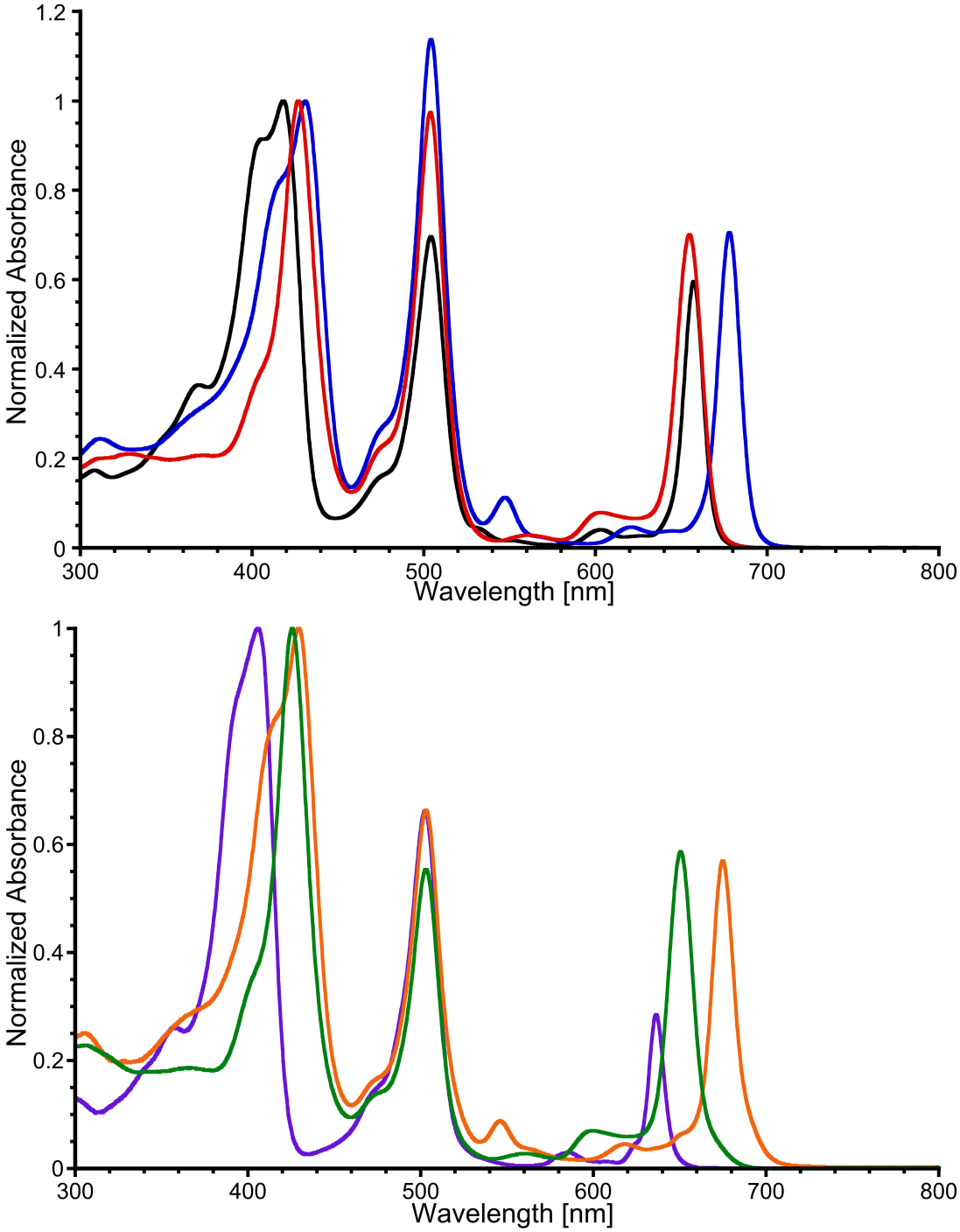

Figure 4.2: Normalized absorption spectra of dyads ET1 (black), ET2 (blue), ZnET2 (red), ET3 (purple), ET4 (orange) and ZnET4 (green). Spectra of dyads ET1, ET2, ZnET2 on top, while spectra of dyads ET3, ET4, ZnET4 on bottom. All spectra acquired in air-equilibrated toluene at ~10μM concentration of array, then normalized at chlorin *B* band.

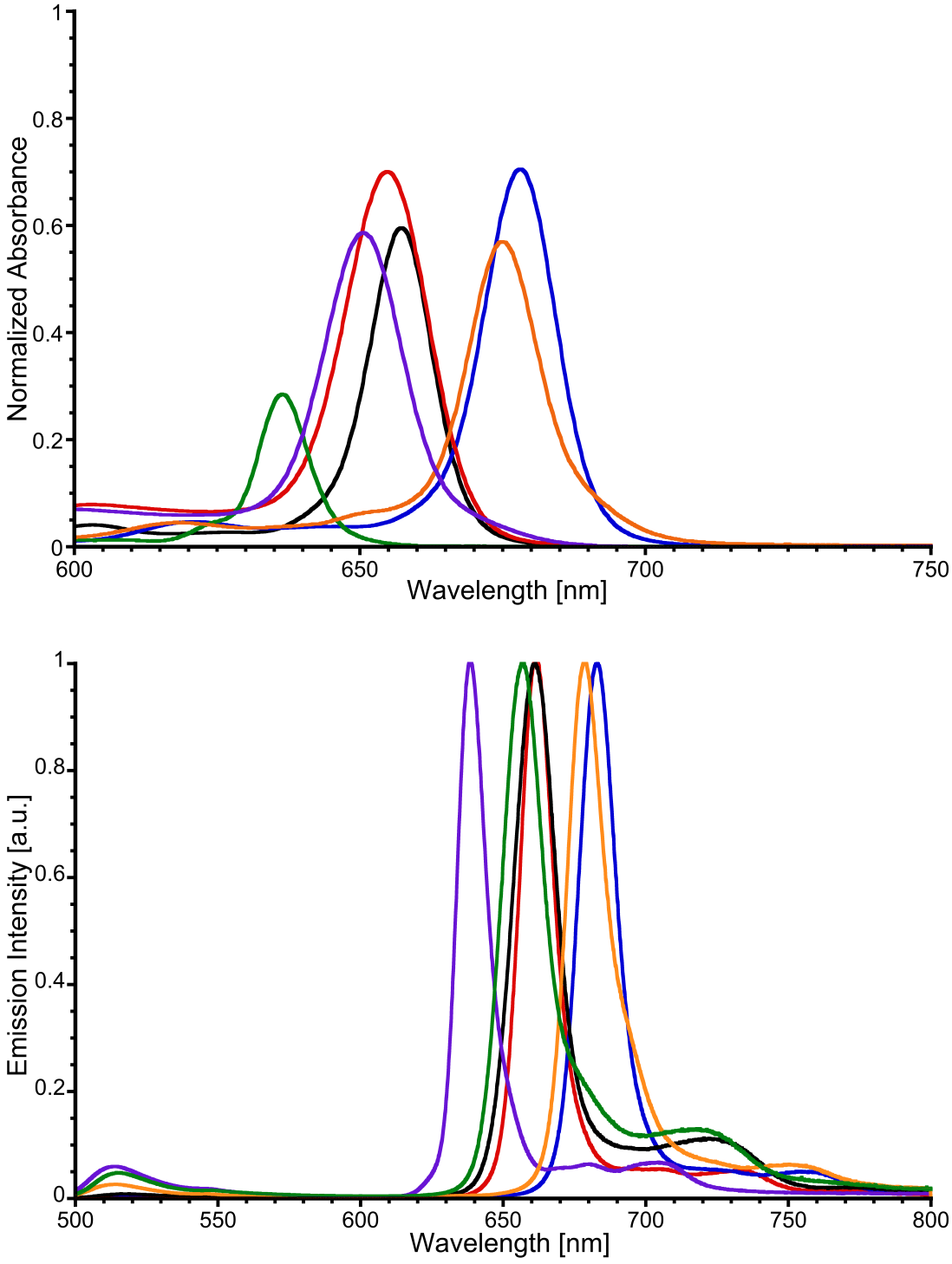

Figure 4.3: Close up of normalized absorption spectra (top) and normalized emission spectra (bottom) of dyads ET1 (black), ET2 (blue), ZnET2 (red), ET3 (purple), ET4 (green) and ZnET4 (orange). All spectra acquired in air-equilibrated toluene, absorption spectra at concentration of ~10 µM and emission spectra at ~1.0 µM. Absorption normalized at *B* band for chlorins, for dyad emission, excitation occurred at blue edge of BODIPY S_0-S_1 band, where slope was minimal (~10-20 nm below λ_{max}).

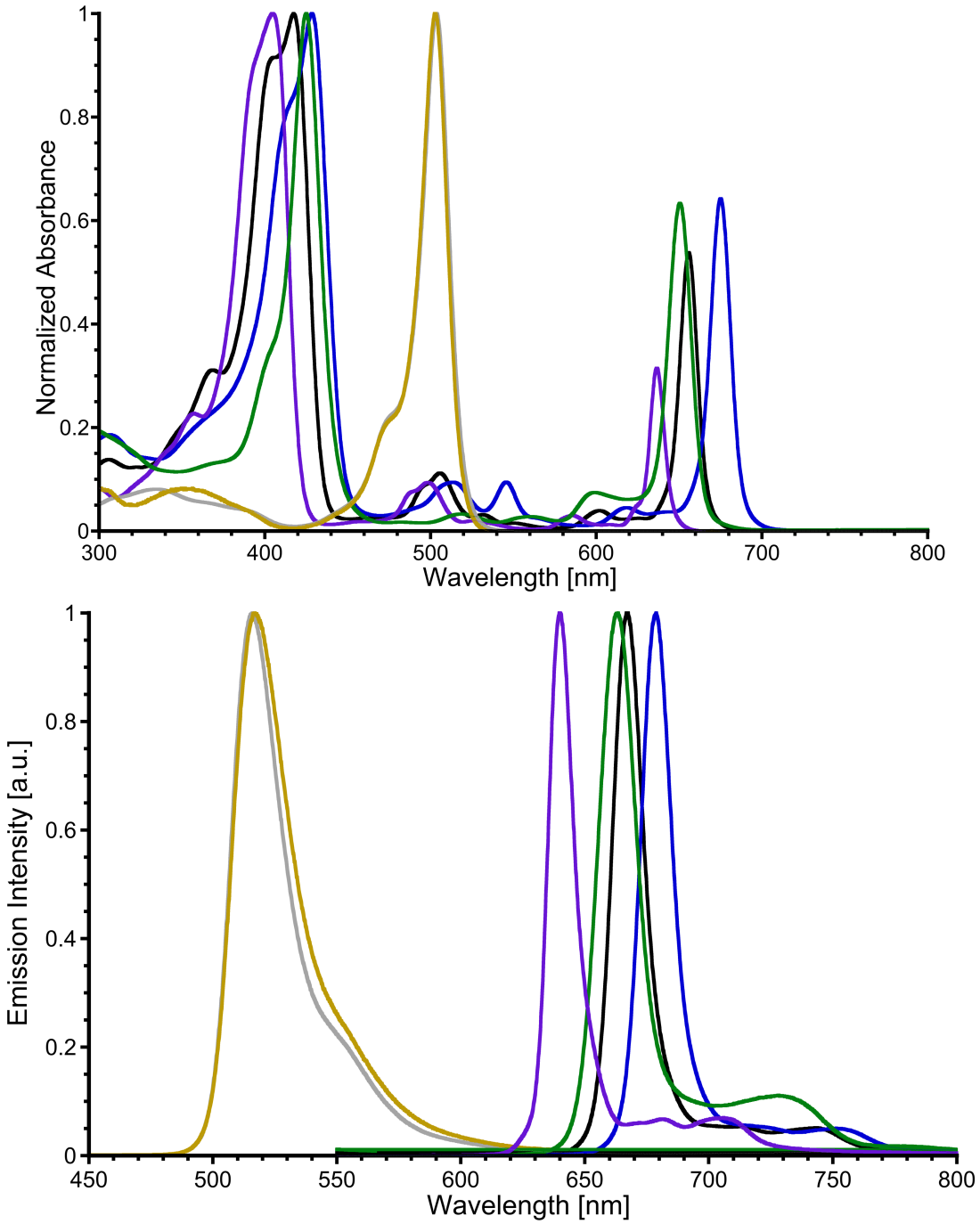

Figure 4.4: Normalized absorption (top) and emission spectra (bottom) of benchmarks C2 (purple), C2-P (black), C2-2P (blue), ZnC2-2P (green) and BODIPY benchmarks B1-TMS (gold) and B2-A (grey). All spectra acquired in air-equilibrated toluene, absorption spectra at ~10μM chromophore concentration and emission at ~1.0μM chromophore concentration; all spectra normalized against most intense band. For emission, chlorins were irradiated at *B* band, BODIPY were irradiated at blue edge of S_0-S_1 absorption band, where slope was minimal (~10-20 nm below λ_{max}).

Compound	Absorption λ_{max} [nm]			λ_{emi} [nm]	Φ_F tol. (DMF)	ETE tol. (DMF)
	$\lambda_{B\ band}$	λ_{BODIPY}/ λ_{Qx}	λ_{Qy}			
energy transfer arrays						
ET1	404, 418	504	657	661	0.35 (0.25)	0.97 (0.96)
ET2	431	504, 548	678	683	0.41 (0.38)	0.96 (0.97)
ET3	406	503	636	641	0.21 (0.20)	0.90 (0.92)
ET4	428	503, 546	675	681	0.37 (0.36)	0.92 (0.88)
ZnET2	427	504	658	661	0.37 (0.011)	0.88[†)]
ZnET4	426	503	651	655	0.31 (0.32)	0.87 (0.80)
chlorin monomers						
C2	405	499	636	641	0.21 (0.20)	
C2-P	402, 417	506	656	659	0.33 (0.34)	
C2-2P	431	514, 546	675	681	0.37 (0.36)	
ZnC2-2P	425	519	651	656	0.33 (0.38)	
BODIPY monomers						
B1-TMS		504		517		
B2-A		503		516		

Table 4.1: Absorption and emission properties of chlorin-BODIPY arrays and benchmark monomers. All values were determined in air-equilibrated toluene, or air-equilibrated DMF where indicated. Reported fluorescence quantum yields were determined upon direct excitation of chlorin component at *B* band. Φ_F values were determined using TPP in air-equilibrated toluene as standard.[109] Energy transfer efficiency (ETE) was defined as Φ_F of chlorin upon excitation at BODIPY, over Φ_F of chlorin upon direct excitation at *B* band. †) ETE was not determined in DMF due to poor emission intensity. Error for quantum yield measurements estimated at ± 5% (see section 2.5.4 for details), error for ETE estimated at ± 10% (see section 4.5.4).

The absorption spectra of all chlorin monomers exhibit the typical *B*, Q_x and Q_y bands in the UV (400-420 nm), green (~515 nm) and red to deep-red (600-650 nm) spectral windows. As demonstrated in Chapter 2, progressively increasing the number of conjugated auxochromes results in the proportional bathochromic shift of the Q_y band, increasing from 636 nm (**C2**) up to 656 nm (**C2-P**) then 675 nm (**C2-2P**). Zinc chelation of **C2-2P** resulted in a hypsochromic shift, as has been well documented for other hydroporphyrins in the literature.[110,281] The absorption spectra of benchmark BODIPYs exhibit the expected S_0-S_1 band in the green region with much weaker S_0-S_2 band in the UV region.

As anticipated, the absorption spectra of the arrays are essentially the sum of the parts, with the chlorin *B* and Q_y bands distinct in the UV and red spectral regions, while the BODIPY S_0-S_1 band appears in the green spectral window (overshadowing the Q_x band of chlorin). This simple assessment is critical because it demonstrates that neither the phenylethynyl nor amide linker provides strong electronic communication between chromophores. For the phenylethynyl linked dyads, absorption maxima were slightly red shifted (1-7 nm) compared to corresponding benchmark monomers (**ET1** ≈ **C2-P** + **B1-TMS**, **ET2** ≈ **C2-2P** + **B1-TMS**, and **ZnET2** ≈ **ZnC2-2P** + **B1-TMS**). While for the amide linked dyads, absorption maxima were identical to those of corresponding monomers (**ET3** = **C2** + **B2-A**, **ET4** = **C2-2P** + **B2-A**, and **ZnET4** = **ZnC2-2P** + **B2-A**).

The emission spectra of all chlorin monomers feature a single, narrow emission band with a small Stokes' shift (1-6 nm). Benchmark BODIPYs **B1-TMS** and **B2-A** show emission maxima at 517 nm and 516 nm, respectively. The emission spectra of

the energy transfer arrays show strong emission from the chlorin unit, with negligible emission from the BODIPY unit, regardless of excitation wavelength (either BODIPY at ~515 nm, or chlorin at ~410 nm). The emission maxima of dyads behave exactly as the maxima of the absorption bands; dyads **ET1**, **ET2** and **ZnET2** share identical emission maxima to respective chlorin monomers while **ET3**, **ET4** and **ZnET4** show a slight bathochromic shift (2-5 nm) relative to their benchmarks. The poor emission of BODIPY upon conjugation to chlorin qualitatively demonstrates that energy transfer is quite efficient in all novel arrays. In addition, we acquired the excitation spectra of all novel dyads when monitoring emission exclusively from the chlorin component. The excitation and absorption spectra closely matched for all dyads, further demonstrating the high efficiency of energy transfer.

Next, we wanted to quantitatively assess the fluorescence properties of all new compounds. We began by determining the fluorescence quantum yields of the chlorin benchmarks. The Φ_F for chlorin monomers increases with the number of phenylethynyl substituents at the 3- and 13- positions, the values were 0.21 for unsubstituted **C2**, 0.33 for monosubstituted **C2-P** and 0.37 for disubstituted **C2-2P**, all in toluene. This is consistent with what we observed in Chapter 2, where Φ_F increased between chlorins **C1-P** and **C2-2P**, except here the chlorin *meso* substituents are identical. Note that values for **C2-2P**, were reported in Chapter 2, they are reproduced here. The zinc coordinated chlorin **ZnC2-2P** showed similarly large Φ_F of 0.33 in toluene, which is consistent behavior for other chlorins in the literature when going from freebase to zinc chelate.[110,281] Fluorescence quantum yields determined in DMF were nearly identical to those determined in toluene, except in the case of **ZnC2-2P**. **ZnC2-2P** showed a

marked increase of Φ_F in DMF. Such behavior agrees with the literature, where zinc porphyrins have been shown to exhibit slight fluorescence enhancement in coordinating vs. non-coordinating solvents (e.g, for zinc (II) chelated tetraphenylporphyrin, Φ_F = 0.033 in toluene and 0.038 in pyridine).[319]

For determination of the Φ_F of chlorin subunits in our arrays, we irradiated the chlorins at the *B* band (410-430 nm) where BODIPY absorbance is minimal. In toluene, the Φ_F of dyads **ET1** and **ET2** were slightly larger than corresponding monomers **C2-P** and **C2-2P**, while **ET3** and **ET4** showed identical Φ_F to monomers **C2-P** and **C2-2P**, respectively. This indicates that in nonpolar solvents, the presence of the BODIPY (which could act as an electron acceptor) does not quench chlorin fluorescence. In DMF, the Φ_F values of **ET3** and **ET4** are identical to those determined in toluene, while arrays **ET1** and **ET2** show some reduction of Φ_F. The Φ_F of **ET1** diminishes from 0.35 to 0.25 (30% decrease) when going from toluene to DMF, while **ET2** drops from 0.41 to 0.38 (7% decrease). The behavior of dyads containing zinc chelated chlorins mirrored that of their freebase counterparts in toluene; dyad **ZnET2** showed slightly enhanced fluorescence relative to monomer **ZnC2-2P**, while **ZnET4** showed nearly identical Φ_F to **ZnC2-2P**. Their behavior in DMF was significantly different, however, as dyad **ZnET4** showed identical Φ_F in either solvent, while the fluorescence quantum yield of **ZnET2** decreased by approximately 30-fold (Φ_F = 0.011).

Energy transfer efficiency is commonly determined by comparing the fluorescence lifetime of the energy donor, in both the presence and absence of the energy acceptor.[8] However, we lacked regular access to time-domain fluorescence spectroscopy, so we assessed ETE slightly differently. ETE was calculated as the ratio

of Φ_F of the energy acceptor upon excitation of the energy donor, over Φ_F of the energy acceptor upon direct excitation. The closer this ratio is to one the more efficient the energy transfer, i.e. an ETE of unity indicates that for each photon absorbed by donor, one photon is emitted by acceptor. In addition, we measured Φ_F in a high polarity solvent (DMF) and compared against Φ_F determined in non-polar solvent (toluene) to probe for quenching processes. The assumption is that the more polar a solvent is, the better it stabilizes a charge separated state, facilitating photoinduced electron transfer (PET). It is shown in the literature that hydroporphyrin monomers typically undergo minimal quenching by PET in polar solvents,[110,281] however, we were concerned it would impact the function of the arrays.

For our arrays, ETE was found as the ratio of Φ_F of the chlorin energy acceptor upon selective excitation of BODIPY maxima (~505 nm) over Φ_F of the chlorin component upon direct excitation (at *B* band, 410-430 nm). Both excitation wavelengths are selected such that the other chromophore possesses minimal absorption in that region. In all cases, ETE for the freebase chlorin containing dyads met or exceeded 0.9 in toluene, and zinc coordinated chlorins were just below 0.9 (ETE = 0.88 for **ZnET2** and 0.87 for **ZnET4**). In DMF, the ETE for freebase dyads did not change significantly (± 0.02 relative to ETE determined in toluene), while dyad **ZnET4** showed approximately one tenth reduction of ETE in DMF (0.80) relative to that in toluene. Due to its weak emission intensity, we were unable to determine the ETE of **ZnET2** in DMF.

We attribute the high ETE in our arrays to the large spectral overlap of the BODIPY emission band with the Q_x absorption band of the chlorin. Because the

BODIPY maxima remain constant, and the Q_x bands change very little between arrays, this was the anticipated result. The lowered ETE for dyad **ZnET2** is most likely the result of lower oscillator strength of the zinc chlorin's Q_x band relative to that of freebase, a trend that has been previously documented.[107,111]

Arrays **ET2**, **ET3** and **ET4** all showed minimal quenching (7% or less decrease relative to Φ_F determined in toluene) while array **ET1** showed greater but incomplete quenching of fluorescence signal (29%). In contrast to this, the zinc chlorin containing dyads behaved dissimilarly in DMF. **ZnET4** showed no change of Φ_F when going from toluene to DMF, where **ZnET2** became nearly non-emissive. This indicates that in DMF **ZnET2** undergoes significant quenching, where **ZnET4** is unaffected. The contrast between **ZnET2** and **ZnET4** clearly demonstrates that the amide linked is less susceptible to quenching, while the phenylethynyl linker is more prone to quenching. This is an important finding because it demonstrates that BODIPY-chlorin energy transfer arrays linked through an amide (such as **ZnET4**) will function much better as imaging agents in solvents of high dielectric constant.

To determine the favorability of electron transfer in each of these systems we utilized the simplified Weller equation[1,2] with solvent parameter omitted:

$$\Delta G = e\left[E_{1/2}^{ox}(donor) - E_{1/2}^{red}(acceptor)\right] - E_{00}$$

where *e* is the electron charge, $E_{1/2}^{ox}(donor)$ is the half-wave oxidation potential of the electron donor, $E_{1/2}^{red}(acceptor)$ is the half-wave reduction potential of the electron acceptor and E_{00} is the energy of the singlet excited state (determined as the average energy between absorption and emission maxima). In lieu of electrochemical data for the compounds used in this study, we found oxidation and reduction half-wave

potentials for hydroporphyrins which closely resemble those studied here (see Table 4.3, Section 4.5.5). In addition, we approximated E_{00} from the Q_y absorption and emission maxima of the hydroporphyrin component of each dyad. We estimated that for **ET2**, ΔG = 0.07 eV, for **ET1** ΔG = -0.10 eV and for **ZnET2** ΔG = -0.27 eV. The trend of decreasing ΔG corresponds to increased quenching for phenylethynyl linked dyads: **ET2** (~0%) < **ET1** (29%) << **ZnET2** (~100%). Suggesting PET from hydroporphyrin to BODIPY is the main mechanism of quenching here. These trends reflect the facts that sequential installation of phenylethynyl substituents at the chlorin 3- and/or 13- positions results in a proportional increase of the chlorin's oxidation potential,[111,282] while installation of zinc reduces the oxidation potential.[282] Also note that we anticipate very similar values of ΔG for electron transfer in the amide linked arrays and the corresponding phenylethynyl linked arrays, further emphasizing the ability of the amide linker to resist quenching.

We also calculated ΔG for the opposite scenario, where the BODIPY component is oxidized and the hydroporphyrin is reduced. For **ET1** and **ZnET2**, the ΔG was positive (0.22-0.24 eV) while for **ET2**, it was only slightly negative (-0.03 eV). Thus, PET from chlorin to BODIPY does not appear energetically favorable for **ET1** and **ZnET2**, while for **ET2** it could be feasible, however, we do not observe any quenching in the case of **ET2**.

Oxidative PET as the mechanism of quenching is further supported by the fact that ETE in dyads is conserved between solvents (in most cases), suggesting quenching occurs after the chlorin becomes excited (either from energy transfer or direct excitation). The other quenching process that would be probable given the solutions

contain only dyad, would be static quenching. For porphyrins and hydroporphyrins static quenching is typically aggregation, which will be apparent in the absorption spectrum.

From a structural design perspective, it is important to emphasize that all of the 10- position/amide linked dyads show negligible quenching in DMF, while the 3,13-phenylethynyl linked dyads are quenched to varying degrees. The most astonishing difference is that between the two zinc containing dyads, because in both possess their chlorin components have comparable oxidation potentials. The lack of quenching for **ZnET4** and near absolute quenching of **ZnET2** demonstrates that the way in which the chlorin and BODIPY chromophores are linked plays a significant role in the resulting properties. It is possible that the linker position plays a role as well, however, for dyads with similar redox properties (**ET2** vs **ET4** and **ZnET2** vs **ZnET4**) the amide linked dyad was always highly fluorescent where the phenylethynyl linked one was subject to quenching in polar solvent, suggesting the type of linker is the most critical factor.

One explanation as to why the phenylethynyl linked dyads are more prone to quenching is the presence of weak electronic coupling, where there is none in the amide linked dyads. There are two key factors which suggest weak electronic coupling between BODIPY and chlorin in dyads **ET1**, **ET2** and **ZnET2**, their increased Φ_F (10-20%) and bathochromically shifted absorption (1-6 nm) and emission maxima (2-5 nm) relative to respective monomers. If there were truly no electronic communication, then these dyads would have identical maxima and Φ_F, to their benchmark monomers, as was the case for amide linked dyads **ET3**, **ET4** and **ZnET4**. Conversely, the complete lack of electronic communication in amide linked dyads is probably the reason they are

highly resistant to PET based quenching. The likelihood that the phenylethynyl linker is responsible for promoting PET through excitonic coupling is supported by Odobel's work on porphyrin dimers.[59,60,320] Odobel's arrays feature linkers comprised of consecutive phenylethynyl moieties that are ultimately conjugated to terminal porphyrins via triple bond. In such arrays they observed ultrafast electron transfer (lifetime of electron transfer below 7 ps) due to the high degree of electronic coupling.[59,60,320] We had originally anticipated that the phenylethynyl moieties in our dyads would fall in plane with respect to the chlorin, and perpendicular to the BODIPY (due to presence of BODIPYs 1,7-position methyl substituents), preventing conjugation. The observed behavior suggests that the BODIPY plane is only twisted relative to that of the linker. We recognize that despite the literature suggesting PET is present, time-resolved spectroscopic and electrochemical measurements are necessary in order to better confirm the mechanism of quenching in our arrays.

To determine if similar quenching is observed in other solvents of high polarity, we also determined Φ_F for our arrays in numerous common organic solvents (Table 4.2). Note that the values presented in Table 4.2 differ slightly from those in Table 4.1, because here we report Φ_F upon excitation at BODIPY, as opposed to direct excitation at chlorin. The Φ_F determined for **ET3**, **ET4** and **ZnET4** further demonstrate the versatility of the amide linked arrays, as their values closely agreed with those found in toluene (i.e., values found in DMSO and toluene are identical within experimental error). Dyad **ET1** showed further decrease of Φ_F relative to that in DMF, while dyad **ZnET2** was again only weakly emissive. In methanol, the Φ_F of **ET3**, **ET4** and **ZnET4** were slightly diminished, retaining ~70% of value found in toluene. Certainly, the

Compound	Solvent (dielectric constant, ε)			
	Toluene (2.38)	Methanol (32.7)	DMF (36.7)	DMSO (46.7)
ET1	0.34	*nd*	0.24	0.20
ZnET2	0.33	*nd*	0.011	0.011
ET3	0.19	0.14	0.18	0.22
ET4	0.34	0.27	0.33	0.36
ZnET4	0.27	0.16	0.28	0.26

Table 4.2: Fluorescence quantum yields of chlorin-BODIPY dyads in solvents of different polarities. Reported Φ_F values determined as emission of chlorin upon excitation at maximum of BODIPY absorption band, sample concentrations were set to ~1.0 µM. *nd* – not determined due to poor solubility. Error for quantum yield measurements estimated at ± 5% (see section 2.5.4 for details). Solvent dielectric constants obtained from sigmaaldritch.com.

protic nature of methanol as opposed to aprotic for all other solvents, played a role, as it was the only protic solvent utilized here. Overall, it is apparent that the amide linked dyads are minimally impacted by solvent polarity, while the properties of phenylethynyl arrays are highly dependent upon environment.

Finally, we sought to demonstrate that the conjugation of BODIPY to chlorin results in increased fluorescence brightness of the chlorin. Fluorescence brightness is defined as the product of the fluorescence quantum yield and the molar absorptivity (ε) at the excitation wavelength. We did not attempt to determine ε for our arrays because they were only prepared on small scale (less than 10 mg), and the resultant error would be significant. Instead, we compared the fluorescence intensity of the given dyad against its benchmark monomer, for samples of the same concentration (absorbance at *B* band set to 0.1) upon excitation at ~515 nm. Note that fluorescence intensity was measured as the integration of the emission band over the same wavelength range, for both benchmark and dyads (data not shown). In toluene, dyad **ET3** showed a 5.2 fold

increase of chlorin fluorescence intensity relative to **C2**, and for **ET4** there was a 5.5 fold increase relative to **C2-2P**. Similar enhancement was seen in DMF for both **ET3** (4.7 fold) and **ET4** (5.2 fold). For **ET1** or **ET2**, signal enhancement was observed, however we did not calculate their relative brightness because it was apparent that the weak electronic communication was altering the properties of the chlorin subunit, and we could not determine if ε at *B* band was conserved relative to respective benchmark monomers.

Section 4.4: Conclusions

We successfully prepared a series of BODIPY-chlorin energy transfer arrays that exhibit bright fluorescence upon excitation of the BODIPY. In all dyads the fluorescence brightness is markedly improved relative to that of chlorin monomers excited in the same spectral window (~515 nm). All arrays showed efficient energy transfer (minimum of 0.87 in toluene, 0.80 in DMF) but dyads possessing phenylethynyl linkers at the chlorin 3- or 3,13- positions had significantly reduced fluorescence in high polarity solvents. The most prominent example of this decreased emission was in the case of zinc containing dyad **ZnET4**, which was barely fluorescent in DMF (Φ_F = 0.011). In sharp contrast, dyads possessing amide linkers at the 10-position of chlorin showed no change to fluorescence quantum yield when introduced to DMF. Thus, we have gained important knowledge for the construction of BODIPY-hydroporphyrin arrays and can begin tailoring them with regard to goal or application. For example, if one wanted to utilize our arrays in a nonpolar medium, either linkage is acceptable to afford high ETE with relatively large Φ_F for the deep-red spectral window. Arguably, arrays **ET1** and **ET2** may perform better in a nonpolar setting due

to their slightly enhanced Φ_F relative to **ET3** and **ET4**. However, for applications such as *in vivo* fluorescence imaging, where environments are complex and contain both polar and nonpolar character, dyads **ET3** and **ET4** would be preferred to maximize emission. Going forward arrays **ET3** and **ET4** provide a viable blueprint for compounds capable of bright red to NIR fluorescence upon excitation in the green or red spectral windows. Also, because the 10-position amide linker is used to establish high ETE with minimal quenching, this leaves the 3,13- positions available for further modification. The glaring problem with these dyads is their poor solubility. This is reflected in our inability to acquire appreciable absorption or emission spectra in select solvents (such as methanol). To afford arrays capable of *in vivo* or *in vitro* imaging significant improvements to water solubility were required, and that is one of the primary foci of Chapter 5. Nonetheless, our early work with the dyads presented here laid the groundwork for the improved constructs that will be discussed in the following chapters.

Section 4.5: Experimental Procedures

Section 4.5.1: General Synthetic and Spectroscopic Procedures

For general procedures involving palladium catalyzed (Sonogashira) reactions and characterization of new compounds by NMR and HRMS, see section 2.5.1. In addition to ^{1}H NMR, and ^{13}C NMR, ^{19}F NMR was collected for completed energy transfer arrays. For final compounds, where ^{13}C NMR is not provided, compound solubility was too low to acquire spectrum. For determination of fluorescence quantum yields see section 2.5.4.

Known compounds **C2-Br**,[122] **9**,[122] **WH**,[115] **WH-Br**,[116] and **B2**[318] were prepared according to published procedures. Known compounds **EH2-2Br**,[122] **B1-TMS**[43,315–317] and **B1**[43,315–317] were prepared by modified procedures and their identity was confirmed against original publications.

Section 4.5.2: Synthesis of Precursors, Chlorins, BODIPY Monomers and BODIPY Standard

Chlorin Precursor (Eastern Half)

*9-bromo-1-formyl-5-[4-(methoxycarbonyl)phenyl]dipyrromethane (**EH2-Br**)*

Following a similar procedure,[161] a solution of **11** (1.08 g, 3.51 mmol) in THF (60 mL) was treated with NBS (0.640 g, 3.60 mmol) at −78 °C. After 40 min, the cooling bath was removed, and a mixture of hexane and water (1:1, 10 mL) was added. The resulting mixture was diluted with ethyl acetate, washed with brine, and dried (Na_2SO_4) and concentrated. Column chromatography [silica, hexane/ethyl acetate (2:1)] provided the desired product as a white powder (1.27 g, 94%): ^{1}H NMR (DMSO-d_6, 400 MHz): δ 3.83 (s, 3 H), 5.54 (s, 1H), 5.67 (t, J = 3.0 Hz, 1H), 6.01−5.93 (m, 2H), 6.91 (t, J = 3.0 Hz, 1H), 7.28 (d, J = 8.2 Hz, 2H), 7.90 (d, J = 8.2 Hz, 2H), 9.39 (s, 1H), 11.46 (br s, 1H), 12.09 (br s, 1H). The product was used immediately in the next step without further characterization.

Chlorins

*18,18-dimethyl-10-(4-methoxycarbonyl)phenyl-chlorin (**C2**)*

Following a similar procedure,[161] a suspension of **WH** (0.620 g, 3.26 mmol) and **EH2-Br** (1.27 g, 3.28 mmol) in CH_2Cl_2 (80 mL) was treated with a solution of *p*-toluenesulfonic acid (3.04 g, 16.0 mmol) in methanol (20 mL) and stirred at room temperature for 40 min. The resulting mixture was treated with TMP (6.60 mL, 38.9

mmol). The reaction mixture was concentrated, and the resulting brown solid was suspended in acetonitrile (300 mL) and treated with zinc acetate (8.78 g, 48.0 mmol), TMP (13.5 mL, 79.5 mmol), and AgOTf (2.50 g, 9.73 mmol). The resulting suspension was refluxed for 17 h. The reaction mixture was cooled down and concentrated, and the residue was purified by column chromatography, collecting all red fluorescent material [silica, hexanes/CH_2Cl_2 (1:2)]. The resulting green solid (crude zinc chlorin) was treated with a solution of TFA (5.80 mL, 75.3 mmol) in CH_2Cl_2 (70 mL) and stirred for 3 hours. The crude reaction mixture was then washed (saturated aqueous $NaHCO_3$ and brine), dried (Na_2SO_4), and concentrated. Column chromatography [silica, hexanes/CH_2Cl_2 (1:2)] provided a green solid (0.422 g, 25%): ^{1}H NMR ($CDCl_3$, 400 MHz): δ −2.34 (s, 1H), −1.96 (s, 1H), 2.07 (s, 6H), 4.13 (s, 3H), 4.64 (s, 2H), 8.27 (d, *J* = 8.3Hz, 2H), 8.45 (d, *J* = 8.3 Hz, 2H), 8.62 (d, *J* = 4.3 Hz, 1H), 8.78 (d, *J* = 4.9 Hz, 1H), 8.85 (d, *J* = 4.3 Hz, 1H), 8.96 (s, 1H), 8.98 (d, *J* = 4.9 Hz, 1H), 9.01 (d, *J* = 4.3 Hz, 1H), 9.05 (s, 1H), 9.26 (d, *J* = 4.9 Hz, 1H), 9.89 (s, 1H); ^{13}C{^{1}H}NMR ($CDCl_3$, 100 MHz): δ 31.2, 46.4, 52.0, 52.4, 94.5, 97.1, 107.3, 119.9, 123.4, 123.8, 127.8, 128.0, 128.4, 129.4, 131.6, 132.6, 134.1, 134.3, 134.7, 139.4, 140.9, 146.6, 150.9, 151.8, 163.0, 167.4, 175.4; HRMS (ESI-FT-ICR) *m/z* $[M+H]^+$ Calcd for $C_{30}H_{26}N_4O_2$, 475.2129; Found 475.2118.

*3,13-dibromo-18,18-dimethyl-10-(4-methoxycarbonyl)phenyl-chlorin (**C2-2Br**)*

Following a reported procedure,[108,161] a solution of **11** (610 mg, 2.00 mmol) in THF (20 mL) and treated with NBS (696 mg, 4.00 mmol) under nitrogen at −78°C. The resulting reaction mixture was stirred for 1 hour at −78°C. The cooling bath was removed, the reaction mixture was warmed up to −20°C, and a hexanes/water mixture

(~10 mL, 1:1) was added. The organic layer was separated, dried (Na_2SO_4), and concentrated. Column chromatography (silica [hexanes/ CH_2Cl_2/EtOAc, 7:3:2]) provided a white/pale yellow solid (0.62 g, 67%). The resulting **EH2-2Br** was immediately used in the next step without further characterization.

Following a reported procedure,[108,161] a mixture of **EH2-2Br** (0.516 g, 1.14 mmol) and **WH-Br** (0.315 g, 1.14 mmol) in CH_2Cl_2 (30 mL) was treated with a solution of *p*-toluenesulfonic acid (1.26 g, 6.65 mmol) in MeOH (10 mL). The resulting mixture was stirred at room temperature for 30 min. Next, TMP (6.65 mL, 38.6 mmol) was added to the reaction flask, and the resulting mixture was concentrated. The resulting orange-red solid was suspended in acetonitrile (100 mL) and treated with $Zn(OAc)_2$ (3.66 g, 20.0 mmol), AgOTf (1.0 g, 4.0 mmol), and TMP (6.78 mL, 39.9 mmol). The resulting mixture was refluxed overnight and then concentrated. The crude zinc complex of chlorin was filtered through silica (CH_2Cl_2), and all green fractions containing chlorin were collected and concentrated. The resulting solid was dissolved in dichloromethane (10 mL), treated with TFA (1.00 mL), and stirred for 4 h. Saturated aqueous $NaHCO_3$ was added and stirred for 5 min. The organic layer was separated, washed (water and brine), dried (Na_2SO_4), and concentrated, to give a red-brown solid. Column chromatography [silica, hexane/CH_2Cl_2 (1:1)] provided a dark-green solid (125 mg, 17%). ^{1}H NMR ($CDCl_3$, 400 MHz): δ −2.17 (s, 1H), −1.78 (s, 1H), 2.04 (s, 6H), 4.13 (s, 3H), 4.63 (s, 2H), 8.18 (d, *J* = 8.0Hz, 2H), 8.43 (d, *J* = 8.0Hz ,2H), 8.50 (d, *J* = 4.0Hz, 1H),8.76 (s, 1H), 8.78 (s, 1H), 8.94 (d, *J* = 4.0 Hz, 1H), 8.96 (s, 1H), 9.15(s, 1H), 9.85 (s, 1H); ^{13}C{^{1}H}NMR ($CDCl_3$, 100 MHz): δ 31.2, 46.5, 52.1, 52.6, 94.8, 95.7, 105.9, 113.8, 118.8, 120.2, 124.7, 128.3, 128.7, 129.9, 132.2, 132.4, 133.3,

134.0, 134.1, 137.2, 140.2, 145.9, 151.2, 152.4, 163.7, 167.4, 176.0; HRMS (ESI-FT-ICR) *m/z* $[M+H]^+$ Calcd for $C_{30}H_{25}N_4O_2Br$, 631.0339; Found 631.03117.

*18,18-dimethyl-10-(4-methoxycarbonyl)phenyl-13-phenylethynylchlorin (**C2-P**)*

Following the general procedure for Sonogashira coupling, a solution of **C2-Br**[122] (15.2 mg, 0.0275 mmol), phenylacetylene **4** (5.6 μL, 0.052 mmol), $(PPh_3)_2PdCl_2$ (3 mg, 0.004 mmol) in DMF/Et_3N (6 mL, 2:1) was degassed and stirred at 80°C for 3 h. The reaction mixture was diluted with ethyl acetate. then was washed (water and brine), dried (Na_2SO_4), and concentrated. Column chromatography [silica, hexanes/CH_2Cl_2 (1:2)] provided a green solid (13 mg, 84%). ^{1}H NMR ($CDCl_3$, 400 MHz): δ −2.11 (br, 1H), −1.72 (br, 1H), 2.08 (s, 6H), 4.12 (s, 3H), 4.70 (s, 2H), 7.45−7.54 (m, 3H), 7.87−7.89 (m, 2H), 8.24 (d, J = 8.2 Hz, 2H), 8.43 (d, J = 8.2 Hz, 2H), 8.58 (d, J = 4.3 Hz, 1H), 8.88 (s, 1H), 8.91 (s, 1H), 8.94 (d, J = 4.4 Hz, 1H), 8.96 (d, J = 4.3 Hz, 1H), 9.22 (d, J = 4.4 Hz, 1H), 9.38 (s, 1H), 9.81 (s, 1H); ^{13}C{^{1}H}NMR ($CDCl_3$, 100 MHz): δ 31.2, 46.8, 52.2, 52.6, 95.0, 95.6, 96.8, 107.3, 117.5, 120.6, 123.6, 124.2, 128.3, 128.76, 128.81, 129.0, 129.3, 129.7, 132.0, 132.3, 132.9, 133.3, 134.2, 135.2, 139.7, 141.7, 146.3, 151.9, 152.1, 163.7, 167.5, 176.4; HRMS (ESI-FT-ICR) *m/z* $[M+H]^+$ Calcd for $C_{38}H_{30}N_4O_2$, 575.2442; Found 575.2451.

18,18-dimethyl-10-(4-methoxycarbonyl)phenyl-3,13-di(phenylethynyl)chlorin (***C2-2P***)

Following the general procedure for Sonogashira coupling, a mixture of **C2-2Br** (20 mg, 0.030 mmol), phenylacetylene **4** (0.013 mL, 0.012 mmol) and $(PPh_3)_2PdCl_2$ (2.1 mg, 0.0030 mmol) in DMF/Et_3N (9 mL, 2:1) was stirred for 4 h at 80°C. The resulting mixture was washed (water and brine), dried (Na_2SO_4), and

concentrated to obtain a dark brown solid. Column chromatography [silica, hexanes/ethyl acetate (5:1)] provided a brown solid (12 mg, 60%). ^{1}H NMR ($CDCl_3$, 400 MHz): δ −1.93 (s, 1H), −1.50 (s, 1H), 2.07 (s, 6H), 4.11 (s, 3H), 4.68 (s, 2H), 7.52 (m, 6H), 7.87 (d, *J* = 8.0 Hz, 2H), 7.99 (d, *J* = 8.0 Hz, 2H), 8.24 (d, *J* = 12 Hz, 2H), 8.43 (d, *J* = 8 Hz, 2H), 8.55 (d, *J* = 4 Hz, 1H), 8.85 (s, 2H, 2 signals overlap), 9.00 (d, *J* = 4 Hz, 1H), 9.04 (s, 1H), 9.33 (s, 1H); ^{13}C{^{1}H}NMR ($CDCl_3$, 100 MHz): δ 31.3, 46.6, 52.3, 52.6, 84.2, 84.4, 95.3, 95.9, 97.2, 98.2, 105.6, 118.3, 120.6, 123.0, 123.4, 123.4, 125.3, 128.4, 128.8, 128.9, 129.0, 129.2, 129.7, 129.8, 132.0, 132.2, 132.5, 133.6, 134.2, 134.3, 135.6, 140.2, 146.2, 152.0, 152.9, 164.2, 167.5, 176.2; HRMS (ESI-FT-ICR) *m/z* $[M+H]^+$ Calcd for $C_{46}H_{35}N_4O_2$, 675.2754; Found 675.2780.

*18,18-dimethyl-10-(4-methoxycarbonyl)phenyl-3,13-di(phenylethynyl)chlorinato Zinc(II) (**ZnC2-2P**)*

A solution of 2 (15.0 mg, 0.0222 mmol) in $CHCl_3$/MeOH (6 mL, 5:1) was treated with $Zn(OAc)_2$ (8.2 mg, 0.045 mmol). The resulting mixture was stirred at 50°C for 30 min. The reaction mixture was diluted with ethyl acetate, washed (water and brine), dried (Na_2SO_4), and concentrated. Column chromatography [silica, hexanes/CH_2Cl_2 (1:3)] provided a green solid, which was further purified by washing with hexanes and MeOH (under sonication). After washing 12.1 mg (71%) was obtained. ^{1}H NMR ($CDCl_3$, 400 MHz): δ 2.05 (s, 6H), 4.08 (s, 3H), 4.58 (s, 2H), 7.55−7.43 (m, 6H), 7.82 (d, *J* = 7.0 Hz, 2H), 7.94 (d, *J* = 7.0 Hz, 2H), 8.16 (d, *J* = 8.0 Hz, 2H), 8.37 (d, *J* = 8.0, 2H), 8.46 (d, *J* = 4.2 Hz, 1H), 8.57 (s, 1H), 8.74 (s, 1H), 8.88 (s, 1H), 8.90 (d, *J* = 4.2 Hz, 1H), 9.05 (s, 1H), 9.85 (s, 1H); HRMS (ESI-FT-ICR) *m/z* $[M]^+$ Calcd for $C_{46}H_{32}N_4O_2Zn$ 736.1811; Found 736.1819.

Boron-dipyrromethenes

*4,4-difluoro-1,3,5,7-tetramethyl-8-[4-(trimethylsilyl)ethynyl]phenyl-4-bora-3a,4a-diaza-s-indacene (**B1-TMS**)*

A mixture of 2,4-dimethylpyrrole **10** (0.440 g, 4.00 mmol) and [4-(trimethylsilyl)ethynyl]benzaldehyde **11** (0.404 g, 2.00 mmol) in anhydrous dichloromethane (100 mL) was treated with trifluoroacetic acid (15 μL, 0.2 mmol), and stirred at room temperature for 6 h, under N_2. The resultant deep-red mixture was treated with DDQ (0.454 g, 2.00 mmol) and stirred for 1 h. Next, Et_3N (3.40 g, 33.6 mmol) and $BF_3{\cdot}OEt_2$ (5.20 g, 36.6 mmol) were added, and the solution was stirred overnight. The mixture was washed with $NaHCO_3$ (sat'd., aq.), then water, and brine before being dried (Na_2SO_4), and concentrated, yielding a viscous, black oil. Column chromatography [silica, hexane/ethyl acetate (20:1)] provided a solid, which was washed with hexanes, and dried under vacuum to obtain pure **B1-TMS** (orange solid, 196 mg, 23%). ^{1}H NMR ($CDCl_3$, 400 MHz): δ 0.28 (s, 9H), 1.40 (s, 6H), 2.56 (6H), 5.98 (s, 2H), 7.25 (d, J = 8.2 Hz, 2H, overlap with $CHCl_3$ peak), 7.61 (d, J = 8.2 Hz, 2H); ^{13}C{^{1}H}NMR ($CDCl_3$, 100 MHz): δ 0.01, 14.7, 95.9, 100.0, 104.3, 121.5, 124.0, 128.2, 131.3, 132.8, 135.3, 140.9, 143.1, 155.9; ^{19}F NMR (376 MHz, $CDCl_3$): δ −146.1 (q, J = 34.0 Hz); HRMS (ESI-FT-ICR) *m/z* $[M+H]^+$ Calcd for $C_{24}H_{27}BF_2N_2Si$, 421.2082; Found 421.2094.

*4,4-difluoro-1,3,5,7-tetramethyl-8-(4-ethynyl)phenyl-4-bora-3a,4a-diaza-s-indacene (**B1**)*

A mixture of **B1-TMS** (0.558 g, 1.33 mmol) and potassium carbonate (0.201 g, 1.459 mmol) in methanol/THF (1:1, 66 mL) was stirred for 1 h. Crude reaction was

diluted with dichloromethane and washed (water then brine), dried (Na_2SO_4) and concentrated. Column chromatography [silica, hexane/ethyl acetate (15:1)] yielded an orange solid (0.278 g, 60%). ^{1}H NMR ($CDCl_3$, 400 MHz): δ 1.39 (s, 6H), 3.17 (s, 1H), 5.98 (s, 2H), 7.26 (d, *J* = 8.3 Hz, 2H, overlaps with $CHCl_3$ peak), 7.62 (d, *J* = 8.2 Hz, 2H); ^{13}C{^{1}H}NMR ($CDCl_3$, 100 MHz): δ 14.65, 14.69, 78.7, 83.0, 121.5, 123.1, 128.3, 131.2, 133.0, 135.7, 140.7, 143.1, 155.9; HRMS (ESI-FT-ICR) *m/z* $[M+H]^+$ Calcd for $C_{21}H_{19}BF_2N_2$, 349.1682; Found 349.1683.

*4,4-difluoro-1,3,5,7-tetramethyl-8-(4-benzamido)phenyl-4-bora-3a,4a-diaza-indacene (**B2-A**)*

A solution of **B2** (0.020 g, 0.059 mmol) in DMF (10 mL) was treated with benzoic acid (0.072 g, 0.590 mmol), EDC·HCl (0.0226 g, 0.118 mmol), and DMAP (0.0144 g, 0.118 mmol) and was stirred at room temperature. After 40 h, the resulting mixture was diluted with ethyl acetate (20 mL), and the organic layer was washed (water and brine), dried (Na_2SO_4), and concentrated. Column chromatography [silica, CH_2Cl_2/hexane/ethyl acetate (20:1:1)] provided a semi-pure solid. Subsequent column chromatography (silica, CH_2Cl_2) provided a bright orange-red solid (20.8 mg, 80%). ^{1}H NMR (400 MHz, $CDCl_3$): δ 1.46 (s, 6H), 2.56 (s, 6H), 5.99 (s, 2H), 7.30 (d, *J* = 8.4 Hz, 2H), 7.56−7.50 (m, 2H), 7.62−7.57 (m, 1H), 7.82 (d, *J* = 8.4 Hz, 2H), 7.94−7.89 (m, 3H); ^{13}C NMR (100 MHz, $CDCl_3$): δ 14.6, 14.7, 120.2, 121.2, 127.0, 128.9, 128.9, 130.9, 131.6, 132.2, 134.6, 138.7, 141.1, 143.1, 155.5, 165.8; ^{19}F NMR (376 MHz, $CDCl_3$): δ −146.2 (q, *J* = 33.7 Hz); HRMS (ESI-FT-ICR) *m/z* $[M+H]^+$ Calcd for $C_{26}H_{24}BF_2N_3O$, 444.2058; Found 444.2052.

Section 4.5.3: Synthesis of Energy Transfer Arrays

3 and 3,13- linked chlorin-BODIPY arrays

ET1

Following the general procedure for Sonogashira coupling, a mixture of **C2-Br** (20 mg, 0.036 mmol), **B1** (15 mg, 0.043 mmol) and $(PPh_3)PdCl_2$ (3.8 mg, 0.0054 mmol) in DMF/Et_3N (2:1, 6 mL) was stirred at 80 °C. After 2 h, TLC [silica, hexanes/CH_2Cl_2 (1:1)] showed complete consumption of the starting chlorin. The reaction mixture was diluted with ethyl acetate, washed (water and brine), dried (Na_2SO_4), and concentrated. Column chromatography [silica, hexane/CH_2Cl_2 (1:2)] provided a brown solid (which appears green in solution and on the chromatography column) in 52% yield (15.0 mg). ^{1}H NMR (400 MHz, $CDCl_3$): δ −2.07 (br, 1H), −1.64 (br, 1H), 1.55 (s, 6H), 2.08 (s, 6H), 2.60 (s, 6H), 4.11 (s, 3H), 4.71 (s, 2H), 6.04 (s, 2H), 7.44 (d, *J* = 8.3 Hz 2H), 8.00 (d, *J* = 8.2Hz, 2H),8.24 (d, *J* = 8.7Hz, 2H), 8.43 (d, *J* = 8.2 Hz, 2H), 8.58 (d, *J* = 4.1 Hz, 1H), 8.91−8.97 (m, 4H), 9.23 (d, J = 4.6 Hz, 1H), 9.37 (s, 1H), 9.80 (s, 1H); ^{13}C NMR (100 MHz, $CDCl_3$): δ 14.3, 14.9, 31.2, 46.8, 52.1, 52.6, 86.0, 95.0, 95.5, 96.0, 107.3, 116.7, 124.4, 124.5, 128.3, 128.6, 129.2, 129.5, 129.8, 131.4, 132.5, 132.6, 133.0, 133.2, 134.2, 135.42, 135.44, 139.6, 141.9, 143.2, 146.3, 152.1, 152.2, 156.0, 163.6, 167.4, 176.7; ^{19}F NMR (376 MHz, $CDCl_3$): δ −146.1 (q, *J* = 30.9 Hz); HRMS (ESI-FT-ICR) *m/z* $[M+H]^+$ Calcd for $C_{51}H_{43}BF_2N_6O_2$, 821.3589; Found 821.3597.

ET2

Following the general procedure for Sonogashira coupling, a mixture of **C2-2Br** (10 mg, 0.016 mmol), **B1** (14 mg, 0.040 mmol), $(PPh_3)PdCl_2$ (1.5 mg, 0.0021 mmol) in DMF/Et_3N (6 mL, 2:1) was stirred at 80 °C for 3 h. The resulting mixture

was diluted with ethyl acetate, washed (water then brine), dried (Na_2SO_4), and concentrated. Column chromatography [silica, hexanes/CH_2Cl_2 (1:1) → (1:10)] provided a brown solid, which was washed (under sonication) with methanol and hexanes (9.1 mg, 47%). ^{1}H NMR (400 MHz, $CDCl_3$): δ −1.88 (br, 1H), −1.45 (br, 1H), 1.55, 1.58 (two singlets overlapped with water signal), 2.09 (s, 6H), 2.60−2.61 (broad, two overlapped singlets, 12H), 4.12 (s, 3H), 4.71 (s, 2H), 6.05 & 6.06 (two overlapped singlets, 4H), 7.46 (d, *J* = 7.3Hz, 2H), 7.51 (d, *J* = 7.3Hz, 2H), 8.00 (d, *J* = 7.3Hz, 2H), 8.12 (d, *J* = 7.3Hz, 2H), 8.24 (d, *J* = 8.2Hz, 2H), 8.44 (d, *J* = 8.2Hz), 8.58 (d, *J* = 4.1 Hz, 1H), 8.87 (s, 1H), 8.89 (s, 1H), 9.02 (d, *J* = 4.1 Hz, 1H), 9.35 (s, 1H), 10.07 (s, 1H); HRMS (MALDI-TOF) *m/z* $[M]^+$ Calcd for $C_{72}H_{60}B_2F_4N_8O_2$, 1167.49995; Found 1167.5024.

ZnET2

A mixture of **ET2** (3.5 mg, 0.0036 mmol) in $CHCl_3$/MeOH (1 mL, 5:1) was treated with $Zn(OAc)_2$ (10 mg, 0.055 mmol), stirred at 50°C for 1 h. then concentrated to dryness. The sample was then dissolved in CH_2Cl_2, washed (water and brine), dried (Na_2SO_4), and concentrated. The resulting solid was washed with MeOH and hexanes (under sonication), to provide a green solid (3.6 mg, 50%). The product, after washing with water, MeOH, and hexanes, showed extremely low solubility in common organic solvents ($CHCl_3$, CH_2Cl_2, THF, DMSO), which prevents recording ^{1}H NMR spectrum of the pure sample. The ^{1}H NMR data reported here were taken on the semi-pure sample, immediately upon concentration, prior to washing. ^{1}H NMR (400 MHz, $CDCl_3$): δ 1.54 (s, 6H), 1.58 (s, 6H), 2.07 (s, 6H), 2.59 (broad, two overlapped singlets, 12H), 4.10 (s, 3H), 4.62 (s, 2H), 6.04 and 6.05 (two overlapped singlets, 4H), 7.43 (d,

J = 8.1 Hz, 2H), 7.49 (d, *J* = 8.1 Hz, 2H), 7.96 (d, *J* = 8.1 Hz, 2H), 8.09 (d, *J* = 8.1 Hz, 2H), 8.18 (d, *J* = 8.1Hz, 2H), 8.40 (d, *J* = 8.1Hz, 2H), 8.50 (d, *J* = 4.2Hz, 1H), 8.63 (s, 1H), 8.80 (s, 1H), 8.96 (s, 1H), 8.96 (d, *J* = 4.2 Hz, 1H), 9.10 (s, 1H), 9.93 (s, 1H); HRMS (MALDI-TOF) *m/z* $[M]^+$ Calcd for $C_{72}H_{58}B_2F_4N_8O_2Zn$, 1228.4113; Found 1228.4092.

10-position linked chlorin-BODIPY arrays

ET3

Following a similar procedure,[122] a solution of **C2** (118 mg, 0.249 mmol) in THF/methanol (2:1, 6 mL) was treated with NaOH (1 M aqueous solution, 2 mL) and stirred under nitrogen for 14 h. The reaction mixture was acidified with aqueous HCl solution (1M, 10 mL) and extracted with CH_2Cl_2. Combined organic layers were dried (Na_2SO_4) and concentrated to afford an intermediate acid **C2-COOH** as a green powder (112 mg, 98%), which was used in the next step without further purification: ^{1}H NMR (400 MHz, DMSO-d_6): δ −2.56 (s, 1H), −2.12 (s, 1H), 2.02 (s, 6H), 4.63 (s, 2H), 8.24 (d, J = 8.3 Hz, 2H), 8.37 (d, J = 8.3 Hz, 2H), 8.49 (d, J = 4.3 Hz, 1H), 8.78 (d, J = 4.9 Hz, 1H), 9.13−9.06 (m, 2H), 9.28− 9.20 (m, 3H), 9.50 (d, J = 4.2 Hz, 1H), 10.08 (s, 1H), 13.27 (br, 1H); ^{13}C NMR (100 MHz, DMSO-d_6): δ 30.8, 46.2, 51.3, 94.8, 97.3, 107.4, 119.4, 124.1, 124.7, 127.7, 128.9, 129.1, 130.2, 131.2, 133.1, 133.8, 134.0, 134.1, 138.9, 140.7, 145.4, 150.3, 151.0, 163.6, 167.6, 175.7; HRMS (ESI-FT-ICR) *m/z* $[M+H]^+$ Calcd for $C_{29}H_{24}N_4O_2$, 461.1972; Found 461.1972.

A solution of **B2** (14.7 mg, 0.0434 mmol) in DMF (5 mL) was treated with crude **C2-COOH** (20.0 mg, 0.0434 mmol), EDC·HCl (83.0 mg 0.434 mmol), and DMAP (5.3 mg, 0.043 mmol) and stirred at room temperature for 14 hours. The

resulting mixture was diluted with ethyl acetate, washed (water then brine), dried (Na_2SO_4), and concentrated. Column chromatography [silica, hexane/CH_2Cl_2 (1:2)] provided a brown-green solid; 18.0 mg, 53%. ^{1}H NMR (400 MHz, $CDCl_3$): δ −2.37 (bs, 1H), −1.98 (bs, 1 H), 1.54 (s, 6H), 2.09 (s, 6H), 2.59 (s, 6H), 4.68 (s, 2H), 6.03 (s, 2H), 7.39 (d, *J* = 8.4 Hz, 2H), 7.99 (d, *J* = 8.4, 2H), 8.25 (s, 1H), 8.28 (d, *J* = 8.2 Hz, 2H), 8.33 (d, *J* = 8.2 Hz, 2H), 8.61 (d, *J* = 4.3Hz,1H), 8.79 (d, *J* = 4.7 Hz, 1H), 8.89 (d, *J* = 4.7 Hz, 1H), 9.00 (d, *J* = 4.3 Hz, 1H), 8.97 (s, 1H), 9.02 (d, *J* = 4.4 Hz, 1H), 9.10 (s, 1H), 9.29 (d, *J* = 4.3, 1H), 9.91 (s, 1H); ^{13}C NMR (100 MHz, $CDCl_3$): δ 14.6, 14.8, 31.2, 46.5, 52.0, 94.6, 97.2, 107.4, 119.5, 120.4, 121.3, 123.5, 123.9, 125.5, 127.7, 128.5, 129.0, 131.0, 131.5, 131.6, 132.7, 133.8, 134.3, 134.5, 134.7, 138.9, 139.4, 141.0, 141.2, 143.1, 146.0, 150.9, 151.8, 155.6, 163.2, 165.9, 175.5; ^{19}F NMR (376 MHz, $CDCl_3$): δ −146.1 (q, J = 33.4 Hz); HRMS (ESI-FT-ICR) *m/z* $[M+H]^+$ Calcd for $C_{48}H_{42}BF_2N_7O$, 782.359; Found 782.3574.

ET4

Following a similar procedure,[122] **C2-2P** (41.7 mg, 0.0617 mmol) was dissolved in THF/methanol (2:1, 6 mL), treated with aqueous NaOH (3 mL, 1.0 M) and stirred vigorously overnight. After 20 h, TLC indicated consumption of all starting material and a single, more polar, red fluorescent spot. The reaction mixture was diluted with CH_2Cl_2 (15 mL), acidified with HCl (~3 mL, 1M), washed (water then brine), dried (Na_2SO_4), and concentrated. ^{1}H NMR clearly indicated the loss of the methoxy group. The yield of hydrolysis was assumed to be quantitative, and the resulting acid **C2-2P-COOH** was used in the next step without further purification. ^{1}H NMR (400 MHz, $CDCl_3$): δ 2.08 (s, 3H), 4.69 (s, 2H), 7.49−7.59 (m, 8H), 7.88−7.90 (m, 2H), 7.98−8.00

(m, 2H), 8.29 (d, *J* = 8.2 Hz, 2H), 8.53 (d, *J* = 8.2 Hz, 2H), 8.58 (d, *J* = 4.4 Hz, 1H), 8.86 (s, 1H), 8.88 (s, 1H), 9.02 (d, *J* = 4.4 Hz, 1H), 9.05 (s, 1H), 9.35 (s, 1H), 10.07 (s, 1H).

A solution of **B2** (18.0 mg, 0.0530 mmol) in DMF (7 mL) was treated with **C2-2P-COOH** (35.0 mg, 0.0530 mmol), EDC·HCl (101 mg, 0.530 mmol), and DMAP (6.5 mg, 0.053 mmol) and stirred at room temperature for 14 hours. The resulting mixture was diluted with ethyl acetate, washed (water then brine), dried (Na_2SO_4), and concentrated. Column chromatography [silica, hexane/CH_2Cl_2 (1:2)] yielded a mixture of product and a green-fluorescent impurity. The resulting sample was dissolved in CH_2Cl_2, mixed with silica (∼2g), and concentrated. The resulting powder was transferred to a short silica column and eluted with MeOH; at which time the green-fluorescent impurity was eluted (whereas insoluble **ET4** stayed atop the column). Elution with MeOH was continued until the green-fluorescent impurity was completely removed. Dyad **ET4** was then eluted with CH_2Cl_2. The resulting powder was washed with MeOH and hexanes to afford a brown solid (13.1 mg, 25%). ^{1}H NMR (400 MHz, $CDCl_3$): δ −1.92 (bs 1H) −1.50 (bs, 1H), 1.55 (s, 6H), 2.08 (s, 6H), 2.59 (s, 6H), 4.69 (s, 2H), 6.03 (s, 2H), 7.40 (d, *J* = 8.5 Hz, 2H), 7.59−7.48 (m, 7H), 7.42−7.38 (m, 2H), 8.00−7.95 (m, 3H), 8.2 (s, 1H) 8.33−8.27 (m, 4H), 8.58 (d, *J* = 4.3 Hz, 1H), 8.86 (s, 1H), 8.87 (s, 1H), 9.02 (d, *J* = 4.4 Hz, 1H), 9.05 (s, 1H), 9.34 (s, 1H), 10.07 (s, 1H); ^{13}C NMR (100 MHz, $CDCl_3$): δ 14.6, 14.7, 31.1, 46.4, 52.1, 84.0, 84.1, 95.2, 95.8, 97.1, 98.1, 105.4, 118.2, 120.0, 120.4, 121.3, 122.9, 123.2, 123.3, 125.2, 125.7, 128.6, 128.7, 128.8, 128.9, 129.0, 129.4, 131.0, 131.6, 131.8, 132.0, 132.1, 133.4, 134.0, 134.1, 134.5, 135.4, 138.9, 140.0, 140.1, 141.2, 143.1, 145.3, 151.8, 152.6, 155.6, 164.1,

165.8, 176.1; ^{19}F NMR (376 MHz, $CDCl_3$): δ −146.1 (q, *J* = 33.1 Hz); HRMS (ESI-FT-ICR) *m/z* $[M+H]^+$ Calcd for $C_{64}H_{50}BF_2N_7O$, 982.4221; Found 982.4193.

ZnET4

A sample of **ET4** (4.7 mg, 0.048 mmol) was dissolved in $CHCl_3$/methanol (5:1, 3 mL) and treated with zinc acetate (1.9 mg, 0.010 mmol). After stirring for 6 h, TLC indicated that all starting material had been consumed. The reaction mixture was then quenched with saturated aqueous $NaHCO_3$, washed (water then brine), dried (Na_2SO_4), and concentrated. Column chromatography [silica, CH_2Cl_2] provided a green solid (3.0 mg, 57%) that became brown after extensive drying. ^{1}H NMR (400 MHz, $CDCl_3$): δ 1.53 (s, 6H, overlapped with water signal), 2.06 (s, 6H), 2.59 (s, 6H), 4.59 (s, 2H), 6.03 (s, 2H), 7.37 (d, *J* = 8.4 Hz, 2H), 7.55−7.40 (m, 6H), 7.81 (d, *J* = 7.0 Hz, 2H), 7.85 (d, *J* = 7.7 Hz, 2H), 7.92 (d, *J* = 6.8 Hz, 2H), 8.10 (d, *J* = 7.5 Hz, 2H), 8.24−8.15 (m, 3H), 8.47 (d, *J* = 4.2 Hz, 1H), 8.60 (s, 1H), 8.77 (s, 1H), 8.91 (s, 1H), 8.92 (d, *J* = 4.0 Hz, 1H), 9.07 (s, 1H), 9.87 (s, 1H); HRMS (ESI-FT-ICR) *m/z* $[M+H]^+$ Calcd for $C_{64}H_{48}BF_2N_7OZn$, 1043.3277; Found 1043.3265.

Section 4.5.4: Determination of Energy Transfer Efficiency

It is worth noting that the typical method for calculating energy transfer efficiency ETE is to determine Φ_F for donor molecule in the absence of acceptor molecule ($\Phi_{F,D}$) and compare against Φ_F for donor molecule in the presence of acceptor molecule ($\Phi_{F,D\text{-}A}$). In this scenario ETE is defined as $1 - (\Phi_{F,D\text{-}A})/(\Phi_{F,D})$. Due to the weak emission intensity of donor molecules in systems with high ETE, $\Phi_{F,D\text{-}A}$ is difficult to accurately measure (as described in section 2.5.4). To improve the accuracy of this measurement many spectroscopists instead measure ETE as a function of lifetime, with the similar relationship, $ETE = 1 - (\tau_{F,D\text{-}A})/(\tau_{F,D})$. Where $\tau_{F,D\text{-}A}$ is

fluorescence lifetime of donor in the presence of acceptor and $\tau_{F,D}$ is the fluorescence lifetime of the donor in absence of acceptor molecule. Because we rely on the equipment of other labs on campus (primarily the Rosenzweig lab) to measure τ_F we instead calculate ETE as the ratio of fluorescence quantum yield of acceptor upon selective excitation of donor ($\Phi_{F,\lambda D}$) divided by fluorescence quantum yield of acceptor upon its direct excitation ($\Phi_{F,\lambda A}$). In our case, donor molecule is always BODIPY and acceptor molecule is always a hydroporphyrin (excited at the B band), so the notation becomes ETE = ($\Phi_{F,\lambda BDP}$)/($\Phi_{F,\lambda Bband}$). Because we are determining ETE as the quotient of two Φ_F values, margin of error in ETE is ± 10%.

Section 4.5.5: Select Oxidation and Reduction Half Reactions

Compound	Reference compound	E^{ox} [V]	E^{red} [V]	E_{00} [eV]	Ref.
C2-P	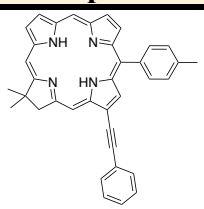	+0.55	-1.53	1.89	Holten[36]
C2-2P	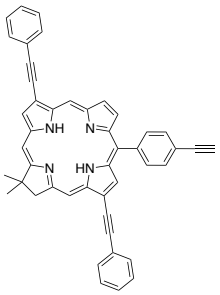	0.66	-1.25	1.83	Holten[282]
ZnC2-2P	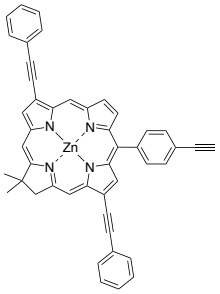	+0.39	-1.50	1.90	Holten[282]
B1-TMS	B1	+1.16	-1.24	2.44	Ziessel[321]

Table 4.3: Reported oxidation and reduction half reactions, for compounds most similar in structure to those studied herein. Also included are values for excited state energy (E_{00}) estimated as the average energy between the absorption and emission maxima.

Chapter 5: Amphiphilic BODIPY-Hydroporphyrin Energy Transfer Arrays

Section 5.1: Introduction

At this stage of our research we had determined the optimal way to link BODIPY and chlorin, to afford improved fluorescence brightness upon excitation in the green spectral window. The apparent brightness resulted from the improved extinction coefficient of BODIPY in the green window (~505 nm) and highly efficient energy transfer to chlorin. Furthermore, we retained the properties that makes chlorins valuable chromophores, such as tunable deep-red to NIR absorption and narrow emission.[112,118,119,210] Collectively, these properties make our arrays strong candidates for applications such as multicolor imaging[267] or fluorescence guided surgery.[268] However, there was one outstanding problem to address, the solubility of arrays.

The arrays presented in Chapter 4, are largely hydrophobic and insoluble due to the two large π systems of the constituent chromophores, making them unsuitable for use in biological media. Often, the method to solubilizing BODIPY or hydroporphyrin monomers incorporates multiple charged functional groups. Examples can be found for one or both dyes that feature negatively charged sulfonates,[322–324] and phosphonates,[325–327] and carboxylates,[325,328] positive ammonium salts,[325,329] and zwitterionic side chains.[330–334] Such an approach is not feasible for us because *in vivo* application requires the use of a targeting moiety to bring the fluorophore to the site of interest,[335,336] and highly charged, particularly polyanionic, chromophores tend to disrupt the specificity of targeting agents.[337] Similarly, highly positively charged chromophores tend to be drawn to negative membrane potential of mitochondria.[338,339] This limits our selection of water solubilizing groups to neutral species, such as

sugars[340] or polyethylene glycol (PEG) ethers.[325,341–351] We opted to use PEG as our water-solubilizer because with strategic placement, the long chains should encompass the chromophore disrupting hydrophobic intermolecular interactions, thus improving solubility. In addition, PEG is known for its biocompatibility,[352] which would avoid complications with later stages of the research.

With the solubilizing moiety selected, we considered that PEG could be installed at either BODIPY or hydroporphyrin, but not both, because it would be cost and labor prohibitive. In addition, we wanted to expand our arrays to incorporate bacteriochlorin, because they possess absorption and emission maxima (710-820 nm) further into the NIR than chlorins, allowing for imaging at greater tissue depths.[275,353,354] By doing so, to the best of our knowledge, we would also be the first to prepare covalently linked BODIPY-bacteriochlorin arrays (a limited number of non-covalent, BODIPY-bacteriochlorin systems are reported).[355,356] By focusing only on modification of the BODIPY, it would allow us to couple PEGylated BODIPY to either chlorin or bacteriochlorin, without requiring separate functionalization of the hydroporphyrins. Ultimately this would lead to amphiphilic arrays, where the chlorin or bacteriochlorin component remains hydrophobic and the BODIPY is modified to become hydrophilic.

Having determined to install PEG on BODIPY, it was now important that we modify BODIPYs solubility, without significantly altering its absorption and emission maxima. On approach, would be to place the PEG substituents on the BODIPY *meso* aryl substituent. Modification at the *meso* position has been extensively studied (similarly to the work discussed in Chapter 2) and it has been shown that phenyl

substituents provide minimal change to λ_{max} due to an orthogonal orientation to the BODIPY core.[98] Thus, the appropriate *meso* aryl substituent can be selected during BODIPY synthesis, if taking this approach. A second method, developed within the last decade, focuses on replacing BODIPY borofluoride moieties. This work, led by Ziessel, has culminated in several boron-substituted BODIPYs, including boro-alkoxy,[357–362] boro-alkyl,[357,358] boro-aryl,[357] and boro-ethynyl.[295,327,330–332,334,340,363,364] While these substitutions appear to coincide with a small decrease in oscillator strength for the BODIPY S_0-S_1 absorption band,[362] all of these derivatives possess very similar absorption maxima. Through either molecular design, the PEG chains should move about the space above and below the plane of the BODIPY core, limiting hydrophobic interactions and aggregation.

The final design point to consider is the synthetic handle for bioconjugation. This should be done by incorporating an N-hydroxy succinimidyl (NHS) ester to completed arrays. A facile way of doing this is to maintain a methyl ester on the hydroporphyrin component (because it will not undergo significant synthetic modification, as opposed to BODIPY). Late-stage hydrolysis will enable the preparation of the NHS ester by EDC mediated coupling.[120] The activated ester can then be conjugated to the biomolecule of interest by the standard procedures.[267,268,365]

At this time, it is important to again consider PET because we anticipate greater fluorescence quenching in more polar media. Keeping to our hypothesis that PET is occurring from photoexcited hydroporphyrin to BODIPY, we anticipate any fluorescence quenching behavior observed in dyads **ET1-ET4** to be exaggerated in new constructs containing bacteriochlorin instead of chlorin (due to bacteriochlorin's

lower oxidation potential).[111,366] Boron-substituted BODIPYs may be a unique solution to this problem, because they possess quite large Φ_F in water and other polar solvents.[327,330–332,334] While it was not explicitly stated in the literature, we suspect that the substitution at boron with less electronegative atoms lowered the reduction potential of the BODIPY, making it less prone to quenching by reductive PET. This could translate into less fluorescence quenching for arrays with boron substituted BODIPY.

Having decided our general approach, we now needed a means of assessing the quenching of amphiphilic arrays in polar media, prior to use by our collaborator. We hypothesized that using an established delivery system/formulation would lead to sufficient water solubility to determine the fluorescence properties of newly constructed arrays. We found several examples of otherwise insoluble fluorophores being solubilized through encapsulation in surfactant micelles. This includes hydroporphyrins and phthalocyanines formulated in Pluronic F-127 micelles,[367,368] and vesicles made by diblock copolymers[137,138,369–372] or phospholipids.[373–375] There was also precedent for amphiphilic hydroporphyrin monomers readily inserting into TX-100 micelles.[376] An additional benefit to these nanostructures is protection against PET, because the nonpolar membranes disfavor formation of a charge-separated state.[376] This may be a more accurate simulation of the environment our arrays would meet *in vivo*, as true biological environments are complex and have non-polar microenvironments (e.g. lipid membranes of organelles or phospholipid bilayer).

All of the design considerations discussed above, as well as cues from the work in Chapter 4, are reflected in the final compounds shown in Chart 5.1.

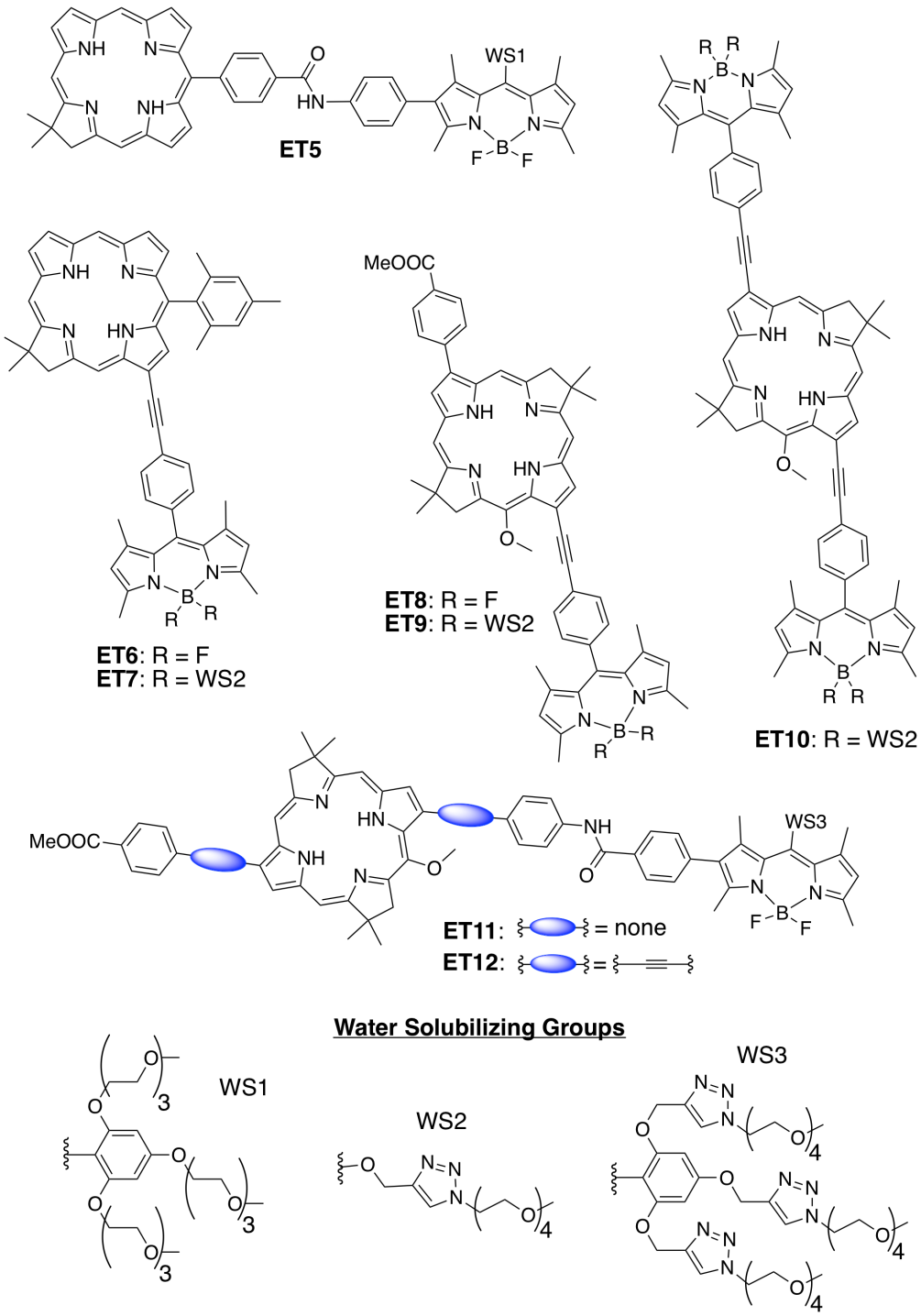

Chart 5.1: Target Hydroporphyrin-BODIPY Arrays discussed in Chapter 5.

Hydroporphyrin-BODIPY dyads **ET5-ET7** feature chlorins while dyads **ET8-ET12** use bacteriochlorins. We began from chlorins because they are easier (and less expensive) to prepare, allowing for a more cost-effective re-design should they provide poor properties. **ET5** features a *meso*-amide linker from chlorin to BODIPY, identical to that seen with **ET3** and **ET4**, as well as a water solubilizing group 2,4,6-tris(triethyleneglycol monomethyl ether)phenyl. (WS1) at the BODIPY 8-position. Array **ET6** is identical to **ET1** except the *p*-methyl benzoate moiety at chlorin 10-position has been replaced with mesityl. Here, we chose mesityl due to its lack of polar functional groups, this would ensure the hydroporphyrin component would remain exclusively hydrophobic, while we improved water solubility of the BODIPY component. We did not want any possibility of hydrogen bonding from chlorin component interfering with amphiphilic nature of arrays, particularly with regard to behavior in aqueous micelles later in the study. **ET6** was prepared by Nithya Santhanam as the hydrophobic model corresponding to dyad **ET7**, which contains novel water solubilizing group WS2. WS2 consists of boro-oxyethyl triazole with tetraethyleneglycol monomethyl ether water solubilizer at triazole 1 position. WS2, was utilized to simultaneously improve water solubility and tune the reduction potential of BODIPY. Recalling that dyad **ET1** underwent significant quenching, **ET6** should exhibit identical quenching in polar solvent (DMF), where redox tuned BODIPY of **ET7** should resist PET and retain a large Φ_F in both polar organic solvent as well as aqueous micelles. Dyads **ET8** and **ET9** are the bacteriochlorin containing equivalents to **ET6** and **ET7**, respectively. We reasoned, that due to the lower oxidation potential of bacteriochlorins, **ET8** should undergo greater quenching than **ET6**. We wanted to

determine if the presence of redox tuned BODIPY in **ET9** would be sufficient to overcome the increased quenching that is typically seen for bacteriochlorins. In the case of triad **ET10**, we wanted to address two concerns. First, we were uncertain if tuning BODIPY alone would overcome the increased quenching of bacteriochlorin, by introducing a second phenylethynyl substituent at bacteriochlorin 3-position, the increased oxidation potential of bacteriochlorin should further prevent PET. Second, creation of a bola-amphiphilic array with a hydrophobic center and water-soluble peripheries could afford greater solubility than otherwise possible. Arrays **ET11** and **ET12** feature an amide linker but differ from previous amide linked chlorins. Due to the synthetic challenge of installing substituents at the bacteriochlorin 10- position we opted to instead link through the 3-position.[113,314] In **ET11**, BODIPY was linked to chlorin through phenyl benzamide similar to hydrophobic **ET3** and **ET4**. Such linker would provide a small impact upon absorption and emission maxima due to steric hindrance making linker orthogonal to the macrocycle. In **ET12**, we wanted to tune the absorption and emission maxima, as well as oxidation potential, similar to **ET4**, yet retain the amide so the linker consists of N-(4-ethynylphenyl)benzamide. Dyads **ET11** and **ET12** feature a different water soluble BODIPY than the other arrays, this BODIPY consists of WS3, which combines the trisubstituted aryl element of WS1 and the tetraethyleneglycol triazole element of WS2 in order to ease synthesis, as discussed below. Note also that all bacteriochlorin dyads possess a methyl benzoate, with the intent to use that as our handle for late-stage bioconjugation following hydrolysis. As a consequence of the placement of the benzoate ester, **ET11** and **ET12** also feature an inverted orientation of the amide, relative to other amide linked constructs. During

synthesis we are forced to prepare asymmetrical bacteriochlorins, where free amine for amide coupling must be present on bacteriochlorin.

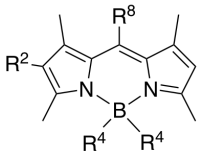

BODIPY	R^2	R^4	R^8
B3	-H	-F	-WS1
B3-NH$_2$	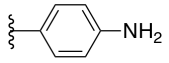	-F	-WS1
B4	-H	-WS2	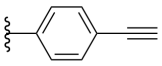
B5	-H	-F	-WS3
B5-COOMe	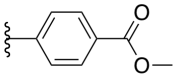	-F	-WS3

Chart 5.2: Target Water Soluble BODIPY Monomers Discussed in Chapter 5.

The target BODIPY monomers as well as novel intermediates are reported in Chart 5.2. The first monomer here, **B3-NH$_2$**, was prepared to closely mimic the amino substituted **B2**, while also affording water solubility through the attachment of WS1 at the meso position. We recognize that a more appropriate surrogate would have placed the amide linker through the *meso* position of BODIPY as was done with **B2**, however, this would have been very challenging to prepare. The next monomer **B4**, is effectively identical to **B1**, but possesses improved water solubility and tuned redox properties by the substitution of WS2 for central fluorine atoms. Finally, BODIPY **B5-COOMe** features the better optimized WS3, with methyl benzoate. Much like the handle for bioconjugation, here the ester will be hydrolyzed then coupled to bacteriochlorin. We have also included BODIPYs **B3** and **B5**, which lack the additional 2-aniline or 2-methyl benzoate moieties, respectively. This is done in order to better characterize fluorescence properties of BODIPYs without strongly electron donating or withdrawing substituents. This is particularly the case for **B3-NH$_2$**, which we anticipate to undergo reductive PET.[289,377,378]

Section 5.2: Synthesis of BODIPY Monomers and ET Arrays

Section 5.2.1: Synthesis of Water Soluble BODIPY Derivatives

We began with the synthesis of **B3-NH₂** (Schemes 5.1 and 5.2) from commercially available 2,4,6-trihydroxybenzaldehyde **12**. Modifying the procedure used to prepare a similar trialkoxy substituted arene,[350] aryl aldehyde **12** was alkylated through substitution reaction with tosyl-terminated triethylene glycol monomethyl ether **13** in the presence of base. This afforded 2,4,6-tris(triethyleneglycol monomethyl ether) benzaldehyde **14** in 47% yield. Benzaldehyde **14** was then used for the standard three step, one-pot synthesis of BODIPY, giving **B3** as a bright orange viscous oil in 9% yield (Scheme 5.1). The yield was low, even for BODIPY synthesis, due to the extensive chromatography required to separate **B3** from the numerous colorful impurities that accompany BODIPY synthesis. The presence of the triethyleneglycol

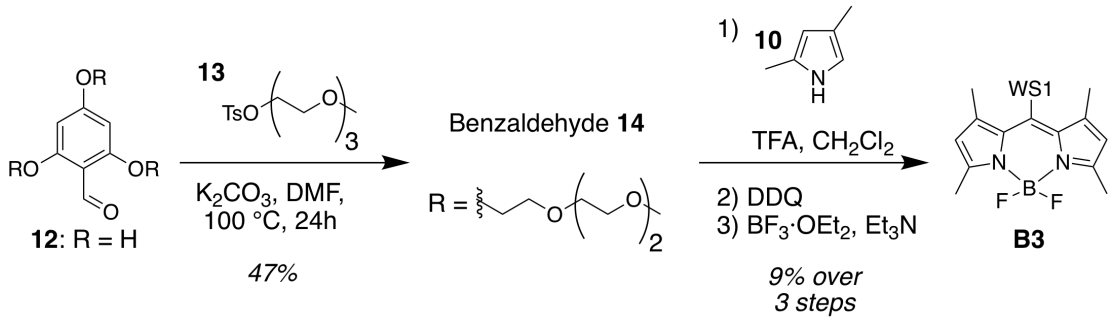

Scheme 5.1: Synthesis of tri-alkoxy aldehyde 14 and BODIPY B3

chains made this BODIPY much more polar than is typical, and lead to decreased separation, one impurity was so similar in retention factor (R_f) and color to target **B3** that its presence was unknown until acquiring ^{1}H NMR. BODIPY **B3** was subsequently iodinated at the 3-position through electrophilic aromatic substitution with iodine

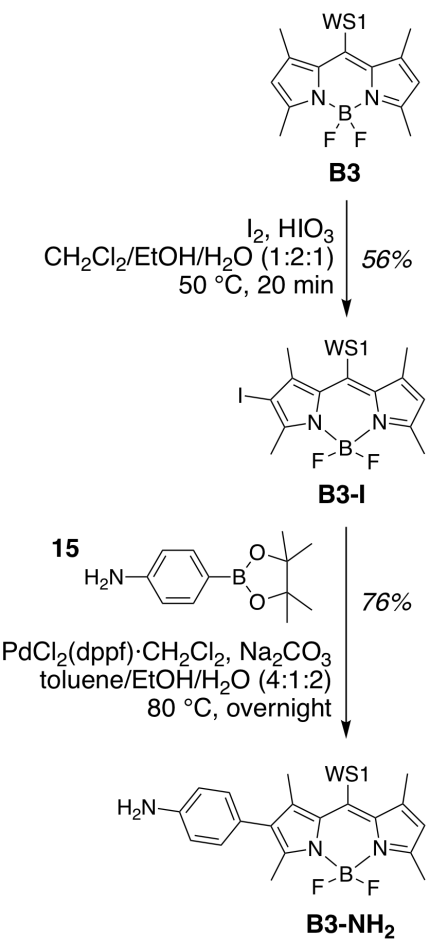

Scheme 5.2: Iodination of B3 and subsequent Suzuki coupling to give target BODIPY B3-NH_2

(Scheme 5.2). This was performed following a published procedure[51,379] which involves I_2/HIO_3 and features comproportionation between HI and HIO_3 to generate additional I_2 *in situ*. The reaction itself worked well, however, monoiodo **B3-I** was only isolated in 56% yield. This is due to the presence of several other byproducts that required challenging chromatography to remove. These impurities were presumed to be a mixture of mono-iodo (at electron rich meso substituent) as well as the various regioisomers of di-iodo BODIPY, based on the change of color from orange-red to pink, and significantly diminished fluorescence upon excitation with UV light. Iodination is known to diminish fluorescence due to increasing intersystem crossing in the photoexcited molecule (heavy atom effect). Incidentally, this was also a good method for qualitatively monitoring reaction progress, a brightly fluorescent reaction mixture indicated little progress. Finally, target monomer **B3-NH_2** was prepared via Suzuki coupling between **B3-I** and 4-aminophenylboronic acid pinacol ester **15**, in 76% yield (Scheme 5.2), following previously established conditions for a similar pegylated BODIPY derivative.[379]

Next, we focused on the preparation of a novel BODIPY monomer with both improved water solubility and tuned redox properties, **B4** (Scheme 5.3). Beginning

from BODIPY **B1-TMS**, we installed boro-propargyloxy substituents by treatment of BODIPY with aluminum chloride at 40ºC in freshly distilled THF for 30 minutes, followed by addition of a large excess of propargyl alcohol and continued stirring at room temperature for 15 minutes. This two step process provided **B4'-TMS** in 86% yield, and coincides with significant visual cues. First the solution changes from red-orange to bright pink upon reaction with $AlCl_3$ (intermediate is hypothesized to be boronium cation),[358] then it returns to red-orange when boro-alkoxy bonds are formed. Our procedure for this is modified from previously published boro-alkoxylation reactions[358,362] that used fewer equivalents of alcohol but required longer reaction times, continued heating and produced lower yields. In our case, the excess propargyl alcohol was readily removed by reduced pressure evaporation. Next, the water solubilizing moiety was installed by Huisgen cycloaddition (1,3-dipolarcycloaddition) between the acetylene groups and known azide-terminated tetraethyleneglycol monomethyl ether **16**.[380] This "Click" reaction was greatly accelerated by use of microwave irradiation,[381–386] providing **B4-TMS** in

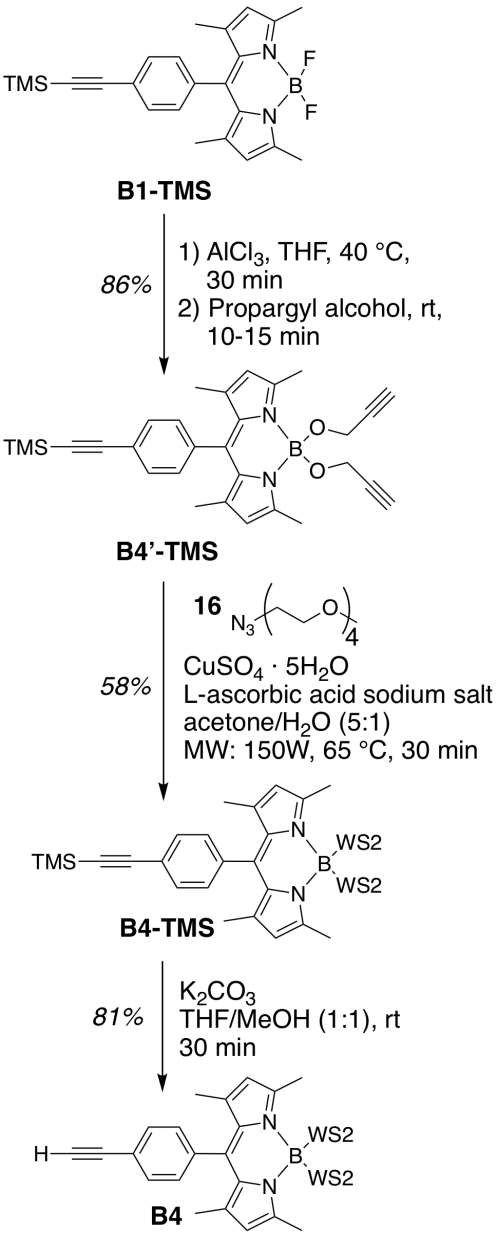

Scheme 5.3: Synthesis of target BODIPY monomer B4

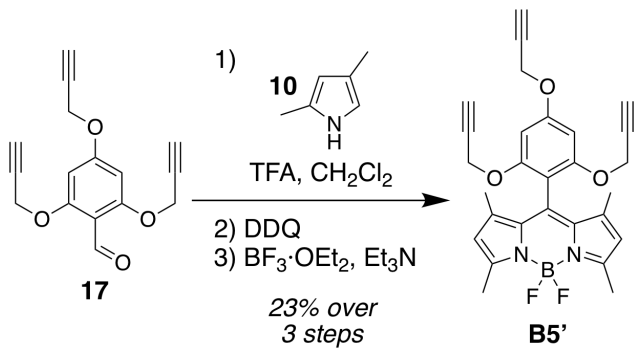

Scheme 5.4: Synthesis of nonpolar intermediate tris(propoargyloxy) substituted BODIPY B5'

58% yield after a single 30 minute microwave exposure. Next, desilylation using standard conditions (K_2CO_3 in THF/MeOH) provided target BODIPY **B4** in 81 % yield.

Despite the relative ease of purification of the **B4** series relative to the **B3** series, we still wanted to prepare a series of dyads with greater hydrophilicity due to a larger number of PEG substituents. As noted above, conjugation to bacteriochlorin would require a BODIPY similar to **B3-NH₂** where 2-(4-amino)phenyl is replaced with 2-(4-carboxymethyl)phenyl. Due to the difficulty involved in purifying **B3-NH₂** and its precursors, we wanted to install the water solubilizing moieties as late as possible. Thus, we adapted the same Click approach to the synthesis of **B5** and **B5-COOMe**. First, we prepared **B5'** by the standard procedure for BODIPY synthesis (condensation, oxidation by DDQ then boron complexation) from 2,4,6-tris(propargyloxy)benzaldehyde **17**[350] and 2,4-dimethylpyrrole **10**. Due to the lack of polar PEG chains at this stage, **B5'** was significantly easier to purify, with yield improving to 23% over the three steps (Scheme 5.4). Next, **B5'** was iodinated at the 2-position (as was done for **B3-I**), yielding **B5'-I** (Scheme 5.5, 61%). The yield was comparable to that for **B3-I**, however, **B5'-I** was significantly easier to separate from the variety of other mono- and di-iodo byproducts, allowing us to scale up this reaction as necessary. Because the propargyl groups are incompatible with the Suzuki coupling

(they will undergo homocoupling in the presence of Pd catalyst), we next performed microwave assisted click reaction on **B5'-I**, obtaining **B5-I** in 80% yield. Finally, 2-iodo BODIPY **B5-I** was reacted with 4-(carboxymethyl)phenylboronic acid pinacol ester **18**, giving **B5-COOMe** in 70% yield. Despite the additional step, the overall yield of target BODIPY **B5-COOMe** (7.9%) was doubled in comparison to **B3-NH$_2$** (3.8%) when determined from respective trisalkoxy benzaldehydes. In a parallel synthesis we were able to prepare model compound **B5** directly from **B5'** via microwave assisted click reaction, in 62% yield (Scheme 5.6).

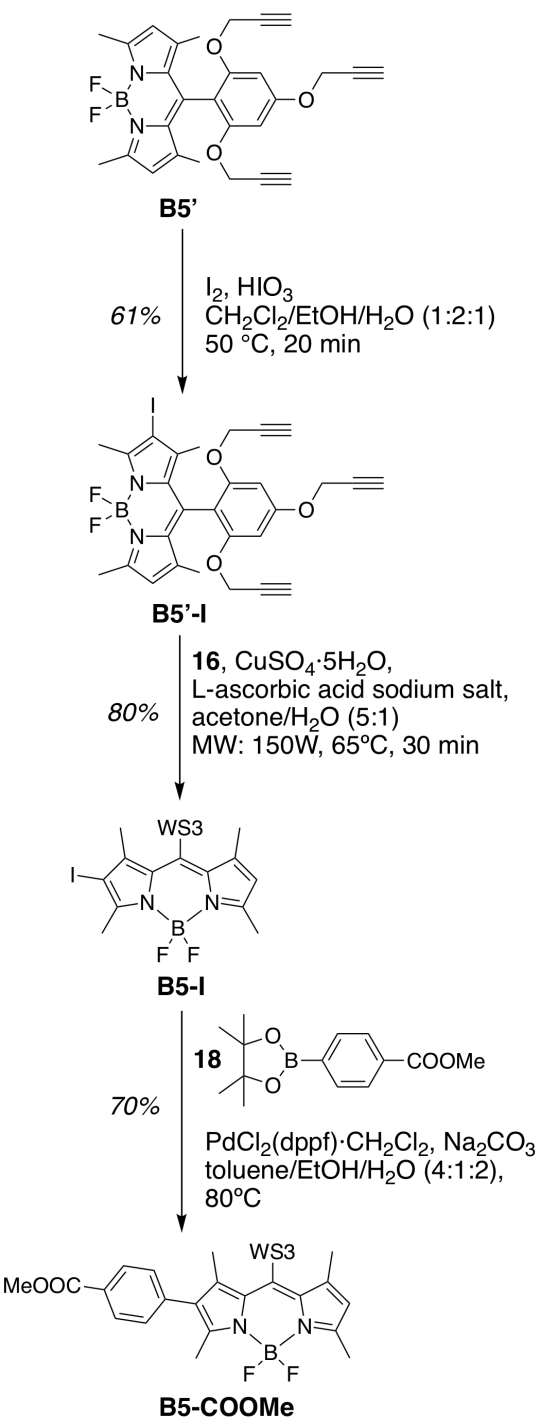

Scheme 5.5: Synthesis of BODIPY B5-COOMe

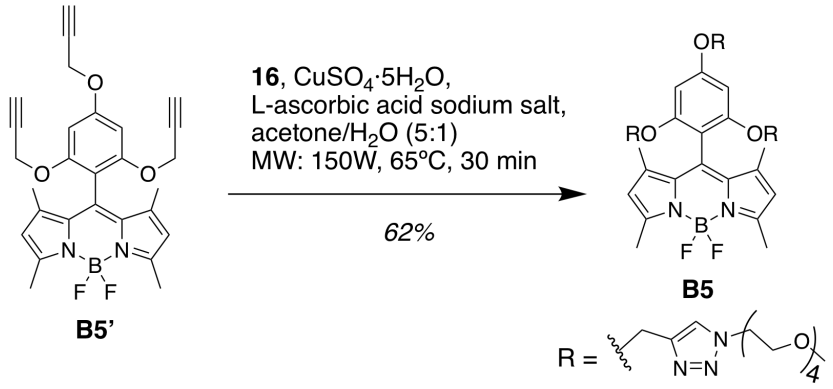

Scheme 5.6: Synthesis of B5 via microwave assisted Click reaction

Section 5.2.2: Synthesis of BODIPY-Hydroporphyrin Arrays

The target arrays **ET5-ET12** were prepared in analogous fashion to that reported for dyads **ET1-ET4**. Arrays **ET5** and **ET11-ET12** were prepared by EDC mediated amide coupling (similar to **ET3-ET4**) while **ET6-ET10** were prepared by Sonogashira reaction (similar to **ET1-ET2**). Syntheses of dyads are presented below in chronological order as opposed to grouping by synthetic method, the chronology was dictated by hydroporphyrin (chlorins first, then bacteriochlorins) and the availability of respective BODIPY coupling partners (we first synthesized **B3-NH$_2$**, then **B4** and finally **B5-COOMe**). All dyads were prepared in low to modest yields (22-35%). Array **ET5**, which can be thought of as the water soluble counterpart to **ET3**, was synthesized by coupling of 10-(4-carboxy)phenyl chlorin **C1-COOH** with amine substituted **B3-NH$_2$**, in 30% yield (Scheme 5.7). It is worth noting that **C1-COOH** was first hydrolyzed from **C1-COOMe** as described in Chapter 4, where **C1-COOH** was treated

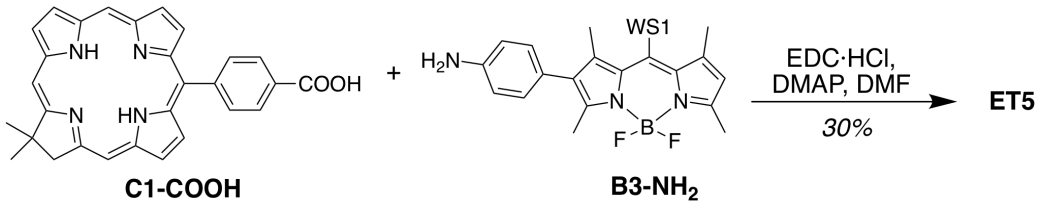

Scheme 5.7: Synthesis of amphiphilic amide linked energy transfer array ET5

as an intermediate. The following 5 arrays were all prepared via copper free Sonogashira cross coupling between bromo-hydroporphyrin and meso-ethnylphenyl substituted BODIPY. Arrays **ET6** and **ET7** were prepared from 13-bromo-10-mesityl chlorin **C1-Br** reacted with either **B1** (by Nithya Santhanam, yielding hydrophobic model array **ET6** in 33% yield) or **B4** (yielding **ET7**, in 29% yield, Scheme 5.8).

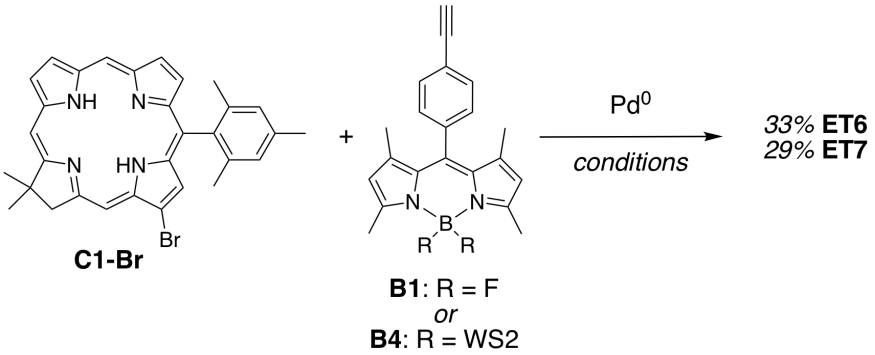

Scheme 5.8: Synthesis of Dyads ET6 and ET7. Conditions - ET6; B1, $Pd_2(dba)_3$, P(*o*-tol)$_3$, toluene/Et_3N, 60ºC. Conditions - ET7; B4, $(PPh_3)_2PdCl_2$, DMF/Et_3N, 80ºC.

Next dyads **ET8** and **ET9** were prepared in the same fashion, except the chlorin component was replaced with 3-bromo-13-(4-methoxycarbonyl)phenyl bacteriochlorin **BC1**. Hydrophobic array **ET8** was prepared by cross coupling between **BC1** and **B1** in 26% yield, where amphiphilic **ET9** was prepared from **BC1** and **B4** in 35% yield (Scheme 5.9, top). The final array prepared through Sonogashira cross coupling was triad **ET10**, which was synthesized from **B4** and 3,13-dibromo bacteriochlorin **BC0** in 33% yield (Scheme 5.9, bottom). The yield reported for **ET10** is approximately 90-95% pure (see experimental section 5.5.5) as we were unable to fully remove a fluorescent BODIPY-type byproduct. All arrays prepared by Sonogashira coupling showed byproducts corresponding to the homocoupling of *meso*-phenylethynyl BODIPY component. Yields are modest due to extensive purification of arrays, which in some cases required both size exclusion chromatography and silica gel

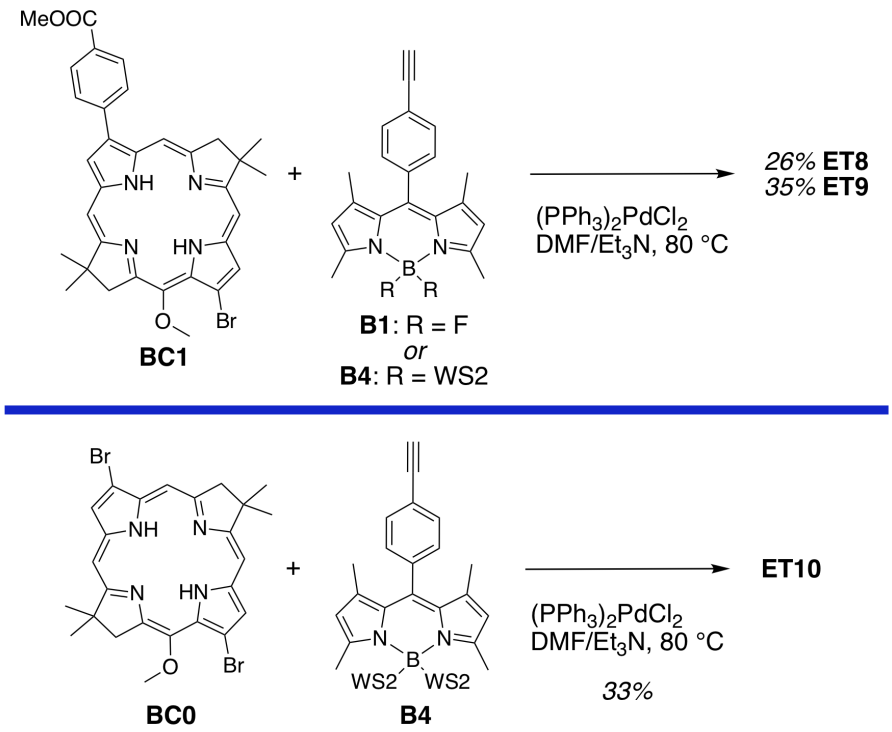

Scheme 5.9: Synthesis of BODIPY-bacteriochlorin dyads ET8 and ET9 (top) and triad ET10 (bottom).

chromatography. Hydrophobic arrays were washed free of fluorescent impurities by methanol following initial silica gel chromatography. In the case of arrays **ET7**, **ET9** and **ET10** the low yield can be in part attributed to the lability of the boron-oxygen bond. This notion was reinforced by the very low yields (below 10%) of our early Sonogashira attempts which utilized K_2CO_3 as base.

For the final two arrays, we first attempted EDC mediated amide coupling (Scheme 5.10) between amino substituted bacteriochlorins **BC1/2-NH$_2$** (provided by Dr. Joshua Akhigbe)[120,122] and the free acid of **B5-COOMe** (hydrolysis product). This route encountered two significant problems. First, the hydrolysis of **B5-COOMe**

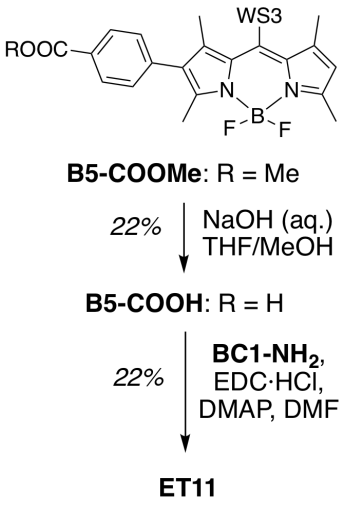

Scheme 5.10: Synthesis of dyad ET11 with amidation as final reaction.

in NaOH (2M, aq.) lead to significant decomposition and a yield of only 22%. We were unable to identify the reason behind the BODIPYs decomposition, as they are known to survive similar hydrolysis conditions.[387,388] Second, the amide synthesis between **B5-COOH** and **BC1-NH$_2$** only provided **ET11** in 22%. This poor yield was in agreement with observations made by Dr. Akhigbe when attempting to couple chlorins and bacteriochlorins.

Due to consecutive poor yields, we rationalized a new route to the target arrays would be necessary. We sought to avoid both hydrolysis of the BODIPY, and a final amide synthesis reaction with multiple large coupling partners. Taking these things into consideration, we changed our approach to include earlier amide coupling between amino bacteriochlorin and the much smaller 4-carboxyphenylboronic acid pinacol ester **20**. This step would provide our amide linker component and also provide a synthetic handle to join with 2-iodo BODIPY **B5-I**. Thus, we synthesized the requisite pinacol boronate bacteriochlorins, **BC1/2-Bpin**, from carboxylic acid **20** and **BC1-NH$_2$** or **BC2-NH$_2$**, respectively (Scheme 5.11). Based upon TLC we observed complete conversion of starting bacteriochlorins, however, upon purification our yields were quite low (29% for **BC1-Bpin** and 33% for **BC2-Bpin**). We suspected that this was due to interaction between the boronic ester and silica and revisited the literature. We found that Isobe *et al*. performed a short study that agreed with our hypothesis, in which they demonstrated that the low yields of boronic esters purified on silica can be improved by first impregnating the silica gel with an excess of boric acid.[389] The greater yields have been attributed to the pretreatment limiting adsorption of the molecule of interest to silica. Because of the high investment of both cost and time with our arrays,

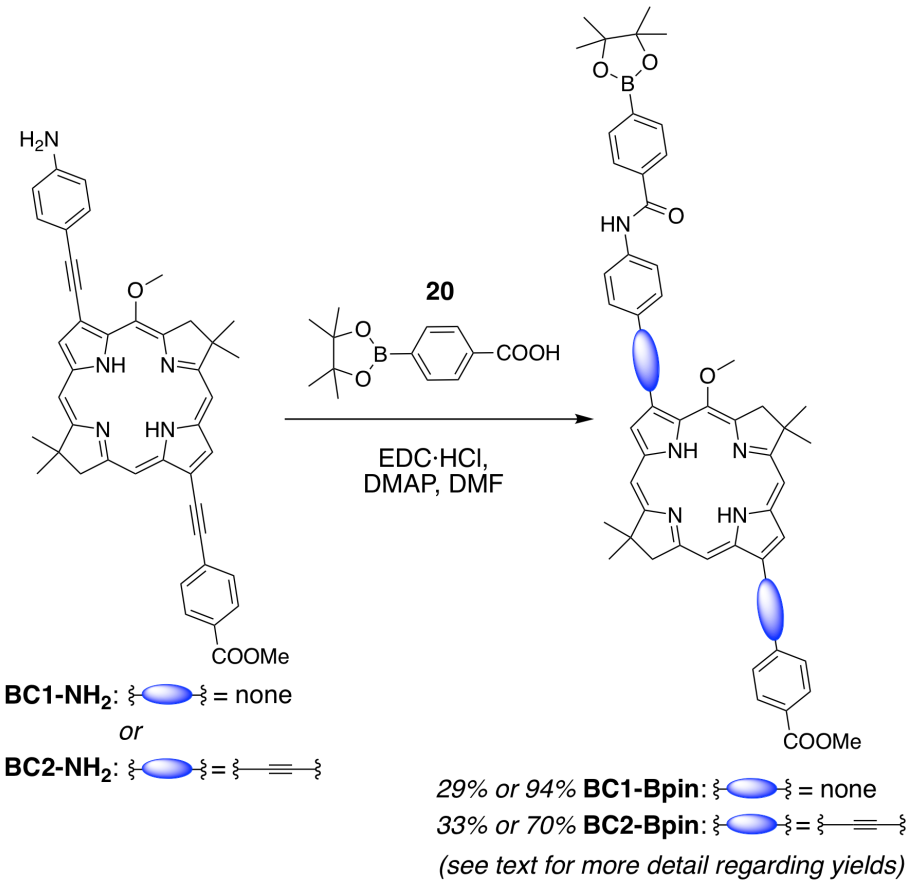

Scheme 5.11: Synthesis of Suzuki coupling ready boronic ester substituted bacteriochlorin intermediates BC1-Bpin and BC2-Bpin.

we were unwilling to risk further loss of material to silica gel, despite the promising outlook of Isobe's method of purification. We ran the syntheses again, and left **BC1/2-Bpin** as crude products following the removal of excess acid through sodium bicarbonate wash. This time, yields were greatly improved for **BC1-Bpin** (94%) and **BC2-Bpin** (70%), with 90% or greater purity (as estimated from ^{1}H NMR). Finally, we prepared dyads **ET11** and **ET12** from Suzuki coupling of **B5-I** with **BC1-Bpin** or **BC2-Bpin** (Scheme 5.12). This provided **ET11** in 22% yield and **ET12** in 30% yield. While the yields were still low (21% after two steps for **ET11** from **BC1-NH$_2$**), it was a great improvement over the initial route (3.4% over three steps from **B5-I** through **B5-COOMe**) and provided us with workable quantities of target arrays.

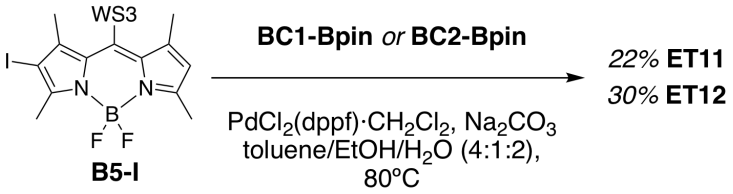

Scheme 5.12: Synthesis of BODIPY-bacteriochlorin dyads ET11 and ET12 via Suzuki coupling

Section 5.3: Characterization

Section 5.3.1: Structure Determination

All novel compounds were characterized by ^{1}H and ^{13}C NMR, and HRMS. All ^{1}H NMR performed on dyads indicated 1:1 ratio of aromatic resonances from hydroporphyrin to BODIPY, where triad **ET10** showed ratio of 1:2. Some compounds (BODIPY monomers and arrays containing water soluble BODIPYs) showed slight excess of protons belonging to PEG substituents. We were unable to change the observed relative integration of those signals through iterative chromatography and have determined it to be a consequence of error when determining integrals. I.e., the reference integral for a single proton was set to one, and we observe consistent over integration for the large overlapping PEG signals. Despite the over-integration, we are confident in the identity of all compounds because in all cases, HRMS *m/z* were consistent with the proposed structures and show no apparent PEG impurities. Unlike the work discussed in Chapter 4, we did not perform ^{19}F NMR for the work presented in Chapter 5. The structural integrity of new BODIPYs and BODIPY containing arrays was instead assessed by absorption and emission spectroscopy after each reaction (in addition to ^{1}H and ^{13}C NMR).

Section 5.3.2: Determination of BODIPY Stability

One of our primary concerns for arrays containing boro-alkoxy substituted BODIPYs (arrays **ET7**, **ET9-ET12**) was the stability of the B-O bond, which has the

potential to react under acid or basic hydrolysis, and is susceptible to nucleophilic attack.[358,362] Primarily, the stability of the B-O bond would have implications in whether or not the completed arrays are stable under imaging conditions.Second, the lability of the B-O bond would dictate our synthetic pathways in obtaining **B4** containing arrays and determine whether or not they were suitable for late-stage manipulation. We first tested the stability of BODIPY **B4** in solution, while stored darkness. Dilute solutions of **B4** in toluene, DMSO and PBS (pH = 7.4) were all prepared, then left for 24 hours. Absorption spectra acquired after 24 hours matched those from the beginning of the experiment, indicating the B-O bonds were stable around neutral pH (spectra not shown). We then performed a similar experiment to assess stability of **B4** against conditions we commonly use for basic [2M NaOH in THF/MeOH (2:1)] or acidic [TFA in CH_2Cl_2 (4:1, v/v)] hydrolysis. In both the basic and acidic conditions, the absorption spectrum of **B4** underwent significant alteration. This includes the loss of the primary S_0-S_1 band of BODIPY around ~515 nm and the appearance of a large broad band in the UV region (spectra not shown). These changes indicate that **B4** underwent significant decomposition under these conditions and indeed the presence of B-O bond limits our available synthetic modifications post boron-alkoxylation step. However, the first set of experiments showed that the arrays should be suitable for imaging around neutral pH.

Section 5.3.3: Photophysical Characterization

The absorption and emission properties of all monomers and arrays were determined in toluene and DMF, in addition, all water soluble BODIPY monomers were measured in PBS while amphiphilic arrays were measured in aqueous micelles/vesicles (prepared from numerous surfactants, see Table 5.3). Here we

focused on the aspects that would demonstrate the usefulness of our constructs in biological media. The key points were; first, the assessment of water-soluble BODIPY emission properties in aqueous media, particularly fluorescence quantum yield; second, the impact on solvent polarity (measured in terms of dielectric constant) on the fluorescence properties of BODIPY-hydroporphyrin arrays, with emphasis on energy transfer efficiency and PET; and third, overall performance of arrays in aqueous micelles (i.e., do they retain the properties we observe in non-polar solvents). The absorption and emission spectra of BODIPY monomers taken in toluene and in PBS (pH = 7.4) can be found in Figure 5.1, emission spectra (toluene only) in Figure 5.2, and a summary of photophysical properties can be found in Table 5.1. Similarly, the absorption spectra of dyads can be found in Figures 5.3 (chlorins) and 5.4 (bacteriochlorins), and emission spectra in Figures 5.5 (toluene only). A summary of the photophysical properties of all arrays can be found in Table 5.2. For comparison, the absorption and emission properties of relevant hydroporphyrin monomers (as well as structures) can be found in the Supporting Information (Table 5.5).

Photophysical Properties for BODIPY Monomers

BODIPY absorption spectra showed the typical S_0-S_1 absorption band centered at ~515 nm with higher energy S_0-S_2 band centered at ~360 nm. All three benchmark monomers (**B3**, **B4**, **B5**) lacking 2-position substituent showed nearly identical absorption maxima, which was blue shifted by 2-5 nm in PBS compared to toluene. Absorption maximum of **B5-COOMe** was red shifted ~15 nm compared to the others due to the presence of 2-(4-methoxycarbonyl)phenyl substituent. Each BODIPY, when compared between toluene and PBS, showed minimal change to the shape of absorption

band, indicating that there was no aggregation at the given concentration (~ 10 μM based on assumed ε of ~100,000 $M^{-1} \cdot cm^{-1}$).[265]

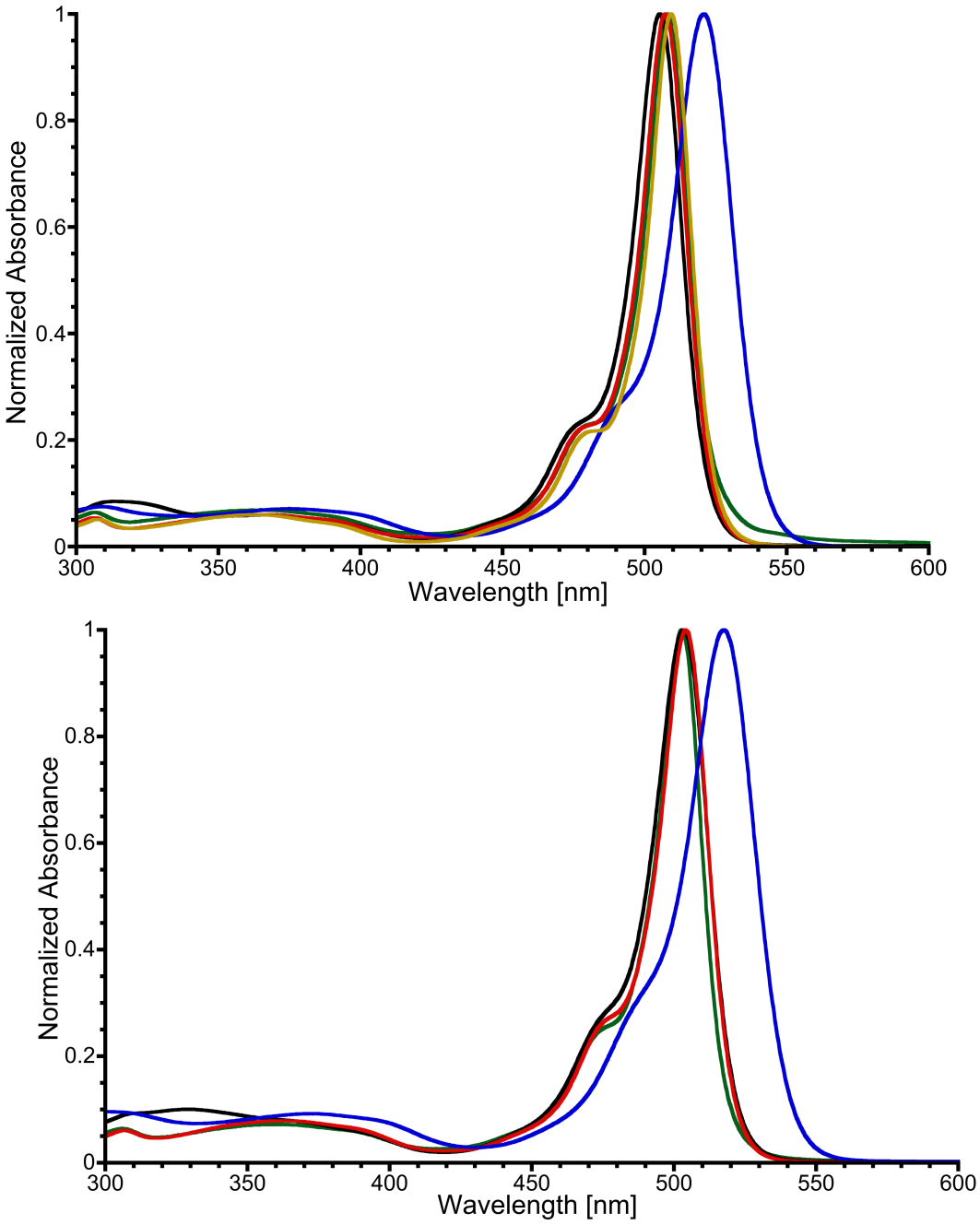

Figure 5.1: Absorption spectra in toluene (top) and PBS (pH = 7.4, bottom) for BODIPY monomers discussed in Chapter 5. B3 (black), B4 (green), B5 (red), B5-COOMe (blue), B5' (gold). All spectra acquired at room temperature at ~10 μM concentration then normalized.

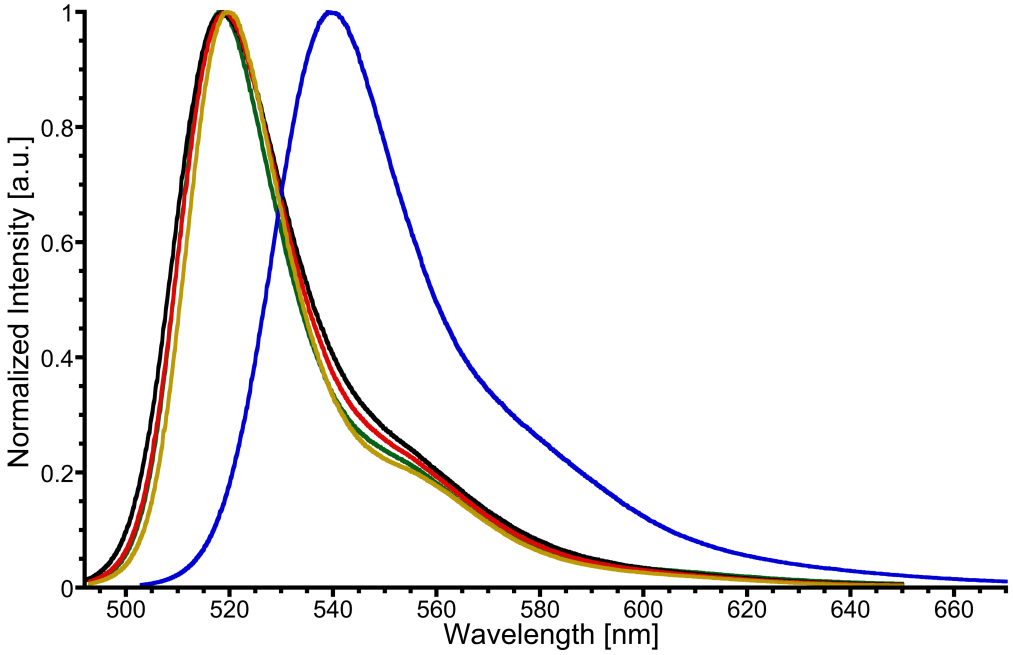

Figure 5.2: Emission spectra for BODIPY monomers discussed in Chapter 5. B3 (black), B4 (green), B5 (red), B5-COOMe (blue), B5' (gold). All spectra acquired in toluene at room temperature at ~1.0 µM concentration, upon excitation at blue edge of primary absorption band (λ ~ 480-490 nm, where slope is minimal), then normalized.

BODIPY	λ_{abs} (nm)	λ_{emi} (nm)	Φ_F tol.	Φ_F DMF	Φ_F PBS
B3	508	518	0.89	0.80	0.25
B4	505	519	0.56	0.56	0.77
B5	507	520	0.97	1.0	1.0
B5-COOMe	521	539	0.89	0.91	0.82
B5'	509	520	1.0	1.0	n/a

Table 5.1: Absorption and emission properties of water soluble BODIPY derivatives and hydrophobic B5', in air-equilibrated toluene [or DMF and PBS (pH = 7.4) where indicated]. Fluorescence quantum yields were determined against rhodamine 6G (Φ_F = 0.88, in air-equilibrated ethanol)[390,391] upon excitation at blue edge of the S_0-S_1 absorption band (λ ~ 480-490 nm, where slope is minimal). n/a – not applicable due to lack of solubility. Absorption spectra acquired at ~10 µM concentration, emission spectra at ~1.0 µM concentration. Error for quantum yield measurements estimated at ± 5% (see section 2.5.4 for details).

The acquired emission spectra were typical for those of BODIPY (Figure 5.2). All monomers possessed a single strong emission band with Stokes' shift in the range of 10-15 nm, and the λ_{max} for emission was minimally blue shifted when going from toluene to PBS (0-4 nm). The fluorescence quantum yields for all BODIPYs met or exceeded 0.56 in toluene. Most BODIPYs showed no fluorescence quenching in DMF compared to toluene, only **B3** fluorescence was quenched (~10%). Water soluble monomers **B4**, **B5** and **B5-COOMe** possess large Φ_F in PBS (≥ 0.76) while **B3** shows a diminished but still large Φ_F (0.25) for PBS. There are a few noteworthy observations regarding these Φ_F values. First, Φ_F is comparable between toluene and PBS for monomers **B4**, **B5** and **B5-COOMe**. This was a bit surprising, because we expected to observe a reduction of Φ_F for the monomers with electron rich trialkoxyphenyl substituents at the 8-position. It is well known that such electron rich *meso* substituents cause reduction of Φ_F in BODIPYs due to electron transfer from *meso* substituent to photoexcited BODIPY.[313] One possible explanation for this lack of quenching is the presence of the four methyl substituents placed around the BODIPY core, increasing the reduction potential (more negative) to the point where PET is disfavored. It is unclear, however, why Φ_F for **B3** is so diminished when its reduction potential is tuned similarly as **B5** and **B5-COOMe**. The only significant difference between **B3** and **B5** is the presence of the triazole moieties as part of the larger water solubilizing group, though it is unclear how they would contribute to limiting PET in **B5**. Second, for **B4**, Φ_F increases from 0.56 in toluene to 0.77 in PBS. My hypothesis is that a tighter solvation shell is formed in PBS, as opposed to toluene, decreasing the extent of non-radiative relaxation in photoexcited **B4**. Third, the presence of 2-aryl substituents does

not significantly influence Φ_F. This is demonstrated by Φ_F of **B5-COOMe** decreasing only 10% relative to **B5**. The slight decrease is likely due to the additional bond providing non-radiative relaxation though rotation. Overall, our results indicate that the **B3** and **B5** series of BODIPY monomers are suitable for use in not only polar organic solvents (DMF) but in PBS as well. On the other hand, the **B2** series of BODIPYs possess decreased fluorescence for reasons currently beyond our understanding, and thus are less desirable for use in imaging applications as stand alone chromophores.

Photophysical Properties of Hydroporphyrin-BODIPY Arrays

Absorption spectra of all novel arrays appeared as anticipated, a sum of the parts, with distinct *B* and Q_y absorption bands from hydroporphyrins and intense absorption band from BODIPY in the green spectral window. All maxima closely match those of their parent monomers (see Table 5.1 for properties of hydroporphyrin monomers) with one exception being the BODIPY absorption band of **ET12** (527 nm), it is red shifted by nearly 6 nm in comparison to **B5-COOMe** (521 nm). The reason for this small bathochromic shift is unclear, because it was not observed in the similarly constructed **ET11**.

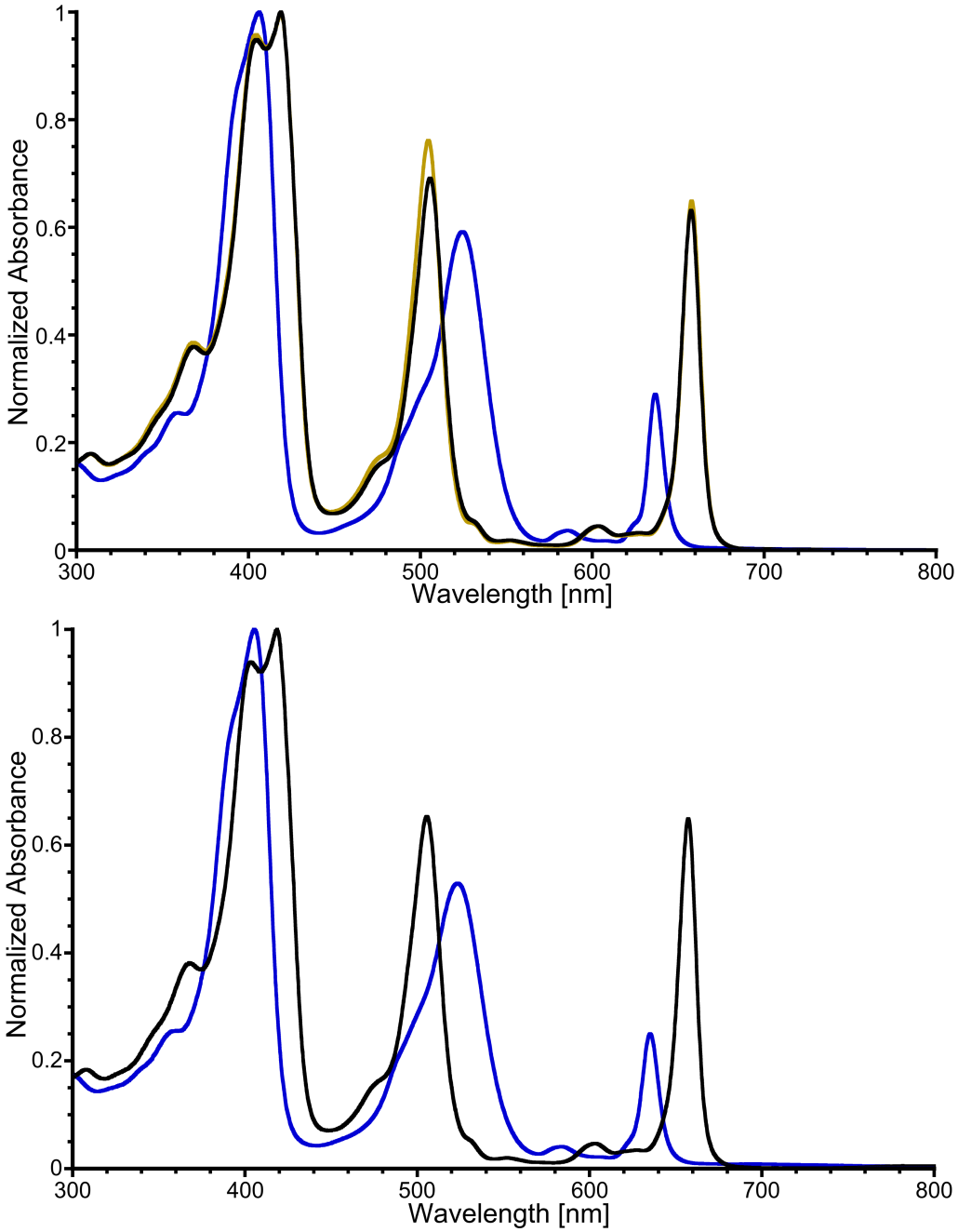

Figure 5.3: Absorption spectra in toluene (top) and TX-100 (3mM in PBS, pH = 7.4, bottom) for chlorin-BODIPY arrays: ET5 (blue), ET6 (gold), and ET7 (black). All spectra acquired at room temperature at ~10 µM concentration and normalized at the hydroporphyrin B band.

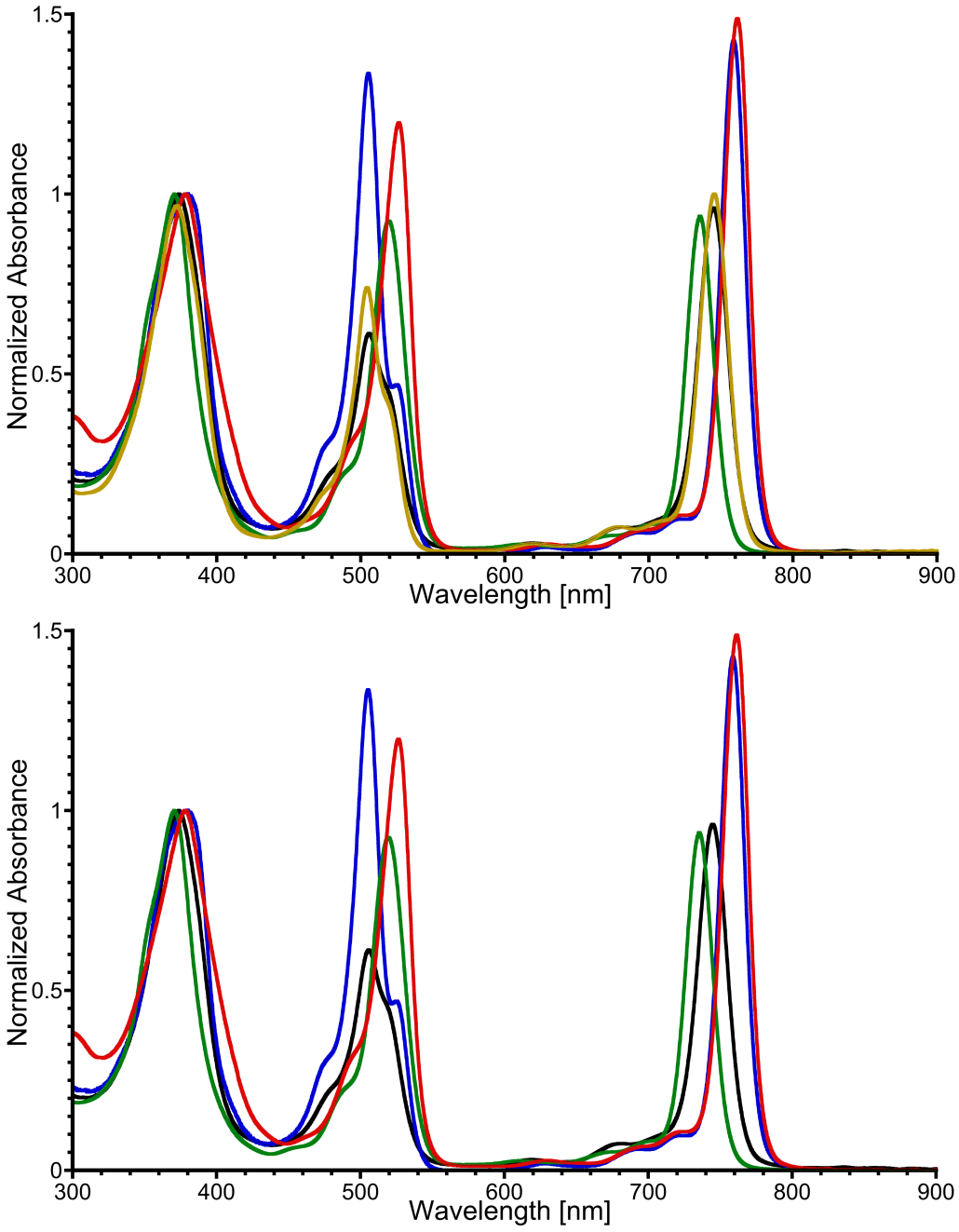

Figure 5.4: Absorption spectra in toluene (top) and TX-100 (3mM in PBS, pH = 7.4, bottom) for bacteriochlorin-BODIPY arrays: ET8 (gold), ET9 (black), ET10 (blue), ET11 (green), and ET12 (red). All spectra acquired at room temperature at ~10 µM concentration and normalized at the hydroporphyrin B band.

We also attempted to acquire the absorption spectra of ET arrays in several aqueous surfactants. Absorption spectra in TX-100 (3mM in PBS, pH = 7.4) are nearly identical to those obtained in toluene (Figures 5.3 and 5.4), under the approximate concentration of 10 μM. The assumption of concentration is made based upon average values of chlorin (150,000 $M^{-1}\cdot cm^{-1}$)[107] and bacteriochlorin (100,000 $M^{-1}\cdot cm^{-1}$)[113] *B* bands and an absorbance set to ~1.0. There are no significant changes to the absorption spectra, ruling out aggregation occurring at this concentration. When we measured absorbance of the ET arrays in Tween 20 (0.1% v/v in PBS), their behavior was noticeably different (Figure 5.5). Only dyads **ET7, ET9** and **ET10** were sufficiently soluble to reach a similar concentration as in TX-100 solution. Dyads **ET7** and **ET9** were well dissolved in Tween 20 solution, the only difference to spectra between the different surfactant solutions is a small change to the relative intensities of *B* and Q_y absorption bands. The absorption spectrum of **ET10**, showed a new band with λ_{max} at 794 nm, in tandem with a reduction of the Q_y band intensity. This behavior is indicative of J-aggregate formation and has been documented for hydrophobic chlorophyll derivatives that were formulated in aqueous micelles.[392–394] Remaining amphiphilic arrays **ET5**, **ET11** and **ET12** were similarly prepared, but there was immediate, extensive broadening of the *B* and Q_y bands, indicating significant aggregation. To remove the aggregates, we filtered the samples through 20 micron membranes, and obtained absorption spectra without exaggerated/broadened features, at significantly diminished concentration (~1 μM or below, corresponding to A< 0.1, Figure 5.5).

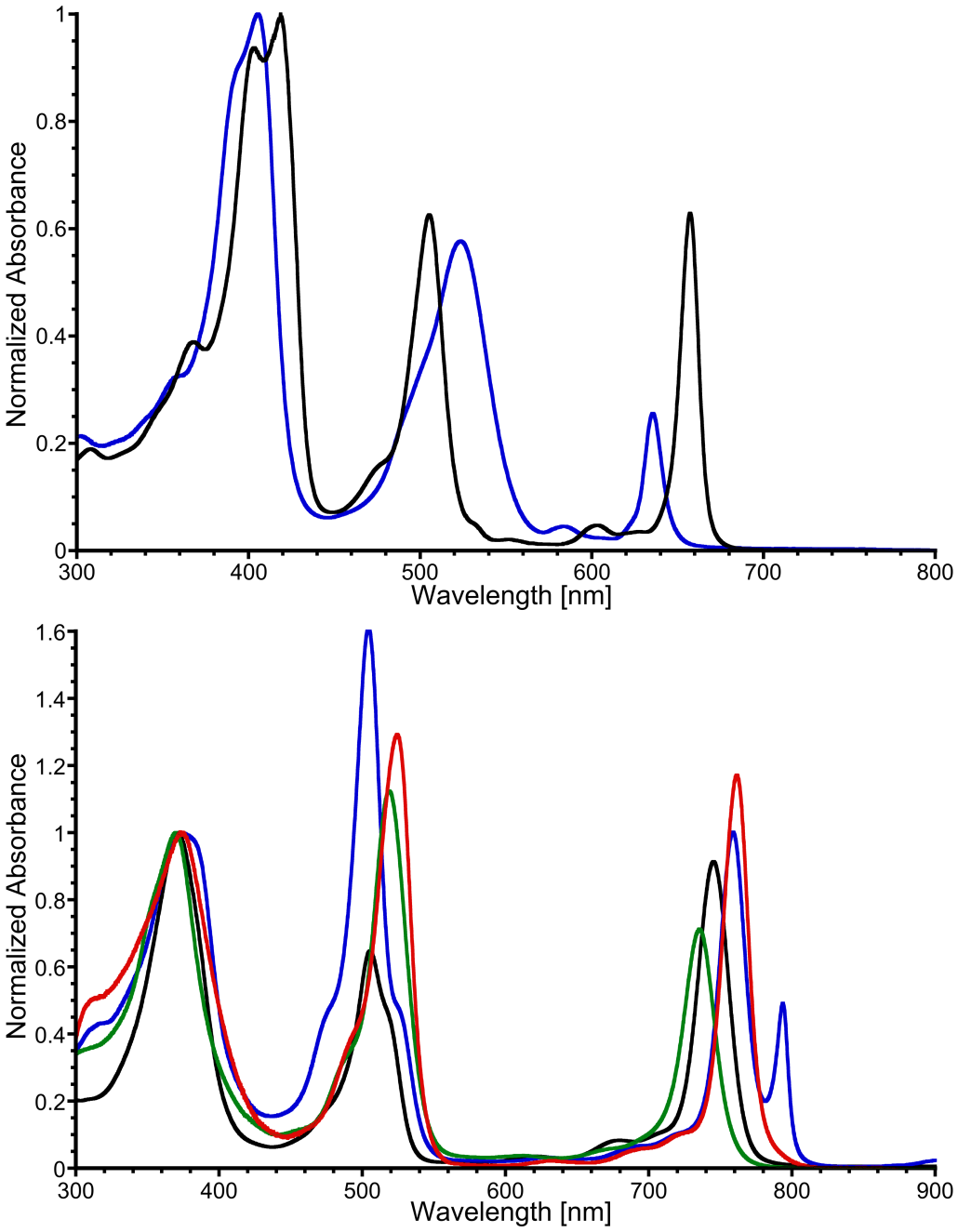

Figure 5.5: Absorption spectra of amphiphilic arrays in Tween-20 (0.1% wt in PBS, pH = 7.4). Top features chlorin-BODIPY arrays: ET5 (blue) and ET7 (black). Bottom features bacteriochlorin-BODIPY arrays: ET9 (black), ET10 (blue), ET11 (green), and ET12 (red). All spectra acquired at room temperature at ~1.0 µM concentration (due to filtration to remove aggregates) and normalized at the hydroporphyrin *B* band.

Note that even after filtration, a J-aggregate was observed in the case of **ET10**. Despite the apparent broadening of the *B* and Q_y bands, the BODIPY absorption bands did not appear to be significantly affected in any of the arrays. Overall, we determined here that all arrays have greater solubility in TX-100 solution rather than Tween 20. Furthermore, those arrays with water solubilizers installed through BODIPY boron (**ET7**, **ET9**, **ET10**) are more soluble in Tween 20 solution and less prone to aggregation than arrays where water solubilizers are installed via BODIPY *meso* (trisalkoxy)phenyl substituent (**ET5**, **ET11**, **ET12**).

The emission spectra of all new BODIPY-hydroporphyrin arrays were similar to what we observed with dyads **ET1-ET4**; they featured nearly exclusive emission (Figure 5.6) from the hydroporphyrin component regardless of excitation wavelength (*B* band or BODIPY). Upon excitation in the green spectral window (BODIPY band) there is only a small amount of residual emission from the BODIPY, except in the case of **ET10**, where we can also attribute BODIPY emission to an impurity (see experimental section 5.5.4 for more detail). Next, we acquired fluorescence excitation spectra for new arrays, when monitoring exclusively the hydroporphyrin emission. In all cases, excitation spectrum (not shown) closely resembled the absorption spectrum of given dyad, qualitatively indicating the high energy transfer efficiency. We then went on to determine the fluorescence quantum yields for all energy transfer arrays, as well as ETE. As in Chapter 4, we again chose to determine ETE as the ratio of Φ_F of hydroporphyrin upon excitation at BODIPY absorption λ_{max}, divided by Φ_F of hydroporphyrin upon direct excitation at *B* band absorption λ_{max}. In toluene, all arrays

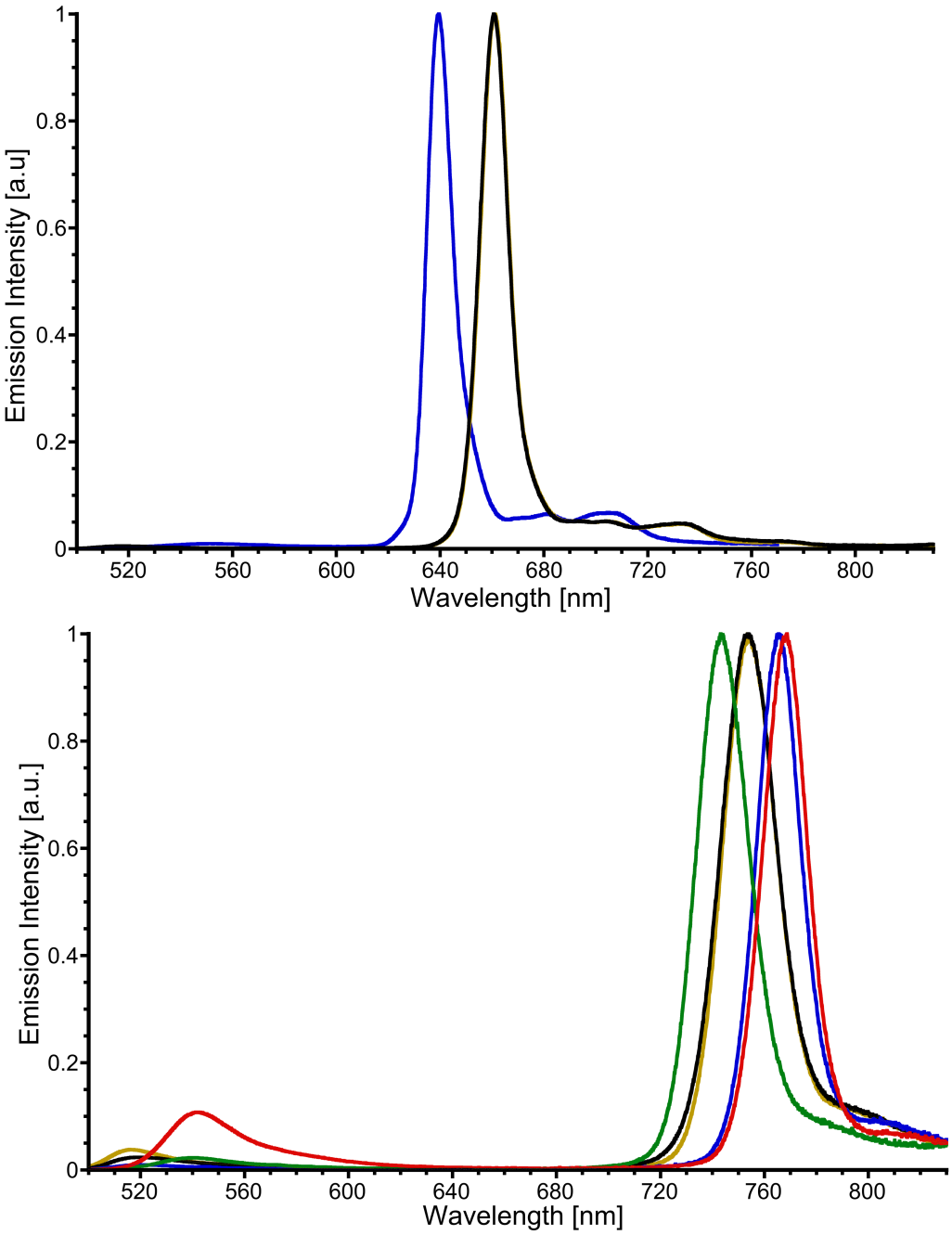

Figure 5.6: Emission spectra of arrays taken in toluene. Top features chlorin-BODIPY arrays: ET5 (blue), ET6 (gold, closely overlapping ET7), and ET7 (black). Bottom features bacteriochlorin-BODIPY arrays: ET8 (gold), ET9 (black), ET10 (blue), ET11 (green), and ET12 (red). All spectra acquired at room temperature at ~1.0 μM concentration, upon excitation at the blue edge of BODIPY S_0-S_1 absorption band (λ ~ 480-490 nm, where slope is minimal), then normalized at the maximum of hydroporphyrin emission band.

Array	Absorption λ_{max} (nm)			λ_{emi} (nm)	$\Phi_{toluene}$ [ETE]	Φ_{DMF} [ETE]	Φ_{TX-100} [ETE]	$\Phi_{Tween-20}$ [ETE]
	$\lambda_{B\ band}$	λ_{BODIPY}	λ_{Qy}					
ET5	406	523	637	639	0.22 [0.97]	0.22 [0.94]	0.16 [0.95]	0.12 [0.78]
ET6	405, 419	503	658	661	0.39 [0.96]	0.21 [0.98]	n/a	n/a
ET7	405, 419	507	658	661	0.35 [0.96]	0.35 [0.95]	0.31 [1.04]	0.33 [1.04]
ET8	372	505	745	754	0.25 [0.96]	0.070 [0.97]	n/a	n/a
ET9	374	505	745	754	0.24 [1.00]	0.19 [0.93]	0.20 [1.20]	0.19 [1.12]
ET10	380	505	759	766	0.24 [0.99]	0.20 [0.96]	0.19 [1.07]	0.10 [0.84]
ET11	371	519	736	744	0.22 [0.90]	0.12 [0.70]	0.12 [0.92]	0.069 [0.80]
ET12	378	527	761	767	0.23 [0.91]	0.20 [0.82]	0.14 [1.0]	0.10 [0.83]

Table 5.2: Absorption and emission properties of BODIPY-hydroporphyrin arrays. All presented wavelength maxima were obtained in toluene. Fluorescence quantum yields are reported for excitation at maximum of BODIPY absorbance, while measuring emission of hydroporphyrin component for sample with absorbance set to A ~ 0.1 at the hydroporphyrin B band (corresponding to ~1.0 μM concentration of array). Where surfactants were used, measurements were performed in 3 mM TX-100 or 0.1% (v/v) Tween-20 in PBS (pH = 7.4). All Φ_F measurements were performed in air-equilibrated solvents, Φ_F was determined against TPP (Φ_F = 0.070 in air-equilibrated toluene)[109] and corrected for differences of refractive index (η) when utilizing solvents other than toluene. For measurements acquired in aqueous surfactants, the value for η used (1.45) was the average between that of pure water (1.33) and pure hydrocarbons (1.55).[395] ETE is determined as the ratio of Φ_F measured upon excitation at maximum of BODIPY divided by Φ_F measured upon direct excitation of hydroporphyrin at maximum of B band. Error for quantum yield measurements estimated at ± 5% (see section 2.5.4 for details), error for ETE estimated at ± 10% (see section 4.5.4). In some cases, ETE measured in aqueous micelles exceeded 1.00, this could be due to experimental uncertainty or due to localization of BODIPY and hydroporphyrin units in environment of different η, causing slightly different illumination of the two components.

exhibited Φ_F comparable to that of respective hydroporphyrin monomers (see Table 5.5) reinforcing that tethering the BODIPY unit(s) to the various hydroporphyrins did not affect their photophysical properties. In all cases, arrays had energy transfer efficiency in excess of 0.90 (Table 5.2).

We next examined the emission properties of our arrays in DMF (Table 5.2), to determine how increasing solvent polarity (as it relates to dielectric constant) affected our arrays, particularly with regard to quenching. For chlorin containing arrays, there was no change to ETE when going from toluene to DMF, and a reduction in Φ_F (42%) was observed only for dyad **ET6**. For bacteriochlorin containing arrays, quenching was observed in all cases, ranging from 13% (in **ET12**) to 72% decrease (in **ET8**) of Φ_F. For most arrays, ETE is comparable between toluene and DMF, except in **ET11** and **ET12** where ETE dropped to 0.70 and 0.82, respectively. The more pronounced decrease in Φ_F for all bacteriochlorin arrays is attributable to the lower oxidation potential of bacteriochlorins relative to chlorins,[211] making bacteriochlorins more likely to undergo oxidative PET. Recall that this was one of the motivations in preparing boron substituted BODIPY derivatives, where we hypothesized that altering the reduction potential at BODIPY could limit quenching of arrays. To assess how replacing BODIPY B-F bonds with less electronegative B-O influenced quenching, we compared the Φ_F of amphiphilic arrays **ET7**, **ET9** and **ET10** against their hydrophobic analogues **ET6** and **ET8** in DMF. For chlorin arrays, amphiphilic **ET7** showed no quenching relative to toluene where **ET6** was quenched by nearly half. For amphiphilic boron substituted bacteriochlorin arrays **ET9** and **ET10**, there was ~20% decrease in Φ_F relative to 72% decrease for B-F containing **ET8**. Because ETE is nearly

quantitative for all of the arrays in consideration, regardless of being in toluene or DMF, we can assume that the difference in quenching is due to the structural differences between the hydrophobic and hydrophilic BODIPYs. Specifically, replacing the B-F bonds with B-O bonds, increases the effective electron density on the BODIPY unit, decreasing its reduction potential. By making the BODIPY unit harder to reduce, PET in the system as a whole becomes less efficient. Our assumption here was reinforced by DFT calculations, which showed that upon replacement of both fluorides with methoxy groups, the HOMO and LUMO energies increase by 0.18 and 0.19 eV, respectively (Figure 5.6.2) This increasing LUMO energy is an indirect measure of decreasing reduction potential.

Next, we compared the arrays where the BODIPY is connected to hydroporphyrin via amide. Dyad **ET5**, showed negligible quenching in DMF compared to toluene, and no change to ETE. This was consistent with the earlier chlorin 10-position amide linked arrays **ET3-4**. For bacteriochlorin arrays, where we are only able to place the amide at the 3- or 13- position, results differed. Dyad **ET11** showed a significant decrease in Φ_F (45%) when going from toluene to DMF, while **ET12** had a much smaller decrease of only 13%. The lower Φ_F in the case of **ET12** is the consequence of less efficient energy transfer in DMF than in toluene (0.82 vs 0.91), and we can attribute the greater quenching in **ET11** relative to **ET12** due to differences in oxidation potential of the bacteriochlorin. This difference is due to the phenylacetylene substituents of **ET12** increasing the oxidation potential more so than phenyl substituents of **ET11**,[36,282] making it more facile for **ET11** to undergo oxidative PET.

The next step was to determine the emission properties of the amphiphilic energy transfer arrays in aqueous micelles, as this would be the closest representation for an *in vivo* environment we have available. For screening surfactants, we began with dyad **ET9**. **ET9** was the dyad of choice because it had shown minimal changes to absorption spectra in both TX-100 and Tween 20 solution, and as a bacteriochlorin containing array, possessed longer emission maxima (most relevant *in vivo*) as well as greater propensity to undergo quenching than chlorin containing dyad **ET7**. We acquired the emission spectra of **ET9** in the following solvents; PBS/DMSO (95:5, v/v), TX-100 (3mM in PBS), Pluronic F-127 (0.13 mM in PBS), Tween 20 (0.1% v/v. in PBS) and poly(ethylene glycol) methyl ether-*block*-poly(*ε*-caprolactone) diblock polymer (PEG-PCl, 1.2 μM in PBS). Note that all surfactant solutions were prepared in at least 10-fold excess of the critical micellar concentration (CMC), for structures of all surfactants used and their CMC values in PBS see Table 5.3 in Section 5.5.1. From emission intensity it was apparent that **ET9** underwent significant quenching (>90% relative to toluene) in PEG-PCl, Pluronic F-127 and PBS/DMSO solutions, while significant signal was retained in TX-100 and Tween-20 solutions. Thus, we only examined the emission of other arrays in TX-100 and Tween-20 solutions. We were already aware, at this time, that select dyads showed poor solubility in Tween-20 formulated micelles, however, after filtration the absorption spectra suggested aggregates were removed, and concentration was sufficient (A~0.1) for us to determine Φ_F. For all dyads except **ET5** and **ET12**, the fluorescence quantum yield in TX-100 (3mM) was comparable to that found in DMF (Table 5.2). Dyad **ET5** showed a decrease of Φ_F from 0.22 to 0.16 despite going unquenched in DMF, while dyad **ET12**

had a decrease of Φ_F to 0.14 (from 0.20 in DMF, and 0.23 in toluene). In both cases, the decrease of Φ_F coincides with nearly quantitative energy transfer, so PET is the most probably cause of quenching. At this time, we also determined if the method by which micelles were formulated significantly affected the calculated Φ_F. The various methods and a table of Φ_F determined in TX-100 micelles, according to those methods are described in section 5.5.6. All differences were minor, and we determined that the formulation method did not influence Φ_F. Relative to TX-100, dyads formulated in Tween 20 micelles underperformed. Most arrays exhibited significant quenching (45-68%) compared to DMF, as well as lowered ETE. Only arrays **ET7** and **ET9**, which did not aggregate at all in Tween 20 solution, were unaffected by quenching.

There are several key points regarding the photophysical data for arrays. First, we observed high energy transfer efficiency (>0.90 from BODIPY to hydroporphyrin unit for all arrays in toluene. ETE diminished for arrays when formulated in aqueous micelles, however, ETE continued to exceed 0.8 in all cases. Second, when going from toluene to aqueous micelles, bacteriochlorin arrays underwent more significant quenching than chlorin arrays. This is consistent with our prediction that the lower oxidation potential of bacteriochlorins promotes oxidative PET. Third, we were able to disfavor quenching of fluorescence by PET, by installation of boro-alkoxy substituents on BODIPY. Amphiphilic arrays with water solubilizing groups installed at boron showed little (~20%) to no reduction of Φ_F in DMF where hydrophobic model arrays with B-F bonds underwent significant fluorescence quenching. Furthermore, arrays where BODIPY was linked to bacteriochlorin by amide underwent more significant quenching in both DMF and aqueous micelles than arrays with phenylethynyl linked

boro-alkoxy BODIPYs. When considering arrays **ET1-4** this is very interesting, because the amide linker discouraged PET where the phenylethynyl one may have contributed to PET. By tuning the BODIPY such that it is more electron rich, not only was this discrepancy overcome, but the arrays with phenylethynyl linked boro-alkoxy BODIPYs outperformed those with an amide linker and untuned BODIPYs.

Section 5.3.4: Photostability of Arrays in Aqueous Environments

Next, we evaluated the stability of amphiphilic arrays in aqueous media, both in darkness and upon light irradiation. We prepared solutions of each array in TX-100 (3mM in PBS) such that all dyads would have approximately the same concentration (~10 μM, absorbance at *B* band set to ~0.1) for this set of experiments. Once prepared, each solution was continuously irradiated at the maximum of bacteriochlorin *B* band by monochromatic light for set time intervals, after which the absorption spectrum was acquired. For more details on individual trials, and sample spectra see Section 5.5.7. In each case we observed a gradual decrease of the hydroporphyrin absorption bands, along with slower decrease in the BODIPY absorption band. The one exception to this was **ET5** where the BODIPY band underwent more rapid bleaching relative to the hydroporphyrin bands. The relative rates of photobleaching have been summarized in Figure 5.7, presented as the ratio of absorbance at Q_y band for given time (A) over the initial absorbance at Q_y band (A_0) vs duration of light exposure at BODIPY band. Bacteriochlorin containing arrays all underwent more rapid photobleaching than chlorin containing arrays, this was again a consequence of the lower oxidation potential of bacteriochlorins. Bacteriochlorin containing arrays with redox tuned BODIPYs underwent photobleaching slower than those with untuned BODIPYs. Array **ET11**

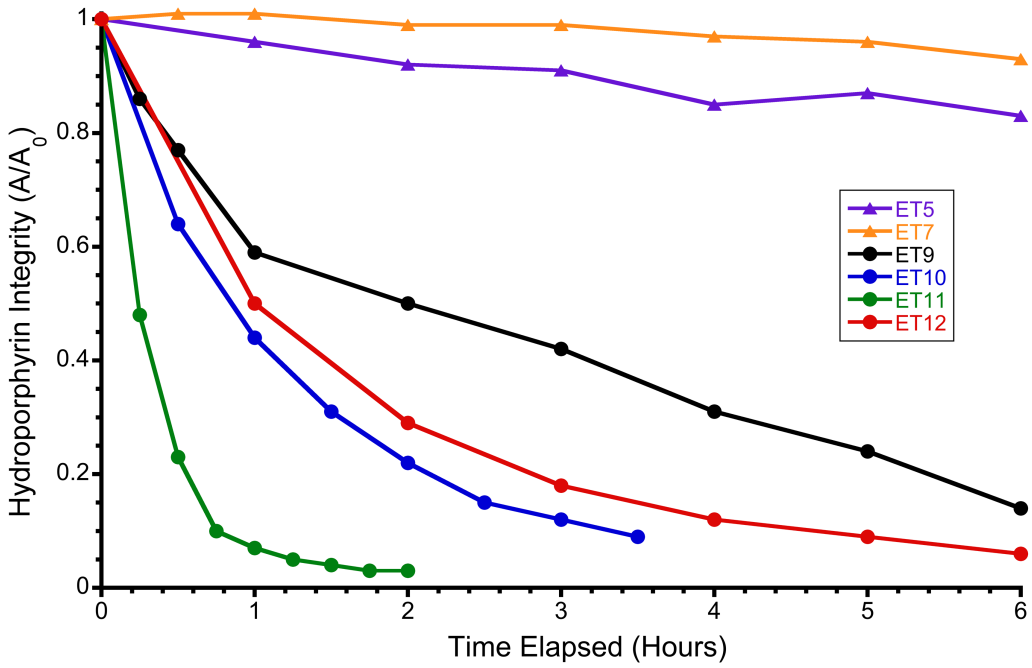

Figure 5.7: Relative rates of photobleaching for BODIPY-hydroporphyrin arrays, measured as the decay in absorbance of the Q_y band upon irradiation at the maxima of the BODIPY absorption band. A – absorbance at Q_y band maximum following irradiation for given duration, A – initial absorbance at Q_y band maximum. For more detail see Section 5.5.7.

underwent the most rapid photobleaching, this was expected because this bacteriochlorin has the lowest oxidation potential of all of those used in this study.[36,282] Note that the data in Figure 5.7 is presented with light exposure at BODIPY absorption maxima. We repeated the measurements with irradiation at hydroporphyrin component (*B* band) and the rate of photobleaching was effectively unchanged, indicating the process is independent of excitation wavelength (data not shown). As a control, we also prepared solutions of all arrays in 3mM TX-100 then left them protected from light for 24 hours, in all cases no changes to the absorption spectrum were observed.

We acknowledge that this was only a crude test for the photostability of our dyads, they nonetheless appear to have comparable stability to those previously utilized for *in vivo* imaging applications.[396–398] We did not choose to study the mechanism of photodegradation more thoroughly, but it could be oxidative decomposition brought on

by PET, or by reaction with singlet oxygen that hydroporphyrins are well known to produce.[396–398]

Section 5.3.5: Selection and Synthesis of Arrays for in vivo Imaging

When deciding which of our arrays were best suitable for our collaborator to image, we considered all of the following: the dyad must possess large ETE, large Φ_F, emit as far into the NIR, be soluble in aqueous micelles, and it must be readily converted into a succinimidyl (NHS) ester.[268] This is a common practice for bioconjugation of small molecules, and one which was previous employed by our collaborators (Kobayashi *et al*.).[120,268] Large ETE was ubiquitous for our arrays, and NIR emission ruled out chlorin containing arrays **ET5** and **ET7**. For bacteriochlorin containing arrays, **ET9** and **ET10** performed better in TX-100 solution (no quenching of fluorescence) than arrays **ET11** and **ET12**, that lacked boro-alkoxy substituents. However, those same boro-alkoxy substituents are too labile to survive the conversion of the methylbenzoate ester (bacteriochlorin 13-position) into NHS ester. This was demonstrated by B-O substituted BODIPYs loss of structural integrity in basic conditions (Section 5.3.2). Thus, we were synthetically restricted to using dyads **ET11** and **ET12**. While less than ideal, **ET11** and **ET12** undergo only partial quenching in aqueous micelles and retain a relatively large Φ_F for that spectral window. To convert **ET11** and **ET12** to their bioconjugatable forms, we separately performed basic hydrolysis, protonated intermediate carboxylate with HCL, then reacted with N-hydroxy succinimide **21** in the presence of EDC·HCl and DMAP, yielding **ET11-NHS** (53%) and **ET12-NHS** (66%), respectively (Scheme 5.13). The integrity of the arrays was confirmed by HRMS, absorption and emission spectroscopy. HRMS showed clearly *m/z* corresponding to target bioconjugatable arrays while there were no notable

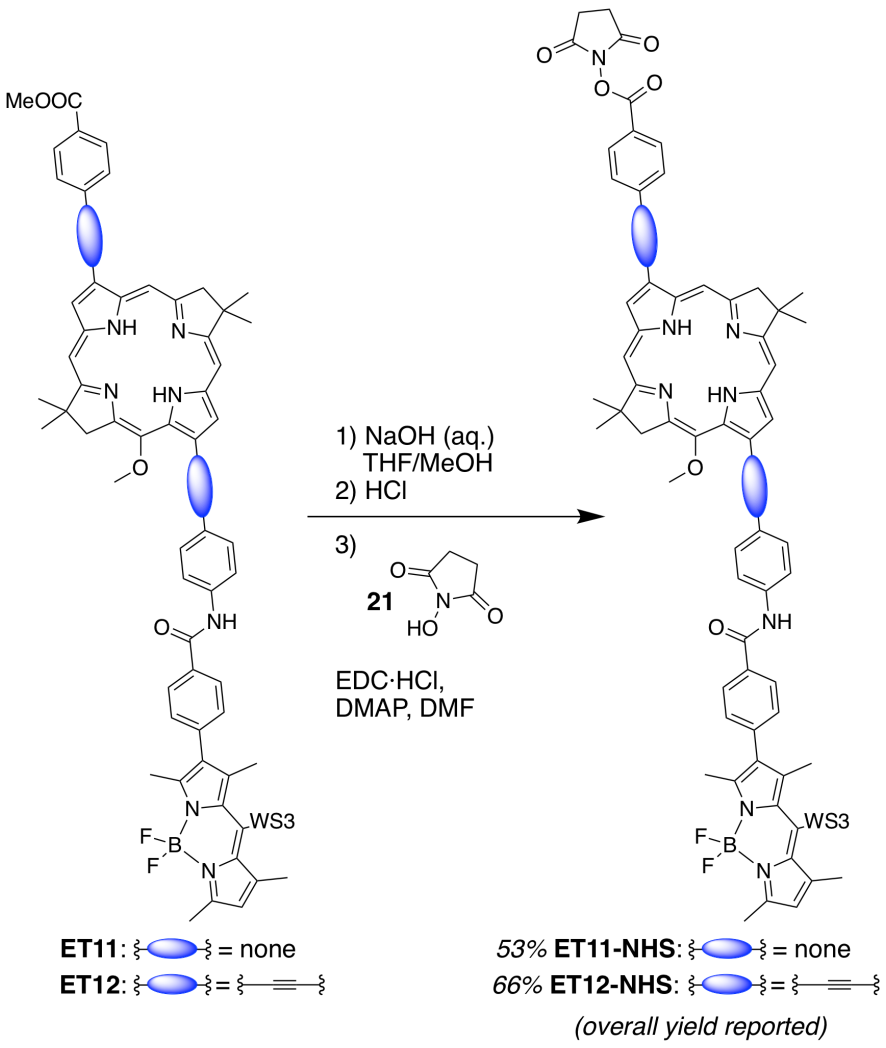

Scheme 5.13: Synthesis of Bioconjugatable BODIPY-bacteriochlorin dyads ET11-NHS and ET12-NHS.

changes in absorption or emission spectra between **ET11/12-NHS** and respective precursor arrays. Our collaborators would go on to demonstrate the effectiveness of dyads **ET11** and **ET12** for visualization of peritoneal cancer metatheses, under the names **NMP11** and **NMP12**, respectively.[128] They performed a series of studies which I will briefly summarize here, the full details of which can be found in *Bioconjugate Chemistry*.[128].

Upon conjugation to either human galactosyl serum albumin (hGSA) or the antibodies panitumumab (Pan) or trastuzumab (Tra), the arrays are soluble but

nonfluorescent in PBS buffer. Introduction of 1% DMSO (v/v) to these solutions restored fluorescence immediately. Similarly, fluorescence of dyad-conjugates was also quenched in mouse serum albumin. The behavior up until this point was expected, because it was previously observed for bacteriochlorin monomers.[120,268] Next, they looked at the various dyad-biomolecule conjugates *in vitro*. The hGSA-**NMP11/12** conjugates were incubated with SHIN3 cells, Pan-**NMP11/12** conjugates were incubated with MDA-MB468 cells, and Tra-**NMP11/12** conjugates were incubated with N87 cells. Essentially, each array-conjugate was incubated against a cancer cell line overexpressing the target protein (lectin receptor for hGSA, EGFR/HER1 for Pan and HER2 for Tra).[399] After incubation, hGSA and Tra conjugates showed negligible fluorescence signal, and Pan conjugates exhibited weak emission. Here, the lack of emission signal from these control experiments is acceptable, because an *in vitro* assay is not representative of the complex, three-dimensional environment found *in vivo*. Next, they tested the hGSA-**NMP11/12** and Tra-**NMP11/12** conjugates *in vivo*, against both large and small tumor models. The first set of trials examined the antibody-array conjugates against highly metathesis prone cancer cell lines, that were injected into the mesentery tissue of mice, and allowed to proliferate for 2-3 weeks (SHIN3 cells for hGSA and N87 cells for Tra). For all four systems, bright fluorescence was observed upon excitation of the BODIPY component, with nearly perfect colocalization of array with the fluorescent proteins being expressed by target cells. Thus, the dyad-conjugates were bright and retained specificity of the targeting moiety. The final test was against a tumor xenograft of 3T3Her2 cells, transfected to express GFP. Again, the Tra-**NMP11/12** showed excellent colocalization with bright emission. These tumors were

then excised by fluorescence guided surgery, using excitation in the green spectral window. Overall, our collaborators were able to demonstrate that our array-antibody conjugates undergo quenching similar to bacteriochlorin monomers while in PBS or *in vitro* but have excellent restoration of fluorescence properties when utilized in a complex environment. Furthermore, they were able to accurately visualize small nodules of highly metastatic cancers and remove a larger xenograft by fluorescence guided surgery.

Section 5.4: Conclusions

In summation, we have successfully prepared a series of novel, neutral water soluble BODIPY derivatives and incorporated them into amphiphilic BODIPY-hydroporphyrin arrays. The monomers were made water soluble through two approaches involving installation of polyethyleneglycol (PEG) ethers at the BODIPY *meso* position or through formation of boro-alkoxy bonds. Where the first PEGylated BODIPYs were difficult to purify from the earliest stages of the synthesis, a modified synthetic pathway enabled us to install PEG ethers at later stage (via microwave assisted Click reaction), increasing overall yields. The completed arrays were synthesized by a combination EDC mediated amide synthesis, Sonogashira and Suzuki cross coupling reactions in low to modest yields.

The majority of the BODIPY benchmarks retained large Φ_F when going from nonpolar to polar media (including PBS). Each of the hydroporphyrin-BODIPY arrays, prepared from hydrophilic BODIPY and hydrophobic chlorin or bacteriochlorin, possessed large ETE from the BODIPY component to hydroporphyrin component. For model hydrophobic arrays, significant quenching was observed when the dyads were

introduced to polar organic solvent (DMF). This quenching of dyads has been attributed to photoinduced electron transfer, and by careful molecular design we were able to limit the extent of PET. First, certain amphiphilic arrays utilized an amide to link the BODIPY and hydroporphyrin. Based on our previous work (Chapter 4) this type of linkage was known to limit PET, compared to phenylethynyl linkers. Second, we tuned the redox properties of the BODIPY moiety to disfavor PET in the phenylethynyl linked systems. This was done by replacement of highly electronegative fluorine atoms at BODIPY 4-position, with less electronegative alkoxy substituents. Such substitution made BODIPY less susceptible to reduction by photoexcited hydroporphyrin without altering absorption and emission maxima. Arrays prepared by the second approach (redox tuned BODIPY, phenylethynyl linker: **ET7**, **ET9**) outperformed those made by the first approach (no tuning of BODIPY, amide linker: **ET5**, **ET10-12**) in both polar organic solvents and aqueous micelles. In fact, amide linked arrays exhibited significant quenching (~50%) and decrease of ETE, where tuned BODIPY containing arrays had no change to ETE in polar media and ETE decreased by 20% or less. These results demonstrate that proper tuning of the BODIPY can overcome the additional quenching that is expected when utilizing a phenylethynyl linker.

Individually, each new array possesses a large pseudo-Stokes' shift due to common excitation at BODIPY. Also, by tethering BODIPY to the hydroporphyrin this increases the effective brightness upon excitation in the green spectral window. These two properties, along with the improved water solubility made our arrays prime candidates for fluorescence imaging, which was performed by our collaborators. Despite the better properties of the arrays containing redox tuned BODIPY, they were

not capable of synthetic modification to allow for conjugation to biomolecules. Thus, we selected amide linked bacteriochlorin-BODIPY arrays **ET11** and **ET12** for testing by our collaborators. Ultimately, it was demonstrated that both dyes provide bright fluorescence images *in vivo* without interfering with the specificity of the targeting moiety. Although it was not demonstrated here, it is worth noting that **ET11** and **ET12** (along with the other BODIPY-hydroporphyrin arrays) are well suited for multicolor fluorescence imaging due to their common excitation band (BODIPY) and tunable emission maxima.

The collective results are encouraging for the design of future arrays; however, we were able to identify a key weakness, the lability in the B-O bond that allowed us to tune the reduction potential of BODIPY **B2**. Due to the inability of the B-O bond to survive acidic or basic hydrolysis, we were unable to make them bioconjugatable, in spite of superior optical properties to other arrays. Exploring substitution at boron with atoms other than oxygen is of primary interest going forward. Some work has demonstrated that replacement of BODIPY fluorine atoms can reduce the stability of the BODIPY,[400,401] particularly strong electron withdrawing groups (one example exists with boro-cyano BODIPY). The reduction of stability leads to rapid conversion of the BODIPY to dipyrromethene under acidic conditions which the fluoro-boro BODIPYs easily survive up to 24 hours.[401] This is concerning considering we require the electron withdrawing character to mitigate quenching in our constructs. Nonetheless, careful design of B-C and B-O ligands should be explored going forward as reduction resistant BODIPYs would be an excellent addition to the growing library of fluorescence imaging probes.

Section 5.5: Experimental Procedures

Section 5.5.1: General Synthetic and Spectroscopic Procedures

For general procedures involving palladium catalyzed (Sonogashira) reactions and characterization of new compounds by NMR and HRMS, see section 2.5.1. For final compounds, where ^{13}C NMR is not provided, compound solubility was too low to acquire spectrum. For determination of fluorescence quantum yields see section 2.5.4, for determination of energy transfer efficiency see section 4.5.4.

Known compounds 1-azido-2-[2-[2-(2-methoxyethoxy)ethoxy]ethoxy]ethane **16,**[380] bacteriochlorins **BC0**,[123] **BC1**,[122] **BC2**,[120] see section 4.5.2 for details regarding BODIPYs **B1** and **B1-TMS**, and section 4.5.3 for chlorin **C2-COOH** (as intermediate in preparation of **ET3**). Dyad **ET6** was prepared as a hydrophobic reference compound by Nithya Santhanam.[126]

General Procedure for Microwave Assisted Click Reactions

Click reactions were all performed under microwave heating, in either 80 mL or 10 mL microwave vessel, with the following parameters: hold time of 30 minutes, temperature of 65ºC, and max power of 150W, for a single reaction cycle unless otherwise indicated. See Section 2.5.1 for details of reaction cycles for microwave assisted reactions.

Spectroscopic Measurements Utilizing Surfactants

In addition to the general absorption and emission parameters noted in section 2.5.1, special care was taken for aqueous solutions containing surfactants. Where TX-100 was used, sample dyad (~0.1 mg) was dissolved in 5.6 mg of TX-100 then diluted with PBS buffer (pH = 7.4) up to a total volume of 3 mL (this provided 3 mM TX-100).

Any dilutions were thereupon performed using a stock solution of 3 mM TX-100 in PBS, until desired absorbance was reached. For surfactants other than TX-100, ~3 mL of stock solution of surfactant (at concentration indicated below) in PBS was added to scintillation vial containing dyad (~0.1-0.3 mg) dissolved in 1mL of CH_2Cl_2. The mixture was then stirred vigorously while open to the atmosphere until all CH_2Cl_2 had evaporated (~1-2 hrs). The resultant dyad-surfactant solution was then diluted with corresponding stock solution until desired absorbance was reached. All surfactants were utilized at concentration above their critical micelle concentration (CMC) in PBS (pH = 7.4), surfactant structures and concentrations used herein are found in Table 5.3.

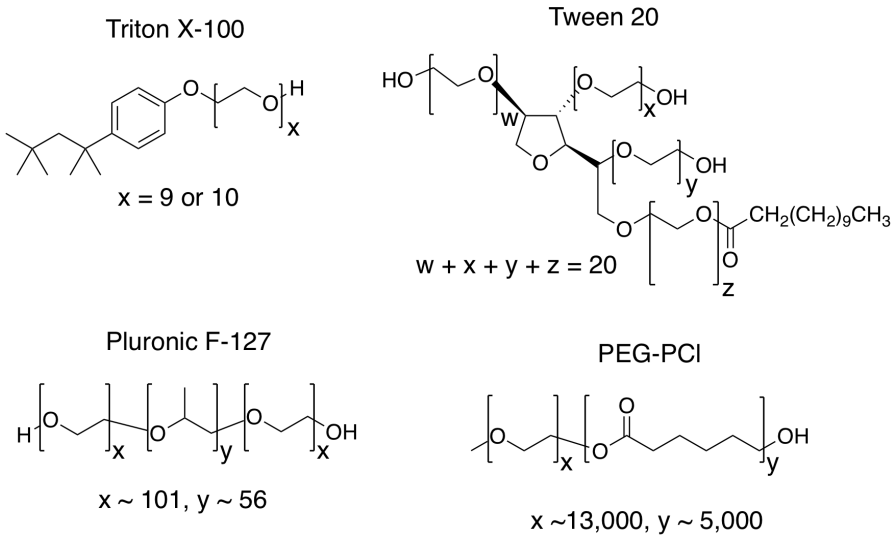

Surfactant	Average Molecular Weight (g/mol)	CMC	Concentration Used
Triton X-100	625	0.24 mM[402]	3 mM
Pluronic F-127	12600	1000 ppm† (0.79 μM)	0.15 mM
Tween 20	1228	60 mg/L[403] (0.05 mM)	0.1% v/v (0.9 mM)
PEG-PCl	1.7 x 10^6	0.8 mg/L[404] (0.4 nM)	1.2 μM

Table 5.3: Surfactants explored for solvation of amphiphilic BODIPY-hydroporphyrin dyads. PEG-PCl is abbreviation for poly(ethyleneglycol)-*block*-poly(*ε*−caprolactone) methyl ether with avg of ~ 5,000 PEG units and ~13,000 PCl units. Critical micellar concentration (CMC) values taken from indicated reference. †) value acquired from sigmaaldritch.com upon purchasing.

Section 5.5.2: Synthesis of Novel Aldehydes

*2,4,6-tris[2-[2-(2-methoxyethoxy)ethoxy]ethoxy]benzaldehyde (**14**)*

A solution of aldehyde **12** (1.30g, 8.43 mmol) and 2-[2-(2-methoxyethoxy)ethoxy]ethyl *p*-toluenesulfonate **13** (8.86 g, 27.84 mmol) in DMF (55 mL) was treated with K_2CO_3 (7.46 g, 54.0 mmol) and stirred at 100°C for 21 hours. Reaction mixture was diluted with CH_2Cl_2, washed (water and brine), dried (Na_2SO_4) and concentrated. Flash column chromatography [silica, CH_2Cl_2/MeOH (50:1)] yielded a viscous, pale brown oil (1.80 g, 47%). ^{1}H NMR ($CDCl_3$, 500 MHz): δ 3.22-3.26 (m, 17H), 3.39-3.43 (m, 13H), 3.45-3.65 (m, 43H), 3.71-3.78 (m, 7H), 4.01-4.05 (m, 6H), 6.00 (s, 2H), 10.22 (s, 1H); ^{13}C NMR ($CDCl_3$, 125 MHz): δ 58.73, 58.76, 61.4, 67.5, 68.6, 69.1, 69.2, 70.1, 70.2, 70.3, 70.35, 70.41, 70.43, 70.6, 70.8, 71.67, 71.68, 72.3, 92.2, 109.2, 162.8, 164.9, 187.1; HRMS (ESI-FT-ICR) *m/z* $[M+Na]^+$ Calcd for $C_{28}H_{48}O_{13}Na$, 615.2987; Found 615.2993.

*2,4,6-tris(prop-2-yn-1-yloxy)benzaldehyde (**17**)*

A solution of 2,4,6-trihydroxybenzaldehyde (1.00 g, 6.49 mmol), in anhydrous DMF (21 mL) was added to flask charged with K_2CO_3 (8.90 g, 64.3 mmol, dried under high vacuum, overnight) then stirred at 60 °C for 30 min. Next, propargyl bromide (2.87 mL, 25.8 mmol, 80% in toluene) was added dropwise and after complete addition the mixture was stirred at 80 °C for 1h. The crude reaction mixture was diluted with ethyl acetate and washed (water and brine), dried (Na_2SO_4) and concentrated. The resulting solid was suspended in diethyl ether (10 mL), sonicated and filtered to yield a light-brown solid (0.960 g, 55%). ^{1}H NMR ($CDCl_3$, 400 MHz): δ 2.56 (t, J = 2.4 Hz, 1H), 2.60 (t, J = 2.4 Hz, 1H), 4.76 (d, J = 2.4 Hz, 2H), 4.78 (d, J = 2.4 Hz, 4H), 6.39

(s, 2H), 10.35 (s, 1H); ^{13}C NMR ($CDCl_3$, 100 MHz): δ 56.3, 56.9, 76.8, 76.9, 77.5, 77.7, 94.1, 110.6, 161.8, 163.5; HRMS (ESI-FT-ICR) *m/z* $[M+H]^+$ Calcd for $C_{16}H_{13}O_4$, 269.0808; Found 269.0809.

Section 5.5.3: Synthesis of Water Soluble and Precursor BODIPYs

Triethyleneglycol substituted BODIPYs

*4,4-difluoro-1,3,5,7-trimethyl-8-[2,4,6-tris[2-[2-(2-methoxyethoxy)ethoxy] ethoxy]phenyl-4-bora-3a,4a-diaza-s-indacene (**B3**)*

A solution of aldehyde **14** (2.29 g, 3.86 mmol) and 2,4-dimethylpyrrole **10** (0.80 mL, 7.73 mmol) in CH_2Cl_2 (40 mL) was treated with trifluoroacetic acid (5 drops) and stirred vigorously at room temperature. After 5 hours, aldehyde **14** appeared fully consumed based upon TLC (silica/CH_2Cl_2). DDQ (0.876 g, 3.86 mmol) was added, and the reaction mixture was stirred for an additional 30 minutes. Then triethylamine (7.5 mL, 54.0 mmol) and $BF_3{\cdot}OEt_3$ (7.6 mL, 61.8 mmol) were added, and the reaction mixture was stirred for an additional 30 minutes. The reaction mixture was concentrated and dried under vacuum, to afford a purple-black residue. Purification required extensive column chromatography. The first column utilized flash chromatography [silica, EtOAc/acetone (9:1)] isolating all green fluorescent material to separate BODIPY from bulk material. The second column (silica, EtOAc) performed was a gravity column that separated out product from a blue colored, red fluorescent impurity. NMR suggested that a BODIPY-like impurity co-eluted with the desired product. A final gravity column (silica, EtOAc), afforded the product as a red-orange, highly viscous oil (270.9 mg, 9%). ^{1}H NMR ($CDCl_3$, 500 MHz): δ 1.52 (s, 6H), 2.47 (s, 6H), 3.23-3.75 (m, 49H), 3.80-3.98 (m, 10H), 5.87 (s, 2H), 6.18 (s, 2H);^{13}C NMR

($CDCl_3$, 125 MHz): δ 13.7, 14.5, 58.9, 59.00, 59.04, 61.7, 67.6, 69.0, 69.4, 69.7, 70.1, 70.3, 70.47, 70.54, 70.6, 70.66, 70.9, 71.0, 71.8, 71.89, 71.93, 72.5, 92.6, 105.5, 120.3, 132.2, 136.2, 142.2, 154.0, 157.2, 161.6; HRMS (ESI-FT-ICR) *m/z* $[M+Na]^+$ Calcd for $C_{40}H_{61}BF_2N_2O_{12}Na$, 833.4185; Found 833.4175.

*2-iodo-4,4-difluoro-1,3,5,7-trimethyl-8-[2,4,6-tris[2-[2-(2-methoxyethoxy)ethoxy] ethoxy]phenyl-4-bora-3a,4a-diaza-s-indacene (**B3-I**)*

In one flask a solution of **B3** (93.2 mg, 0.115 mmol) and iodine (14.6 mg, 0.057 mmol) in ethanol/CH_2Cl_2 (2:1, 30 mL) were prepared. In a second flask, iodic acid (10.0 mg, 0.057 mmol) was dissolved in deionized water (10 mL), then added dropwise to the flask containing **B3**. Once transfer was complete, the solution was stirred vigorously for 45 min at 50°C. The crude reaction mixture was diluted with CH_2Cl_2, washed (water and brine), dried (Na_2SO_4) and concentrated. Gravity column chromatography [silica, EtOAc/acetone (8:1) → (4:1) → (2:1)] yielded a highly viscous pink/light red oil (59.8 mg, 56%). Note that there are numerous byproducts in varying amounts due to the statistical nature of this reaction. The byproducts are presumed to be an assortment of the other possible mono- and di- iodo BODIPYs. The desired product is the major spot when viewed on TLC and is weakly fluorescent under UV light. Diiodo- byproducts are readily identified because they are non-fluorescent. ^1H NMR ($CDCl_3$, 500 MHz): δ 1.57 (s, 3H), 1.59 (s, 3H), 2.52 (s, 3H), 2.58 (s, 3H), 3.31-3.42 (m, 18H), 3.47-3.58 (m, 12H), 3.62-3.78 (m, 11H), 3.87-3.91 (m, 2H), 3.98-4.03 (m, 4H), 4.12-4.17 (m, 2H), 5.98 (s, 1H), 6.22 (s, 2H); ^{13}C NMR ($CDCl_3$, 125 MHz): δ 14.0, 14.8, 15.8, 29.8, 59.1, 59.2, 67.8, 69.1, 69.5, 69.8, 70.4, 70.73, 70.74, 70.8, 71.0, 71.1, 71.9, 72.1, 83.3, 92.7, 105.4, 121.6, 131.6, 132.9, 136.5, 142.2, 144.6, 152.94,

156.7, 157.3, 162.0; HRMS (ESI-FT-ICR) *m/z* $[M+Na]^+$ Calcd for $C_{40}H_{60}BF_2IN_2O_{12}Na$, 959.3134; Found 959.3151.

*4,4-difluoro-1,3,5,7-trimethyl-2-(4-amino)phenyl-8-[2,4,6-tris[2-[2-(2-methoxyethoxy)ethoxy]ethoxy]phenyl-4-bora-3a,4a-diaza-s-indacene (**B3-NH$_2$**)*

Following the general procedure for palladium catalyzed cross coupling reactions, a solution of **B3-I** (70.9 mg, 0.0757 mmol) and 4-aminophenylboronic acid pinacol ester **15** (49.6 mg, 0.227 mmol), Na_2CO_3 (80.2 mg, 0.757 mmol), and $PdCl_2(dppf)\cdot CH_2Cl_2$ (3.1 mg, 3.79 μmol) in toluene/ethanol/water (7 mL, 4:1:2), was stirred at 80°C for 18 hours. Crude reaction mixture was concentrated to dryness, and the residue was dissolved in CH_2Cl_2, washed (water and brine), dried (Na_2SO_4) and concentrated. Column chromatography [silica, EtOAc/acetone (5:1) → (4:1) → (3:1) → (2:1)] yielded a red-pink film that is orange fluorescent (51.6 mg, 76%). ^{1}H NMR ($CDCl_3$, 500 MHz): δ 1.48 (s, 3H), 1.56 (s, 3H), 2.47 (s, 3H), 2.51 (s, 3H), 3.29-3.57 (m, 32H), 3.63-3.77 (m, 14H), 3.85-3.90 (m, 2H), 3.99-4.05 (m, 4H), 4.10-4.16 (m, 2H), 5.29 (s, 1H), 6.21 (s, 2H), 6.68 (d, *J* = 7.9 Hz, 2H), 6.94 (d, *J* = 7.9 Hz, 2H);^{13}C NMR ($CDCl_3$, 125 MHz): δ 12.0, 13.4, 13.8, 14.6, 53.5, 59.0, 59.2, 67.7, 69.2, 69.5, 69.8, 70.2, 70.7, 70.8, 71.0, 71.1, 71.9, 72.0, 92.7, 106.0, 115.0, 120.2, 123.8, 131.2, 132.1, 132.2, 133.1, 136.1, 138.4, 141.7, 145.4, 153.5, 153.6, 157.3, 161.7;
HRMS (ESI-FT-ICR) *m/z* $[M+Na]^+$ Calcd for $C_{46}H_{66}BF_2N_3O_{12}Cs$, 1034.3765; Found 1034.3742.

Alkoxyboron-substituted BODIPYs

*1,3,5,7-trimethyl-8-[4-(trimethylsilyl)ethynyl]phenyl-4,4-bis(prop-2-yn-1-yloxy)-4-bora-3a,4a-diaza-s-indacene (**B4'-TMS**)*

A solution of **B1-TMS** (50.0 mg, 119 μmol) and aluminum chloride (79.3 mg, 595 μmol) in freshly distilled THF (15 mL), was stirred vigorously at 40°C. After 30 minutes, the reaction mixture was cooled to room temperature and treated with propargyl alcohol (1.00 mL, 17.8 mmol) and stirred for an additional 10 minutes. At this time TLC [silica, CH_2Cl_2/EtOAc (9:1)] indicated all starting material and intermediate were consumed. Crude reaction mixture was concentrated, and the residue was dissolved in EtOAc, washed (water and brine), dried (Na_2SO_4), and concentrated. Flash column chromatography [silica, CH_2Cl_2/EtOAc (5:1)] yielded a red-orange foam (50.5 mg, 86%). ^{1}H NMR ($CDCl_3$, 500 MHz): δ 0.28 (s, 9H), 1.40 (s, 6H), 2.06 (t, *J* =2.2 Hz, 2H), 2.58 (s, 6H), 3.81-3.83 (m, 4H), 5.96 (s, 2H), 7.25 (d, *J* = 8.4 Hz, 2H), 7.60 (d, *J* = 8.0 Hz, 2H); ^{13}C NMR ($CDCl_3$, 125 MHz): δ 0.04, 14.8, 15.2, 50.0, 70.8, 83.2, 95.9, 104.5, 121.7, 124.0, 128.5, 132.6, 132.8, 135.9, 140.5, 142.1, 157.0; HRMS (ESI-FT-ICR) *m/z* $[2M+Na]^+$ Calcd for $C_{60}H_{66}B_2N_4O_4Si_2Na$, 1007.4720; Found 1007.4718.

*4,4-bis[1-[2-[2-[2-(2-methoxyethoxy)ethoxy]ethoxy]ethoxy]-1H-1,2,3-triazol-4-ylmethoxyl]-1,3,5,7-trimethyl-8-[4-(trimethylsilyl)ethynyl]phenyl-4-bora-3a,4a-diaza-s-indacene (**B4'**)*

A 80 mL microwave reaction vessel was charged with samples of **B4'-TMS** (134.0 mg, 0.272 mmol), 1-azido-2-[2-[2-(2-methoxyethoxy)ethoxy]ethoxy]ethane **16** (171.3 mg, 0.734 mmol), copper (II) sulfate pentahydrate (34.0 mg, 0.136 mmol), L-ascorbic acid sodium salt (26.9 mg, 0.136 mmol) and acetone/water (5:1, 24 mL). The solution was then irradiated as described in General Procedure for Microwave Assisted Click Reactions. Once the vessel cooled, the product was diluted with EtOAc, washed

(water and brine), dried (Na_2SO_4), and concentrated. Flash column chromatography [silica, CH_2Cl_2/methanol (100:0) → (40:1) → (20:1)] yielded a viscous red oil (151 mg, 58%, third fraction, red-orange color and green fluorescent): It is worth noting that TLC suggests the reaction is incomplete after a single cycle of microwave exposure, however, a second exposure results in both decrease of product yield and introduction of a new impurity that elutes closely following the product, making purification difficult. ^{1}H NMR ($CDCl_3$, 500 MHz): δ 0.24 (s, 9H), 1.36 (s, 6H), 2.50 (s, 6H), 3.32 (s, 6H), 3.46-3.51 (m, 4H), 3.56-3.64 (m, 20H), 3.76-3.84 (m, 4H), 4.25 (s, 4H), 4.37-4.46 (m, 4H), 5.90 (s, 2H), 7.27 (d, J = 7.7 Hz, 2H), 7.56 (d, J = 7.7 Hz, 2H); ^{13}C NMR ($CDCl_3$, 125 MHz): δ -0.1, 14.7, 15.0, 50.0, 56.7, 59.0, 69.6, 70.6, 70.7, 72.0, 95.7, 104.4, 121.5, 122.6, 123.9, 128.4, 132.6, 132.7, 135.7, 141.0, 141.9, 148.6, 155.9; HRMS (ESI-FT-ICR) *m/z* $[M+Na]^+$ Calcd for $C_{48}H_{71}BN_8O_{10}SiNa$, 981.5056; 981.5073.

4,4-bis[[1-[2-[2-[2-(2-methoxyethoxy)ethoxy]ethoxy]ethoxy]-1H-1,2,3-triazol-4-yl]methoxyl]-1,3,5,7-trimethyl-8-(4-ethynyl)phenyl-4-bora-3a,4a-diaza-s-indacene ***(B4)***

A solution of **B4'** (151.3 mg, 0.158 mmol) in THF/methanol (1:1, 30 mL), was treated with K_2CO_3 (28.4 mg, 0.205 mmol) and stirred vigorously for 30 minutes. The reaction mixture was diluted with EtOAc, washed (water and brine), dried (Na_2SO_4), and concentrated to afford a viscous red oil (113.0 mg, 81%). ^{1}H NMR ($CDCl_3$, 400 MHz): δ 1.35 (s, 6H), 2.49 (s, 6H), 3.16 (s, 1H), 3.31 (s, 6H), 3.46-3.50 (m, 4H), 3.56-3.60 (m, 20H), 3.78 (t, J = 5.3 Hz, 4H), 4.24 (s, 4H), 4.41 (t, J = 5.3 Hz, 4H), 5.90 (s, 2H), 7.30 (d, J = 8.1 Hz, 2H), 7.55 (s, 2H), 7.60 (d, J = 8.2 Hz, 2H); ^{13}C NMR ($CDCl_3$,

125 MHz): δ 14.8, 15.0, 50.1, 56.7, 59.1, 69.7, 70.54, 70.56, 70.64, 72.0, 78.5, 83.1, 121.6, 122.77, 122.84, 128.5, 132.5, 132.9, 136.1, 140.8, 141.9, 148.6, 156.0; HRMS (ESI-FT-ICR) *m/z* $[M+Na]^+$ Calcd for $C_{45}H_{63}BN_8O_{10}Na$, 909.4660; Found 909.4652.

Tris-triazolylphenyl substituted BODIPY and precursors

*4,4-difluoro-1,3,5,7-trimethyl-8-[2,4,6-tris(prop-2-yn-1-yloxy)]phenyl-4-bora-3a,4a-diaza-s-indacene (**B5'**)*

A solution of aldehyde **17** (3.00 g, 11.2 mmol) and 2,4-dimethylpyrrole **10** (2.30 mL, 22.4 mmol) in CH_2Cl_2 (110 mL) was treated with trifluoroacetic acid (5 drops) and stirred vigorously. After 30 minutes, **17** appeared fully consumed based upon TLC (silica/CH_2Cl_2). A sample of DDQ (2.53 g, 11.2 mmol) was added, and stirring was continued for another 30 minutes. Then, triethylamine (22.0 mL, 157 mmol) and $BF_3 \cdot OEt_2$ (22.0 mL, 179 mmol) were added, and the resulting mixture was stirred for an additional 30 minutes. The crude reaction mixture was filtered through silica, and all green fluorescent material was collected then concentrated. The resultant viscous oil was dissolved in 30 mL EtOAc and washed (water and brine), dried (Na_2SO_4) and concentrated. Column chromatography [silica, CH_2Cl_2/hexanes (3:1)] yielded a nearly pure product, with a minor pink-red impurity. To remove the impurity, product was dissolved in dichloromethane (40 mL), diluted with hexanes (20 mL) then dichloromethane was removed via rotary evaporator, being cautious to avoid concentration to dryness. The resulting precipitate was filtered and dried over vacuum to afford a red-orange solid (1.23 g, 23%). ^{1}H NMR ($CDCl_3$, 500 MHz): δ 1.58 (s, 6H), 2.44 (t, J = 2.3 Hz, 2H), 2.54 (s, 6H), 2.58 (t, J = 2.4 Hz, 1H), 4.62 (d, J = 2.3 Hz, 4H) 4.77 (d, J = 2.4 Hz, 2H), 5.94 (s, 2H), 6.52 (s, 2H);^{13}C NMR ($CDCl_3$, 125 MHz): δ

13.8, 14.8, 55.9, 56.5, 76.17, 76.21, 78.1, 78.4, 94.4, 106.9, 120.7, 132.1, 134.9, 142.4, 154.6, 155.9, 160.0; HRMS (ESI-FT-ICR) *m/z* $[M+Na]^+$ Calcd for $C_{28}H_{25}BF_2N_2O_3Na$, 509.1823; Found 509.1818.

*4,4-difluoro-1,3,5,7-trimethyl-8-[2,4,6-tris[[1-[2-[2-[2-(2-methoxyethoxy)ethoxy]ethoxy]ethoxy]-1H-1,2,3-triazol-4-yl]methoxyl]phenyl-4-bora-3a,4a-diaza-s-indacene (**B5**)*

A 10 mL microwave reaction vessel was charged with **B5'** (40.0 mg, 0.0823 mmol), 1-azido-2-[2-[2-(2-methoxyethoxy)ethoxy]ethoxy]ethane **16** (76.7 mg, 0.329 mmol), copper(II) sulfate pentahydrate (10.3 mg, 0.0412 mmol), L-ascorbic acid sodium salt (8.2 mg, 0.0412 mmol), and acetone/water (6 mL, 5:1). The solution was then irradiated as described in General Procedure for Microwave Assisted Click Reactions. Crude reaction mixture was diluted with EtOAc, washed (water and brine), dried (Na_2SO_4) and concentrated. Note that the product exhibits water solubility and it may be necessary to wash aqueous layer with EtOAc in a back extraction to recover all product. Column chromatography [silica, CH_2Cl_2/methanol (25:1)] afforded a highly viscous red-orange oil (60.5 mg, 62%). ^{1}H NMR ($CDCl_3$, 500 MHz): δ 1.45 (s, 6H), 2.50 (s, 6H), 3.31 (s, 6H), 3.32 (s, 3H), 3.46-3.57 (m, 27H), 3.59-3.64 (m, 11H), 3.78 (t, J = 5.4 Hz, 4H), 3.88 (t, J = 5.1 Hz, 2H), 4.40 (t, J = 5.4 Hz, 4H), 4.57 (t, J = 5.2 Hz, 2H), 5.11 (s, 4H), 5.21 (s, 2H), 5.89 (s, 2H), 6.58 (s, 2H), 7.33 (s, 2H), 7.93 (s, 1H);^{13}C NMR ($CDCl_3$, 125 MHz): δ 13.6, 14.6, 50.2, 50.4, 59.0, 59.1, 62.2, 63.4, 69.3, 69.5, 70.5, 70.55, 70.62, 70.65, 71.9, 72.0, 94.6, 106.6, 120.6, 123.8, 124.5, 132.2, 136.1, 142.3, 143.0, 144.0, 154.2, 156.7, 161.3; HRMS (ESI-FT-ICR) *m/z* $[M+Na]^+$ Calcd for $C_{55}H_{82}BF_2N_{11}O_{15}Na$, 1208.5954; Found 1208.5973.

*2-iodo-4,4-difluoro-1,3,5,7-trimethyl-8-[2,4,6-tris(prop-2-yn-1-yloxy)]phenyl-4-bora-3a,4a-diaza-s-indacene (**B5'-I**)*

In one flask a solution of **B5'** (500 mg, 1.03 mmol) and iodine (131 mg, 0.517 mmol) in CH_2Cl_2/ethanol (1:2, 240 mL) was prepared. In a second flask, a solution of iodic acid (90.9 mg, 0.517 mmol) in deionized water (80 mL) was prepared. Once homogenous, the iodic acid solution was added slowly to the **B5'** solution. When transfer was complete, the reaction mixture was then stirred at 50°C for 20 minutes. Upon completion, crude reaction mixture was cooled, diluted with CH_2Cl_2, washed (water and brine), dried (Na_2SO_4) and concentrated. Column chromatography [silica, CH_2Cl_2/hexane (1:1)] yielded the desired product (the second to last compound to elute, appearing bright orange, and weakly green fluorescent on TLC). Bright orange solid (313.0 mg, 50%). Note that the desired product is the major product, however, there is a distribution of other iodo-BODIPY products as in the case of **B3-I**. ^{1}H NMR ($CDCl_3$, 500 MHz): δ 1.58 (s, 3H), 1.59 (s, 3H), 2.45 (t, J = 2.3 Hz, 2H), 2.55 (s, 3H), 2.59 (t, J = 2.4 Hz, 1H), 2.62 (s, 3H), 4.62 (d, J = 2.2 Hz, 4H), 4.77 (d, J = 2.4 Hz, 2H), 6.00 (s, 1H), 6.53 (s, 2H); ^{13}C NMR ($CDCl_3$, 125 MHz): δ 14.1, 15.0, 15.9, 55.9, 56.5, 76.30, 76.34, 78.0, 78.2, 83.8, 94.4, 106.6, 121.8, 131.5, 132.7, 134.9, 142.3, 144.6, 153.5, 155.8, 157.1, 160.2; HRMS (ESI-FT-ICR) *m/z* $[M+Na]^+$ Calcd for $C_{28}H_{24}BF_2IN_2O_3Na$, 635.0799; Found 635.0786.

*2-iodo-4,4-difluoro-1,3,5,7-trimethyl-8-[2,4,6-tris[[1-[2-[2-[2-(2-methoxyethoxy)ethoxy]ethoxy]ethoxy]-1H-1,2,3-triazol-4-yl]methoxyl]phenyl-4-bora-3a,4a-diaza-s-indacene (**B5-I**)*

A microwave reaction vessel (80 mL) was charged with **B5'-I** (300.0 mg, 0.499 mmol), 1-azido-2-[2-[2-(2-methoxyethoxy)ethoxy]ethoxy]ethane **16** (465.6 mg, 2.00 mmol), copper(II)sulfate pentahydrate (62.4 mg, 0.250 mmol), L-ascorbic acid sodium salt (49.5 mg, 0.250 mmol), and acetone/water (44 mL, 5:1). The solution was then irradiated as described in General Procedure for Microwave Assisted Click Reactions. Crude reaction mixture was diluted with EtOAc, washed (water and brine), dried (Na_2SO_4) and concentrated. Note that product exhibits water solubility and it may be necessary to wash aqueous layer with EtOAc in a back extraction to recover all product. Column chromatography [silica, CH_2Cl_2/methanol (40:1) → (30:1) → (20:1) → (15:1)] yielded a highly viscous red-orange oil (515.4 mg, 80%). Note that product began eluting with the CH_2Cl_2/methanol (30:1) solvent system, however, product stuck to the silica and eluent polarity was increased to (20:1) with addition of pressure and eventual increase in polarity to (15:1) to force remaining product to elute. ^{1}H NMR ($CDCl_3$, 500 MHz): δ 1.44 (s, 3H), 1.48 (s, 3H), 2.54 (s, 3H), 2.60 (s, 3H), 3.33 (s, 6H), 3.35 (s, 3H), 3.48-3.51 (m, 4H), 3.52-3.60 (m, 23H), 3.62-3.66 (m 10H), 3.81 (t, J = 5.4 Hz, 4H), 3.91 (t, J = 5.1 Hz, 2H), 4.43 (t, J = 5.4 Hz, 4H), 4.59 (t, J = 5.1 Hz, 2H), 5.10-5.16 (m, 4H) 5.23 (s, 2H), 5.98 (s, 1H), 6.62 (s, 2H), 7.36 (s, 2H), 7.95 (s, 1H); ^{13}C NMR ($CDCl_3$, 125 MHz): δ 13.7, 14.6, 15.4, 15.6, 50.0, 50.2, 58.8, 58.9, 62.0, 62.9, 69.1, 69.3, 70.26, 70.30, 70.35, 70.41, 70.44, 71.7, 71.8, 83.2, 94.5, 105.9, 121.6, 123.7, 124.4, 131.4, 132.7, 136.1, 141.9, 142.7, 143.6, 144.6, 152.6, 156.4, 156.7, 161.3; HRMS (ESI-FT-ICR) *m/z* $[M+H]^+$ Calcd for $C_{55}H_{82}BF_2IN_{11}O_{15}$, 1312.5101; Found 1312.5124.

*4,4-difluoro-1,3,5,7-trimethyl-2-(4-methoxycarbonyl)phenyl-8-[2,4,6-tris[[1-[2-[2-[2-(2-methoxyethoxy)ethoxy]ethoxy]ethoxy]-1H-1,2,3-triazol-4-yl]methoxyl]phenyl-4-bora-3a,4a-diaza-s-indacene (**B5-COOMe**)*

Following the general procedure for palladium catalyzed cross coupling reactions, **B5-I** (100.0 mg, 0.0764 mmol), 4-methoxycarbonylphenylboronic acid pinacol ester **18** (60.0 mg, 0.229 mmol), Na_2CO_3 (81.0 mg, 0.764 mmol) and $PdCl_2(dppf)\cdot CH_2Cl_2$ (6.2 mg, 7.63 μmol) in toluene/ethanol/water (7 mL, 4:1:2) were stirred at 80°C for 15 hours. Crude reaction mixture was diluted with EtOAc, washed (water and brine), dried (Na_2SO_4) and concentrated. Column chromatography [silica, CH_2Cl_2/methanol (30:1) → (20:1)] yielded a viscous pink oil (70.3 mg, 70%). Note that as with **B5-I** the product stuck to silica and increased polarity was necessary to remove all product from column. It is challenging to distinguish product from any unreacted starting material based solely on TLC, however the product is highly fluorescent in comparison to starting material. ^{1}H NMR ($CDCl_3$, 400 MHz): δ 1.43 (s, 3H), 1.47 (s, 3H), 2.50 (s, 3H), 2.56 (s, 3H) 3.33 (s, 6H), 3.35 (s, 3H), 3.47-3.59 (m, 31H), 3.61-3.66 (m, 11H), 3.80 (t, *J* = 5.3 Hz, 4H), 3.92 (t, *J* = 5.1 Hz, 2H), 3.93 (s, 3H), 4.35-4.46 (m, 4H), 4.58 (t, *J* = 5.2 Hz, 2H), 5.16 (s, 2H), 5.17 (s, 2H), 5.22 (s, 2H), 5.96 (s, 1H), 6.61 (s, 2H), 7.23 (d, *J* = 8.4 Hz, 2H), 7.41 (s, 2H), 7.94 (s, 1H), 8.04 (d, *J* = 8.4 Hz, 2H); ^{13}C NMR ($CDCl_3$, 125 MHz): δ 11.8, 13.3, 13.8, 14.7, 50.2, 50.4, 52.1, 58.96, 59.01, 62.1, 63.3, 70.45, 70.52, 70.59, 70.61, 71.89, 71.94, 94.6, 106.5, 121.1, 123.8, 124.5, 128.6, 129.6, 130.2, 131.6, 131.8, 132.8, 136.7, 138.1, 138.9, 142.9, 143.1, 143.9, 151.8, 155.3, 156.7, 161.4, 166.9; HRMS (ESI-FT-ICR) *m/z* $[M+H]^+$ Calcd for $C_{63}H_{88}BF_2N_{11}O_{17}Na$, 1342.6323; Found 1342.6353.

Section 5.5.4: Synthesis of Bacteriochlorins en route to ET11 and ET12

*3-[4-(amino)phenyl]-5-methoxy-8,8,18,18-tetramethyl-13-[4-(methoxycarbonyl)phenyl]-bacteriochlorin (**BC1-NH$_2$**)*

Following the general procedure for palladium catalyzed reactions, a mixture of **BC1** (30.0 mg, 0.0489 mmol), 4-aminophenylboronic acid pinacol ester **16** (11.6 mg, 0.0528 mmol), Cs_2CO_3 (161 mg, 0.0489 mmol), and $Pd(PPh_3)_4$ (9.1 mg, 0.0079 mmol) in toluene (6 mL) and DMF (3 mL) was stirred at 85 °C. After 17 h, the mixture was diluted with ethyl acetate, washed (water and brine), dried (Na_2SO_4) and concentrated. Column chromatography [silica, CH_2Cl_2 → CH_2Cl_2/methanol (49:1)] to afford a dark green solid (26 mg, 69%). ^{1}H NMR ($CDCl_3$, 400 MHz): δ −2.06 (s, 1H), −1.68 (s, 1H), 1.96 (s, 6H), 1.98 (s, 6H), 3.73 (s, 3H), 3.89 (br s, 2H), 4.07 (s, 3H), 4.40 (s, 2H), 4.42 (s, 2H), 6.98 (d, *J* = 8.44 Hz, 2H), 7.94 (d, *J* = 8.44Hz, 2H), 8.28 (d, *J* = 8.44 Hz, 2H), 8.42 (d, *J* = 8.44 Hz, 2H), 8.62 (s, 1H), 8.63 (s, 1H), 8.70 (s, 1H), 8.82 (s, 2H); ^{13}C NMR ($CDCl_3$, 100 MHz): δ 31.4, 31.5, 45.6, 46.2, 48.4, 51.9, 52.6, 63.8, 96.5, 96.8, 97.6, 114.9, 121.5, 123.3, 128.5, 128.6, 128.9, 130.5, 131.2, 132.4, 133.9, 134.1, 134.5, 135.3, 136.5, 141.8, 145.9, 155.7, 159.8, 167.7, 168.9, 170.3; HRMS (ESI-FT-ICR) *m/z* $[M]^+$ Calcd for $C_{39}H_{39}N_5O_3$, 625.3047; Found 625.3047.

*3-[4-(aminophenyl)ethynyl]-5-methoxy-8,8,18,18-tetramethyl-13-[4-(methoxycarbonyl)phenylethynyl]-bacteriochlorin (**BC2-NH$_2$**)*

Following the general procedure for Sonogashira coupling, a mixture of **BC2** (20 mg, 0.031 mmol), 4-ethynylaniline **19** (4.3 mg, 0.037 mmol), and $PdCl_2(PPh_3)_2$ (3.5 mg, 0.0050 mmol) in Et_3N/DMF (1:2, 6 mL) was stirred at 80 °C. After 2 h, the mixture was diluted with ethyl acetate, washed (water and brine), dried (Na_2SO_4) and concentrated. The residue was purified with silica column chromatography [silica,

hexane/CH_2Cl_2 (1:3)] to afford a dark reddish powder (14 mg, 67%). ^{1}H NMR ($CDCl_3$, 500 MHz): δ −1.87 (s, 1H), −1.57 (s, 1H), 1.95 (s, 12H), 3.93 (br s, 2H), 3.99 (s, 3H), 4.43 (s, 2H), 4.45 (s, 2H), 4.50 (s, 3H), 6.79 (d, *J* = 8.45 Hz, 1H), 7.68 (d, *J* = 8.45 Hz, 1H), 7.94 (d, *J* = 8.40 Hz, 1H), 8.19 (d, *J* = 8.40 Hz, 1H), 8.53 (s, 1H), 8.58 (s, 1H), 8.78 (d, *J* = 2.2 Hz, 1H), 8.81 (d, *J* = 1.9 Hz, 1H), 8.92 (s, 1H); ^{13}C NMR ($CDCl_3$, 100 MHz): δ 31.3, 41.7, 46.2, 48.2, 51.8, 52.7, 64.9, 85.4, 88.4, 95.3, 95.8, 96.6, 96.9, 98.1, 114.0, 114.8, 115.1, 115.3, 124.6, 125.3, 128.8, 129.9, 130.1, 131.9, 132.1, 133.5, 135.2, 135.7, 135.9, 137.9, 147.1, 156.4, 160.9, 167.0, 169.8, 171.1; HRMS (ESI-FT-ICR) *m/z* $[M]^+$ Calcd for $C_{43}H_{39}N_5O_3$, 673.3047; Found 673.3052.

BC1-BPin

A solution of **BC1-NH₂** (17.6 mg, 0.0281 mmol), 4-carboxylphenylboronic acid pinacol ester **20** (14.0 mg, 0.0562 mmol), EDC·HCl (10.8 mg, 0.0562 mmol), and DMAP (6.9 mg, 0.0562 mmol) in DMF (2 mL) was treated with hydroxybenzotriazole monohydrate (8.8 mg, 0.0562 mmol) and stirred for 64 hours. The reaction crude was diluted with EtOAc, washed [saturated aqueous $NaHCO_3$ (3x), water, and brine], dried (Na_2SO_4) and concentrated, yielding a green solid (22.7 mg, 94%). ^{1}H NMR indicates a product with approximately 90% purity, which was deemed acceptable for subsequent reactions. Column chromatography of this compound leads to significantly lower yields (20-30% overall), streaking observed during TLC suggests this diminished yield is due to product adhering to silica. ^{1}H NMR ($CDCl_3$, 400 MHz): δ -1.97 (s, 1H), -1.66 (s, 1H), 1.39 (s, 3H), 1.40 (s, 12H), 1.96 (s, 6H), 1.98 (s, 6H), 3.71 (s, 2H), 4.06 (s, 2H), 7.95-8.05 (m, 6H), 8.10 (s, 1H), 8.16 (d, *J* = 8.5 Hz, 2H), 8.25-8.30 (m, 3H),

8.42 (d, J = 8.3 Hz, 2H), 8.66 (s, 1H), 8.69 (s, 1H), 8.80 (s, 1H), 8.82 (s, 1H); HRMS (ESI-FT-ICR) *m/z* $[M]^+$ Calcd for $C_{52}H_{54}BN_5O_6$, 855.4170; Found 855.4172.

BC2-BPin

A solution of **BC2-NH₂** (35.0 mg, 0.0519 mmol), 4-carboxylphenylboronic acid pinacol ester **20** (25.8 mg, 0.104 mmol), EDC·HCl (19.9 mg, 0.104 mmol), and DMAP (12.7 mg, 0.104 mmol) in DMF (3 mL) was stirred for 46 hours. The crude reaction mixture was diluted with EtOAc, washed (saturated aqueous $NaHCO_3$ (3x), water, and brine, then dried (Na_2SO_4) and concentrated, yielding a red-brown solid (32.9 mg, 70%). Proton NMR indicates a product with greater than 95% purity, and was used for the next step without purification. ^{1}H NMR ($CDCl_3$, 400 MHz): δ -1.80 (s, 1H), -1.55 (s, 1H), 1.39 (s, 12H), 1.96 (s, 12H), 3.99 (s, 3H), 4.44 (s, 2H), 4.45 (s, 2H), 4.51 (s, 3H), 7.79 (d, J = 8.7 Hz, 2H), 7.83 (d, J = 8.7 Hz, 2H), 7.89 (d, J = 8.5 Hz, 2H), 7.92 (d, J = 8.2 Hz, 2H), 7.97 (d, J = 8.2 Hz, 2H), 8.07 (s, 1H), 8.14 (d, J = 8.5 Hz, 2H), 8.55 (s, 1H), 8.57 (s, 1H), 8.81 (s, 1H), 8.82 (s, 1H), 8.91 (s, 1H); HRMS (ESI-FT-ICR) *m/z* $[M]^+$ Calcd for $C_{56}H_{54}BN_5O_6$, 903.4171; 903.4164.

Section 5.5.5: Synthesis of Amphiphilic Hydroporphyrin-BODIPY Arrays

ET5

A solution of **B3-NH₂** (35.0 mg, 0.0388 mmol), **C2-COOH** (15.0 mg, 0.0326 mmol), EDC·HCl (12.5 mg, 0.0652 mmol) and DMAP (8.0 mg, 0.0652 mmol) in DMF (3 mL) was stirred at room temperature for 4 days. The crude reaction mixture was diluted with EtOAc, washed (water and brine), dried (Na_2SO_4), and concentrated. Column chromatography [silica, EtOAc/acetone (6:1) → (4:1)] yielded a red-purple solid (12.9 mg, 30%). ^{1}H NMR ($CDCl_3$, 500 MHz): δ -2.36 (s, 1H), -1.97 (s, 1H), 1.59

(s, 3H), 1.62 (s, 3H), 2.08 (s, 6H), 2.58 (s, 6H), 3.37 (s, 6H), 3.39 (s, 3H), 3.47-3.54 (m, 4H), 3.47-3.54 (m, 8H), 3.54-3.59 (m, 6H), 3.66-3.70 (m, 2H), 3.70-3.76 (m, 6H), 3.76-3.79 (m, 2H), 3.89-3.92 (m, 2H), 4.05-4.10 (m, 4H), 4.15-4.19 (m, 2H), 4.76 (s, 2H), 5.97 (s, 1H), 6.27 (s, 2H), 7.29 (d, J = 8.4 Hz, 2H), 7.84 (d, J = 8.4 Hz, 2H), 8.20 (s, 1H), 8.24 (d, J = 8.1 Hz, 2H), 8.30 (d, J = 8.1 Hz, 2H), 8.62 (d, J = 4.3 Hz, 1H), 8.79 (d, J = 4.7 Hz, 1H), 8.87 (d, J = 4.7 Hz, 1H), 8.96 (s, 1H), 8.99 (d, J = 4.5 Hz, 1H), 9.01 (d, J = 4.3 Hz, 1H), 9.08 (s, 1H), 9.27 (d, J = 4.4 Hz, 1H), 9.90 (s, 1H); ^{13}C NMR ($CDCl_3$, 125 MHz): δ 12.0, 13.5, 13.9, 14.8, 29.8, 31.3, 46.6, 52.2, 59.1, 59.2, 67.8, 69.3, 69.5, 69.8, 70.4, 70.7, 70.78, 70.81, 71.0, 71.2, 72.0, 72.1, 92.8, 94.7, 97.3, 105.9, 107.5, 119.8, 120.3, 120.7, 123.6, 124.1, 125.7, 127.9, 128.6, 130.5, 131.2, 131.8, 132.0, 132.2, 132.7, 132.8, 134.3, 134.5, 134.6, 134.9, 136.7, 137.0, 138.4, 139.6, 141.2, 142.6, 145.8, 151.1, 152.0, 152.6, 154.5, 157.4, 161.8, 163.3, 166.0, 175.6; HRMS (ESI-FT-ICR) *m/z* $[M]^+$ Calcd for $C_{75}H_{88}BF_2N_7O_{13}$, 1343.6508; Found 1343.6494.

ET7

Following the general procedure for Sonogashira cross coupling reactions, samples of **C1-Br** (15.0 mg, 27.9 μmol), **B4** (26.0 mg, 29.3 μmol), $(PPh_3)_2PdCl_2$ (2.9 mg, 4.2 μmol) in DMF/Et_3N (2:1, 6 mL) were stirred at 80°C for 15 hours. The crude reaction mixture was diluted with EtOAc, washed (water and brine), dried (Na_2SO_4) and concentrated. Flash column chromatography [silica, CH_2Cl_2/methanol (1:0) → (50:1) → (30:1) → (25:1) → (15:1) → (11:1)] followed by a second gravity column chromatography [silica, CH_2Cl_2/methanol (1:0) → (25:1) → (15:1)] afforded target dyad as a green solid (10.8 mg, 29%). ^{1}H NMR ($CDCl_3$, 500 MHz): δ -1.90 (s, 1H), -

1.57 (s, 1H), 1.55 (s, 6H), 1.87 (s, 6H), 2.08 (s, 6H), 2.58 (s, 6H), 2.62 (s, 3H), 3.38 (s, 6H), 3.53-3.57 (m, 5H), 3.61-3.67 (m, 23H), 3.86 (t, J = 5.2 Hz, 4H), 4.36 (s, 4H), 4.49 (t, J = 5.2 Hz, 4H), 4.71 (s, 2H), 6.01 (s, 2H), 7.53 (d, J = 7.9 Hz, 2H), 7.64 (s, 1H), 8.02 (d, J = 7.9 Hz, 2H), 8.47 (d, J = 4.2 Hz, 1H), 8.78 (s, 1H), 8.86 (s, 2H), 8.92 (d, J= 4.4 Hz, 1H), 9.18 (d, J = 4.4 Hz, 1H), 9.32 (s, 1H), 9.73 (s, 1H); ^{13}C NMR ($CDCl_3$, 125 MHz): δ 15.0, 15.1, 21.4, 21.6, 29.8, 31.2, 46.8, 50.2, 52.0, 56.8, 59.2, 69.8, 70.66, 70.74, 72.1, 86.2, 94.6, 95.0, 95.8, 106.9, 116.4, 121.0, 121.7, 122.9, 124.1, 124.4, 127.9, 128.8, 128.9, 131.8, 132.6, 132.8, 133.0, 133.1, 135.3, 135.8, 137.5, 137.9, 139.2, 139.7, 141.2, 141.8, 142.1, 148.7, 152.3, 152.8, 156.1, 163.3, 176.3; HRMS (ESI-FT-ICR) *m/z* $[M+Na]^+$ Calcd for $C_{76}H_{91}BN_{12}O_{10}Na$, 1365.6978; Found 1365.6953.

ET8

Following the general procedure for Sonogashira cross coupling reactions, samples of **BC1** (20.0 mg, 32.6 μmol), **B1** (17.0 mg, 48.9 μmol), $(PPh_3)_2PdCl_2$ (4.6 mg, 6.5 μmol) in DMF/Et_3N (2:1, 9 mL) were reacted at 80°C for 16 hours. The crude reaction mixture was diluted with EtOAc, washed (water and brine), dried (Na_2SO_4) and concentrated. Column chromatography [silica, CH_2Cl_2/hexanes (1:1) → (2:1)] yielded a red-brown solid (7.4 mg, 26%). ^{1}H NMR ($CDCl_3$, 500 MHz): δ -1.47 (s, 1H), -1/26 (s, 1H), 1.57 (s, 6H), 1.93 (s, 6H), 1.96 (s, 6H), 2.60 (s, 6H), 4.06 (s, 3H), 4.34 (s, 2H), 4.43 (s, 2H), 4.55 (s, 3H), 6.04 (s, 2H), 7.42 (d, J = 8.1 Hz, 2H), 7.99 (d, J = 8.1 Hz, 2H), 8.23 (d, J = 8.2 Hz, 2H), 8.42 (d, J = 8.2 Hz, 2H), 8.53 (s, 1H), 8.57 (s, 1H), 8.67 (s, 1H) 8.77 (s, 2H); ^{13}C NMR ($CDCl_3$, 125 MHz): δ 14.5, 14.9, 30.9, 31.2, 45.3, 46.2, 47.2, 52.4, 52.5, 64.6, 89.2, 92.5, 97.0, 97.1, 97.6, 110.7, 121.5, 123.5,

123.6, 125.5, 128.5, 129.3, 130.4, 131.0, 131.2, 131.5, 132.4, 133.7, 134.7, 135.6, 136.1, 136.5, 136.8, 140.8, 141.3, 143.3, 153.9, 155.9, 162.2, 167.3, 169.0, 171.5; HRMS (ESI-FT-ICR) *m/z* $[M]^+$ $C_{54}H_{51}BF_2N_6O_3$, 880.4087; Found 880.4079.

ET9

Following the general procedure for Sonogashira cross coupling reactions, samples of **BC1** (20.0 mg, 32.6 μmol), **B4** (43.4 mg, 48.9 μmol), $(PPh_3)_2PdCl_2$ (4.6 mg, 6.5 μmol) in DMF/Et_3N (2:1, 9 mL) were reacted at 80°C for 4 hours. The crude reaction was diluted with EtOAc, washed (water and brine), dried (Na_2SO_4) and concentrated. Column chromatography [silica, CH_2Cl_2/methanol (100:0) → (20:1)] yielded a red-brown solid (13.4 mg, 29%). ^1H NMR ($CDCl_3$, 500 MHz): δ -1.49 (s, 1H), -1.28 (s, 1H), 1.56 (s, 6H), 1.66 (s, 6H), 1.94 (s, 6H), 1.97 (s, 6H), 2.59 (s, 6H), 3.38 (s, 6H), 3.54-3.57 (m, 5H), 3.61-3.66 (m, 23H), 3.86 (t, *J* = 5.4 Hz, 4H), 4.06 (s, 3H), 4.34-4.36 (m, 6H), 4.47 (t, *J* = 5.4 Hz, 4H), 4.57 (s, 3H), 7.50 (d, *J* = 8.3 Hz, 2H), 7.64 (s, 2H), 8.01 (d, *J* = 8.3 Hz, 2H), 8.23 (d, *J* = 8.5 Hz, 2H), 8.41 (d, *J* = 8.5 Hz, 2H), 8.53 (s, 1H), 8.58 (s, 1H), 8.67 (s, 1H), 8.76-8.79 (m, 2H); ^{13}C NMR ($CDCl_3$, 125 MHz): δ 15.0, 15.2, 30.9, 31.2, 45.3, 46.1, 47.2, 50.2, 52.4, 52.5, 56.8, 59.2, 64.6, 69.8, 70.7, 70.67, 70.74, 72.1, 89.0, 92.7, 97.0, 97.1, 97.6, 110.9, 121.7, 122.9, 123.5, 123.7, 125.3, 128.6, 128.69, 128.72, 129.3, 130.6, 131.0, 131.2, 132.2, 132.3, 132.4, 132.8, 133.8, 135.2, 135.7, 136.0, 136.4, 136.7, 140.8, 141.4, 142.2, 148.8, 154.0, 155.9, 162.1, 167.3, 169.0, 171.4; HRMS (ESI-FT-ICR) *m/z* $[M+Na]^+$ Calcd for $C_{78}H_{95}BF_2N_{12}O_{13}Na$, 1441.7139; Found 1441.7142.

ET10

Following the general procedure for palladium catalyzed cross coupling reactions, samples of **BC0** (10.0 mg, 17.9 μmol), **B4** (39.7 mg, 44.8 μmol), $(PPh_3)_2PdCl_2$ (2.6 mg, 3.6 μmol) were reacted in DMF/Et_3N (2:1, 9 mL) at 80°C for 2.5 hours. The crude reaction was diluted with EtOAc, washed (water and brine), dried (Na_2SO_4) and concentrated. During extraction a precipitate was observed in the aqueous phase, this was extracted using CH_2Cl_2, which was subsequently washed with brine, dried (Na_2SO_4) and combined with the first extract (TLC indicated the two mixtures were nearly identical). Two size exclusion chromatography columns (Bio-Beads S-X1 Support#152-2151, THF) were performed to remove byproduct, followed with column chromatography [silica, CH_2Cl_2/methanol (100:0) → (20:1) → (10:1) → (5:1)] yielded a red-brown solid (13.0 mg, 33%). ^{1}H NMR shows impurities in the aromatic region which was identified on the basis of HRMS data {(ESI-FT-ICR) *m/z* $[M+Na]^+$ Calcd for $C_{90}H_{124}B_2N_{16}O_{20}Na$, 1794.9300; Found 1794.9300}as a product of homo-coupling of **B4**. Relative integration of ^{1}H NMR suggests this impurity is present in ~5-10%. This impurity was removed through rigorous, iterative crystallization, however, the yield of highly pure **ET10** is negligible. The presence of the impurity does not appear to have any impact on the photochemical properties of the sample (Φ_F and Φ_{ETE} recrystallized and non-recrystallized samples are the same within experimental uncertainty). ^{1}H NMR ($CDCl_3$, 500 MHz): δ -1.65 (s, 1H), -1.45 (s, 1H), 1.56 (s, 6H), 1.57 (s, 6H), 1.97 (s, 12H), 2.59 (s, 12H), 3.38 (s, 12H), 3.54-3.57 (m, 10H), 3.60-3.67 (m, 50H), 3.86 (t, *J* = 5.2 Hz, 9H), 4.34-4.36 (m, 10H), 4.46 (s, 3H), 4.49 (t, *J* = 5.0 Hz, 4H), 4.56 (s, 3H), 6.01 (s, 2H), 6.02 (s,2H), 7.51 (d, *J* = 8.5 Hz, 2H), 7.55 (d, *J* = 8.5 Hz, 2H), 7.63 (s, 2H), 7.64 (s, 2H), 8.02 (d, *J* = 8.5 Hz, 2H), 8.05

(d, J = 8.5 Hz, 2H), 8.57 (d, J = 8.5 Hz, 2H), 8.82-8.84 (m, 2H), 8.95 (s, 1H); ^{13}C NMR ($CDCl_3$, 125 MHz): δ 15.0, 15.2, 31.0, 31.1, 45.7, 45.8, 50.2, 52.0, 56.8, 59.2, 64.7, 69.8, 70.7, 70.8, 72.1, 121.69, 121.74, 122.9, 124.4, 124.7, 128.8, 128.9, 132.4, 132.6, 132.8, 134.7, 135.7, 135.9, 138.4, 141.2, 141.4, 142.1, 142.2, 148.8, 156.0, 156.1, 170.2; HRMS (ESI-FT-ICR) *m/z* $[M+2Na]^{2+}$ Calcd for $C_{115}H_{150}B_2N_{20}O_{21}Na_2$, 1107.0650; Found 1107.0650.

ET11 (*Prepared by Suzuki Cross Coupling Reaction)*

Following the general procedure for palladium catalyzed cross coupling reactions, **BC1-NH$_2$** (90% pure, 22.7 mg, 0.0239 mmol), **B5-I** (37.6 mg, 0.0286 mmol), Na_2CO_3 (25.3 mg, 0.239 mmol) and $PdCl_2(dppf)\cdot CH_2Cl_2$ (3.9 mg, 4.78 μmol) in toluene/ethanol/water (7 mL, 4:1:2) were reacted at 80°C for 2 hours. Crude reaction mixture was diluted with EtOAc, washed (water and brine), dried (Na_2SO_4) and concentrated. Size exclusion chromatography (Bio-Beads S-X1 Support#152-2151, THF), followed with chromatography column [silica, CH_2Cl_2/methanol (35:1) → (30:1) → (25:1)] yielded a purple solid (10.0 mg, 22%). ^{1}H NMR ($CDCl_3$, 400 MHz): δ 1.46 (s, 3H), 1.53 (s, 3H), 1.96 (s, 6H), 1.98 (s, 6H), 2.59 (s, 3H), 2.60 (2, 3H), 3.33-3.37 (m, 10H), 3.51-3.67 (m, 43H), 3.71 (s, 3H), 3.82 (t, J = 5.3 Hz, 4H), 3.91 (t, J = 5.0 Hz, 2H), 4.06 (s, 3H), 4.40 (s, 4H), 4.43 (t, J = 5.3 Hz, 4H), 4.60 (t, J = 5.0 Hz, 2H), 5.20 (s, 2H), 5.21 (s, 2H), 5.26 (s, 2H), 6.00 (s, 1H), 6.65 (s, 2H), 7.36 (d, J = 7.9 Hz, 2H), 7.44 (s, 2H), 7.97 (s, 1H), 7.98 (d, J = 8.3 Hz, 2H), 8.08 (d, J = 8.0 Hz, 2H), 8.15 (d, J = 8.2 Hz, 2H), 8.27 (d, J = 8.0 Hz, 2H), 8.41 (d, J = 8.1 Hz, 2H), 8.51 (s, 1H), 8.63-8.70 (m, 3H), 8.80 (s, 1H), 8.82 (s, 1H);^{13}C NMR ($CDCl_3$, 125 MHz): δ 11.9, 13.9, 14.9, 29.8, 31.18, 31.23, 45.6, 45.8, 48.0, 50.3, 50.5, 51.9, 52.4, 59.08, 59.14,

62.2, 63.4, 63.5, 69.4, 69.6, 70.5, 70.57, 70.64, 70.67, 70.70, 70.72, 72.02, 72.05, 94.8, 96.7, 97.3, 106.6, 119.6, 121.9, 123.0, 124.0, 124.7, 127.5, 127.9, 128.9, 130.3, 130.7, 131.0, 131.9, 134.3, 134.5, 134.6, 134.9, 136.3, 136.8, 143.1, 144.0, 154.9, 155.6, 156.8, 160.2, 161.5, 165.9, 167.4, 169.4, 169.9; HRMS (ESI-FT-ICR) *m/z* $[M+2Na]^{2+}$ Calcd for $C_{101}H_{123}BF_2N_{16}O_{19}Na_2$, 979.4506; Found 979.4524.

ET11 *(Prepared by EDC Mediated Amide Synthesis)*

A solution of **B5-COOMe** (63.2 mg, 0.0479 mmol) in THF/methanol (1:1, 6 mL) was treated with aqueous NaOH (1 mL, 3M) and stirred vigorously at room temperature for 1 h. Crude reaction mixture was diluted with EtOAc, washed (5% HCl and brine), and dried (Na_2SO_4). Note that considerable nonfluorescent color was observed in aqueous phase suggesting decomposition of BODIPY during reaction. Residue was then purified by column chromatography [silica, CH_2Cl_2/MeOH (20:1) → (15:1) → (5:1)] yielding **B5-COOH** as a pink film (13.5 mg, 22%). ^{1}H NMR ($CDCl_3$, 400 MHz): δ 1.38 (s, 3H), 1.49 (s, 3H), 2.51 (s, 3H), 2.57 (s, 3H) 3.34 (s, 6H), 3.35 (s, 3H), 3.48−3.66 (m, 48H), 3.77 (t, *J* = 5.4 Hz, 4H), 3.90 (t, *J* = 5.2 Hz, 2H), 4.40 (t, *J* = 5.4 Hz, 4H), 4.59 (t, *J* = 5.2 Hz, 2H), 5.16 (s, 2H), 5.17 (s, 2H), 5.23 (s, 2H), 5.97 (s, 1H), 6.61 (s, 2H), 7.22 (d, *J* = 8.2 Hz, 2H), 7.40 (s, 2H), 7.95 (s, 1H), 8.09 (d, *J* = 8.2 Hz, 2H).

Intermediate **B5-COOH** was then immediately used in the subsequent reaction without further characterization. Bactetiochlorin **BC1-BPin** (7.5 mg, 12 μmol), **B5-COOH** (13.0 mg, 9.96 μmol), EDC·HCl (3.8 mg, 20 μmol), and DMAP (2.4 mg, 20 μmol) were dissolved in 3 mL of CH_2Cl_2 and stirred at room temperature, in darkness, for 18 h. Crude reaction mixture was purified by column chromatography [silica,

CH_2Cl_2/methanol (30:1)], to afford a purple film (5.0 mg, 22%) from **B5-COOH**. Overall yield for both steps beginning from **B5-COOMe** is low at 4.8%. Characterization data (^{1}H NMR, absorption, emission) are consistent with those obtained for the sample prepared via Suzuki cross-coupling.

ET12

Following the general procedure for palladium coupling reactions, **BC2-NH$_2$** (95% pure, 32.0 mg, 0.035 mmol), **B5-I** (55.7 mg, 0.042 mmol), sodium carbonate (37.1 mg, 0.35 mmol) and $PdCl_2(dppf)\cdot CH_2Cl_2$ (5.7 mg, 7.0 μmol) in toluene/ethanol/water (7 mL, 4:1:2) were reacted at 80°C for 2 hours. Crude reaction mixture was diluted with EtOAc, washed (water and brine), dried (Na_2SO_4), and concentrated. Column chromatography [silica, CH_2Cl_2/methanol (25:1)] yielded a purple-brown solid (28.5 mg, 41%). ^{1}H NMR ($CDCl_3$, 500 MHz): δ -1.80 (s, 1H), -1.55 (s. 1H), 1.43 (s, 3H), 1.53 (s, 3H), 1.95 (s, 12H), 2.56 (s, 3H), 2.59 (s, 3H), 3.33 (s, 6H), 3.36 (s, 3H), 3.48-3.66 (m, 41H), 3.79 (t, J = 5.2 Hz, 4H), 3.90 (t, J = 5.0 Hz, 2H), 3.99 (s, 3H), 4.38-4.46 (m, 8H), 4.50 (s, 3H), 4.59 (t, J = 4.9 Hz, 2H), 5.19 (s, 2H), 5.20 (s, 2H), 5.25 (s, 2H), 6.60 (s, 1H), 6.64 (s, 2H), 7.32 (d, J = 8.0 Hz, 2H), 7.43 (s, 2H), 7.85 (s, 3H), 7.91 (d, J = 8.1 Hz, 2H), 7.96 (s, 1H), 8.03 (d, J = 8.0 Hz, 2H), 8.15 (d, J = 8.1 Hz, 2H), 8.54 (s, 1H), 8.57 (s, 1H), 8.65 (s, 1H), 8.79-8.83 (m, 2H), 8.91 (s, 1H);^{13}C NMR ($CDCl_3$, 125 MHz): δ 11.9, 13.5, 13.9, 14.9, 31.0, 31.1, 45.6, 45.8, 47.8, 50.3, 50.5, 51.7, 52.5, 59.06, 59.13, 62.1, 63.3, 64.7, 69.3, 69.6, 70.4, 70.5, 70.59, 70.61, 70.66, 70.69, 71.96, 72.01, 94.7, 97.1, 97.8, 106.5, 113.3, 115.5, 120.3, 124.0, 124.7, 124.9, 125.0, 127.6, 128.5, 129.6, 129.8, 130.6, 131.70, 131.73, 132.6, 133.4, 135.0, 135.4, 135.7, 137.9, 138.0, 143.0, 144.0, 155.7, 156.7, 161.1, 161.5, 165.8, 166.8,

170.2, 170.6; HRMS (ESI-FT-ICR) *m/z* $[M+2Na]^{2+}$ Calcd for $C_{105}H_{123}BF_2N_{16}O_{19}Na_2$, 1003.9541; Found 1003.9541.

Section 5.5.5: Synthesis of Bioconjugatable Arrays

ET11-NHS

A sample of **ET11** (20.2 mg, 10.6 μmol) was dissolved in THF/MeOH (2:1, 3 mL) and treated with 2 M NaOH (1 mL). Mixture was stirred at room temperature for 1 h, then diluted with EtOAc, washed with water, then acidified (5% HCl), washed with brine, dried (Na_2SO_4) and concentrated. Intermediate carboxylic acid was a purple solid upon concentration and drying. Intermediate integrity was confirmed by absorption spectrum and HRMS [(ESI-FT-ICR) *m/z* $[M+Na]^+$ Calcd for $C_{100}H_{121}BF_2N_{16}O_{19}Na$, 1922.8987; found 1922.8930]. Dyad carboxylic acid intermediate (12.5 mg, 6.58 μmol), DMAP (3.2 mg, 26.3 μmol), and EDC·HCl (5.1 mg, 26.3 μmol) were dissolved in DMF (1 mL), treated with N-hydroxysuccinimide (7.6 mg, 65.8 μmol), then stirred at room temperature. After 24 h, the reaction was diluted with EtOAc, washed with water, brine, dried (Na_2SO_4) and concentrated. Product was yielded as a purple solid (11.3 mg, 86%). Absorption and emission spectra (in DMF) are identical with those of methyl ester, confirming integrity of array. HRMS (ESI-FT-ICR) *m/z* $[M+Na]^+$ Calcd for $C_{104}H_{124}BF_2N_{17}O_{21}Na$, 2019.9150; found 2019.9087.

ET12-NHS

A sample of **ET12** (20.1 mg, 10.2 μmol) was dissolved in THF/MeOH (2:1, 3 mL) and treated with 2 M NaOH (1 mL). Mixture was stirred at room temperature for 1 h, then diluted with EtOAc, washed with water, then acidified (5% HCl), washed

with brine, dried (Na_2SO_4) and concentrated. Carboxylic acid intermediate was yielded as a purple solid (15.2 mg, 78%), and identity confirmed by HRMS [(ESI-TOF) *m/z* $[M+Na]^+$ Calcd for $C_{104}H_{121}BF_2N_{16}O_{19}Na$, 1970.8987; found 1970.8944]. Dyad carboxylic acid inter- mediate (15.2 mg, 7.80 μmol), DMAP (3.2 mg, 31.2 μmol), and EDC·HCl (6.0 mg, 31.2 μmol) were dissolved in DMF (1 mL), treated with N-hydroxysuccinimide (9.0 mg, 78.0 μmol), and stirred at room temperature. After 24 h, the reaction was diluted with EtOAc, washed with water, brine, dried (Na_2SO_4) and concentrated. Product was yielded as a purple solid (13.5 mg, 86%). Absorption and emission spectra (in DMF) are identical with those of methyl ester, confirming integrity of array. HRMS (ESI-TOF) *m/z* $[M+Na]^+$ Calcd for $C_{108}H_{124}BF_2N_{17}O_{21}Na$, 2067.9151; found 2067.9049.

Section 5.5.6: Examination of Aqueous Micelle Preparation Methods

To determine if the method of micelle preparation influenced photophysical properties we prepared several solutions of dyad (**ET7** or **ET9**) in 3 mM TX-100 in PBS (pH = 7.4) and measured both Φ_F and ETE. The four different methods we employed are described below, and in all cases, dilutions were performed with 3 mM TX-100 in PBS (pH = 7.4) stock solution (as needed for measurements).

Sample Preparation Methods

Method A: 0.1-0.3 mgs of compound were dissolved in dichloromethane and mixed with 3 mL of 3 mM TX-100 in PBS (pH = 7.4). Resultant biphasic mixture was then stirred in an open vial for two hours, with protection from ambient light, until all dichloromethane evaporated.

Method B: 0.1-0.3 mgs of compound were dissolved in 5.6 mg of TX-100 surfactant and diluted to total volume of 3 mL using PBS (pH = 7.4) solution (this provided 3 mM TX-100).

Method C: 0.1-0.3 mgs of compound were dissolved directly into 3 mL of 3 mM TX-100 in PBS (pH = 7.4). The mixture was initially vortexed and sonicated then left stirring overnight in darkness, if visible solid remained, sonication and stirring was repeated until dissolved.

Method D: 0.1-0.3 mgs of compound and TX-100 (5.6 mg) were dissolved in dichloromethane then concentrated under reduced pressure. Resultant film was then dried under high vacuum for 30-60 mins to ensure removal of dichloromethane. The dry film was then dissolved in 3 mL of PBS (pH = 7.4) to attain 3 mM TX-100.

Compound	Property	Method A	Method B	Method C	Method D
ET7	Φ_F	0.31	0.31	0.32	0.31
	ETE	1.07	1.04	1.02	1.04
ET9	Φ_F	0.15	0.193	0.15	0.18
	ETE	1.01	1.20	1.10	1.09

Table 5.4: Fluorescence quantum yields and ETE of amphiphilic dyads ET7 and ET7 in 3 mM TX-100 solution, following different methods of sample preparation. Error for quantum yield measurements estimated at ± 5% (see section 2.5.4 for details), error for ETE estimated at ± 10% (see section 4.5.4).

Overall, the results (summarized in Table 5.4) indicate that both Φ_F and ETE vary depending on the method of solution preparation, however these variations do not have an impact on the overall conclusions. More rigorous and systematic studies, regarding both array concentration and method of solution preparation, on the structure and properties of the resulting micelles are required to fully understand the observed variations. Ultimately, we chose to report Φ_F and ETE for dyads in Table 5.2 by Method

B because we had measured several dyads by this preparation method prior to assessing the other three methods described above, and repeating all measurements following a different preparation method would be unnecessarily time consuming.

Section 5.5.7: Photostability Testing of Dyads in Aqueous Micelles

In order to determine the ability of amphiphilic dyads to serve as imaging agents in a biological environment, we assessed their photostability in aqueous micelles. All samples prepared for the examination of photostability were prepared in 3 mM TX-100 in PBS (pH = 7.4) by Method A (see section 5.5.6 for details), with dyad concentration adjusted through dilution to a final absorbance of A $\approx$ 0.1 at hydroporphyrin B band. Solutions were then divided evenly, with one half stored in darkness while the other was subjected to irradiation. Irradiated samples were exposed to monochromatic light (set to λ_{max} of *B* band) generated by xenon lamp, with maximum excitation slit width (20 nm) possible in PTI-Quantamaster Spectrofluorometer. Samples were all stirred at maximum setting for entirety of irradiation time, using micro-stirbar and fluorometer built in magnetic stirrer. Absorption spectrum of irradiated samples was recorded at the noted time intervals (representative traces can be found in Figures 5.8 and 5.9), while the absorption of dark samples was recorded after 24 hours of storage. Absorption of dark samples are not shown as there were no notable differences relative to freshly prepared samples. The y axis demonstrated in figure 5.7 is the ratio of absorbance over initial absorbance at the maximum of the Q_y absorption band, at the time indicated.

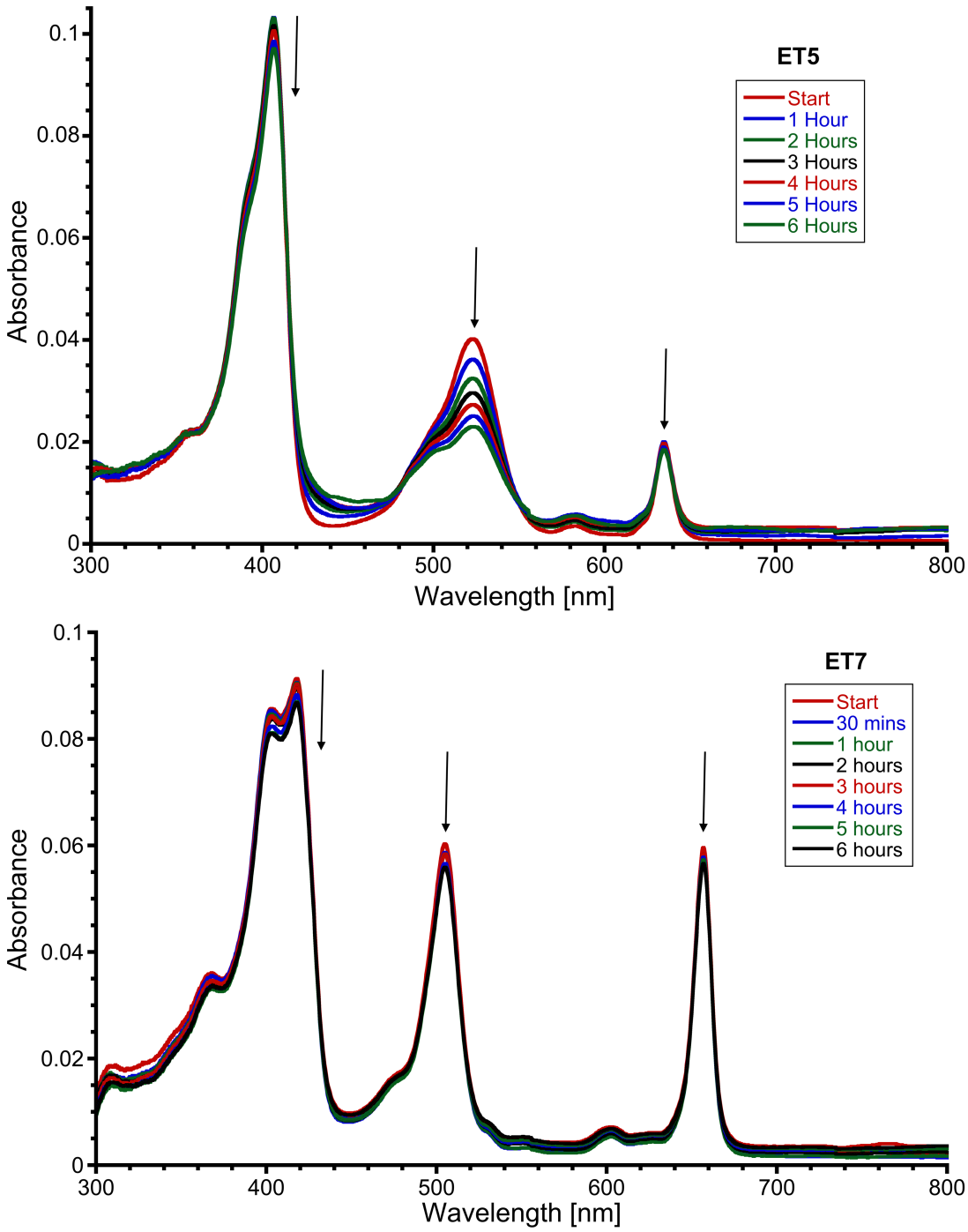

Figure 5.8: Change in absorption over time for chlorin-BODIPY dyads ET5 (top) and ET7 (bottom), upon selective irradiation at the maximum of the BODIPY absorption band.

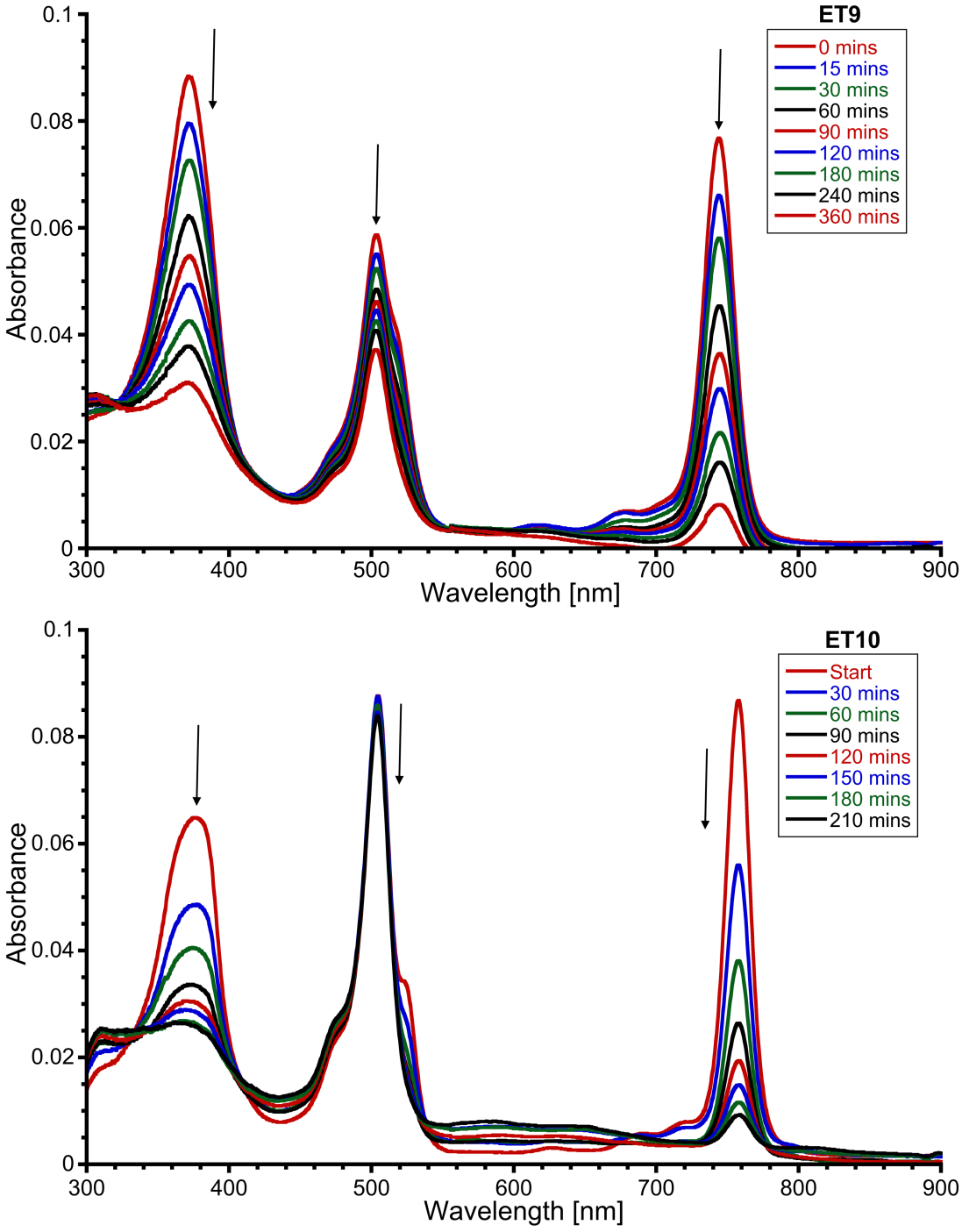

Figure 5.9: Change in absorption over time for bacteriochlorin-BODIPY dyads ET9 (top) and ET10 (bottom), upon selective irradiation at the maximum of the BODIPY absorption band.

Section 5.6: Supplemental Information

Section 5.6.1: Photophysical Properties and Structures of Hydroporphyrin Monomers

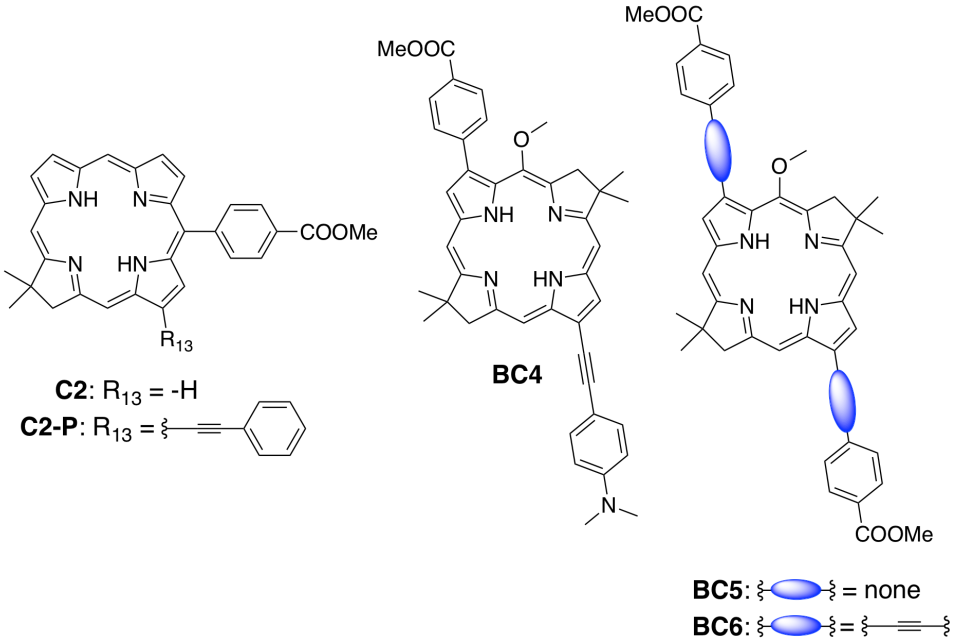

Monomer [related dyad]	Absorption λ_{max} (nm)			λ_{emi} (nm)	Φ_F tol. (DMF)
	$\lambda_{B\ band}$	λ_{Qx}	λ_{Qy}		
C2 [ET5]	405	499	636	641	0.21 (0.20)
C2-P [ET6-7]	402, 417	506	656	659	0.33 (0.34)
BC4 [ET11]	369	514	735	744	0.25 (0.23)
BC5 [ET8-9]	369	522	750	761	0.25 (0.21)
BC6 [ET10 & ET12]	380	529	761	765	0.23 (0.21)

Table 5.5: Photophysical properties of hydroporphyrin monomers closely related to those utilized in arrays ET5-ET12. Data for C2,[126] C2-P,[124] BC4,[268] and BC5[129] taken from our publications, BC6 was prepared and characterized in house following standard procedure (Section 2.5.4) but is currently unpublished. Error for quantum yield measurements estimated at ± 5% (see section 2.5.4 for details).

Section 5.6.2: DFT Calculated Data

Compound	HOMO (eV)	LUMO (eV)
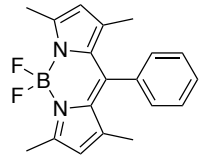 **B-F**	-5.34	-2.33
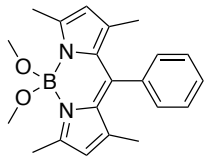 **B-OMe**	-5.16	-2.14

Table 5.6: DFT Calculated HOMO & LUMO Energies for model 4,4-difluoro (B-F) and 4,4-dimethoxy (B-OMe) BODIPYs

For general details on DFT calculations see Section 2.5.6 or Section 3.5.3.

Chapter 6: BODIPY-Bacteriochlorin Energy Transfer Arrays with Multiple Excitation and Single Emission

Section 6.1: Introduction

In the previous two chapters we demonstrated how to prepare weakly conjugated arrays that feature dual excitation (green and red-NIR spectral windows) and a single red-NIR emission band. In Chapter 4 the focus was on understanding molecular design to afford large ETE and low fluorescence quenching. In Chapter 5, we made the early hydrophobic constructs suitable for *in vivo* application with neutral water solubilizing functionalities strategically placed on the BODIPY energy donor. All arrays presented to this point feature a common BODIPY donor (absorption λ_{max} ~505 nm) with variable emission maxima, that was controlled by tuning the hydroporphyrin energy acceptor. Here, we want to expand upon the capabilities of our growing library of arrays by taking the opposite approach, tuning the absorption maxima while keeping the maximum emission wavelength constant. Such a series of arrays would be valuable for multiplexed imaging applications. For example, a microscopist who wants to visualize several targets in a complex sample, could label the targets with different arrays, then select which target to visualize based upon the excitation wavelength, without need to alter the detection system.

For this new series of arrays, we considered that we must retain a significant separation between the maxima of donor emission and acceptor absorption (~20 nm or more), to preserve the large pseudo-Stokes' shift and greater imaging resolution. To do this, the energy acceptor's absorption and emission maxima should already be quite bathochromically shifted, giving us more flexibility with the tuning of the energy donor

properties. We opted to retain bacteriochlorin as the energy acceptor, because of our familiarity and the fact its Q_y band maxima is situated in the NIR (> 715 nm).[113] We considered chlorin as the energy donor, however, its lowest energy transition is already quite red shifted even for unsubstituted chlorin (~620 nm),[107] leaving us little room for tuning before bacteriochlorin would undergo direct excitation. Also, on the practical side, using two fully synthetic hydroporphyrins for our arrays would drive cost needlessly high. Thus, we evaluated BODIPY as a cheaper alternative.

BODIPY continued to be an appealing energy donor, because the maximum of the S_0-S_1 absorption band can be tuned by expanding the π system similar to what was examined in Chapter 2 with chlorins. Unlike hydroporphyrins, it is not necessary to install halides as synthetic handles on BODIPY, rather, styryl substituents can be installed wherever there are pyrrolic methyl substituents.[265,308,405–409] This is a common approach where styryl substituents are connected to BODIPY through Knoevenagel condensation between the 5- and 7- position methyl substituents and an aryl aldehyde. The addition of each styryl group results in a bathochromic shift of ~50-100 nm (depending on electron donating/withdrawing groups on the auxochrome) of the BODIPY S_0-S_1 band.[265,308,406–409] This makes it straightforward to prepare a short series of BODIPYs, with different λ_{max} when beginning from a common, green absorbing BODIPY. This approach has been taken to prepare numerous styryl BODIPY derivatives that have been used as single chromophores for imaging,[410–413] or photodynamic therapy.[345,414,415] Styryl substituted BODIPYs have also been seen in energy transfer arrays as either the energy donor or energy acceptor. Due to absorption and emission maxima falling around ~550-600 nm, mono-styryl BODIPYs are often

seen either as energy donor,[85,302,307,416–418] or acceptor.[364,419] Meanwhile, di-styryl BODIPYs (maxima ~630-700 nm) occasionally seen as energy acceptor.[85,364,417,418,420–426] and rarely used as energy donor.[420,422] The general approach by Knoevenagel

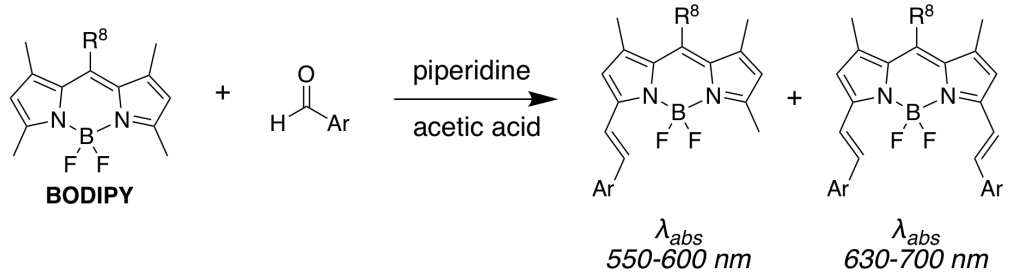

Figure 6.1: General Synthesis of Styryl Substituted BODIPYs

condensation can be seen in Scheme 6.1.

Up until this point, all arrays which we have prepared featured a common donor emission (BODIPY) and common acceptor absorption (hydroporphyrin Q_x band). Under the assumption that FRET was the primary mechanism of energy transfer, ETE is highly dependent upon the overlap of the donor emission and acceptor absorption (overlap integral, J).[2,427,428] Thus the main question we encounter here is, how will altering the spectral properties of BODIPY affect ETE of the system. Either ETE will remain high, as was observed for the previous arrays, or there will be a decrease. Here, we can attempt to promote larger ETE in all cases by proper choice of a common linker.

The rate of energy transfer is inversely proportional to inter pigment distance (*r,* measured as center-to-center distance between transition dipole moments) to the sixth power.[2] Because of this great sensitivity to distance, we want to utilize the shortest linker possible, that is easy to install and also prohibits strong electronic conjugation. For our purposes, the only logical choice was to use a phenyl linker, which we demonstrated in the previous chapter does not significantly alter the absorption and emission properties of bacteriochlorins. Like before, we can expect quenching due to

PET to occur in polar media, but that is only a secondary concern for these arrays, as the primary goal is to attain arrays with large ETE regardless of the excitation wavelength. Should quenching become a significant problem, that can be addressed later with different molecular design.

The new set of arrays (Chart 6.1) feature BODIPY monomers with 0, 1 and 2 styryl substituents linked to bacteriochlorin (arrays **ET13**, **ET14** and **ET15**, respectively). By increasing the number of styryl substituents, we will address the question of how ETE will be affected by varying the degree of spectral overlap between donor emission and acceptor absorption. Our choice of styryl BODIPY energy donors are 3-[2-(2,4,6-trimethoxyphenyl)ethenyl] BODIPY for **ET14** and 3,5-bis[2-(2,4,6-trimethoxyphenyl)ethenyl] BODIPY for **ET15**. The 2,4,6-trimethoxyphenyl substituents were selected because it is well documented that the more electron rich the auxochrome, the greater the resultant bathochromic shift.[308,406–409] Array **ET13**, featuring 1,3,5,7-tetramethyl BODIPY will serve as a benchmark similar to our earlier arrays with common green emissive BODIPYs. For benchmark compounds, we included 3,13-bis[(4-methoxycarbonyl)phenyl]bacteriochlorin **BC3**, and BODIPY monomers **B6-B8** which feature 0-2 styryl substituents, respectively (Chart 6.1). Note that **B6-B8** also possess boron pinacol esters, for use as a synthetic handle in dyad synthesis.

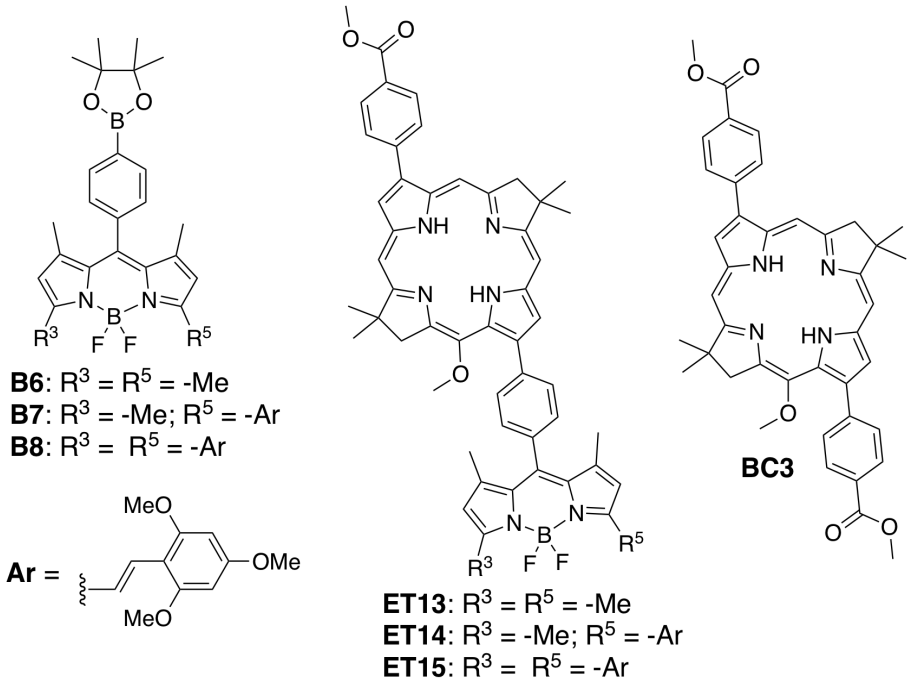

Chart 6.1: BODIPY Monomers and Energy Transfer Arrays Discussed in Chapter 6.

Section 6.2: Synthesis of BODIPY Monomers and Arrays

Section 6.2.1: Synthesis of red light absorbing and emitting BODIPYs

BODIPY monomer **B6** was prepared following the standard one-pot, 3 step synthesis of 1,3,5,7-tetramethyl-8-(4-bromo)phenyl BODIPY with subsequent Miyaura borylation.[429] **B7** and **B8** were prepared from **B6** following established conditions for Knoevenagel condensation,[308] with microwave irradiation to expedite the reaction (Scheme 6.2).[430] These standard conditions feature reaction **B6** and aryl aldehyde (2,4,6-trimethoxybenzaldehyde **22**) with piperidine/acetic acid in DMF. Reaction with 1 equivalent of **22** provided **B7** in 13% yield, while the same reaction with 4 equivalents of **22** provided **B8** in 9% yield. Several attempts were made to improve the yields, including different solvent systems and the return to conventional heating. We found that the prolonged (overnight) reaction times of conventional heating lead to increased decomposition rather than improved yields, similar results

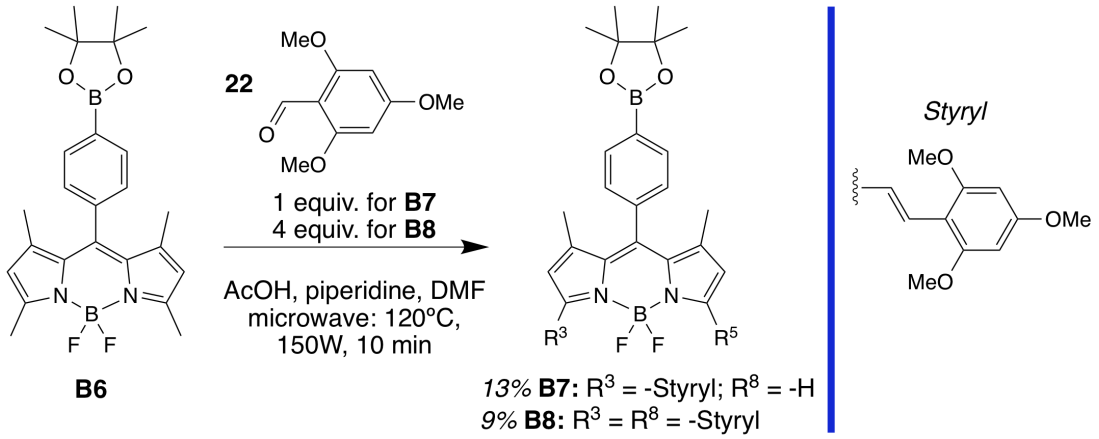

Scheme 6.2: Synthesis of styryl substituted BODIPYs, B7 and B8.

were seen with over-exposure in the microwave reactor. Optimal yields were attained when all starting material was consumed, and product spot was the major one observed on TLC (easily distinguished by color, mono-styryl BODIPY is deep blue in color and bright pink fluorescent under UV irradiation, di-styryl BODIPY is blue-green in color and red fluorescent under UV irradiation). Even then, some byproducts (di- and tri-styryl BODIPYs) accompanied the major product and required column chromatography for complete removal. The necessity of column chromatography is presumably responsible for the low yield, at least in part, due to the interaction between boron pinacolate esters and silica.[389]

Section 6.2.2: Synthesis of BODIPY-Bacteriochlorin Arrays and Benchmark Bacteriochlorin Monomer

Benchmark bacteriochlorin monomer **BC3**, was isolated as the side product of the routine synthesis of known 3-bromo-13-(4-methoxycarbonyl)phenyl bacteriochlorin **BC1** (Scheme 6.3).[122] The disubstituted byproduct was isolated in 37% yield from unoptimized conditions for Suzuki cross-coupling reaction.

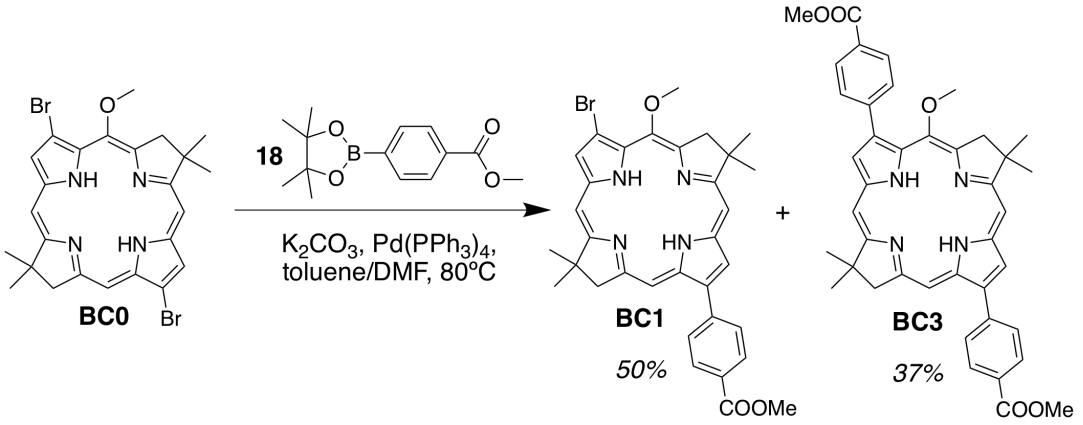

Scheme 6.3: Synthesis of bacteriochlorin benchmark BC3 and mono-bromo bacteriochlorin BC1 for preparation of arrays.

The phenyl linked BODIPY-bacteriochlorin arrays were all prepared via Suzuki cross-coupling reaction bacteriochlorin **BC1** and one of the boronic ester substituted BODIPYs **B6-8** (Scheme 6.4). Here we utilized two sets of conditions. The first are the conditions we sued for the synthesis of amphiphilic dyads **ET11-12**,[379] the second are established Suzuki reaction conditions for coupling of commercially available boronic esters to bromo-bacteriochlorins.[122] The yields were comparable in all cases, regardless of the conditions used; **ET13** in 49% yield and both **ET14** and **ET15** in 56% yield. All dyads were isolated by column chromatography and required additional trituration with hexanes and/or methanol to remove minor fluorescent impurities that appeared to be residual BODIPY.

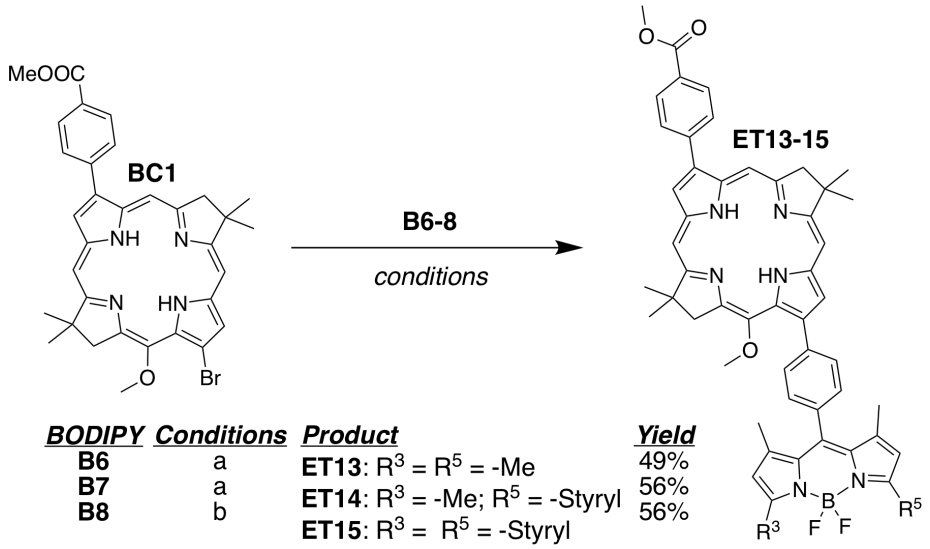

BODIPY	Conditions	Product	Yield
B6	a	ET13: $R^3 = R^5 =$ -Me	49%
B7	a	ET14: $R^3 =$ -Me; $R^5 =$ -Styryl	56%
B8	b	ET15: $R^3 = R^5 =$ -Styryl	56%

Scheme 6.4: Synthesis of BODIPY-bacteriochlorin arrays, ET13-ET15. Conditions a) Na_2CO_3, $PdCl_2(dppf)\cdot CH_2Cl_2$, toluene/EtOH/$H_2O$ (4:1:2), 80ºC; b) K_2CO_3, $Pd(PPh_3)_4$ toluene/DMF (2:1), 80ºC

Section 6.3: Characterization

Section 6.3.1: Structure Determination

All new compounds were characterized by high-resolution mass spectrometry, as well as ^{1}H and ^{13}C NMR spectroscopy. All data are consistent with the target structures. The ^{1}H NMR of **B7** and **B8** showed two doublets at 7.6 ppm and 7.2 ppm, which correspond to the ethenyl component of 3,5-styryl substituents, as well as loss of the resonance at 2.35 ppm, corresponding to 3,5-methyl substituents (visible in ^{1}H NMR of **B6**). The coupling constant for both vinyl protons ($^3J \approx 16.5$ Hz) is consistent with *E* stereochemistry of the styryl double bonds, in all novel BODIPY monomers and in arrays. For arrays, ^{1}H NMR resonances assigned to BODIPY and bacteriochlorin were found to be in 1:1 ratio.

Section 6.3.2: Photophysical Characterization

We acquired the absorption and emission spectra of all novel compounds in toluene, and determined fluorescence quantum yields (and energy transfer efficiency

for arrays) in both toluene and DMF. Absorption and emission spectra of BODIPY monomers are shown in Figure 6.1, with absorption of benchmark **BC3** included to clearly show the spectral overlap between **BC3** absorption and BODIPY monomers emission. Figure 6.2 features the absorption and emission spectra of arrays **ET13-15**, respectively. Emission of **BC3** is also included in Figure 6.2. All spectra are acquired in air-equilibrated toluene, absorption spectra are acquired at a ~10 μM concentration while emission spectra are acquired at ~ 1.0 μM concentration, under the assumed ε (~100,000 $M^{-1} \cdot cm^{-1}$) at either BODIPY S_0-S_1 absorption band[265] or hydroporphyrin *B* band.[109,113] A summary of photophysical properties for BODIPY monomers, benchmark bacteriochlorin **BC3** and arrays can be found in Table 6.1.

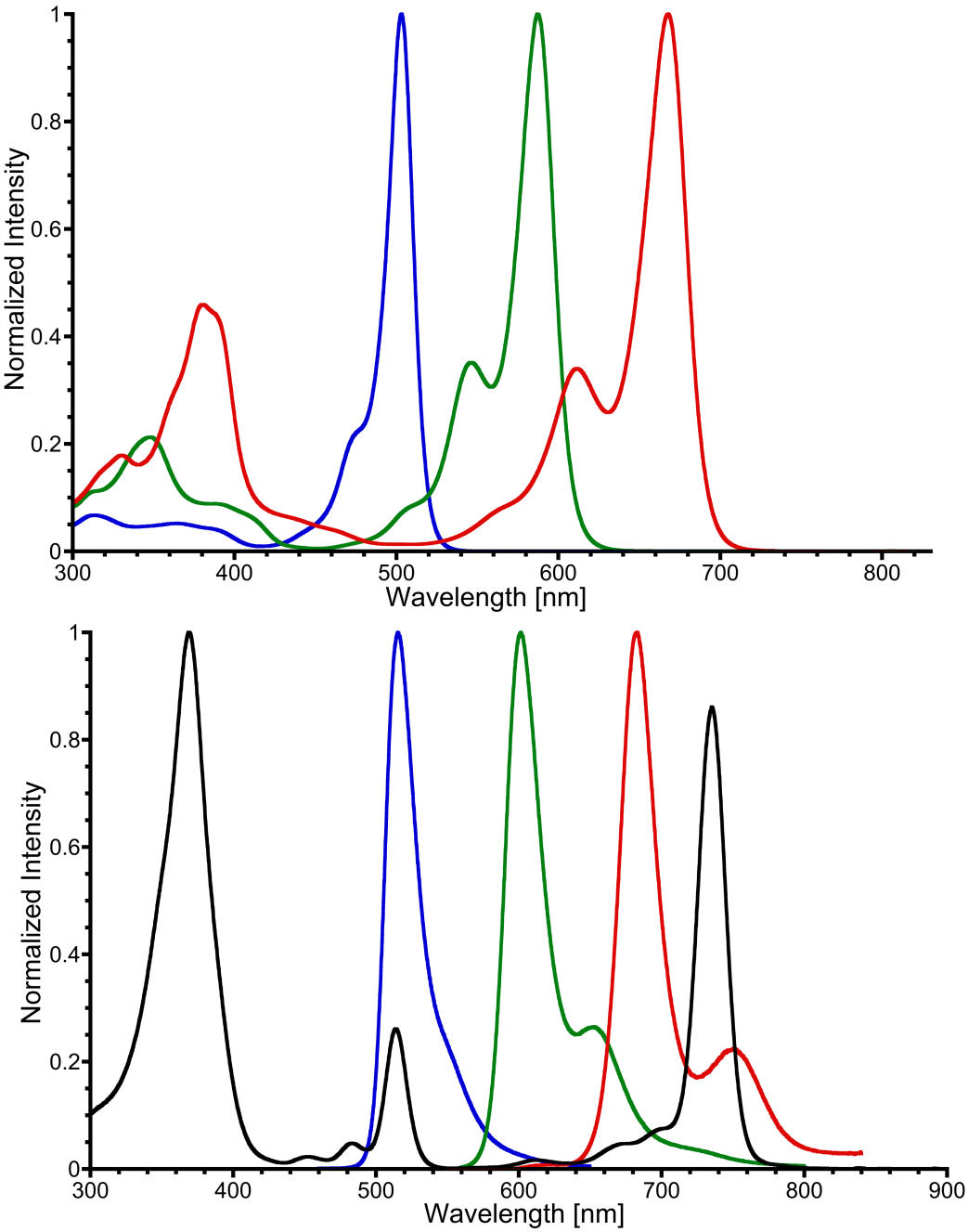

Figure 6.1: Absorption (top) and emission spectra (bottom) of BODIPY monomers B6 (blue), B7 (green) and B8 (red). For bottom: Absorption spectrum of benchmark bacteriochlorin BC3 (black) also included. All absorption spectra acquired in toluene at ~10 µM concentration and normalized at maximum of most intense band. Emission acquired at ~1.0 µM concentration, upon excitation at blue edge of BODIPY S_0-S_1 absorption band where slope is minimal (~10-20 nm below λ_{max}).

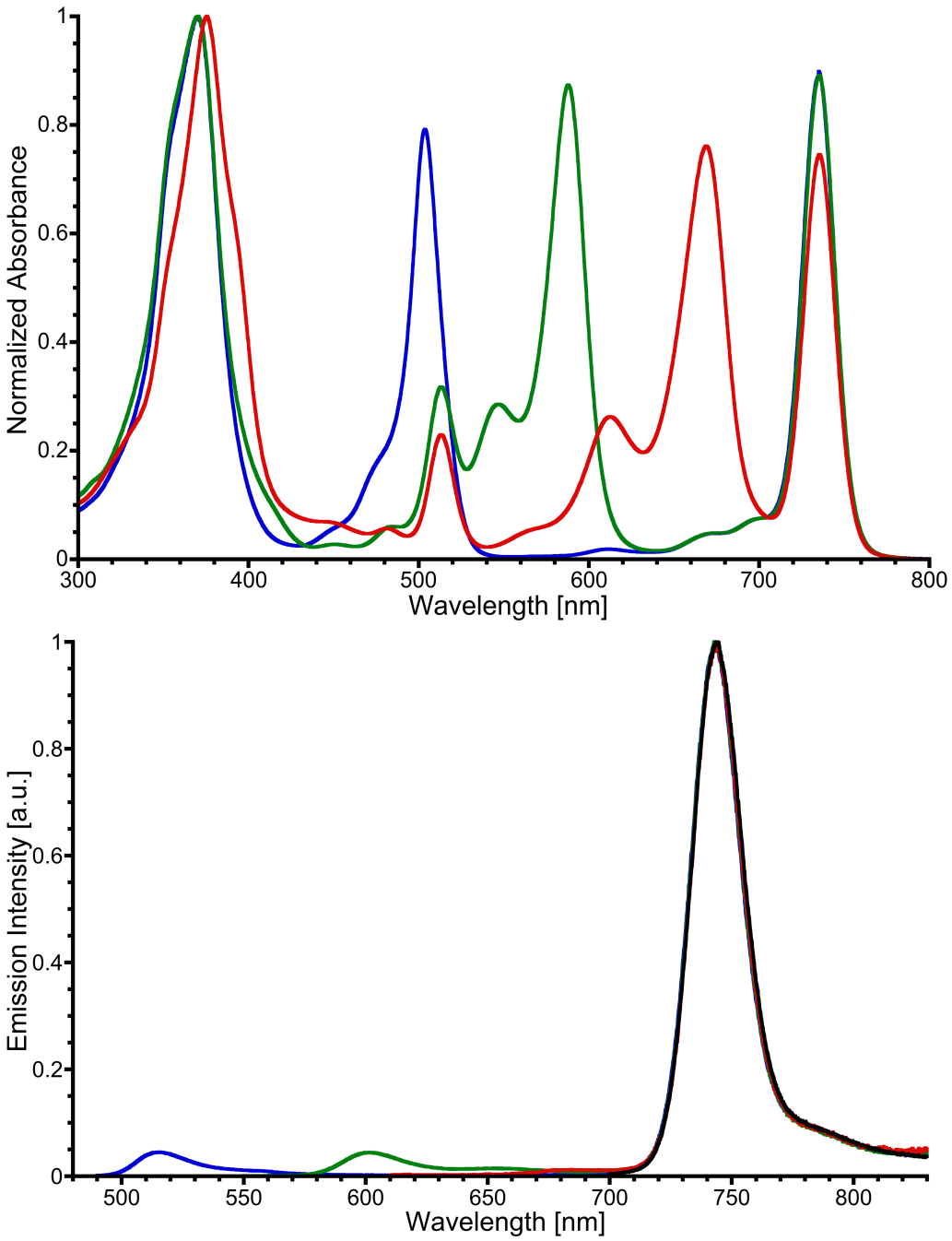

Figure 6.2: Absorption (top) and emission spectra (bottom) of arrays ET13 (blue), ET14 (green) and ET15 (red). For bottom: Emission spectrum of benchmark bacteriochlorin BC3 (black) also included. All absorption spectra acquired in toluene at ~10 µM concentrationand normalized at maximum of most intense band. Emission acquired at ~1.0 µM concentration, upon excitation at blue edge of BODIPY S_0-S_1 absorption band where slope is minimal (~10-20 nm below λ_{max}) for arrays, for BC3 excitation occurred at maximum of the *B* band.

Compound	Absorption λ_{max} (nm)			λ_{emi} (nm)	Φ_F toluene [ETE]	Φ_F DMF
	$\lambda_{B\ band}$	λ_{BDP}	λ_{Qy}			
BODIPY monomers						
B6	503			515	0.69	0.54
B7	587			602	0.84	0.75
B8	668			683	0.56	0.45
benchmark bacteriochlorin						
BC3	369	514[†)]	735	744	0.25	0.23
energy transfer arrays						
ET13	371	504	735	744	0.23 [0.93]	0.026
ET14	370	588	735	743	0.24 [0.92]	0.018
ET15	373	669	736	744	0.24 [0.96]	<0.005

Table 6.1: Absorption and emission properties of BODIPY and bacteriochlorin monomers and bacteriochlorin-BODIPY arrays. Fluorescence quantum yields were determined using rhodamine 6G as standard for BODIPY monomers (Φ_F = 0.88 in air-equilibrated methanol)[56,391] and TPP as standard for BC1 and arrays (Φ_F = 0.070 in air-equilibrated toluene).[109] BODIPY monomers were excited at the blue edge of S_0-S_1 absorption band (~10-20 nm shorter than λ_{max} where change in slope is at a minimum), benchmark BC1 was excited upon maximum of B band, and dyads were excited at either the maximum of the bacteriochlorin B band or BODIPY band. For dyads, only the emission from bacteriochlorin was measured, for samples where concentration was ~1.0 μM or less. ETE is determined as the ratio of Φ_F measured upon excitation at maximum of BODIPY divided by Φ_F measured upon direct excitation of bacteriochlorin at maximum of B band. ETE was not determined in DMF due to the weak fluorescence. †) value corresponds to bacteriochlorin Q_x band. Error for quantum yield measurements estimated at ± 5% (see section 2.5.4 for details), error for ETE estimated at ± 10% (see section 4.5.4 for details).

Photophysical Properties of BODIPY Monomers

The absorption spectra of each BODIPY monomer (Figure 6.1) features a strong S_0-S_1 band that is red shift by ~80 nm for each styryl substituent when going from **B6-B8**. The styryl substituents also result in significant broadening of the S_0-S_1 band, with an increase to the intensity and resolution of the shoulder on the blue edge of the primary band. Each styryl substituent increases the intensity of the higher energy S_0-S_2 absorption band and causes it to bathochromically shift by ~20 nm. Each BODIPY possesses intense emission and Stokes' shift in the typical range for BODIPY (12-15 nm). Fluorescence quantum yields were large for all monomers in toluene at 0.69, 0.84 and 0.56 for **B6-B8**, respectively. Additionally, they showed limited quenching of fluorescence in DMF, where Φ_F only decreased by 22% at most.

Photophysical Properties of BODIPY-Bacteriochlorin Arrays

The absorption spectra of all arrays are the sum of the absorption for bacteriochlorin and BODIPY components (Figure 6.2), with effectively unchanged maxima, this behavior is consistent with all other weakly conjugated arrays. This was the desired effect resulting from the linker's orientation being orthogonal to both chromophores, as opposed to just the BODIPY unit (in the case of phenylethynyl linker).

The emission spectra of dyads (Figure 6.4), upon selective excitation at the BODIPY component, shows nearly exclusive emission from the bacteriochlorin, with only weak residual fluorescence signal from BODIPY. The emission λ_{max} of the arrays remains unchanged from that of benchmark bacteriochlorin **BC3** (744 nm), as can be seen by the nearly identical emission spectra for all dyads and **BC3**. This demonstrates

that even in the excited state, electronic conjugation between the two chromophores is being prevented by the phenyl linker.

Next, we examined the energy transfer efficiency and determined fluorescence quantum yields for all arrays. We acquired the fluorescence excitation spectra of each dyad to quickly assess ETE, and in all cases observed close agreement with excitation spectra and absorption spectra (Section 6.6, Figures 6.3 and 6.4), reinforcing what we observed with emission spectra. Satisfied, we determined the Φ_F for each dyad upon excitation at each component and then took the ratio as Φ_F upon excitation at BODIPY band with monitoring of bacteriochlorin emission, divided by Φ_F determined upon direct excitation of the bacteriochlorin (see section 4.5.4 for more detail). In toluene, the values for Φ_F upon direct excitation of bacteriochlorin (0.23-0.24) closely match that of the monomer, indicating that the attachment of the BODIPY does not influence emission intensity of bacteriochlorin. The ETE determined in toluene exceeds 0.90 for all arrays. This indicates that either, the spectral overlap is sufficient in all arrays to afford large ETE, or it is possible that through-bond energy transfer is at work here, at least to partial degree.[427,428] Elucidating the mechanism of energy transfer in these constructs is the subject of our growing collaboration with Dr. Matthew Pelton.

In contrast to what we observed for toluene, fluorescence is significantly reduced in DMF, regardless of the excitation wavelength. Emission became so weak (>90% quenching) that we were unable to accurately determine ETE in DMF. Quenching is greater in phenyl linked **ET13** than in phenylethynyl linked **ET8** (Chapter 5, Φ_F = 0.25 in toluene, 0.07 in DMF). This could be due to the increased oxidation

potential of chlorin in **ET8** partially prohibiting PET and/or the smaller distance between chromophores in the case of phenyl linker.[431]

In order to probe the mechanism of quenching further, we measured Φ_F and ETE for dyad **ET15** in solvents with a wide range of dielectric constants (ε, Table 6.2).

Solvent (ε)	C_6H_5-Me (2.38)	C_6H_5-Cl (5.62)	THF (7.58)	CH_2Cl_2 (8.93)	*i*-PrOH† (17.9)	Acetone (20.7)	C_6H_5-CN (26.0)	DMF (36.7)
Φ_F	0.25	0.26	0.22	0.059	0.19	0.03	0.033	0.024
Φ_{ETE}	0.97	0.96	0.95	1.0	1.0	1.0	n/a	n/a

Table 6.2: Emission Properties of array ET15 in solvents of varying polarity (expressed in dielectric constant (ε). Fluorescence quantum yields reported for excitation at *B* band, determined using TPP as standard (Φ_F = 0.070 in air-equilibrated toluene).[109] Φ_F determined at concentration of array ~1.0 μM. ETE is determined as the ratio of Φ_F measured upon excitation at maximum of BODIPY divided by Φ_F measured upon direct excitation of bacteriochlorin at maximum of B band. †) contains 2.5% THF. n/a- data not reported due to weak emission intensity and overlap with residual emission from B8 (either as impurity or due to incomplete energy transfer). Dielectric constants (ε) obtained from sigmaaldritch.com. Error for quantum yield measurements estimated at ± 5% (see section 2.5.4 for details), error for ETE estimated at ± 10% (see section 4.5.4 for details).

Only dyad **ET15** was used for this purpose, because it showed the greatest quenching in DMF. We found that both Φ_F and ETE remain high ($\Phi_F > 0.21$, ETE > 0.9) for solvents of dielectric constant below 8, with significant quenching occurring at $\varepsilon \sim 9$ or above. The one exception to this was isopropanol, for which $\Phi_F = 0.19$ and ETE was near unity. We suspect that the need for a small amount of THF cosolvent (2.5% v) has led to this discrepancy. Overall, the trend shows a decrease in fluorescence quantum yield as solvent dielectric constant increases. This behavior is very different from hydroporphyrin monomers, for which quenching is independent of solvent dielectric constant (this is demonstrated in Chapter 2, with chlorin monomers in DMF, Table 2.1). The diminished Φ_F, with large ETE indicates that the quenching is occurring regardless of the excitation wavelength (BODIPY or bacteriochlorin) and must follow the energy transfer process. Thus, quenching is occurring from photoexcited

bacteriochlorin, most probably as oxidative PET, which is consistent with the behavior of all of our previous arrays, and reported porphyrin containing arrays.[421]

Section 6.4: Conclusions

We successfully prepared a short series of new long wavelength absorbing and emitting styryl BODIPY derivatives via microwave assisted Knoevenagel condensation. Each styryl BODIPY, and one green emitting BODIPY, was then incorporated into a bacteriochlorin-BODIPY energy transfer array by Suzuki cross coupling. These new molecular designs enabled us to broadly tune the absorption maxima of arrays with a constant energy acceptor and NIR emission maxima. Each array exhibited highly efficient energy transfer from BODIPY to bacteriochlorin. The absorption and emission maxima of the BODIPY component varied from 505-685 nm and had differing spectral overlap with the Q_x and Q_y absorption bands of bacteriochlorin. This minimal dependence on spectral overlap could be an advantageous feature for the synthesis of future arrays with tunable excitation maxima. In particular, our arrays with deep-red absorption and NIR emission would be well suited towards biological application because both maxima are well within the optical therapeutic window (650-900 nm). There are limited examples of such arrays,[122,134,397,398,432,433] and most examples[134,432] (including those prepared by our gro. up)[122] have relied upon chlorins as the energy donor with bacteriochlorins as energy acceptor. Distyryl BODIPYs are well suited to replace the chlorins in such arrays. Distyryl BODIPYs possess larger molar absorptivity relative to chlorins (~100,000 $M^{-1} \cdot cm^{-1}$ vs 80,000 $M^{-1} \cdot cm^{-1}$, respectively)[134,308] absorbing in the same spectral window, have been demonstrated here as efficient energy donors to bacteriochlorin, and are

significantly easier to synthesize than chlorins (a few days as opposed to several weeks of labor).

The high solvent-polarity dependence of quenching and Φ_F in the BODIPY-bacteriochlorin arrays is the primary concern for their application *in vivo*. Because cells are complex, with bulk water (high polarity) and nonpolar compartments (low polarity) it is unclear how they will perform in a real setting. To address the quenching by PET, we can consider the modulation of BODIPY reduction potential or formulate in aqueous micelles (as done with arrays prepared in Chapter 5). It is also possible that these arrays, being very nonpolar in nature, would be naturally drawn to the subcellular compartments with low polarity (e.g., proteins, lipid membrane)[434–437] where fluorescence is restored upon leaving the polar media. From what we experienced with the dyads prepared in Chapter 5, however, it is more likely that significant improvement to water solubility will also be necessary. Thus, the next stage is to incorporate both motifs, of improved water solubility and redox properties to reduce quenching (Chapter 5) and the long wavelength excitation of styryl BODIPYs (Chapter 6) to achieve arrays better suited for *in vivo* application. This phase of research is currently underway.

Section 6.5: Experimental Procedures

Section 6.5.1: General Synthetic and Spectroscopic Procedures

For general procedures involving palladium catalyzed (Sonogashira) reactions and characterization of new compounds by NMR and HRMS, see section 2.5.1. For final compounds, where ^{13}C NMR is not provided, compound solubility was too low to acquire spectrum. For determination of fluorescence quantum yields see section 2.5.4, for determination of energy transfer efficiency see section 4.5.4.

Known compounds **B6**,[429] **BC1**[122] and **BC0**[123] were prepared according to literature procedure.

Microwave Assisted Knoevenagel Condensation

Styryl substituted BODIPYs were prepared via Knoevenagel condensation under microwave heating with the following parameters: hold time of 10 minutes, temperature of 120ºC, and max power of 150W, for one reaction cycle in 10 mL microwave safe test tube. See Section 2.5.1 for details of reaction cycles for microwave assisted reactions.

Section 6.5.2: Synthesis of Styryl Substituted BODIPYs and Bacteriochlorin Standard

*4,4-difluoro-3-[E-2-(1,3,5-trimethoxyphenyl)ethenyl]-1,5,7-trimethyl-8-[4-(4,4,5,5-tetramethyl-1,3,2-dioxaborolan-2-yl)phenyl]-4-bora-3a,4a-diaza-s-indacene (**B7**)*

A mixture of **B6** (106 mg, 0.235 mmol), 2,4,6-trimethoxybenzaldehyde **22** (46.2 mg, 0.235 mmol), acetic acid (6 drops) and piperidine (6 drops) in DMF (5 mL) were reacted following the General Procedure for Microwave Assisted Knoevenagel Condensation. The crude reaction mixture was diluted with EtOAc, washed (water and brine) and concentrated. Flash column chromatography [silica, CH_2Cl_2/hexanes (5:1)]

yielded a blue/pink solid (19.6 mg, 13%). ^{1}H NMR ($CDCl_3$, 400 MHz): 1.36 (s, 3H), 1.39 (s, 12H), 1.41 (s, 3H), 2.57 (s, 3H), 3.84 (s, 3H), 3.91 (s, 6H), 5.93 (s, 1H), 6.12 (s, 2H), 6.65 (s, 1H), 7.33 (d, *J* = 8.1 Hz, 2H), 7.64 (d, *J* = 16.5 Hz, 1H), 7.89 (d, *J* = 8.1 Hz, 2H), 8.12 (d, *J* = 16.6 Hz, 1H); ^{13}C NMR ($CDCl_3$, 100 MHz): 14.6, 14.7, 15.1, 25.1, 55.5, 56.0, 84.2, 90.7, 108.3, 117.8, 120.1, 120.3, 128.0, 128.9, 130.9, 133.1, 135.3, 138.6, 138.9, 140.6, 143.0, 152.8, 157.0, 160.7, 162.0; HRMS (ESI-FT-ICR) *m/z* $[M+Cs]^+$ Calcd for $C_{35}H_{40}B_2F_2N_2O_5Cs$ 761.2152; Found 761.2154.

*4,4-difluoro-3,5-bis[E-2-(1,3,5-trimethoxyphenyl)ethenyl]-1,7-dimethyl-8-[4-(4,4,5,5-tetramethyl-1,3,2-dioxaborolan-2-yl)phenyl]-4-bora-3a,4a-diaza-s-indacene (**B8**)*

A mixture of **B6** (106 mg, 0.200 mmol), 2,4,6-trimethoxybenzaldehyde **22** (156 mg, 0.8 mmol), acetic acid (6 drops) and piperidine (6 drops) in DMF (5 mL) were placed in a 10 mL microwave tube and reacted following the General Procedure for Microwave Assisted Knoevenagel Condensation. After a single microwave exposure TLC indicated that **B8** was present, however, further irradiation leads to extensive decomposition rather than increased yield. The crude reaction mixture was diluted with EtOAc, washed (water then brine) and concentrated. Flash column chromatography [silica, CH_2Cl_2/hexanes (5:1)] yielded a teal solid (14.5 mg, 9%). ^{1}H NMR ($CDCl_3$, 400MHz): 1.39 (s, 12H), 1.41 (s, 6H), 3.84 (s, 6H), 3.92 (s, 12H), 6.13 (s, 4H), 6.64 (s, 2H), 7.36 (d, *J* = 7.9Hz, 2H), 7.59 (d, *J* = 16.6 Hz, 2H), 7.89 (d, *J* = 8.0 Hz, 2H), 8.19 (d, *J* = 16.6 Hz, 2H); ^{13}C NMR ($CDCl_3$, 100MHz): 15.0, 25.1, 55.5, 55.9, 84.2, 90.8, 108.7, 117.1, 120.8, 127.0, 128.4, 132.9, 135.2, 136.5, 139.0, 140.9, 154.7, 160.5, 161.5; HRMS (ESI-FT-ICR) *m/z* $[M]^+$ Calcd for $C_{45}H_{50}B_2F_2N_2O_8$ 806.3731; Found 806.3708.

*5-methoxy-8,8,18,18-tetramethyl-3,13-bis[4-(methoxycarbonyl)phenyl] bacteriochlorin (**BC3**)*

This compound was prepared in non-optimized reaction, as a side product in synthesis of **BC1**. Following the general procedure for palladium catalyzed cross-couplings (Section 2.5.1), a mixture of **BC0** (100.0 mg, 0.179 mmol), 4-methoxycarbonylphenylboronic acid pinacol ester **18** (56.3 mg, 0.215 mmol), potassium carbonate (247.4 mg, 1.79 mmol), and $Pd(PPh_3)_4$ (41.4 mg, 0.0358 mmol) in toluene/DMF (2:1, 21 mL) was stirred at 80ºC, under N_2 for 15 hours. The reaction mixture was diluted with EtOAc, washed (water and brine), dried (Na_2SO_4) and concentrated. Column chromatography [silica, hexanes/CH_2Cl_2 (1:2) → EtOAc] yielded **BC1** (54.5 mg, 50%) as a green solid, and **BC3** (second fraction, green). **BC3** was further purified by flash column chromatography [silica, CH_2Cl_2 → CH_2Cl_2/EtOAc (20:1)] to remove residual pinacol ester **18**, **BC3** was obtained as a green solid (26.6 mg, 37%). ^{1}H NMR ($CDCl_3$, 400 MHz): δ -1.82 (s, 1H), -1.57 (s, 1H), 1.95 (s, 6H), 1.98 (s, 6H), 3.64 (s, 3H), 4.05 (s, 3H), 4.06 (s, 3H), 4.37 (s, 2H), 4.39 (s, 2H), 8.20 (d, *J* = 8.5 Hz, 2H), 8.27 (d, *J* = 8.5 Hz, 2H), 8.32 (d, *J* = 8.5 Hz, 2H), 8.42 (d, *J* = 8.5 Hz, 2H), 8.64 (s, 1H), 8.65 (d, *J* = 2.8 Hz, 1H), 8.67 (s, 1H), 8.77 (s, 1H), 8.82 (d, *J* = 2.1Hz, 1H); ^{13}C NMR ($CDCl_3$, 125 MHz): δ 31.16, 31.23, 45.7, 45.8, 47.7, 52.1, 52.3, 52.5, 63.4, 96.8, 97.1, 97.3, 122.5, 122.6, 127.4, 128.6, 129.08, 129.14, 130.4, 131.0, 131.4, 132.9, 134.2, 135.1, 135.2, 135.6, 136.3, 141.20, 143.23, 154.5, 160.9, 167.4, 167.7, 169.5, 170.1. HRMS (ESI-FT-ICR) *m/*z $[M]^+$ Calcd for $C_{41}H_{40}N_4O_5$ 668.2993; Found 668.2997.

Section 6.5.3: Synthesis of BODIPY-bacteriochlorin Arrays

ET13

Following the general procedure for palladium catalyzed cross-couplings (section 2.5.1), a mixture of **BC1** (10.0 mg, 0.0163 mmol), **B6** (8.8 mg, 0.0196 mmol), sodium carbonate (17.3 mg, 0.163 mmol) and $PdCl_2(dppf)\cdot CH_2Cl_2$ (2.7 mg, 3.26 μmol) in toluene/ethanol/water (4:1:2, 7 mL) was stirred under N_2 at 80°C for 20 hours. The reaction mixture was diluted with EtOAc, washed (water and brine), dried (Na_2SO_4) and concentrated. Column chromatography [silica, hexanes/CH_2Cl_2 (1:3)], yielded a nearly pure solid. Trituration and filtration of with hexanes (performed until filtrate was no longer green fluorescent) yielded a red-brown solid (6.8 mg, 49%). ^{1}H NMR ($CDCl_3$, 500 MHz): -1.83 (s, 1H), -1.57 (s, 1H), 1.74 (s, 6H), 1.96 (s, 6H), 1.99 (s, 6H), 2.63 (s, 6H), 3.73 (s, 3H), 4.07 (s, 3H), 4.40 (s, 4H), 6.09 (s, 2H), 7.55 (d, J = 7.8 Hz, 2H), 8.25-8.30 (m, 4H), 8.42 (d, J = 8.0 Hz, 2H), 8.65-8.70 (m, 3H), 8.79 (s, 1H), 8.83 (s, 1H); ^{13}C NMR ($CDCl_3$, 125 MHz); 14.8, 15.0, 31.2, 31.3, 45.7, 45.8, 47.8, 52.0, 52.5, 63.7, 96.8, 97.0, 97.3, 121.4, 122.5, 123.0, 127.2, 127.6, 129.1, 130.4, 131.0, 131.8, 132.0, 133.0, 133.6, 134.1, 135.0, 135.2, 135.5, 136.2, 139.2, 141.2, 142.3, 143.3, 154.4, 155.6, 160.8, 167.4, 169.6, 170.1; HRMS (ESI-FT-ICR) *m/z* $[M]^+$ Calcd for $C_{52}H_{51}BF_2N_6O_3$ 856.4087; Found 856.4074.

ET14

Following the general procedure for palladium catalyzed cross-couplings (section 2.5.1), a mixture of **BC1** (10.0 mg, 0.0163 mmol), **B7** (12.3 mg, 0.0196 mmol), sodium carbonate (17.3 mg, 0.163 mmol) and $PdCl_2(dppf)\cdot CH_2Cl_2$ (2.7 mg, 3.26 μmol) in toluene/ethanol/water (4:1:2, 7 mL) was stirred under N_2 at 80°C for 17 hours. The

reaction mixture was diluted with EtOAc, washed (water and brine), dried (Na_2SO_4) and concentrated. Column chromatography [silica, hexanes/CH_2Cl_2 (1:3)] yielded a dark blue solid, which contained a minor fluorescent impurity. This impurity was removed by trituration and filtration of solid product with hexanes until filtrate was no longer orange-red fluorescent, resulting in an overall yield of 9.5 mg (56%). ^{1}H NMR ($CDCl_3$, 500 MHz): -1.86 (s, 1H), -1.59 (s, 1H), 1.73 (s, 3H), 1.78 (s, 3H), 1.96 (s, 6H), 2.00 (s, 6H), 2.65 (s, 3H), 3.74 (s, 3H), 3.87 (s, 3H), 3.96 (s, 6H), 4.06 (s, 3H), 4.40 (s, 2H), 4.41 (s, 2H), 6.06 (s, 1H), 6.16 (s, 2H), 6.77 (s, 1H), 7.58 (d, J = 7.9 Hz, 2H), 7.72 (d, J = 16.5 Hz, 1H), 8.21 (d, J = 16.6 Hz, 1H), 8.24-8.29 (m, 4H), 8.42 (d, J = 8.1 Hz, 2H), 8.66-8.70 (m, 2H), 8.79 (s, 1H), 8.83 (s, 1H);^{13}C NMR ($CDCl_3$, 125 MHz); 14.8, 14.9, 15.4, 31.2, 31.2, 45.7, 45.8, 47.8, 52.0, 52.5, 55.5, 56.0, 63.7, 90.8, 96.8, 96.9, 97.3, 108.3, 117.9, 120.2, 120.4, 122.4, 123.2, 127.3, 128.1, 128.9, 129.0, 130.3, 131.0, 131.4, 131.8, 133.4, 133.6, 134.15, 134.23, 134.9, 135.0, 135.3, 136.2, 138.9, 139.4, 140.6, 141.3, 142.9, 152.8, 154.5, 157.0, 160.68, 160.72, 162.0, 167.4, 169.6, 169.9; HRMS (ESI-FT-ICR) *m/z* $[M]^+$ Calcd for $C_{62}H_{61}BF_2N_6O_6$ 1,034.4718; Found 1,034.4706.

ET15

Following the general procedure for palladium catalyzed cross-couplings (section 2.5.1), a mixture of **BC1** (8.9 mg, 14.5 μmol), **B8** (14.0 mg, 17.4 μmol), potassium carbonate (20.0 mg, 145 μmol) and $Pd(PPh_3)_4$ (4.0 mg, 3.5 μmol) in toluene/DMF (2:1, 6 mL) was stirred under N_2 at 80°C for 14 hours. The reaction mixture was diluted with EtOAc, washed with water, brine, dried (Na_2SO_4) and concentrated. Flash column chromatography (silica, CH_2Cl_2) yielded a teal green solid,

9.9 mg (56%). ^{1}H NMR ($CDCl_3$, 500 MHz): -1.88 (s, 1H), -1.60 (s, 1H), 1.78 (s, 6H), 1.96 (s, 6H), 2.00 (s, 6H), 3.76 (s, 3H), 3.87 (s, 6H), 3.97 (s, 12H), 4.06 (s, 3H), 4.40 (s, 2H), 4.42 (s, 2H), 6.17 (s, 4H), 6.76 (s, 2H), 7.61 (d, J = 7.8 Hz, 2H), 7.67 (d, J = 16.6 Hz, 2H), 8.23-8.30 (m, 6H), 8.42 (d, J = 8.1 Hz, 2H), 8.67-8.71 (m, 3H), 8.80 (s, 1H), 8.83 (s, 1H); ^{13}C NMR ($CDCl_3$, 125 MHz); 15.3, 25.1, 29.8, 31.2, 45.8, 51.9, 55.5, 55.87, 55.91, 63.8, 90.9, 96.9, 97.3, 108.7, 117.2, 120.9, 122.3, 123.3, 127.1, 127.4, 128.5, 129.0, 130.3, 131.0, 131.7, 131.7, 133.4, 133.7, 134.3, 134.6, 134.8, 134.9, 135.19, 135.23, 136.3, 137.0, 138.7, 140.89, 140.91, 141.3, 154.7, 160.5, 160.6, 161.5, 167.4, 169.8; HRMS (ESI-FT-ICR) *m/*z $[M]^+$ Calcd for $C_{72}H_{71}BF_2N_6O_9$ 1,213.0365; Found 1,213.0357.

Section 6.6: Additional Spectra

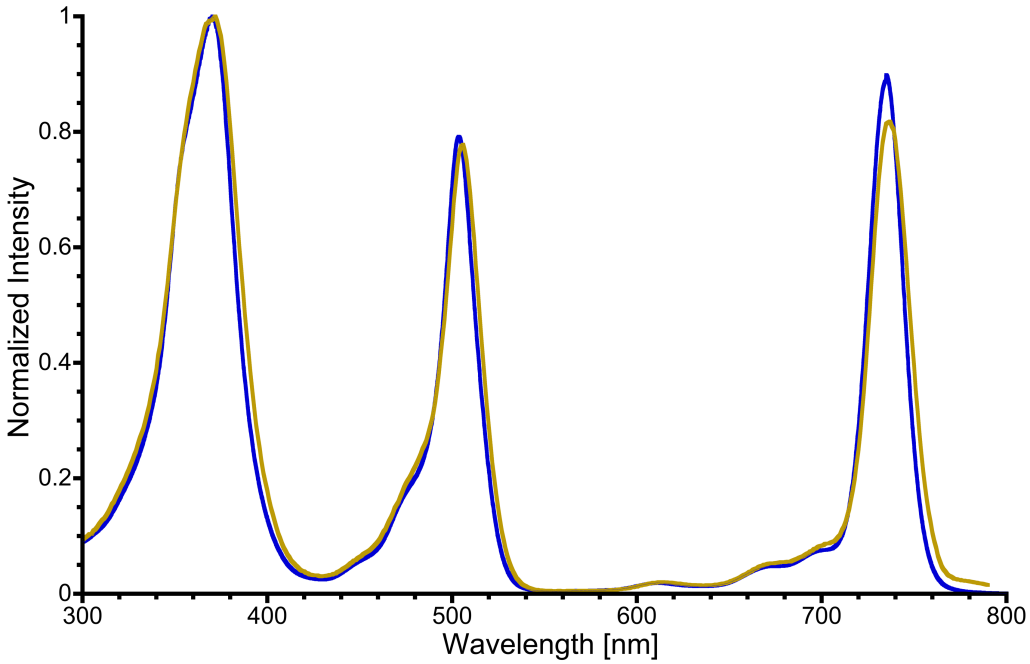

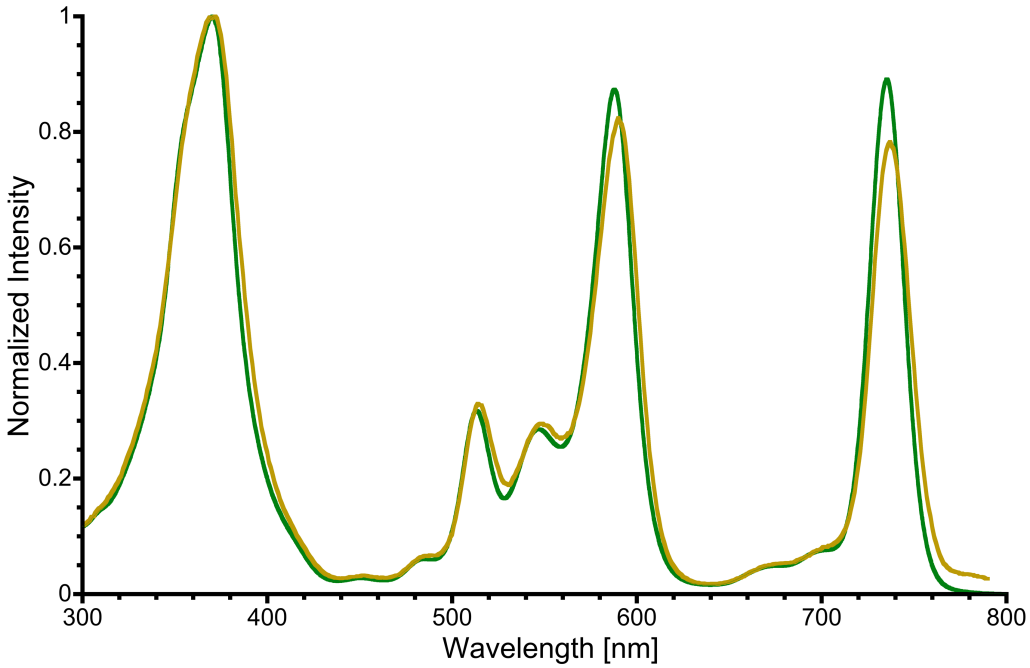

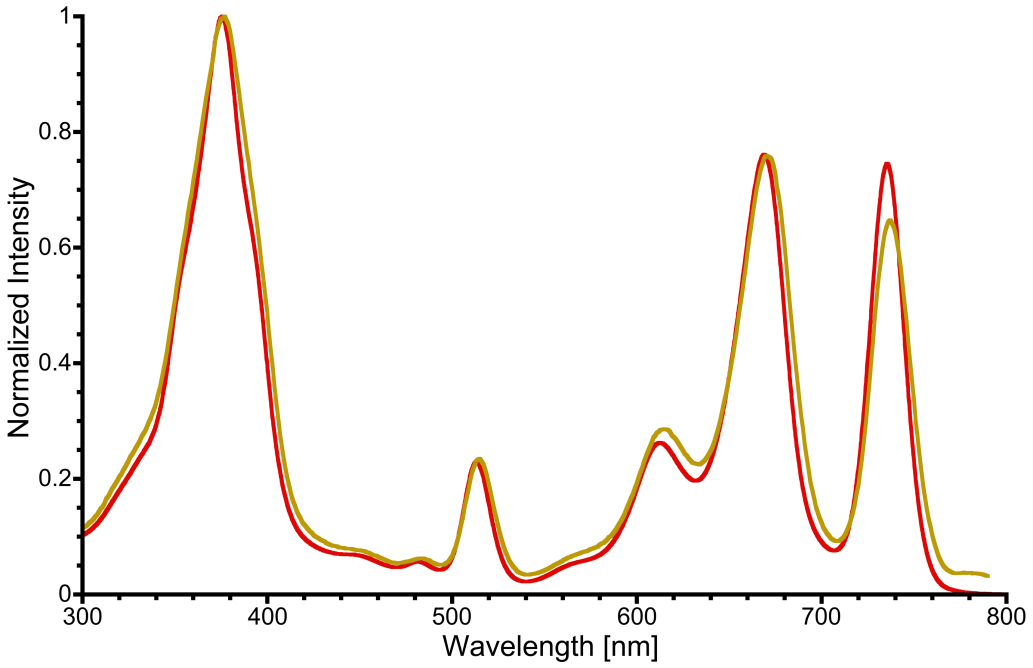

Above, the absorption spectra of dyads **ET13 (blue)**, **ET14** (**green**) and **ET15** (**red**) are presented with corresponding excitation spectra (**gold**) overlaid. Excitation and absorption all closely match, indicating highly efficient energy transfer. Minor deviations between the relative intensity or shape of bands are due to instrument response

Bibliography

(1) Turro, N. J.; Ramamurthy, V.; Scaiano, J. C. *Principles of Molecular Photochemistry: An Introduction*; University Science Books: Sausalito, Calif, 2009.

(2) Valeur, B.; Berberan-Santos, M. N. *Molecular Fluorescence: Principles and Applications*, Second edition.; Wiley-VCH ; Wiley-VCH Verlag GmbH & Co. KGaA: Weinheim, Germany : [Chichester, England], 2012.

(3) Adan, A.; Alizada, G.; Kiraz, Y.; Baran, Y.; Nalbant, A. Flow Cytometry: Basic Principles and Applications. *Crit. Rev. Biotechnol.* **2017**, *37* (2), 163–176. https://doi.org/10.3109/07388551.2015.1128876.

(4) Han, Y.; Gu, Y.; Zhang, A. C.; Lo, Y.-H. Review: Imaging Technologies for Flow Cytometry. *Lab. Chip* **2016**, *16* (24), 4639–4647. https://doi.org/10.1039/C6LC01063F.

(5) Bendall, S. C.; Nolan, G. P.; Roederer, M.; Chattopadhyay, P. K. A Deep Profiler's Guide to Cytometry. *Trends Immunol.* **2012**, *33* (7), 323–332. https://doi.org/10.1016/j.it.2012.02.010.

(6) Rogers, M. V. Light on High-Throughput Screening: Fluorescence-Based Assay Technologies. *Drug Discov. Today* **1997**, *2* (4), 156–160. https://doi.org/10.1016/S1359-6446(97)01016-7.

(7) Hall, M. D.; Yasgar, A.; Peryea, T.; Braisted, J. C.; Jadhav, A.; Simeonov, A.; Coussens, N. P. Fluorescence Polarization Assays in High-Throughput Screening and Drug Discovery: A Review. *Methods Appl. Fluoresc.* **2016**, *4* (2), 022001. https://doi.org/10.1088/2050-6120/4/2/022001.

(8) Lakowicz, J. R. *Principles of Fluorescence Spectroscopy*, Third edition, corrected at 4. printing.; Springer: New York, NY, 2010.

(9) Umezawa, K.; Citterio, D.; Suzuki, K. New Trends in Near-Infrared Fluorophores for Bioimaging. *Anal. Sci.* **2014**, *30* (3), 327–349. https://doi.org/10.2116/analsci.30.327.

(10) Lovell, J. F.; Liu, T. W. B.; Chen, J.; Zheng, G. Activatable Photosensitizers for Imaging and Therapy. *Chem. Rev.* **2010**, *110* (5), 2839–2857. https://doi.org/10.1021/cr900236h.

(11) Celli, J. P.; Spring, B. Q.; Rizvi, I.; Evans, C. L.; Samkoe, K. S.; Verma, S.; Pogue, B. W.; Hasan, T. Imaging and Photodynamic Therapy: Mechanisms, Monitoring, and Optimization. *Chem. Rev.* **2010**, *110* (5), 2795–2838. https://doi.org/10.1021/cr900300p.

(12) Abrahamse, H.; Hamblin, M. R. New Photosensitizers for Photodynamic Therapy. *Biochem. J.* **2016**, *473* (4), 347–364. https://doi.org/10.1042/BJ20150942.

(13) Baskaran, R.; Lee, J.; Yang, S.-G. Clinical Development of Photodynamic Agents and Therapeutic Applications. *Biomater. Res.* **2018**, *22* (1), 25. https://doi.org/10.1186/s40824-018-0140-z.

(14) Moghissi, K.; Dixon, K.; Stringer, M.; Freeman, T.; Thorpe, A.; Brown, S. The Place of Bronchoscopic Photodynamic Therapy in Advanced Unresectable Lung Cancer: Experience of 100 Cases1. *Eur. J. Cardiothorac. Surg.* **1999**, *15* (1), 1–6. https://doi.org/10.1016/S1010-7940(98)00295-4.

(15) Moghissi, K.; Dixon, K. Photodynamic Therapy (PDT) in Esophageal Cancer: A Surgical View of Its Indications Based on 14 Years Experience. *Technol. Cancer Res. Treat.* **2003**, *2* (4), 319–326. https://doi.org/10.1177/153303460300200406.
(16) Gray, J.; Fullarton, G. The Current Role of Photodynamic Therapy in Oesophageal Dysplasia and Cancer. *Photodiagnosis Photodyn. Ther.* **2007**, *4* (3), 151–159. https://doi.org/10.1016/j.pdpdt.2007.04.003.
(17) Grosjean, P.; Wagnieres, G.; Fontolliet, C. Clinical Photodynamic Therapy for Superficial Cancer in the Oesophagus and the Bronchi: 514 Nm Compared with 630 Nm Light Irradiation after Sensitization with Photofrin 1. **1998**, 7.
(18) Wen, X.; Li, Y.; Hamblin, M. R. Photodynamic Therapy in Dermatology beyond Non-Melanoma Cancer: An Update. *Photodiagnosis Photodyn. Ther.* **2017**, *19*, 140–152. https://doi.org/10.1016/j.pdpdt.2017.06.010.
(19) Bissonnette, R.; Tremblay, J.-F.; Lui, H.; Juzenas, P.; Boushira, M. Systemic Photodynamic Therapy with Aminolevulinic Acid Induces Apoptosis in Lesional T Lymphocytes of Psoriatic Plaques. *J. Invest. Dermatol.* **2002**, *119* (1), 77–83. https://doi.org/10.1046/j.1523-1747.2002.01827.x.
(20) Kim, M.; Jung, H.; Park, H. Topical PDT in the Treatment of Benign Skin Diseases: Principles and New Applications. *Int. J. Mol. Sci.* **2015**, *16* (10), 23259–23278. https://doi.org/10.3390/ijms161023259.
(21) Lin, J.; Wan, M. T. Current Evidence and Applications of Photodynamic Therapy in Dermatology. *Clin. Cosmet. Investig. Dermatol.* **2014**, 145. https://doi.org/10.2147/CCID.S35334.
(22) Schmidt-Erfurth, U.; Schlo¨tzer-Schrehard, U.; Cursiefen, C.; Michels, S.; Beckendorf, A.; Naumann, G. O. H. Influence of Photodynamic Therapy on Expression of Vascular Endothelial Growth Factor (VEGF), VEGF Receptor 3, and Pigment Epithelium–Derived Factor. *Investig. Opthalmology Vis. Sci.* **2003**, *44* (10), 4473. https://doi.org/10.1167/iovs.02-1115.
(23) Michels, S.; Schmidt-Erfurth, U. Sequence of Early Vascular Events after Photodynamic Therapy. *Investig. Opthalmology Vis. Sci.* **2003**, *44* (5), 2147. https://doi.org/10.1167/iovs.02-0604.
(24) Newman, D. K. Photodynamic Therapy: Current Role in the Treatment of Chorioretinal Conditions. *Eye* **2016**, *30* (2), 202–210. https://doi.org/10.1038/eye.2015.251.
(25) Drees, M.; Davis, R. M.; Heflin, J. R. Improved Morphology of Polymer-Fullerene Photovoltaic Devices with Thermally Induced Concentration Gradients. *J. Appl. Phys.* **2005**, *97* (3), 036103. https://doi.org/10.1063/1.1845574.
(26) Grätzel, M. Molecular Photovoltaics That Mimic Photosynthesis. *Pure Appl. Chem.* **2001**, *73* (3), 459–467. https://doi.org/10.1351/pac200173030459.
(27) Nikolis, V. C.; Mischok, A.; Siegmund, B.; Kublitski, J.; Jia, X.; Benduhn, J.; Hörmann, U.; Neher, D.; Gather, M. C.; Spoltore, D.; et al. Strong Light-Matter Coupling for Reduced Photon Energy Losses in Organic Photovoltaics. *Nat. Commun.* **2019**, *10* (1), 3706. https://doi.org/10.1038/s41467-019-11717-5.
(28) Wu, J.; Luke, J.; Lee, H. K. H.; Shakya Tuladhar, P.; Cha, H.; Jang, S.-Y.; Tsoi, W. C.; Heeney, M.; Kang, H.; Lee, K.; et al. Tail State Limited Photocurrent

Collection of Thick Photoactive Layers in Organic Solar Cells. *Nat. Commun.* **2019**, *10* (1), 5159. https://doi.org/10.1038/s41467-019-12951-7.
(29) Reineke, S.; Lindner, F.; Schwartz, G.; Seidler, N.; Walzer, K.; Lüssem, B.; Leo, K. White Organic Light-Emitting Diodes with Fluorescent Tube Efficiency. *Nature* **2009**, *459* (7244), 234–238. https://doi.org/10.1038/nature08003.
(30) Fröbel, M.; Fries, F.; Schwab, T.; Lenk, S.; Leo, K.; Gather, M. C.; Reineke, S. Three-Terminal RGB Full-Color OLED Pixels for Ultrahigh Density Displays. *Sci. Rep.* **2018**, *8* (1), 9684. https://doi.org/10.1038/s41598-018-27976-z.
(31) Sasabe, H.; Kido, J. Multifunctional Materials in High-Performance OLEDs: Challenges for Solid-State Lighting †. *Chem. Mater.* **2011**, *23* (3), 621–630. https://doi.org/10.1021/cm1024052.
(32) Kim, G. W.; Lampande, R.; Choe, D. C.; Ko, I. J.; Park, J. H.; Pode, R.; Kwon, J. H. Next Generation Smart Window Display Using Transparent Organic Display and Light Blocking Screen. *Opt. Express* **2018**, *26* (7), 8493. https://doi.org/10.1364/OE.26.008493.
(33) Hu, G.; Liu, R.; Alexy, E. J.; Mandal, A. K.; Bocian, D. F.; Holten, D.; Lindsey, J. S. Panchromatic Chromophore-Tetrapyrrole Light-Harvesting Arrays Constructed from Bodipy, Perylene, Terrylene, Porphyrin, Chlorin, and Bacteriochlorin Building Blocks. *New J. Chem.* **2016**, *40* (9), 8032–8052. https://doi.org/10.1039/c6nj01782g.
(34) Mandal, A. K.; Diers, J. R.; Niedzwiedzki, D. M.; Hu, G.; Liu, R.; Alexy, E. J.; Lindsey, J. S.; Bocian, D. F.; Holten, D. Tailoring Panchromatic Absorption and Excited-State Dynamics of Tetrapyrrole-Chromophore (Bodipy, Rylene) Arrays - Interplay of Orbital Mixing and Configuration Interaction. *J. Am. Chem. Soc.* **2017**, *139* (48), 17547–17564. https://doi.org/10.1021/jacs.7b09548.
(35) Yu, Z.; Pancholi, C.; Bhagavathy, G. V.; Kang, H. S.; Nguyen, J. K.; Ptaszek, M. Strongly Conjugated Hydroporphyrin Dyads: Extensive Modification of Hydroporphyrins Properties by Expanding the Conjugated System. *J. Org. Chem.* **2014**, *79* (17), 7910–7925. https://doi.org/10.1021/jo501041b.
(36) Kang, H. S.; Esemoto, N. N.; Diers, J. R.; Niedzwiedzki, D. M.; Greco, J. A.; Akhigbe, J.; Yu, Z.; Pancholi, C.; Viswanathan Bhagavathy, G.; Nguyen, J. K.; et al. Effects of Strong Electronic Coupling in Chlorin and Bacteriochlorin Dyads. *J. Phys. Chem. A* **2016**, *120* (3), 379–395. https://doi.org/10.1021/acs.jpca.5b10686.
(37) Sasaki, S. I.; Mizutani, K.; Kunieda, M.; Tamiaki, H. Synthesis and Optical Properties of C3-Ethynylated Chlorin and π-Extended Chlorophyll Dyads. *Tetrahedron* **2011**, *67* (33), 6065–6072. https://doi.org/10.1016/j.tet.2011.06.020.
(38) Kelley, R. F.; Suk, J. L.; Wilson, T. M.; Nakamura, Y.; Tiede, D. M.; Osuka, A.; Hupp, J. T.; Wasielewski, M. R. Intramolecular Energy Transfer within Butadiyne-Linked Chlorophyll and Porphyrin Dimer-Faced, Self-Assembled Prisms. *J. Am. Chem. Soc.* **2008**, *130* (13), 4277–4284. https://doi.org/10.1021/ja075494f.
(39) Wang, X. F.; Kitao, O.; Zhou, H.; Tamiaki, H.; Sasaki, S. I. Extension of π-Conjugation Length along the Qy Axis of a Chlorophyll a Derivative for

Efficient Dye-Sensitized Solar Cells. *Chem. Commun.* **2009**, No. 12, 1523–1525. https://doi.org/10.1039/b820540j.
(40) Cho, H. S.; Jeong, D. H.; Cho, S.; Kim, D.; Matsuzaki, Y.; Tanaka, K.; Tsuda, A.; Osuka, A. Photophysical Properties of Porphyrin Tapes. *J. Am. Chem. Soc.* **2002**, *124* (49), 14642–14654. https://doi.org/10.1021/ja020826w.
(41) Tanaka, T.; Osuka, A. Conjugated Porphyrin Arrays: Synthesis, Properties and Applications for Functional Materials. *Chem. Soc. Rev.* **2015**, *44* (4), 943–969. https://doi.org/10.1039/c3cs60443h.
(42) Morel, Y.; Stephan, O.; Andraud, C.; Baldeck, P. L. Enhanced Two-Photon Absorption with Dimers of p-Conjugated Molecules. *Synth. Met.* **2001**, 3.
(43) Hayek, A.; Bolze, F.; Bourgogne, C.; Baldeck, P. L.; Didier, P.; Arntz, Y.; Mély, Y.; Nicoud, J. F. Boron Containing Two-Photon Absorbing Chromophores. 2. Fine Tuning of the One- and Two-Photon Photophysical Properties of Pyrazabole Based Fluorescent Bioprobes. *Inorg. Chem.* **2009**, *48* (19), 9112–9119. https://doi.org/10.1021/ic900627g.
(44) Amanpour, J.; Hu, G.; Alexy, E. J.; Mandal, A. K.; Kang, H. S.; Yuen, J. M.; Diers, J. R.; Bocian, D. F.; Lindsey, J. S.; Holten, D. Tuning the Electronic Structure and Properties of Perylene–Porphyrin–Perylene Panchromatic Absorbers. *J. Phys. Chem. A* **2016**, *120* (38), 7434–7450. https://doi.org/10.1021/acs.jpca.6b06857.
(45) High, J. S.; Virgil, K. A.; Jakubikova, E. Electronic Structure and Absorption Properties of Strongly Coupled Porphyrin–Perylene Arrays. *J. Phys. Chem. A* **2015**, *119* (38), 9879–9888. https://doi.org/10.1021/acs.jpca.5b05600.
(46) Auerhammer, N.; Schulz, A.; Schmiedel, A.; Holzapfel, M.; Hoche, J.; Röhr, M. I. S.; Mitric, R.; Lambert, C. Dynamic Exciton Localisation in a Pyrene–BODIPY–Pyrene Dye Conjugate. *Phys. Chem. Chem. Phys.* **2019**, *21* (18), 9013–9025. https://doi.org/10.1039/C9CP00908F.
(47) Kuimova, M. K.; Collins, H. A.; Balaz, M.; Dahlstedt, E.; Levitt, J. A.; Sergent, N.; Suhling, K.; Drobizhev, M.; Makarov, N. S.; Rebane, A.; et al. Photophysical Properties and Intracellular Imaging of Water-Soluble Porphyrin Dimers for Two-Photon Excited Photodynamic Therapy. *Org. Biomol. Chem.* **2009**, *7* (5), 889–896. https://doi.org/10.1039/b814791d.
(48) Beverina, L.; Sassi, M. Twists and Turns Around a Square: The Many Faces of Squaraine Chemistry. *Synlett* **2014**, *25* (04), 477–490. https://doi.org/10.1055/s-0033-1340482.
(49) Khadria, A.; Gawel, P.; Roche, C.; Anderson, H. L.; de Coene, Y.; Clays, K. Push-Pull Pyropheophorbides for Nonlinear Optical Imaging. *Org. Biomol. Chem.* **2017**, *15* (4), 947–956. https://doi.org/10.1039/c6ob02319c.
(50) Urbani, M.; Grätzel, M.; Nazeeruddin, M. K.; Torres, T. Meso-Substituted Porphyrins for Dye-Sensitized Solar Cells. *Chem. Rev.* **2014**, *114* (24), 12330–12396. https://doi.org/10.1021/cr5001964.
(51) Ahrens, J.; Haberlag, B.; Scheja, A.; Tamm, M.; Bröring, M. Conjugated BODIPY DYEmers by Metathesis Reactions. *Chem. - Eur. J.* **2014**, *20* (10), 2901–2912. https://doi.org/10.1002/chem.201303468.

(52) Lambert, C.; Scherpf, T.; Ceymann, H.; Schmiedel, A.; Holzapfel, M. Coupled Oscillators for Tuning Fluorescence Properties of Squaraine Dyes. *J. Am. Chem. Soc.* **2015**, *137* (10), 3547–3557. https://doi.org/10.1021/ja512338w.
(53) Kuster, S.; Sauvage, F.; Nazeeruddin, Md. K.; Grätzel, M.; Nüesch, F. A.; Geiger, T. Unsymmetrical Squaraine Dimer with an Extended π-Electron Framework: An Approach in Harvesting near Infra-Red Photons for Energy Conversion. *Dyes Pigments* **2010**, *87* (1), 30–38. https://doi.org/10.1016/j.dyepig.2010.01.019.
(54) Screen, T. E. O.; Blake, I. M.; Rees, L. H.; Clegg, W.; Anderson, H. L. Making Conjugated Connections to Porphyrins: A Comparison of Alkyne, Alkene, Imine and Azo Links. *J. Chem. Soc. Perkin 1* **2002**, *2* (3), 320–329. https://doi.org/10.1039/b109915a.
(55) Wasielewski, M. R.; Studier, M. H.; Katz, J. J. Covalently Linked Chlorophyll a Dimer: A Biomimetic Model of Special Pair Chlorophyll. *Proc. Natl. Acad. Sci.* **1976**, *73* (12), 4282–4286. https://doi.org/10.1073/pnas.73.12.4282.
(56) Jaquinod, L.; Nurco, D. J.; Medforth, C. J.; Pandey, R. K.; Forsyth, T. P.; Olmstead, M. M.; Smith, K. M. Synthesis and Characterization of Bis(Chlorin)s from the McMurry Reaction of Formylchlorins. *Angew. Chem. - Int. Ed.* **1996**, *35* (9), 1013–1016. https://doi.org/10.1002/anie.199610131.
(57) Jaquinod, L.; Forsyth, T. P.; Smith, K. M. Planar Bischlorophyll Derivatives with a Completely Conjugated N-System :Model Com- Pounds for the Special Pair in Photosynthesis*. 3.
(58) Drobizhev, M.; Stepanenko, Y.; Dzenis, Y.; Karotki, A.; Rebane, A.; Taylor, P. N.; Anderson, H. L. Understanding Strong Two-Photon Absorption in π-Conjugated Porphyrin Dimers via Double-Resonance Enhancement in a Three-Level Model. *J. Am. Chem. Soc.* **2004**, *126* (47), 15352–15353. https://doi.org/10.1021/ja0445847.
(59) Fortage, J.; Göransson, E.; Blart, E.; Becker, H. C.; Hammarström, L.; Odobel, F. Strongly Coupled Zinc Phthalocyanine-Tin Porphyrin Dyad Performing Ultra-Fast Single Step Charge Separation over a 34 \AA Distance. *Chem. Commun.* **2007**, No. 44, 4629–4631. https://doi.org/10.1039/b711642j.
(60) Fortage, J.; Boixel, J.; Blart, E.; Hammarström, L.; Becker, H. C.; Odobel, F. Single-Step Electron Transfer on the Nanometer Scale: Ultra-Fast Charge Shift in Strongly Coupled Zinc Porphyrin-Gold Porphyrin Dyads. *Chem. - Eur. J.* **2008**, *14* (11), 3467–3480. https://doi.org/10.1002/chem.200701335.
(61) Fortage, J.; Scarpaci, A.; Viau, L.; Pellegrin, Y.; Blart, E.; Falkenström, M.; Hammarström, L.; Asselberghs, I.; Kellens, R.; Libaers, W.; et al. Charge-Transfer State and Large First Hyperpolarizability Constant in a Highly Electronically Coupled Zinc and Gold Porphyrin Dyad. *Chem. - Eur. J.* **2009**, *15* (36), 9058–9067. https://doi.org/10.1002/chem.200900262.
(62) Sutton, J. M.; Boyle, R. W. First Synthesis of Porphyrin–Phthalocyanine Heterodimers with a Direct Ethynyl Linkage. *Chem. Commun.* **2001**, No. 19, 2014–2015. https://doi.org/10.1039/b105840c.
(63) Ventura, B.; Barigelletti, F.; Lodato, F.; Officer, D. L.; Flamigni, L. Energy Transfer Processes in Electronically Coupled Porphyrin Hetero-Dyads

Connected at the β Position. *Phys. Chem. Chem. Phys.* **2009**, *11* (13), 2166. https://doi.org/10.1039/b819138g.
(64) Le Roy, J. J.; Cremers, J.; Thomlinson, I. A.; Slota, M.; Myers, W. K.; Horton, P. H.; Coles, S. J.; Anderson, H. L.; Bogani, L. Tailored Homo- and Hetero-Lanthanide Porphyrin Dimers: A Synthetic Strategy for Integrating Multiple Spintronic Functionalities into a Single Molecule. *Chem. Sci.* **2018**, *9* (45), 8474–8481. https://doi.org/10.1039/C8SC03762K.
(65) Hu, G.; Kang, H. S.; Mandal, A. K.; Roy, A.; Kirmaier, C.; Bocian, D. F.; Holten, D.; Lindsey, J. S. Synthesis of Arrays Containing Porphyrin, Chlorin, and Perylene-Imide Constituents for Panchromatic Light-Harvesting and Charge Separation. *RSC Adv.* **2018**, *8* (42), 23854–23874. https://doi.org/10.1039/C8RA04052D.
(66) Grin, M. A.; Lonin, I. S.; Fedyunin, S. V.; Tsiprovskiy, A. G.; Strizhakov, A. A.; Tsygankov, A. A.; Krasnovsky, A. A.; Mironov, A. F. Synthesis and Properties of the Zn-Chlorin–Bacteriochlorin Dimer. *Mendeleev Commun.* **2007**, *17* (4), 209–211. https://doi.org/10.1016/j.mencom.2007.06.007.
(67) Vicente, M. G. H.; Smith, K. M. Vilsmeier Reactions of Porphyrins and Chlorins with 3-(Dimethy1amino)AcroleinTo Give Meso-(2-Formylvinyl)Porphyrins: New Syntheses of Benzochlorins, Benzoisobacteriochlorins, and Benzobacteriochlorins and Reductive Coupling of Porphyrins and Chlorins Using Low-Valent Titanium Complexes. 12.
(68) Mirkovic, T.; Ostroumov, E. E.; Anna, J. M.; Van Grondelle, R.; Govindjee; Scholes, G. D. Light Absorption and Energy Transfer in the Antenna Complexes of Photosynthetic Organisms. *Chem. Rev.* **2017**, *117* (2), 249–293. https://doi.org/10.1021/acs.chemrev.6b00002.
(69) Durrant, J. R.; Klug, D. R.; Kwa, S. L.; van Grondelle, R.; Porter, G.; Dekker, J. P. A Multimer Model for P680, the Primary Electron Donor of Photosystem II. *Proc. Natl. Acad. Sci. U. S. A.* **1995**, *92* (11), 4798–4802. https://doi.org/10.1073/pnas.92.11.4798.
(70) Konar, A.; Sechrist, R.; Song, Y.; Policht, V. R.; Laible, P. D.; Bocian, D. F.; Holten, D.; Kirmaier, C.; Ogilvie, J. P. Electronic Interactions in the Bacterial Reaction Center Revealed by Two-Color 2D Electronic Spectroscopy. *J. Phys. Chem. Lett.* **2018**, *9* (18), 5219–5225. https://doi.org/10.1021/acs.jpclett.8b02394.
(71) Knapp, E. W.; Fischer, S. F.; Zinth, W.; Sander, M.; Kaiser, W.; Deisenhofer, J.; Michel, H. Analysis of Optical Spectra from Single Crystals of Rhodopseudomonas Viridis Reaction Centers. *Proc. Natl. Acad. Sci. U. S. A.* **1985**, *82* (24), 8463–8467. https://doi.org/10.1073/pnas.82.24.8463.
(72) Arnett, D. C.; Moser, C. C.; Dutton, P. L.; Scherer, N. F. The First Events in Photosynthesis: Electronic Coupling and Energy Transfer Dynamics in the Photosynthetic Reaction Center from Rhodobacter Sphaeroides. *J. Phys. Chem. B* **1999**, *103* (11), 2014–2032. https://doi.org/10.1021/jp984464j.
(73) Jordanides, X. J.; Scholes, G. D.; Fleming, G. R. The Mechanism of Energy Transfer in the Bacterial Photosynthetic Reaction Center. *J. Phys. Chem. B* **2001**, *105* (8), 1652–1669. https://doi.org/10.1021/jp003572e.

(74) Hannestad, J. K.; Sandin, P.; Albinsson, B. Self-Assembled DNA Photonic Wire for Long-Range Energy Transfer. *J. Am. Chem. Soc.* **2008**, *130* (47), 15889–15895. https://doi.org/10.1021/ja803407t.
(75) Teo, Y. N.; Kool, E. T. Polyfluorophore Excimers and Exciplexes as FRET Donors in DNA. 10.
(76) Nishimura, T.; Ogura, Y.; Tanida, J. Fluorescence Resonance Energy Transfer-Based Molecular Logic Circuit Using a DNA Scaffold. *Appl. Phys. Lett.* **2012**, *101* (23), 233703. https://doi.org/10.1063/1.4769812.
(77) Lewis, F. D. DNA Photonics. *Pure Appl. Chem.* **2006**, *78* (12), 2287–2295. https://doi.org/10.1351/pac200678122287.
(78) Chen, J.; Liu, T. W. B.; Lo, P.-C.; Wilson, B. C.; Zheng, G. "Zipper" Molecular Beacons: A Generalized Strategy to Optimize the Performance of Activatable Protease Probes. *Bioconjug. Chem.* **2009**, *20* (10), 1836–1842. https://doi.org/10.1021/bc900207k.
(79) Marras, S. A. E.; Kramer, F. R.; Tyagi, S. Efficiencies of Fluorescence Resonance Energy Transfer and Contact-Mediated Quenching in Oligonucleotide Probes. *Nucleic Acids Res.* **2002**, *30* (21), 8.
(80) dos Remedios, C. G.; Moens, P. D. J. Fluorescence Resonance Energy Transfer Spectroscopy Is a Reliable "Ruler" for Measuring Structural Changes in Proteins. *J. Struct. Biol.* **1995**, *115* (2), 175–185. https://doi.org/10.1006/jsbi.1995.1042.
(81) Daly, B.; Ling, J.; de Silva, A. P. Current Developments in Fluorescent PET (Photoinduced Electron Transfer) Sensors and Switches. *Chem. Soc. Rev.* **2015**, *44* (13), 4203–4211. https://doi.org/10.1039/C4CS00334A.
(82) Algar, W. R.; Hildebrandt, N.; Vogel, S. S.; Medintz, I. L. FRET as a Biomolecular Research Tool — Understanding Its Potential While Avoiding Pitfalls. *Nat. Methods* **2019**, *16* (9), 815–829. https://doi.org/10.1038/s41592-019-0530-8.
(83) Mula, S.; Ulrich, G.; Ziessel, R. Dual Bodipy Fluorophores Linked by Polyethyleneglycol Spacers. *Tetrahedron Lett.* **2009**, *50* (46), 6383–6388. https://doi.org/10.1016/j.tetlet.2009.08.091.
(84) Mula, S.; Elliott, K.; Harriman, A.; Ziessel, R. Energy Transfer by Way of an Exciplex Intermediate in Flexible Boron Dipyrromethene-Based Allosteric Architectures. *J. Phys. Chem. A* **2010**, *114* (39), 10515–10522. https://doi.org/10.1021/jp106626v.
(85) Brizet, B.; Desbois, N.; Bonnot, A.; Langlois, A.; Dubois, A.; Barbe, J.-M.; Gros, C. P.; Goze, C.; Denat, F.; Harvey, P. D. Slow and Fast Singlet Energy Transfers in BODIPY-Gallium(III)Corrole Dyads Linked by Flexible Chains. *Inorg. Chem.* **2014**, *53* (7), 3392–3403. https://doi.org/10.1021/ic402798f.
(86) Basumatary, B.; Ramana Reddy, R. V.; Bhandary, S.; Sankar, J. Gallium(III)Corrole-BODIPY Hybrid: Novel Photophysical Properties and First Observation of B-F···F Interactions. *Dalton Trans.* **2015**, *44* (48), 20817–20821. https://doi.org/10.1039/c5dt03104d.
(87) Khan, T. K.; Bröring, M.; Mathur, S.; Ravikanth, M. Boron Dipyrrin-Porphyrin Conjugates. *Coord. Chem. Rev.* **2013**, *257* (15–16), 2348–2387. https://doi.org/10.1016/j.ccr.2013.04.007.

(88) Ohya, Y.; Yabuki, K.; Hashimoto, M.; Nakajima, A.; Ouchi, T. Multistep Fluorescence Resonance Energy Transfer in Sequential Chromophore Array Constructed on Oligo-DNA Assemblies. *Bioconjug. Chem.* **2003**, *14* (6), 1057–1066. https://doi.org/10.1021/bc034028m.
(89) Zhang, Y.; Bi, J.; Xia, S.; Mazi, W.; Wan, S.; Mikesell, L.; Luck, R.; Liu, H. A Near-Infrared Fluorescent Probe Based on a FRET Rhodamine Donor Linked to a Cyanine Acceptor for Sensitive Detection of Intracellular PH Alternations. *Molecules* **2018**, *23* (10), 2679. https://doi.org/10.3390/molecules23102679.
(90) Yasarapudi, V. B.; Frazer, L.; Webb, J. E. A.; Gallaher, J. K.; Macmillan, A.; Falber, A.; Thordarson, P.; Schmidt, T. W. Competing Energy Transfer Pathways in a Five-Chromophore Perylene Array. *J. Phys. Chem. C* **2018**, *122* (25), 13937–13943. https://doi.org/10.1021/acs.jpcc.8b01084.
(91) Liu, T. W.; Akens, M. K.; Chen, J.; Wise-Milestone, L.; Wilson, B. C.; Zheng, G. Imaging of Specific Activation of Photodynamic Molecular Beacons in Breast Cancer Vertebral Metastases. *Bioconjug. Chem.* **2011**, *22* (6), 1021–1030. https://doi.org/10.1021/bc200169x.
(92) Zheng, G.; Chen, J.; Stefflova, K.; Jarvi, M.; Li, H.; Wilson, B. C. Photodynamic Molecular Beacon as an Activatable Photosensitizer Based on Protease-Controlled Singlet Oxygen Quenching and Activation. *Proc. Natl. Acad. Sci.* **2007**, *104* (21), 8989–8994. https://doi.org/10.1073/pnas.0611142104.
(93) Cló, E.; Snyder, J. W.; Voigt, N. V.; Ogilby, P. R.; Gothelf, K. V. DNA-Programmed Control of Photosensitized Singlet Oxygen Production. *J. Am. Chem. Soc.* **2006**, *128* (13), 4200–4201. https://doi.org/10.1021/ja058713a.
(94) Weissleder, R.; Tung, C.-H.; Mahmood, U.; Bogdanov, A. In Vivo Imaging of Tumors with Protease-Activated near-Infrared Fluorescent Probes. *Nat. Biotechnol.* **1999**, *17* (4), 375–378. https://doi.org/10.1038/7933.
(95) Popov, A. V.; Mawn, T. M.; Kim, S.; Zheng, G.; Delikatny, E. J. Design and Synthesis of Phospholipase C and A2-Activatable near-Infrared Fluorescent Smart Probes. *Bioconjug. Chem.* **2010**, *21* (10), 1724–1727. https://doi.org/10.1021/bc100271v.
(96) Ozlem, S.; Akkaya, E. U. Thinking Outside the Silicon Box: Molecular AND Logic As an Additional Layer of Selectivity in Singlet Oxygen Generation for Photodynamic Therapy. *J. Am. Chem. Soc.* **2009**, *131* (1), 48–49. https://doi.org/10.1021/ja808389t.
(97) Erbas-Cakmak, S.; Kolemen, S.; Sedgwick, A. C.; Gunnlaugsson, T.; James, T. D.; Yoon, J.; Akkaya, E. U. Molecular Logic Gates: The Past, Present and Future. *Chem. Soc. Rev.* **2018**, *47* (7), 2228–2248. https://doi.org/10.1039/C7CS00491E.
(98) Orte, A.; Debroye, E.; Ruedas-Rama, M. J.; Garcia-Fernandez, E.; Robinson, D.; Crovetto, L.; Talavera, E. M.; Alvarez-Pez, J. M.; Leen, V.; Verbelen, B.; et al. Effect of the Substitution Position (2, 3 or 8) on the Spectroscopic and Photophysical Properties of BODIPY Dyes with a Phenyl, Styryl or Phenylethynyl Group. *RSC Adv.* **2016**, *6* (105), 102899–102913. https://doi.org/10.1039/C6RA22340K.

(99) Mass, O.; Ptaszek, M.; Taniguchi, M.; Diers, J. R.; Kee, H. L.; Bocian, D. F.; Holten, D.; Lindsey, J. S. Synthesis and Photochemical Properties of 12-Substituted versus 13-Substituted Chlorins. *J. Org. Chem.* **2009**, *74* (15), 5276–5289. https://doi.org/10.1021/jo900706x.
(100) Springer, J. W.; Faries, K. M.; Diers, J. R.; Muthiah, C.; Mass, O.; Kee, H. L.; Kirmaier, C.; Lindsey, J. S.; Bocian, D. F.; Holten, D. Effects of Substituents on Synthetic Analogs of Chlorophylls. Part 3: The Distinctive Impact of Auxochromes at the 7- versus 3-Positions. *Photochem. Photobiol.* **2012**, *88* (3), 651–674. https://doi.org/10.1111/j.1751-1097.2012.01083.x.
(101) Ra, D.; Gauger, K. A.; Muthukumaran, K.; Balasubramanian, T.; Chandrashaker, V.; Taniguchi, M.; Yu, Z.; Talley, D. C.; Ehudin, M.; Ptaszek, M.; et al. Progress towards Synthetic Chlorins with Graded Polarity, Conjugatable Substituents, and Wavelength Tunability. *J. Porphyr. Phthalocyanines* **2015**, *19* (04), 547–572. https://doi.org/10.1142/S1088424615500042.
(102) Esdaile, L. J.; Jensen, P.; McMurtrie, J. C.; Arnold, D. P. Azoporphyrin: The Porphyrin Analogue of Azobenzene. *Angew. Chem. Int. Ed.* **2007**, *46* (12), 2090–2093. https://doi.org/10.1002/anie.200604658.
(103) Shin, E. J.; Kim, D. Substituent Effect on the Fluorescence Quenching of Various Tetraphenylporphyrins by Ruthenium Tris(2,2′-Bipyridine) Complex. *J. Photochem. Photobiol. Chem.* **2002**, *152* (1–3), 25–31. https://doi.org/10.1016/S1010-6030(02)00189-2.
(104) Guy, J.; Caron, K.; Dufresne, S.; Michnick, S. W.; Skene; Keillor, J. W. Convergent Preparation and Photophysical Characterization of Dimaleimide Dansyl Fluorogens: Elucidation of the Maleimide Fluorescence Quenching Mechanism. *J. Am. Chem. Soc.* **2007**, *129* (39), 11969–11977. https://doi.org/10.1021/ja0738125.
(105) Greene, L. E.; Lincoln, R.; Cosa, G. Tuning Photoinduced Electron Transfer Efficiency of Fluorogenic BODIPY- *α* -Tocopherol Analogues. *Photochem. Photobiol.* **2019**, *95* (1), 192–201. https://doi.org/10.1111/php.13062.
(106) Kee, H. L.; Kirmaier, C.; Yu, L.; Thamyongkit, P.; Youngblood, W. J.; Calder, M. E.; Ramos, L.; Noll, B. C.; Bocian, D. F.; Scheidt, W. R.; et al. Structural Control of the Photodynamics of Boron−Dipyrrin Complexes. *J. Phys. Chem. B* **2005**, *109* (43), 20433–20443. https://doi.org/10.1021/jp0525078.
(107) Strachan, J. P.; O'Shea, D. F.; Balasubramanian, T.; Lindsey, J. S. Rational Synthesis of Meso-Substituted Chlorin Building Blocks. *J. Org. Chem.* **2000**, *65* (10), 3160–3172. https://doi.org/10.1021/jo991942t.
(108) Laha, J. K.; Muthiah, C.; Taniguchi, M.; McDowell, B. E.; Ptaszek, M.; Lindsey, J. S. Synthetic Chlorins Bearing Auxochromes at the 3- and 13-Positions. *J. Org. Chem.* **2006**, *71* (11), 4092–4102. https://doi.org/10.1021/jo060208o.
(109) Yang, E.; Kirmaier, C.; Krayer, M.; Taniguchi, M.; Kim, H.-J.; Diers, J. R.; Bocian, D. F.; Lindsey, J. S.; Holten, D. Photophysical Properties and Electronic Structure of Stable, Tunable Synthetic Bacteriochlorins: Extending the Features

of Native Photosynthetic Pigments. *J. Phys. Chem. B* **2011**, *115* (37), 10801–10816. https://doi.org/10.1021/jp205258s.
(110) Kee, H. L.; Kirmaier, C.; Tang, Q.; Diers, J. R.; Muthiah, C.; Taniguchi, M.; Laha, J. K.; Ptaszek, M.; Lindsey, J. S.; Bocian, D. F.; et al. Effects of Substituents on Synthetic Analogs of Chlorophylls. Part 1: Synthesis, Vibrational Properties and Excited-State Decay Characteristics. *Photochem. Photobiol.* **2007**, *83* (5), 1110–1124. https://doi.org/10.1111/j.1751-1097.2007.00150.x.
(111) Kee, H. L.; Kirmaier, C.; Tang, Q.; Diers, J. R.; Muthiah, C.; Taniguchi, M.; Laha, J. K.; Ptaszek, M.; Lindsey, J. S.; Bocian, D. F.; et al. Effects of Substituents on Synthetic Analogs of Chlorophylls. Part 2: Redox Properties, Optical Spectra and Electronic Structure. *Photochem. Photobiol.* **2007**, *83* (5), 1125–1143. https://doi.org/10.1111/j.1751-1097.2007.00151.x.
(112) Tamiaki, H.; Kunieda, M. 51 Photochemistry of Chlorophylls and Their Synthetic Analogs. In *Handbook of Porphyrin Science (Volume 11)*; World Scientific Publishing Company, 2011; Vol. 15, pp 223–290. https://doi.org/10.1142/9789814322386_0003.
(113) Kim, H. J.; Lindsey, J. S. De Novo Synthesis of Stable Tetrahydroporphyrinic Macrocycles: Bacteriochlorins and a Tetradehydrocorrin. *J. Org. Chem.* **2005**, *70* (14), 5475–5486. https://doi.org/10.1021/jo050467y.
(114) Taniguchi, M.; Cramer, D. L.; Bhise, A. D.; Kee, H. L.; Bocian, D. F.; Holten, D.; Lindsey, J. S. Accessing the Near-Infrared Spectral Region with Stable, Synthetic, Wavelength-Tunable Bacteriochlorins. *New J. Chem.* **2008**, *32* (6), 947–958. https://doi.org/10.1039/b717803d.
(115) Ptaszek, M.; Bhaumik, J.; Kim, H.-J.; Taniguchi, M.; Lindsey, J. S. Refined Synthesis of 2,3,4,5-Tetrahydro-1,3,3-Trimethyldipyrrin, a Deceptively Simple Precursor to Hydroporphyrins. *Org. Process Res. Dev.* **2005**, *9* (5), 651–659. https://doi.org/10.1021/op050087e.
(116) Krayer, M.; Balasubramanian, T.; Ruzié, C.; Ptaszek, M.; Cramer, D. L.; Taniguchi, M.; Lindsey, J. S. Refined Syntheses of Hydrodipyrrin Precursors to Chlorin and Bacteriochlorin Building Blocks. *J. Porphyr. Phthalocyanines* **2009**, *13* (10), 1098–1110. https://doi.org/10.1142/s1088424609001406.
(117) Ptaszek, M.; McDowell, B. E.; Taniguchi, M.; Kim, H.-J.; Lindsey, J. S. Sparsely Substituted Chlorins as Core Constructs in Chlorophyll Analogue Chemistry. Part 1: Synthesis. *Tetrahedron* **2007**, *63* (18), 3826–3839. https://doi.org/10.1016/j.tet.2007.02.038.
(118) Lindsey, J. S. De Novo Synthesis of Gem-Dialkyl Chlorophyll Analogues for Probing and Emulating Our Green World. *Chem. Rev.* **2015**, *115* (13), 6534–6620. https://doi.org/10.1021/acs.chemrev.5b00065.
(119) Lindsey, J. S.; Mass, O.; Chen, C. Y. Tapping the Near-Infrared Spectral Region with Bacteriochlorin Arrays. *New J. Chem.* **2011**, *35* (3), 511–516. https://doi.org/10.1039/c0nj00977f.
(120) Yu, Z.; Ptaszek, M. Multifunctional Bacteriochlorins from Selective Palladium-Coupling Reactions. *Org. Lett.* **2012**, *14* (14), 3708–3711. https://doi.org/10.1021/ol3015545.

(121) Mass, O.; Pandithavidana, D. R.; Ptaszek, M.; Santiago, K.; Springer, J. W.; Jiao, J.; Tang, Q.; Kirmaier, C.; Bocian, D. F.; Holten, D.; et al. De Novo Synthesis and Properties of Analogues of the Self-Assembling Chlorosomal Bacteriochlorophylls. *New J. Chem.* **2011**, *35* (11), 2671–2690. https://doi.org/10.1039/c1nj20611g.
(122) Yu, Z.; Ptaszek, M. Near-IR Emissive Chlorin-Bacteriochlorin Energy-Transfer Dyads with a Common Donor and Acceptors with Tunable Emission Wavelength. *J. Org. Chem.* **2013**, *78* (21), 10678–10691. https://doi.org/10.1021/jo4016858.
(123) Krayer, M.; Ptaszek, M.; Kim, H.-J.; Meneely, K. R.; Fan, D.; Secor, K.; Lindsey, J. S. Expanded Scope of Synthetic Bacteriochlorins via Improved Acid Catalysis Conditions and Diverse Dihydrodipyrrin-Acetals. *J. Org. Chem.* **2010**, *75* (4), 1016–1039. https://doi.org/10.1021/jo9025572.
(124) Meares, A.; Bhagavathy, G. V.; Zik, S. R.; Gallagher, T.; Ptaszek, M. Expanding π-Conjugation in Chlorins Using Ethenyl Linker. *J. Org. Chem.* **2018**, *83* (16), 9076–9087. https://doi.org/10.1021/acs.joc.8b01186.
(125) Meares, A.; Yu, Z.; Viswanathan Bhagavathy, G.; Satraitis, A.; Ptaszek, M. Photoisomerization of Enediynyl Linker Leads to Slipped Cofacial Hydroporphyrin Dyads with Strong Through-Bond and Through-Space Electronic Interactions. *J. Org. Chem.* **2019**, *84* (12), 7851–7862. https://doi.org/10.1021/acs.joc.9b00731.
(126) Meares, A.; Satraitis, A.; Santhanam, N.; Yu, Z.; Ptaszek, M. Deep-Red Emissive BODIPY-Chlorin Arrays Excitable with Green and Red Wavelengths. *J. Org. Chem.* **2015**, *80* (8), 3858–3869. https://doi.org/10.1021/acs.joc.5b00119.
(127) Meares, A.; Satraitis, A.; Akhigbe, J.; Santhanam, N.; Swaminathan, S.; Ehudin, M.; Ptaszek, M. Amphiphilic BODIPY-Hydroporphyrin Energy Transfer Arrays with Broadly Tunable Absorption and Deep Red/Near-Infrared Emission in Aqueous Micelles. *J. Org. Chem.* **2017**, *82* (12), 6054–6070. https://doi.org/10.1021/acs.joc.7b00357.
(128) Ogata, F.; Nagaya, T.; Maruoka, Y.; Akhigbe, J.; Meares, A.; Lucero, M. Y.; Satraitis, A.; Fujimura, D.; Okada, R.; Inagaki, F.; et al. Activatable Near-Infrared Fluorescence Imaging Using PEGylated Bacteriochlorin-Based Chlorin and BODIPY-Dyads as Probes for Detecting Cancer. *Bioconjug. Chem.* **2019**, *30* (1), 169–183. https://doi.org/10.1021/acs.bioconjchem.8b00820.
(129) Meares, A.; Satraitis, A.; Ptaszek, M. BODIPY–Bacteriochlorin Energy Transfer Arrays: Toward Near-IR Emitters with Broadly Tunable, Multiple Absorption Bands. *J. Org. Chem.* **2017**, *82* (24), 13068–13075. https://doi.org/10.1021/acs.joc.7b02031.
(130) LeCours, S. M.; DiMagno, S. G.; Therien, M. J. Exceptional Electronic Modulation of Porphyrins through Meso-Arylethynyl Groups. Electronic Spectroscopy, Electronic Structure, and Electrochemistry of [5,15-Bis](Aryl)Ethynyl]-10,20-Diphenylporphinato]Zinc(II) Complexes. *J. Am. Chem. Soc.* **1996**, *118* (47), 11854–11864. https://doi.org/10.1021/ja962403y.
(131) Yang, E.; Ruzié, C.; Krayer, M.; Diers, J. R.; Niedzwiedzki, D. M.; Kirmaier, C.; Lindsey, J. S.; Bocian, D. F.; Holten, D. Photophysical Properties and

Electronic Structure of Bacteriochlorin-Chalcones with Extended near-Infrared Absorption. *Photochem. Photobiol.* **2013**, *89* (3), 586–604. https://doi.org/10.1111/php.12053.
(132) Yang, E.; Zhang, N.; Krayer, M.; Taniguchi, M.; Diers, J. R.; Kirmaier, C.; Lindsey, J. S.; Bocian, D. F.; Holten, D. Integration of Cyanine, Merocyanine and Styryl Dye Motifs with Synthetic Bacteriochlorins. *Photochem. Photobiol.* **2016**, *92* (1), 111–125. https://doi.org/10.1111/php.12547.
(133) de Assis, F. F.; Ferreira, M. A. B.; Brocksom, T. J.; de Oliveira, K. T. NIR Bacteriochlorin Chromophores Accessed by Heck and Sonogashira Cross-Coupling Reactions on a Tetrabromobacteriochlorin Derivative. *Org. Biomol. Chem.* **2016**, *14* (4), 1402–1412. https://doi.org/10.1039/c5ob02228b.
(134) Kee, H. L.; Nothdurft, R.; Muthiah, C.; Diers, J. R.; Fan, D.; Ptaszek, M.; Bocian, D. F.; Lindsey, J. S.; Culver, J. P.; Holten, D. Examination of Chlorin-Bacteriochlorin Energy-Transfer Dyads as Prototypes for near-Infrared Molecular Imaging Probes. *Photochem. Photobiol.* **2008**, *84* (5), 1061–1072. https://doi.org/10.1111/j.1751-1097.2008.00409.x.
(135) Anderson, H. L. Building Molecular Wires from the Colours of Life: Conjugated Porphyrin Oligomers. *Chem. Commun.* **1999**, *31* (23), 2323–2330. https://doi.org/10.1039/a904209a.
(136) Frampton, M. J.; Akdas, H.; Cowley, A. R.; Rogers, J. E.; Slagle, J. E.; Fleitz, P. A.; Drobizhev, M.; Rebane, A.; Anderson, H. L. Synthesis, Crystal Structure, and Nonlinear Optical Behavior of β-Unsubstituted Meso−meso E-Vinylene-Linked Porphyrin Dimers. *Org. Lett.* **2005**, *7* (24), 5365–5368. https://doi.org/10.1021/ol0520525.
(137) Christian, N. A.; Milone, M. C.; Ranka, S. S.; Li, G.; Frail, P. R.; Davis, K. P.; Bates, F. S.; Therien, M. J.; Ghoroghchian, P. P.; June, C. H.; et al. Tat-Functionalized near-Infrared Emissive Polymersomes for Dendritic Cell Labeling. *Bioconjug. Chem.* **2007**, *18* (1), 31–40. https://doi.org/10.1021/bc0601267.
(138) Wu, S. P.; Lee, I.; Ghoroghchian, P. P.; Frail, P. R.; Zheng, G.; Glickson, J. D.; Therien, M. J. Near-Infrared Optical Imaging of B16 Melanoma Cells via Low-Density Lipoprotein-Mediated Uptake and Delivery of High Emission Dipole Strength Tris[(Porphinato)Zinc(II)] Fluorophores. *Bioconjug. Chem.* **2005**, *16* (3), 542–550. https://doi.org/10.1021/bc0497416.
(139) Kuimova, M. K.; Botchway, S. W.; Parker, A. W.; Balaz, M.; Collins, H. A.; Anderson, H. L.; Suhling, K.; Ogilby, P. R. Imaging Intracellular Viscosity of a Single Cell during Photoinduced Cell Death. *Nat. Chem.* **2009**, *1* (1), 69–73. https://doi.org/10.1038/nchem.120.
(140) Hammerer, F.; Garcia, G.; Charles, P.; Sourdon, A.; Achelle, S.; Teulade-Fichou, M. P.; Maillard, P. Glycoconjugated Porphyrin Dimers as Robust Ratiometric Temperature Sensors. *Chem. Commun.* **2014**, *50* (67), 9529–9532. https://doi.org/10.1039/c4cc03367a.
(141) Duncan, T. V.; Susumu, K.; Sinks, L. E.; Therien, M. J. Exceptional Near-Infrared Fluorescence Quantum Yields and Excited-State Absorptivity of Highly Conjugated Porphyrin Arrays. *J. Am. Chem. Soc.* **2006**, *128* (28), 9000–9001. https://doi.org/10.1021/ja061897o.

(142) Parkinson, P.; Kamonsutthipaijit, N.; Anderson, H. L.; Herz, L. M. Size-Independent Energy Transfer in Biomimetic Nanoring Complexes. *ACS Nano* **2016**, *10* (6), 5933–5940. https://doi.org/10.1021/acsnano.6b01265.
(143) Drobizhev, M.; Stepanenko, Y.; Dzenis, Y.; Karotki, A.; Rebane, A.; Taylor, P. N.; Anderson, H. L. Extremely Strong Near-IR Two-Photon Absorption in Conjugated Porphyrin Dimers: Quantitative Description with Three-Essential-States Model. *J. Phys. Chem. B* **2005**, *109* (15), 7223–7236. https://doi.org/10.1021/jp044261x.
(144) Ogawa, K.; Hasegawa, H.; Inaba, Y.; Kobuke, Y.; Inouye, H.; Kanemitsu, Y.; Kohno, E.; Hirano, T.; Ogura, S.; Okura, I. Water-Soluble Bis(Imidazolylporphyrin) Self-Assemblies with Large Two-Photon AbsorptionCross Sections as Potential Agents for Photodynamic Therapy. *J. Med. Chem.* **2006**, *49* (7), 2276–2283. https://doi.org/10.1021/jm051072+.
(145) Rao, P. D.; Dhanalekshmi, S.; Littler, B. J.; Lindsey, J. S. Rational Syntheses of Porphyrins Bearing up to Four Different Meso Substituents. *J. Org. Chem.* **2000**, *65* (22), 7323–7344. https://doi.org/10.1021/jo000882k.
(146) Taniguchi, M.; Ra, D.; Mo, G.; Balasubramanian, T.; Lindsey, J. S. Synthesis of Meso-Substituted Chlorins via Tetrahydrobilene-a Intermediates. *J. Org. Chem.* **2001**, *66* (22), 7342–7354. https://doi.org/10.1021/jo0104835.
(147) Esemoto, N. N.; Satraitis, A.; Wiratan, L.; Ptaszek, M. Symmetrical and Nonsymmetrical Meso-Meso Directly Linked Hydroporphyrin Dyads: Synthesis and Photochemical Properties. *Inorg. Chem.* **2018**, *57* (6), 2977–2988. https://doi.org/10.1021/acs.inorgchem.7b02200.
(148) Yamamoto, Y.; Tamiaki, H. Synthesis, Optical Properties and Protonation of Chlorophyll Derivatives Appending a Pyridyl Group in the C3-Substituent. *Dyes Pigments* **2015**, *118*, 159–165. https://doi.org/10.1016/j.dyepig.2015.03.006.
(149) Shinozaki, Y.; Richards, G.; Ogawa, K.; Yamano, A.; Ohara, K.; Yamaguchi, K.; Kawano, S. I.; Tanaka, K.; Araki, Y.; Wada, T.; et al. Double Helices of a Pyridine-Appended Zinc Chlorophyll Derivative. *J. Am. Chem. Soc.* **2013**, *135* (14), 5262–5265. https://doi.org/10.1021/ja400493e.
(150) Zimmerman, G.; Chow, L.-Y.; Paik, U.-J. The Photochemical Isomerization of Azobenzene. *J. Am. Chem. Soc.* **1958**, *80* (14), 3528–3531. https://doi.org/10.1021/ja01547a010.
(151) Burrell, A. K.; Officer, D. L.; Plieger, P. G.; Reid, D. C. W. Synthetic Routes to Multiporphyrin Arrays. *Chem. Rev.* **2001**, *101* (9), 2751–2796. https://doi.org/10.1021/cr0000426.
(152) Chachisvilis, M.; Chirvony, V. S.; Shulga, A. M.; Källebring, B.; Larsson, S.; Sundström, V. Spectral and Photophysical Properties of Ethylene-Bridged Side-to-Side Porphyrin Dimers. 1. Ground-State Absorption and Fluorescence Study and Calculation of Electronic Structure of Trans-1,2-Bis(Meso-Octaethylporphyrinyl)Ethene. *J. Phys. Chem.* **1996**, *100* (32), 13857–13866. https://doi.org/10.1021/jp9607374.
(153) Chachisvilis, M.; Chirvony, V. S.; Shulga, A. M.; Källebring, B.; Larsson, S.; Sundström, V. Spectral and Photophysical Properties of Ethylene-Bridged Side-to-Side Porphyrin Dimers. 2. Femtosecond Transient Absorption and Picosecond Fluorescence Study of Trans-1,2-Bis(Meso-

Octaethylporphyrinyl)Ethene. *J. Phys. Chem.* **1996**, *100* (32), 13867–13873. https://doi.org/10.1021/jp960738w.
(154) Locos, O.; Bašić, B.; McMurtrie, J. C.; Jensen, P.; Arnold, D. P. Homo-and Heteronuclear Meso,Meso-(E)-Ethene-1,2-Diyl-Linked Diporphyrins: Preparation, X-Ray Crystal Structure, Electronic Absorption and Emission Spectra and Density Functional Theory Calculations. *Chem. - Eur. J.* **2012**, *18* (18), 5574–5588. https://doi.org/10.1002/chem.201102995.
(155) Locos, O. B.; Arnold, D. P. The Heck Reaction for Porphyrin Functionalisation: Synthesis of Meso-Alkenyl Monoporphyrins and Palladium-Catalysed Formation of Unprecedented Meso-β Ethene-Linked Diporphyrins. *Org. Biomol. Chem.* **2006**, *4* (5), 902–916. https://doi.org/10.1039/b516989e.
(156) Johnson, D. G.; Svec, W. A.; Wasielewski, M. R. Solvent Polarity Dependent Photophysics of a Fixed-Distance, Symmetric Chlorophyll Dimer. A Model of the Special Pair in Photosynthetic Reaction Centers. *Isr. J. Chem.* **1988**, *28* (2–3), 193–203. https://doi.org/10.1002/ijch.198800030.
(157) Johnson, S. G.; Small, G. J.; Johnson, D. G.; Svec, W. A.; Wasielewski, M. R. Temperature and Solvent-Polarity Dependence of the Absorption and Fluorescence Spectra of a Fixed-Distance Symmetric Chlorophyll Dimer. *J. Phys. Chem.* **1989**, *93* (14), 5437–5444. https://doi.org/10.1021/j100351a025.
(158) Jaquinod, L.; Senge, M. O.; Pandey, R. K.; Forsyth, T. P.; Smith, K. M. Planar Bischlorophyll Derivatives with a Completely Conjugated π-System: Model Compounds for the Special Pair in Photosynthesis. *Angew. Chem. - Int. Ed.* **1996**, *35* (16), 1840–1842. https://doi.org/10.1002/anie.199618401.
(159) Li, G.; Dobhal, M. P.; Graham, A.; Shibata, M.; Zheng, G.; Kozyrev, A.; Pandey, R. K. Thermolysis of Vic-Dihydroxybacteriochlorins: Effect of the Nature of Substrates in Directing the Formation of Chlorin−Chlorin Dimers with Fixed and Flexible Orientations and Their Preliminary in Vitro Photosensitizing Efficacy. *J. Org. Chem.* **2003**, *68* (10), 3762–3772. https://doi.org/10.1021/jo0207630.
(160) Smith, K. M.; Goff, D. A. Synthesis of Nickel(II) Isobacteriochlorins from Nickel(II) Complexes of Chlorophyll Derivatives. *J. Am. Chem. Soc.* **1985**, *107* (17), 4954–4964. https://doi.org/10.1021/ja00303a022.
(161) Ptaszek, M.; Lahaye, D.; Krayer, M.; Muthiah, C.; Lindsey, J. S. De Novo Synthesis of Long-Wavelength Absorbing Chlorin-13,15-Dicarboximides. *J. Org. Chem.* **2010**, *75* (5), 1659–1673. https://doi.org/10.1021/jo902649d.
(162) Muthiah, C.; Bhaumik, J.; Lindsey, J. S. Rational Routes to Formyl-Substituted Chlorins. *J. Org. Chem.* **2007**, *72* (15), 5839–5842. https://doi.org/10.1021/jo0707885.
(163) Taniguchi, M.; Ptaszek, M.; McDowell, B. E.; Boyle, P. D.; Lindsey, J. S. Sparsely Substituted Chlorins as Core Constructs in Chlorophyll Analogue Chemistry. Part 3: Spectral and Structural Properties. *Tetrahedron* **2007**, *63* (18), 3850–3863. https://doi.org/10.1016/j.tet.2007.02.040.
(164) Sol, V.; Chaleix, V.; Granet, R.; Krausz, P. An Efficient Route to Dimeric Porphyrin-RGD Peptide Conjugates via Olefin Metathesis. *Tetrahedron* **2008**, *64* (2), 364–371. https://doi.org/10.1016/j.tet.2007.10.092.

(165) Langford, S. J.; Latter, M. J.; Woodward, C. P. Construction of Multiporphyrin Arrays via Selective Cross-Metathesis. *Org. Lett.* **2006**, *8* (12), 2595–2598. https://doi.org/10.1021/ol060867n.
(166) da Silva, F. D. C.; Ferreira, V. F.; de Souza, M. C. B. V.; Tomé, A. C.; Neves, M. G. P. M. S.; Silva, A. M. S.; Cavaleiro, J. A. S. Synthesis of Glycoporphyrins by Cross-Metathesis Reactions. *Synlett* **2008**, No. 8, 1205–1207. https://doi.org/10.1055/s-2008-1072718.
(167) Jiao, L.; Hao, E.; Fronczek, F. R.; Vicente, M. G. H.; Smith, K. M. Benzoporphyrins via an Olefin Ring-Closure Metathesis Methodology. *Chem. Commun.* **2006**, No. 37, 3900–3902. https://doi.org/10.1039/b607711k.
(168) Sergeeva, N. N.; Bakar, M. B.; Senge, M. O. Synthesis, Transformations, and Comparative Studies of Porphyryl Acrylic Acids and Their Homologues. *J. Org. Chem.* **2009**, *74* (4), 1488–1497. https://doi.org/10.1021/jo8021764.
(169) Liu, X.; Sternberg, E.; Dolphin, D. Cross-Metathesis of the Vinyl Group on Tetrapyrrolic Macrocycles: Reactivity, Selectivity, and Mechanism. *J. Org. Chem.* **2008**, *73* (17), 6542–6550. https://doi.org/10.1021/jo8007989.
(170) Liu, X.; Sternberg, E.; Dolphin, D. Cross-Metathesis Reactions of Vinyl-Chlorins and -Porphyrins Catalyzed by a "Second Generation" Grubbs' Catalyst. *Chem. Commun.* **2004**, *4* (7), 852–853. https://doi.org/10.1039/b400001c.
(171) Coquerel, Y.; Rodriguez, J. Microwave-Assisted Olefin Metathesis. *Eur. J. Org. Chem.* **2008**, *2008* (7), 1125–1132. https://doi.org/10.1002/ejoc.200700696.
(172) Mee, S. P. H.; Lee, V.; Baldwin, J. E. Significant Enhancement of the Stille Reaction with a New Combination of Reagents—Copper(I) Iodide with Cesium Fluoride. *Chem. - Eur. J.* **2005**, *11* (11), 3294–3308. https://doi.org/10.1002/chem.200401162.
(173) Kim, W. S. Copper Replacement of Magnesium in the Chlorophylls and Bacteriochlorophyll. *Z. Für Naturforschung B* **1967**, *22* (10), 1054–1061. https://doi.org/10.1515/znb-1967-1014.
(174) Crossley, M. J.; Harding, M. M.; Tansey, C. W. A Convenient Synthesis of 2-Alkyl-5,10,15,20-Tetraphenylporphyrins: Reaction of Metallo-2-Nitro-5,10,15,20-Tetraphenylporphyrins with Grignard and Organolithium Reagents. *J. Org. Chem.* **1994**, *59* (16), 4433–4437. https://doi.org/10.1021/jo00095a018.
(175) Muthiah, C.; Ptaszek, M.; Nguyen, T. M.; Flack, K. M.; Lindsey, J. S. Two Complementary Routes to 7-Substituted Chlorins. Partial Mimics of Chlorophyll b. *J. Org. Chem.* **2007**, *72* (20), 7736–7749. https://doi.org/10.1021/jo701500d.
(176) Deraedt, C.; d'Halluin, M.; Astruc, D. Metathesis Reactions: Recent Trends and Challenges. *Eur. J. Inorg. Chem.* **2013**, n/a-n/a. https://doi.org/10.1002/ejic.201300682.
(177) Grubbs, R. H.; Wenzel, A. G.; Chatterjee, A. K. Olefin Cross-Metathesis. In *Comprehensive Organometallic Chemistry*; Elsevier, 2007; Vol. 11, pp 179–205.
(178) Blacquiere, J. M.; McDonald, R.; Fogg, D. E. Integrating the Schrock and Grubbs Catalysts: Ruthenium-Binaphtholate Catalysts for Olefin Metathesis. *Angew. Chem. Int. Ed.* **2010**, *49* (22), 3807–3810. https://doi.org/10.1002/anie.200906635.

(179) Chang, Raymond. *Physical Chemistry for the Chemical and Biological Sciences*, 3rd ed.; University Science Books, 2000.
(180) Senge, M. O.; Vicente, M. G. H.; Gerzevske, K. R.; Forsyth, T. P.; Smith, K. M. Models for the Photosynthetic Reaction Center: Preparation, Spectroscopy, and Crystal and Molecular Structures of Cofacial Bisporphyrins Linked by Cis-1,2- and Trans-1,2-Ethene Bridges and of 1,1-Carbinol-Bridged Bisporphyrins. *Inorg. Chem.* **1994**, *33* (25), 5625–5638. https://doi.org/10.1021/ic00103a006.
(181) Aravindu, K.; Kim, H.-J.; Taniguchi, M.; Dilbeck, P. L.; Diers, J. R.; Bocian, D. F.; Holten, D.; Lindsey, J. S. Synthesis and Photophysical Properties of Chlorins Bearing 0–4 Distinct Meso-Substituents. *Photochem. Photobiol. Sci.* **2013**, *12* (12), 2089. https://doi.org/10.1039/c3pp50240f.
(182) Hoffmann, R. Geometry Changes in Excited States. *Pure Appl. Chem.* **1970**, *24* (3), 567–584. https://doi.org/10.1351/pac197024030567.
(183) Yuen, J. M.; Harris, M. A.; Liu, M.; Diers, J. R.; Kirmaier, C.; Bocian, D. F.; Lindsey, J. S.; Holten, D. Effects of Substituents on Synthetic Analogs of Chlorophylls. Part 4: How Formyl Group Location Dictates the Spectral Properties of Chlorophylls b, d and f. *Photochem. Photobiol.* **2015**, *91* (2), 331–342. https://doi.org/10.1111/php.12401.
(184) Frimer, A. A. The Reaction of Singlet Oxygen with Olefins: The Question of Mechanism. *Chem. Rev.* **1979**, *79* (5), 359–387. https://doi.org/10.1021/cr60321a001.
(185) Ogilby, P. R. Singlet Oxygen: There Is Indeed Something New under the Sun. *Chem. Soc. Rev.* **2010**, *39* (8), 3181. https://doi.org/10.1039/b926014p.
(186) Clennan, E. L. New Mechanistic and Synthetic Aspects of Singlet Oxygen Chemistry. *Tetrahedron* **2000**, *56* (47), 9151–9179. https://doi.org/10.1016/S0040-4020(00)00794-8.
(187) Redmond, R. W.; Gamlin, J. N. A Compilation of Singlet Oxygen Yields from Biologically Relevant Molecules. *Photochem. Photobiol.* **1999**, *70* (4), 391–475. https://doi.org/10.1111/j.1751-1097.1999.tb08240.x.
(188) You, Y. Chemical Tools for the Generation and Detection of Singlet Oxygen. *Org. Biomol. Chem.* **2018**, *16* (22), 4044–4060. https://doi.org/10.1039/C8OB00504D.
(189) Jiang, M. Y.; Dolphin, D. Site-Specific Prodrug Release Using Visible Light. *J. Am. Chem. Soc.* **2008**, *130* (13), 4236–4237. https://doi.org/10.1021/ja800140g.
(190) Bartusik, D.; Aebisher, D.; Ghosh, G.; Minnis, M.; Greer, A. Fluorine End-Capped Optical Fibers for Photosensitizer Release and Singlet Oxygen Production. *J. Org. Chem.* **2012**, *77* (10), 4557–4565. https://doi.org/10.1021/jo3006107.
(191) Zamadar, M.; Ghosh, G.; Mahendran, A.; Minnis, M.; Kruft, B. I.; Ghogare, A.; Aebisher, D.; Greer, A. Photosensitizer Drug Delivery via an Optical Fiber. *J. Am. Chem. Soc.* **2011**, *133* (20), 7882–7891. https://doi.org/10.1021/ja200840p.
(192) Sakamoto, R.; Murata, M.; Nlshihara, H. Visible-Light Photochromism of Bis(Ferrocenylethynyl)Ethenes Switches Electronic Communication between

Ferrocene Sites. *Angew. Chem. - Int. Ed.* **2006**, *45* (29), 4793–4795. https://doi.org/10.1002/anie.200601067.
(193) Hayashi, M.; Sakamoto, R.; Nishihara, H. Extremely Efficient and Reversible Visible-Light Photochromism and Accompanying Switch of Electronic Communication in N-Phenylcarbazole-Appended Diethynylethene. *Chem. - Eur. J.* **2012**, *18* (28), 8610–8613. https://doi.org/10.1002/chem.201200794.
(194) Ponomarev, G. V.; Borovkov, V. V.; Sugiura, K.; Sakata, Y.; Shul'ga, A. M. Synthesis and Properties of Cis - 1,2 - Bis (Octaethylporphyrinyl)Ethylene. *Tetrahedron Lett.* **1993**, *34* (13), 2153–2156. https://doi.org/10.1016/S0040-4039(00)60369-6.
(195) Faries, K. M.; Diers, J. R.; Springer, J. W.; Yang, E.; Ptaszek, M.; Lahaye, D.; Krayer, M.; Taniguchi, M.; Kirmaier, C.; Lindsey, J. S.; et al. Photophysical Properties and Electronic Structure of Chlorin-Imides: Bridging the Gap between Chlorins and Bacteriochlorins. *J. Phys. Chem. B* **2015**, *119* (24), 7503–7515. https://doi.org/10.1021/jp511257w.
(196) Gottlieb, H. E.; Kotlyar, V.; Nudelman, A. NMR Chemical Shifts of Common Laboratory Solvents as Trace Impurities. *J. Org. Chem.* **1997**, *62* (21), 7512–7515. https://doi.org/10.1021/jo971176v.
(197) Mandal, A. K.; Taniguchi, M.; Diers, J. R.; Niedzwiedzki, D. M.; Kirmaier, C.; Lindsey, J. S.; Bocian, D. F.; Holten, D. Photophysical Properties and Electronic Structure of Porphyrins Bearing Zero to Four Meso-Phenyl Substituents: New Insights into Seemingly Well Understood Tetrapyrroles. *J. Phys. Chem. A* **2016**, *120* (49), 9719–9731. https://doi.org/10.1021/acs.jpca.6b09483.
(198) Seybold, P. G.; Gouterman, M. Porphyrins: XIII: Fluorescence Spectra and Quantum Yields. *J. Mol. Spectrosc.* **1969**, *31* (1–13), 1–13. https://doi.org/10.1016/0022-2852(69)90335-X.
(199) Kasha, M.; Rawls, H. R.; El-Bayoumi, M. A. The Exciton Model in Molecular Spectroscopy. *Pure Appl. Chem.* **1965**, *11* (3–4), 371–392. https://doi.org/DOI: 10.1351/pac196511030371.
(200) Hestand, N. J.; Spano, F. C. Expanded Theory of H- and J-Molecular Aggregates: The Effects of Vibronic Coupling and Intermolecular Charge Transfer. *Chem. Rev.* **2018**, *118* (15), 7069–7163. https://doi.org/10.1021/acs.chemrev.7b00581.
(201) Jendrny, M.; Aartsma, T. J.; Köhler, J. Insights into the Excitonic States of Individual Chlorosomes from Chlorobaculum Tepidum. *Biophys. J.* **2014**, *106* (9), 1921–1927. https://doi.org/10.1016/j.bpj.2014.03.020.
(202) Orf, G. S.; Blankenship, R. E. Chlorosome Antenna Complexes from Green Photosynthetic Bacteria. *Photosynth. Res.* **2013**, *116* (2–3), 315–331. https://doi.org/10.1007/s11120-013-9869-3.
(203) Allen, J. P.; Feher, G.; Yeates, T. O.; Komiya, H.; Rees, D. C. Structure of the Reaction Center from Rhodobacter Sphaeroides R-26: The Cofactors. *Proc. Natl. Acad. Sci.* **1987**, *84* (16), 5730–5734. https://doi.org/10.1073/pnas.84.16.5730.

(204) Kim, D.; Osuka, A. Directly Linked Porphyrin Arrays with Tunable Excitonic Interactions. *Acc. Chem. Res.* **2004**, *37* (10), 735–745. https://doi.org/10.1021/ar030242e.
(205) Aratani, N.; Kim, D.; Osuka, A. Discrete Cyclic Porphyrin Arrays as Artificial Light-Harvesting Antenna. *Acc. Chem. Res.* **2009**, *42* (12), 1922–1934. https://doi.org/10.1021/ar9001697.
(206) Harvey, P. D.; Stern, C.; Gros, C. P.; Guilard, R. The Photophysics and Photochemistry of Cofacial Free Base and Metallated Bisporphyrins Held Together by Covalent Architectures. *Coord. Chem. Rev.* **2007**, *251* (3), 401–428. https://doi.org/10.1016/j.ccr.2006.06.009.
(207) Fletcher, J. T.; Therien, M. J. Strongly Coupled Porphyrin Arrays Featuring Both π-Cofacial and Linear-π-Conjugative Interactions. *Inorg. Chem.* **2002**, *41* (2), 331–341. https://doi.org/10.1021/ic010871p.
(208) Fletcher, J. T.; Therien, M. J. Extreme Electronic Modulation of the Cofacial Porphyrin Structural Motif. *J. Am. Chem. Soc.* **2002**, *124* (16), 4298–4311. https://doi.org/10.1021/ja012489h.
(209) Balaban, T. S.; Tamiaki, H.; Holzwarth, A. R. Chlorins Programmed for Self-Assembly. In *Supermolecular Dye Chemistry*; Springer, 2005; Vol. 258, pp 1–38.
(210) Taniguchi, M.; Lindsey, J. S. Synthetic Chlorins, Possible Surrogates for Chlorophylls, Prepared by Derivatization of Porphyrins. *Chem. Rev.* **2017**, *117* (2), 344–535. https://doi.org/10.1021/acs.chemrev.5b00696.
(211) Chang, C. K.; Hanson, L. K.; Richardson, P. F.; Young, R.; Fajer, J. π-Cation Radicals of Ferrous and Free Base Isobacteriochlorins: Models for Siroheme and Sirohydrochlorin. *Proc. Natl. Acad. Sci. U. S. A.* **1981**, *78* (5), 2652–2656. https://doi.org/10.1073/pnas.78.5.2652.
(212) Ouyang, Q.; Yan, K.-Q.; Zhu, Y.-Z.; Zhang, C.-H.; Liu, J.-Z.; Chen, C.; Zheng, J.-Y. An Efficient PIFA-Mediated Synthesis of a Directly Linked Zinc Chlorin Dimer via Regioselective Oxidative Coupling. *Org. Lett.* **2012**, *14* (11), 2746–2749. https://doi.org/10.1021/ol300969g.
(213) Xiong, R.; Arkhypchuk, A. I.; Kovacs, D.; Orthaber, A.; Borbas, K. E. Directly Linked Hydroporphyrin Dimers. *Chem. Commun.* **2016**, *52* (58), 9056–9058. https://doi.org/10.1039/c6cc00516k.
(214) Wasielewski, M. R.; Svec, W. A.; Cope, B. T. Bis(Chlorophyll)Cyclophanes. New Models of Special Pair Chlorophyll. *J. Am. Chem. Soc.* **1978**, *100* (6), 1961–1962. https://doi.org/10.1021/ja00474a070.
(215) Pellin, M. J.; Kaufmann, K. J.; Wasielewski, M. R. In Vitro Duplication of the Primary Light-Induced Charge Separation in Purple Photosynthetic Bacteria. *Nature* **1979**, *278* (5699), 54–55. https://doi.org/10.1038/278054a0.
(216) Pellin, M. J.; Wasielewski, M. R.; Kaufmann, K. J. Picosecond Photophysics of Covalently Linked Pyrochlorophyllide a Dimer. Unique Kinetics within the Singlet Manifold. *J. Am. Chem. Soc.* **1980**, *102* (6), 1868–1873. https://doi.org/10.1021/ja00526a017.
(217) Yuen, M. J.; Closs, G. L.; Katz, J. J.; Roper, J. A.; Wasielewski, M. R.; Hindman, J. C. Photophysical Properties of Zinc and Magnesium Tris(Pyrochlorophyllide a) 1,1,1-Tris(Hydroxymethyl)Ethane Triesters. *Proc.*

Natl. Acad. Sci. U. S. A. **1980**, *77* (10), 5598–5601. https://doi.org/10.1073/pnas.77.10.5598.
(218) Overfield, R. E.; Scherz, A.; Kaufmann, K. J.; Wasielewski, M. R. Photophysics of Bis(Chlorophyll)Cyclophanes: Models of Photosynthetic Reaction Centers. *J. Am. Chem. Soc.* **1983**, *105* (13), 4256–4260. https://doi.org/10.1021/ja00351a024.
(219) Boxer, S. G.; Bucks, R. R. A Structural Model for the Photosynthetic Reaction Center. *J. Am. Chem. Soc.* **1979**, *101* (7), 1883–1885. https://doi.org/10.1021/ja00501a045.
(220) Periasamy, N.; Linschitz, H.; Closs, G. L.; Boxer, S. G. Photoprocesses in Covalently Linked Pyrochlorophyllide Dimer: Triplet State Formation and Opening and Closing of Hydroxylic Linkages. *Proc. Natl. Acad. Sci. U. S. A.* **1978**, *75* (6), 2563–2566. https://doi.org/10.1073/pnas.75.6.2563.
(221) Bucks, R. R.; Boxer, S. G. Synthesis and Spectroscopic Properties of a Novel Cofacial Chlorophyll-Based Dimer. *J. Am. Chem. Soc.* **1982**, *104* (1), 340–343. https://doi.org/10.1021/ja00365a085.
(222) Bucks, R. R.; Netzel, T. L.; Fujita, I.; Boxer, S. G. Picosecond Spectroscopic Study of Chlorophyll-Based Models for the Primary Photochemistry of Photosynthesis. *J. Phys. Chem.* **1982**, *86* (11), 1947–1955. https://doi.org/10.1021/j100208a009.
(223) Kosaka, N.; Tamiaki, H. Synthesis of a Novel Cyclic Chlorophyll Hetero-Dyad as a Model Compound for Stacked Chlorophylls Found in Photosynthetic Systems. *Eur. J. Org. Chem.* **2004**, *2004* (11), 2325–2330. https://doi.org/10.1002/ejoc.200400027.
(224) Sasaki, S.; Tamiaki, H. Synthesis of Cyclic Chlorophyll Oligomers. *Tetrahedron Lett.* **2006**, *47* (28), 4965–4968. https://doi.org/10.1016/j.tetlet.2006.04.159.
(225) Hunt, J. E.; Katz, J. J.; Svirmickas, A.; Hindman, J. C. Photoprocesses in Photosystem I Model Systems. *J. Am. Chem. Soc.* **1984**, *106* (8), 2242–2250. https://doi.org/10.1021/ja00320a004.
(226) Vasudevan, J.; Stibrany, R. T.; Bumby, J.; Knapp, S.; Potenza, J. A.; Emge, T. J.; Schugar, H. J. An Edge-over-Edge Zn(II) Bacteriochlorin Dimer Having an Unshifted Qy Band. The Importance of π-Overlap. *J. Am. Chem. Soc.* **1996**, *118* (46), 11676–11677. https://doi.org/10.1021/ja9624376.
(227) Knapp, S.; Huang, B.; Emge, T. J.; Sheng, S.; Krogh-Jespersen, K.; Potenza, J. A.; Schugar, H. J. A Pyropheophorbide Dimer with Single Pyrrole π Overlap and a Low-Energy Q Absorption. *J. Am. Chem. Soc.* **1999**, *121* (34), 7977–7978. https://doi.org/10.1021/ja991632s.
(228) Nikkonen, T.; Haavikko, R.; Helaja, J. Hydrogen Bond Driven Self-Assembled C2-Symmetric Chlorin Syn Dimers; Unorthodox Models for Chlorophyll "special Pairs" in Photosynthetic Reaction Centres. *Org. Biomol. Chem.* **2009**, *7* (10), 2046–2052. https://doi.org/10.1039/b819764d.
(229) Thanh, N. T. V.; Könekamp, T.; Hanke, D.; Löwer, F.; Borrmann, T.; Montforts, F.-P. Synthesis of a Cofacial Chlorin Dimer of Defined Symmetry. *J. Porphyr. Phthalocyanines* **2012**, *16* (05n06), 626–632. https://doi.org/10.1142/s1088424612500666.

(230) Cohen-Ofri, I.; Van Gastel, M.; Grzyb, J.; Brandis, A.; Pinkas, I.; Lubitz, W.; Noy, D. Zinc-Bacteriochlorophyllide Dimers in de Novo Designed Four-Helix Bundle Proteins. A Model System for Natural Light Energy Harvesting and Dissipation. *J. Am. Chem. Soc.* **2011**, *133* (24), 9526–9535. https://doi.org/10.1021/ja202054m.
(231) McCleese, C.; Yu, Z.; Esemoto, N. N.; Kolodziej, C.; Maiti, B.; Bhandari, S.; Dunietz, B. D.; Burda, C.; Ptaszek, M. Excitonic Interactions in Bacteriochlorin Homo-Dyads Enable Charge Transfer: A New Approach to the Artificial Photosynthetic Special Pair. *J. Phys. Chem. B* **2018**, *122* (14), 4131–4140. https://doi.org/10.1021/acs.jpcb.8b02123.
(232) Sugiyama, Y.; Shinohara, Y.; Momotake, A.; Takahashi, K.; Kanna, Y.; Nishimura, Y.; Arai, T. Photochemistry of Linear-Shaped Phenylacetylenyl- and (Phenylacetylenyl) Phenylacetylenyl-Substituted Aromatic Enediynes. *J. Phys. Chem. A* **2010**, *114* (41), 10929–10935. https://doi.org/10.1021/jp1054827.
(233) Nakano, Y.; Ishizuka, K.; Muraoka, K.; Ohtani, H.; Takayama, Y.; Sato, F. Synthesis of Conjugated Oligomers Having Aromatic and Enediyne Units Alternately in the Backbone That Show Intense Fluorescence Emission. *Org. Lett.* **2004**, *6* (14), 2373–2376. https://doi.org/10.1021/ol049277k.
(234) Nielsen, M. B.; Diederich, F. Conjugated Oligoenynes Based on the Diethynylethene Unit. *Chem. Rev.* **2005**, *105* (5), 1837–1867. https://doi.org/10.1021/cr9903353.
(235) Schenning, A. P. H. J.; Arndt, J. D.; Ito, M.; Stoddart, A.; Schreiber, M.; Siemsen, P.; Martin, R. E.; Boudon, C.; Gisselbrecht, J. P.; Gross, M.; et al. Insulated Molecular Wires: Dendritic Encapsulation of Poly(Triacetylene) Oligomers, Attempted Dendritic Stabilization of Novel Poly(Pentaacetylene) Oligomers, and an Organometallic Approach to Dendritic Rods. *Helv. Chim. Acta* **2001**, *84* (2), 296–334. https://doi.org/10.1002/1522-2675(20010228)84:2<296::AID-HLCA296>3.0.CO;2-X.
(236) Kivala, M.; Diederich, F. Acetylene-Derived Strong Organic Acceptors for Planar and Nonplanar Push-Pull Chromophores. *Acc. Chem. Res.* **2009**, *42* (2), 235–248. https://doi.org/10.1021/ar8001238.
(237) Edelmann, M. J.; Raimundo, J.-M.; Utesch, N. F.; Diederich, F.; Boudon, C.; Gisselbrecht, J.-P.; Gross, M. Dramatically Enhanced Fluorescence of Heteroaromatic Chromophores upon Insertion as Spacers into Oligo(Triacetylene)s. *Helv. Chim. Acta* **2002**, *85* (7), 2195–2213. https://doi.org/10.1002/1522-2675(200207)85:7<2195::AID-HLCA2195>3.0.CO;2-G.
(238) Martin, R. E.; Wytko, J. A.; Diederich, F.; Boudon, C.; Gisselbrecht, J. P.; Gross, M. Modulation of π-Electron Conjugation in Oligo(Triacetylene) Chromophores by Incorporation of a Central Spacer. *Helv. Chim. Acta* **1999**, *82* (9), 1470–1485. https://doi.org/10.1002/(SICI)1522-2675(19990908)82:9<1470::AID-HLCA1470>3.0.CO;2-N.
(239) Wytko, J.; Berl, V.; McLaughlin, M.; Tykwinski, R. R.; Schreiber, M.; Diederich, F.; Boudon, C.; Gisselbrecht, J.-P.; Gross, M. Porphyrin-[(E)-1,2-Diethynylethene] Scaffolding: Synthesis and Optical and Electrochemical Properties of Multinanometer-Sized Porphyrin Arrays. *Helv. Chim. Acta* **1998**,

81 (11), 1964–1977. https://doi.org/10.1002/(SICI)1522-2675(19981111)81:11<1964::AID-HLCA1964>3.0.CO;2-I.
(240) Sakamoto, R.; Kume, S.; Nishihara, H. Visible-Light Photochromism of Triarylamine- Or Ferrocene-Bound Diethynylethenes That Switches Electronic Communication between Redox Sites and Luminescence. *Chem. - Eur. J.* **2008**, *14* (23), 6978–6986. https://doi.org/10.1002/chem.200800732.
(241) Martin, R. E.; Bartek, J.; Diederich, F.; Tykwinski, R. R.; Meister, E. C.; Hilger, A.; Lüthi, H. P. Photochemical Trans–Cis Isomerisation of Donor/Acceptor-Substituted (E)-Hex-3-Ene-1,5-Diynes (1,2-Diethynylethenes, DEEs) and 3,4-Diethynylhex-3-Ene-1,5-Diynes (Tetraethynylethenes, TEEs). *J. Chem. Soc. Perkin Trans. 2* **1998**, No. 2, 233–242. https://doi.org/10.1039/a707679g.
(242) Wu, Y. L.; Ferroni, F.; Pieraccini, S.; Schweizer, W. B.; Frank, B. B.; Spada, G. P.; Diederich, F. 1,2-Di(Phenylethynyl)Ethenes with Axially Chiral, 2,2′-Bridged 1,1′-Binaphthyl Substituents: Potent Cholesteric Liquid-Crystal Inducers. *Org. Biomol. Chem.* **2012**, *10* (39), 8016–8026. https://doi.org/10.1039/c2ob25983d.
(243) Melinger, J. S.; Pan, Y.; Kleiman, V. D.; Peng, Z.; Davis, B. L.; McMorrow, D.; Lu, M. Optical and Photophysical Properties of Light-Harvesting Phenylacetylene Monodendrons Based on Unsymmetrical Branching. *J. Am. Chem. Soc.* **2002**, *124* (40), 12002–12012. https://doi.org/10.1021/ja020380j.
(244) Schuh, K.; Glorius, F. A Domino Copper-Catalyzed C-N and C-O Cross-Coupling for the Conversion of Primary Amides into Oxazoles. *Synthesis* **2007**, No. 15, 2297–2306. https://doi.org/10.1055/s-2007-983782.
(245) Bowling, N. P.; McMahon, R. J. Enediyne Isomers of Tetraethynylethene. *J. Org. Chem.* **2006**, *71* (16), 5841–5847. https://doi.org/10.1021/jo052505j.
(246) Song, R.; Robert, A.; Bernadou, J.; Meunier, B. Illustrating Atropisomerism in the Porphyrin Series Using NMR Spectroscopy. *Analusis* **1999**, *27* (5), 464–467. https://doi.org/10.1051/analusis:1999126.
(247) Allen, M. T.; Whitten, D. G. The Photophysics and Photochemistry of .Alpha.,.Omega.-Diphenylpolyene Singlet States. *Chem. Rev.* **1989**, *89* (8), 1691–1702. https://doi.org/10.1021/cr00098a003.
(248) Boldi, A. M.; Anthony, J.; Knobler, C. B.; Diederich, F. New Cross-Conjugated Compounds Derived from Tetraethynylethene. *Angew. Chem. Int. Ed.* **1992**, *31* (9), 1240–1242.
(249) Fornari, R. P.; Rowe, P.; Padula, D.; Troisi, A. Importance and Nature of Short-Range Excitonic Interactions in Light Harvesting Complexes and Organic Semiconductors. *J. Chem. Theory Comput.* **2017**, *13* (8), 3754–3763. https://doi.org/10.1021/acs.jctc.7b00328.
(250) Ehrlich, S.; Moellmann, J.; Grimme, S. Dispersion-Corrected Density Functional Theory for Aromatic Interactions in Complex Systems. *Acc. Chem. Res.* **2013**, *46* (4), 916–926. https://doi.org/10.1021/ar3000844.
(251) Kaufmann, C.; Kim, W.; Nowak-Król, A.; Hong, Y.; Kim, D.; Würthner, F. Ultrafast Exciton Delocalization, Localization, and Excimer Formation Dynamics in a Highly Defined Perylene Bisimide Quadruple π-Stack. *J. Am. Chem. Soc.* **2018**, *140* (12), 4253–4258. https://doi.org/10.1021/jacs.7b11571.

(252) Son, M.; Park, K. H.; Shao, C.; Würthner, F.; Kim, D. Spectroscopic Demonstration of Exciton Dynamics and Excimer Formation in a Sterically Controlled Perylene Bisimide Dimer Aggregate. *J. Phys. Chem. Lett.* **2014**, *5* (20), 3601–3607. https://doi.org/10.1021/jz501953a.
(253) Sung, J.; Nowak-Król, A.; Schlosser, F.; Fimmel, B.; Kim, W.; Kim, D.; Würthner, F. Direct Observation of Excimer-Mediated Intramolecular Electron Transfer in a Cofacially-Stacked Perylene Bisimide Pair. *J. Am. Chem. Soc.* **2016**, *138* (29), 9029–9032. https://doi.org/10.1021/jacs.6b04591.
(254) Lindquist, R. J.; Lefler, K. M.; Brown, K. E.; Dyar, S. M.; Margulies, E. A.; Young, R. M.; Wasielewski, M. R. Energy Flow Dynamics within Cofacial and Slip-Stacked Perylene-3,4-Dicarboximide Dimer Models of π-Aggregates. *J. Am. Chem. Soc.* **2014**, *136* (42), 14912–14923. https://doi.org/10.1021/ja507653p.
(255) Margulies, E. A.; Shoer, L. E.; Eaton, S. W.; Wasielewski, M. R. Excimer Formation in Cofacial and Slip-Stacked Perylene-3,4:9,10-Bis(Dicarboximide) Dimers on a Redox-Inactive Triptycene Scaffold. *Phys. Chem. Chem. Phys.* **2014**, *16* (43), 23735–23742. https://doi.org/10.1039/c4cp03107e.
(256) Schubert, A.; Settels, V.; Liu, W.; Würthner, F.; Meier, C.; Fink, R. F.; Schindlbeck, S.; Lochbrunner, S.; Engels, B.; Engel, V. Ultrafast Exciton Self-Trapping upon Geometry Deformation in Perylene-Based Molecular Aggregates. *J. Phys. Chem. Lett.* **2013**, *4* (5), 792–796. https://doi.org/10.1021/jz4000752.
(257) Brown, K. E.; Salamant, W. A.; Shoer, L. E.; Young, R. M.; Wasielewski, M. R. Direct Observation of Ultrafast Excimer Formation in Covalent Perylenediimide Dimers Using Near-Infrared Transient Absorption Spectroscopy. *J. Phys. Chem. Lett.* **2014**, *5* (15), 2588–2593. https://doi.org/10.1021/jz5011797.
(258) Mauck, C. M.; Young, R. M.; Wasielewski, M. R. Characterization of Excimer Relaxation via Femtosecond Shortwaveand Mid-Infrared Spectroscopy. *J. Phys. Chem. A* **2017**, *121* (4), 784–792. https://doi.org/10.1021/acs.jpca.6b11388.
(259) Hunter, C. A.; Sanders, J. K. M. The Nature of π-π Interactions. *J. Am. Chem. Soc.* **1990**, *112* (14), 5525–5534. https://doi.org/10.1021/ja00170a016.
(260) Gouterman, M.; Wagnière, G. H.; Snyder, L. C. Spectra of Porphyrins Part II. Four Orbital Model. *J. Mol. Spectrosc.* **1963**, *11* (1–6), 108–127. https://doi.org/10.1016/0022-2852(63)90011-0.
(261) Shrestha, K.; González-Delgado, J. M.; Blew, J. H.; Jakubikova, E. Electronic Structure of Covalently Linked Zinc Bacteriochlorin Molecular Arrays: Insights into Molecular Design for NIR Light Harvesting. *J. Phys. Chem. A* **2014**, *118* (42), 9901–9913. https://doi.org/10.1021/jp507749c.
(262) Samori, S.; Tojo, S.; Fujitsuka, M.; Ryhding, T.; Fix, A. G.; Armstrong, B. M.; Haley, M. M.; Majima, T. Emission from Regioisomeric Bis(Phenylethynyl)Benzenes during Pulse Radiolysis. *J. Org. Chem.* **2009**, *74* (10), 3776–3782. https://doi.org/10.1021/jo900494j.
(263) Berthelot, J.; Benammar, Y.; Desmazières, B. Solvent Incorporation in Bromination of Alkynes With Tetrabutylammonium Tribromide in Methanol.

Synth. Commun. **1997**, *27* (16), 2865–2876. https://doi.org/10.1080/00397919708004163.
(264) Rossi, R.; Bellina, F.; Carpita, A.; Mazzarella, F. Palladium-Mediated Cross-Coupling Reactions Involving 3-Substituted Alkyl (E)-2,3-Dibromopropenoates and Arylzinc or Aryltin Derivatives. *Tetrahedron* **1996**, *52* (11), 4095–4110. https://doi.org/10.1016/S0040-4020(96)00071-3.
(265) Loudet, A.; Burgess, K. BODIPY Dyes and Their Derivatives: Syntheses and Spectroscopic Properties. *Chem. Rev.* **2007**, *107* (11), 4891–4932. https://doi.org/10.1021/cr078381n.
(266) Mishra, A.; Behera, R. K.; Behera, P. K.; Mishra, B. K.; Behera, G. B. Cyanines during the 1990s: A Review. *Chem. Rev.* **2000**, *100* (6), 1973–2012. https://doi.org/10.1021/cr990402t.
(267) Harada, T.; Sano, K.; Sato, K.; Watanabe, R.; Yu, Z.; Hanaoka, H.; Nakajima, T.; Choyke, P. L.; Ptaszek, M.; Kobayashi, H. Activatable Organic Near-Infrared Fluorescent Probes Based on a Bacteriochlorin Platform: Synthesis and Multicolor in Vivo Imaging with a Single Excitation. *Bioconjug. Chem.* **2014**, *25* (2), 362–369. https://doi.org/10.1021/bc4005238.
(268) Alexander, V. M.; Sano, K.; Yu, Z.; Nakajima, T.; Choyke, P. L.; Ptaszek, M.; Kobayashi, H. Galactosyl Human Serum Albumin-NMP1 Conjugate: A near Infrared (NIR)-Activatable Fluorescence Imaging Agent to Detect Peritoneal Ovarian Cancer Metastases. *Bioconjug. Chem.* **2012**, *23* (8), 1671–1679. https://doi.org/10.1021/bc3002419.
(269) Croce, A. C.; Bottiroli, G. Autofluorescence Spectroscopy and Imaging: A Tool for Biomedical Research and Diagnosis. *Eur. J. Histochem.* **2014**, *58* (4). https://doi.org/10.4081/ejh.2014.2461.
(270) Nagaya, T.; Nakamura, Y. A.; Choyke, P. L.; Kobayashi, H. Fluorescence-Guided Surgery. *Front. Oncol.* **2017**, *7*, 314. https://doi.org/10.3389/fonc.2017.00314.
(271) Nguyen, Q. T.; Tsien, R. Y. Fluorescence-Guided Surgery with Live Molecular Navigation — a New Cutting Edge. *Nat. Rev. Cancer* **2013**, *13* (9), 653–662. https://doi.org/10.1038/nrc3566.
(272) DSouza, A. V.; Lin, H.; Henderson, E. R.; Samkoe, K. S.; Pogue, B. W. Review of Fluorescence Guided Surgery Systems: Identification of Key Performance Capabilities beyond Indocyanine Green Imaging. *J. Biomed. Opt.* **2016**, *21* (8), 080901. https://doi.org/10.1117/1.JBO.21.8.080901.
(273) Resch-Genger, U.; Grabolle, M.; Cavaliere-Jaricot, S.; Nitschke, R.; Nann, T. Quantum Dots versus Organic Dyes as Fluorescent Labels. *Nat. Methods* **2008**, *5* (9), 763–775. https://doi.org/10.1038/nmeth.1248.
(274) Lavis, L. D.; Raines, R. T. Bright Ideas for Chemical Biology-Supplement. *ACS Chem. Biol.* **2008**, *3* (3), 142–55. https://doi.org/10.1021/cb700248m.
(275) Parrish, J. A. New Concepts in Therapeutic Photomedicine; Photochemistry, Optical Targeting and the Therapeutic Window. *J. Invest. Dermatol.* **1981**, *77* (1), 45–50. https://doi.org/10.1111/1523-1747.ep12479235.
(276) Gupta, A.; Avci, P.; Dai, T.; Huang, Y.-Y.; Hamblin, M. R. Ultraviolet Radiation in Wound Care: Sterilization and Stimulation. *Adv. Wound Care* **2013**, *2* (8), 422–437. https://doi.org/10.1089/wound.2012.0366.

(277) Umezawa, K.; Matsui, A.; Nakamura, Y.; Citterio, D.; Suzuki, K. Bright, Color-Tunable Fluorescent Dyes in the Vis/NIR Region: Establishment of New "Tailor-Made" Multicolor Fluorophores Based on Borondipyrromethene. *Chem. - Eur. J.* **2009**, *15* (5), 1096–1106. https://doi.org/10.1002/chem.200801906.
(278) Lovell, J. F.; Chan, M. W.; Qi, Q.; Chen, J.; Zheng, G. Porphyrin FRET Acceptors for Apoptosis Induction and Monitoring. *J. Am. Chem. Soc.* **2011**, *133* (46), 18580–18582. https://doi.org/10.1021/ja2083569.
(279) Taniguchi, M.; Ra, D.; Kirmaier, C.; Hindin, E.; Schwartz, J. K.; Diers, J. R.; Knox, R. S.; Bocian, D. F.; Lindsey, J. S.; Holten, D. Comparison of Excited-State Energy Transfer in Arrays of Hydroporphyrins (Chlorins, Oxochlorins) versus Porphyrins: Rates, Mechanisms, and Design Criteria. *J. Am. Chem. Soc.* **2003**, *125* (44), 13461–13470. https://doi.org/10.1021/ja035987u.
(280) Muthukumaran, K.; Loewe, R. S.; Kirmaier, C.; Hindin, E.; Schwartz, J. K.; Sazanovich, I. V.; Diers, J. R.; Bocian, D. F.; Holten, D.; Lindsey, J. S. Synthesis and Excited-State Photodynamics of A Perylene-Monoimide-Oxochlorin Dyad. A Light-Harvesting Array. *J. Phys. Chem. B* **2003**, *107* (15), 3431–3442. https://doi.org/10.1021/jp026941a.
(281) Muthiah, C.; Kee, H. L.; Diers, J. R.; Fan, D.; Ptaszek, M.; Bocian, D. F.; Holten, D.; Lindsey, J. S. Synthesis and Excited-State Photodynamics of a Chlorin–Bacteriochlorin Dyad—Through-Space Versus Through-Bond Energy Transfer in Tetrapyrrole Arrays. *Photochem. Photobiol.* **2008**, *84* (3), 786–801. https://doi.org/10.1111/j.1751-1097.2007.00258.x.
(282) Kee, H. L.; Diers, J. R.; Ptaszek, M.; Muthiah, C.; Fan, D.; Lindsey, J. S.; Bocian, D. F.; Holten, D. Chlorin-Bacteriochlorin Energy-Transfer Dyads as Prototypes for near-Infrared Molecular Imaging Probes: Controlling Charge-Transfer and Fluorescence Properties in Polar Media. *Photochem. Photobiol.* **2009**, *85* (4), 909–920. https://doi.org/10.1111/j.1751-1097.2008.00532.x.
(283) Laakso, J.; Rosser, G. A.; Szíjjártó, C.; Beeby, A.; Borbas, K. E. Synthesis of Chlorin-Sensitized near Infrared-Emitting Lanthanide Complexes. *Inorg. Chem.* **2012**, *51* (19), 10366–10374. https://doi.org/10.1021/ic3015354.
(284) Voznyak, D. A.; Zakharova, G. V.; Chibisov, A. K.; Kharitonova, O. V.; Grin, M. A.; Semenikhin, K. O.; Mironov, A. F. Primary Photochemical Processes in Dyads Based on Indocarbocyanine Dyes and Chlorin E6. *High Energy Chem.* **2010**, *44* (1), 31–36. https://doi.org/10.1134/S0018143910010066.
(285) Kataoka, Y.; Shibata, Y.; Tamiaki, H. Intramolecular Excitation Energy Transfer from Visible-Light Absorbing Chlorophyll Derivatives to a Near-Infrared-Light Emitting Boron Dipyrromethene Moiety. *Chem. Lett.* **2010**, *39* (9), 953–955. https://doi.org/10.1246/cl.2010.953.
(286) Finikova, O. S.; Troxler, T.; Senes, A.; DeGrado, W. F.; Hochstrasser, R. M.; Vinogradov, S. A. Energy and Electron Transfer in Enhanced Two-Photon-Absorbing Systems with Triplet Cores. *J. Phys. Chem. A* **2007**, *111* (30), 6977–6990. https://doi.org/10.1021/jp071586f.
(287) Mani, T.; Niedzwiedzki, D. M.; Vinogradov, S. A. Generation of Phosphorescent Triplet States via Photoinduced Electron Transfer: Energy and Electron Transfer Dynamics in Pt Porphyrin-Rhodamine b Dyads. *J. Phys. Chem. A* **2012**, *116* (14), 3598–3610. https://doi.org/10.1021/jp301345h.

(288) Ziessel, R.; Ulrich, G.; Harriman, A. The Chemistry of Bodipy: A New El Dorado for Fluorescence Tools. *New J. Chem.* **2007**, *31* (4), 496–501. https://doi.org/10.1039/b617972j.
(289) Boens, N.; Leen, V.; Dehaen, W. Fluorescent Indicators Based on BODIPY. *Chem. Soc. Rev.* **2012**, *41* (3), 1130–1172. https://doi.org/10.1039/c1cs15132k.
(290) Ziessel, R.; Harriman, A. Artificial Light-Harvesting Antennae: Electronic Energy Transfer by Way of Molecular Funnels. *Chem. Commun.* **2011**, *47* (2), 611–631. https://doi.org/10.1039/c0cc02687e.
(291) El-Khouly, M. E.; Fukuzumi, S.; D'Souza, F. Photosynthetic Antenna-Reaction Center Mimicry by Using Boron Dipyrromethene Sensitizers. *ChemPhysChem* **2014**, *15* (1), 30–47. https://doi.org/10.1002/cphc.201300715.
(292) Erbas-Cakmak, S.; Akkaya, E. U. Toward Singlet Oxygen Delivery at a Measured Rate: A Self-Reporting Photosensitizer. *Org. Lett.* **2014**, *16* (11), 2946–2949. https://doi.org/10.1021/ol501084n.
(293) Kostereli, Z.; Ozdemir, T.; Buyukcakir, O.; Akkaya, E. U. Tetrastyryl-BODIPY-Based Dendritic Light Harvester and Estimation of Energy Transfer Efficiency. *Org. Lett.* **2012**, *14* (14), 3636–3639. https://doi.org/10.1021/ol301462x.
(294) Ziessel, R.; Ulrich, G.; Haefele, A.; Harriman, A. An Artificial Light-Harvesting Array Constructed from Multiple Bodipy Dyes. *J. Am. Chem. Soc.* **2013**, *135* (30), 11330–11344. https://doi.org/10.1021/ja4049306.
(295) Harriman, A.; Mallon, L.; Elliot, K.; Heafele, A.; Ulrich, G.; Ziessel, R. Length Dependence for Intramolecular Energy Transfer in Three- and Four-Color Donor-Spacer-Acceptor Arrays. *J. Am. Chem. Soc.* **2009**, *131* (1), 13375–13386.
(296) Thivierge, C.; Han, J.; Jenkins, R. M.; Burgess, K. Fluorescent Proton Sensors Based on Energy Transfer. *J. Org. Chem.* **2011**, *76* (13), 5219–5228. https://doi.org/10.1021/jo2005654.
(297) Wu, L.; Loudet, A.; Barhoumi, R.; Burghardt, R. C.; Burgess, K. Fluorescent Cassettes for Monitoring Three-Component Interactions in Vitro and in Living Cells. *J. Am. Chem. Soc.* **2009**, *131* (26), 9156–9157. https://doi.org/10.1021/ja9029413.
(298) Zhang, X.; Xiao, Y.; He, L.; Zhang, Y. Through-Bond Energy Transfer Cassettes for Multicolor Encoding. *J. Org. Chem.* **2014**, *79* (13), 6315–6320. https://doi.org/10.1021/jo500653r.
(299) Pochorovski, I.; Knehans, T.; Nettels, D.; Müller, A. M.; Schweizer, W. B.; Caflisch, A.; Schuler, B.; Diederich, F. Experimental and Computational Study of BODIPY Dye-Labeled Cavitand Dynamics. *J. Am. Chem. Soc.* **2014**, *136* (6), 2441–2449. https://doi.org/10.1021/ja4104292.
(300) Zhang, C.; Zhao, J.; Wu, S.; Wang, Z.; Wu, W.; Ma, J.; Guo, S.; Huang, L. Intramolecular RET Enhanced Visible Light-Absorbing Bodipy Organic Triplet Photosensitizers and Application in Photooxidation and Triplet-Triplet Annihilation Upconversion. *J. Am. Chem. Soc.* **2013**, *135* (28), 10566–10578. https://doi.org/10.1021/ja405170j.
(301) Ueno, Y.; Jose, J.; Loudet, A.; Pérez-Bolívar, C.; Anzenbacher, P.; Burgess, K. Encapsulated Energy-Transfer Cassettes with Extremely Well Resolved

Fluorescent Outputs. *J. Am. Chem. Soc.* **2011**, *133* (1), 51–55. https://doi.org/10.1021/ja107193j.
(302) Shi, W. J.; El-Khouly, M. E.; Ohkubo, K.; Fukuzumi, S.; Ng, D. K. P. Photosynthetic Antenna-Reaction Center Mimicry with a Covalently Linked Monostyryl Boron-Dipyrromethene-Aza-Boron-Dipyrromethene-C60 Triad. *Chem. - Eur. J.* **2013**, *19* (34), 11332–11341. https://doi.org/10.1002/chem.201300318.
(303) Bandi, V.; Ohkubo, K.; Fukuzumi, S.; D'Souza, F. A Broad-Band Capturing and Emitting Molecular Triad: Synthesis and Photochemistry. *Chem. Commun.* **2013**, *49* (28), 2867–2869. https://doi.org/10.1039/c3cc40471d.
(304) Bandi, V.; El-Khouly, M. E.; Nesterov, V. N.; Karr, P. A.; Fukuzumi, S.; D'Souza, F. Self-Assembled via Metal-Ligand Coordination AzaBODIPY-Zinc Phthalocyanine and AzaBODIPY-Zinc Naphthalocyanine Conjugates: Synthesis, Structure, and Photoinduced Electron Transfer. *J. Phys. Chem. C* **2013**, *117* (11), 5638–5649. https://doi.org/10.1021/jp400046b.
(305) El-Khouly, M. E.; Amin, A. N.; Zandler, M. E.; Fukuzumi, S.; D'Souza, F. Near-IR Excitation Transfer and Electron Transfer in a BF 2-Chelated Dipyrromethane-Azadipyrromethane Dyad and Triad. *Chem. - Eur. J.* **2012**, *18* (17), 5239–5247. https://doi.org/10.1002/chem.201103074.
(306) Liu, J. Y.; Ermilov, E. A.; Röder, B.; Ng, D. K. P. Switching the Photo-Induced Energy and Electron-Transfer Processes in BODIPY-Phthalocyanine Conjugates. *Chem. Commun.* **2009**, No. 12, 1517–1519. https://doi.org/10.1039/b821630d.
(307) Liu, J. Y.; Huang, Y.; Menting, R.; Röder, B.; Ermilov, E. A.; Ng, D. K. P. A Boron Dipyrromethene-Phthalocyanine Pentad as an Artificial Photosynthetic Model. *Chem. Commun.* **2013**, *49* (29), 2998–3000. https://doi.org/10.1039/c3cc00262d.
(308) Lu, H.; MacK, J.; Yang, Y.; Shen, Z. Structural Modification Strategies for the Rational Design of Red/NIR Region BODIPYs. *Chem. Soc. Rev.* **2014**, *43* (13), 4778–4823. https://doi.org/10.1039/c4cs00030g.
(309) Kowada, T.; Maeda, H.; Kikuchi, K. BODIPY-Based Probes for the Fluorescence Imaging of Biomolecules in Living Cells. *Chem. Soc. Rev.* **2015**, *44* (14), 4953–4972. https://doi.org/10.1039/C5CS00030K.
(310) Kirmaier, C.; Hindin, E.; Schwartz, J. K.; Sazanovich, I. Y.; Diers, J. R.; Muthukumaran, K.; Taniguchi, M.; Bocian, D. F.; Lindsey, J. S.; Holten, D. Synthesis and Excited-State Photodynamics of Perylene-Bis(Imide)-Oxochlorin Dyads. A Charge-Separation Motif. *J. Phys. Chem. B* **2003**, *107* (15), 3443–3454. https://doi.org/10.1021/jp0269423.
(311) Kelley, R. F.; Tauber, M. J.; Wasielewski, M. R. Intramolecular Electron Transfer through the 20-Position of a Chlorophyll a Derivative: An Unexpectedly Efficient Conduit for Charge Transport. *J. Am. Chem. Soc.* **2006**, *128* (14), 4779–4791. https://doi.org/10.1021/ja058233j.
(312) Gunderson, V. L.; Smeigh, A. L.; Kim, C. H.; Co, D. T.; Wasielewski, M. R. Electron Transfer within Self-Assembling Cyclic Tetramers Using Chlorophyll-Based Donor-Acceptor Building Blocks. *J. Am. Chem. Soc.* **2012**, *134* (9), 4363–4372. https://doi.org/10.1021/ja211329k.

(313) Sunahara, H.; Urano, Y.; Kojima, H.; Nagano, T. Design and Synthesis of a Library of BODIPY-Based Environmental Polarity Sensors Utilizing Photoinduced Electron-Transfer-Controlled Fluorescence ON/OFF Switching. *J. Am. Chem. Soc.* **2007**, *129* (17), 5597–5604. https://doi.org/10.1021/ja068551y.
(314) Liu, Y.; Lindsey, J. S. Northern–Southern Route to Synthetic Bacteriochlorins. *J. Org. Chem.* **2016**, *81* (23), 11882–11897. https://doi.org/10.1021/acs.joc.6b02334.
(315) Ast, S.; Fischer, T.; Müller, H.; Mickler, W.; Schwichtenberg, M.; Rurack, K.; Holdt, H. J. Integration of the 1,2,3-Triazole "Click" Motif as a Potent Signalling Element in Metal Ion Responsive Fluorescent Probes. *Chem. - Eur. J.* **2013**, *19* (9), 2990–3005. https://doi.org/10.1002/chem.201201575.
(316) Bura, T.; Nastasi, F.; Puntoriero, F.; Campagna, S.; Ziessel, R. Ultrafast Energy Transfer in Triptycene-Grafted Bodipy Scaffoldings. *Chem. - Eur. J.* **2013**, *19* (27), 8900–8912. https://doi.org/10.1002/chem.201300413.
(317) Godoy, J.; Vives, G.; Tour, J. M. Synthesis of Highly Fluorescent BODIPY-Based Nanocars. *Org. Lett.* **2010**, *12* (7), 1464–1467. https://doi.org/10.1021/ol100108r.
(318) Chen, Y.; Wang, H.; Wan, L.; Bian, Y.; Jiang, J. 8-Hydroxyquinoline-Substituted Boron-Dipyrromethene Compounds: Synthesis, Structure, and OFF-ON-OFF Type of PH-Sensing Properties. *J. Org. Chem.* **2011**, *76* (10), 3774–3781. https://doi.org/10.1021/jo200050a.
(319) Ambroise, A.; Li, J.; Yu, L.; Lindsey, J. S. A Self-Assembled Light-Harvesting Array of Seven Porphyrins in a Wheel and Spoke Architecture. *Org. Lett.* **2000**, *2* (17), 2563–2566. https://doi.org/10.1021/ol006036d.
(320) Wielopolski, M.; Atienza, C.; Clark, T.; Guldi, D. M.; Martín, N. P-Phenyleneethynylene Molecular Wires: Influence of Structure on Photoinduced Electron-Transfer Properties. *Chem. - Eur. J.* **2008**, *14* (21), 6379–6390. https://doi.org/10.1002/chem.200800159.
(321) Bura, T.; Leclerc, N.; Fall, S.; Lévêque, P.; Heiser, T.; Ziessel, R. Absorption Tuning of Monosubstituted Triazatruxenes for Bulk Heterojunction Solar Cells. *Org. Lett.* **2011**, *13* (22), 6030–6033. https://doi.org/10.1021/ol202443g.
(322) Li, L.; Han, J.; Nguyen, B.; Burgess, K. Syntheses and Spectral Properties of Functionalized, Water-Soluble BODIPY Derivatives. *J. Org. Chem.* **2008**, *73* (5), 1963–1970. https://doi.org/10.1021/jo702463f.
(323) Nierth, A.; Kobitski, A. Y.; Ulrich Nienhaus, G.; Jäschke, A. Anthracene-Bodipy Dyads as Fluorescent Sensors for Biocatalytic Diels-Alder Reactions. *J. Am. Chem. Soc.* **2010**, *132* (8), 2646–2654. https://doi.org/10.1021/ja9084397.
(324) Michael Luciano; Christian Brückner. Modifications of Porphyrins and Hydroporphyrins for Their Solubilization in Aqueous Media. *Molecules* **2017**, *22* (6), 980. https://doi.org/10.3390/molecules22060980.
(325) Jiang, J.; Yang, E.; Reddy, K. R.; Niedzwiedzki, D. M.; Kirmaier, C.; Bocian, D. F.; Holten, D.; Lindsey, J. S. Synthetic Bacteriochlorins Bearing Polar Motifs (Carboxylate, Phosphonate, Ammonium and a Short PEG). Water-Solubilization, Bioconjugation, and Photophysical Properties. *New J. Chem.* **2015**, *39* (7), 5694–5714. https://doi.org/10.1039/c5nj00759c.

(326) Borbas, K. E.; Chandrashaker, V.; Muthiah, C.; Hooi, L. K.; Holten, D.; Lindsey, J. S. Design, Synthesis, and Photophysical Characterization of Water-Soluble Chlorins. *J. Org. Chem.* **2008**, *73* (8), 3145–3158. https://doi.org/10.1021/jo7026728.
(327) Bura, T.; Ziessel, R. Water-Soluble Phosphonate-Substituted BODIPY Derivatives with Tunable Emission Channels. *Org. Lett.* **2011**, *13* (12), 3072–3075. https://doi.org/10.1021/ol200969r.
(328) Jiang, J.; Vairaprakash, P.; Reddy, K. R.; Sahin, T.; Pavan, M. P.; Lubian, E.; Lindsey, J. S. Hydrophilic Tetracarboxy Bacteriochlorins for Photonics Applications. *Org. Biomol. Chem.* **2014**, *12* (1), 86–103. https://doi.org/10.1039/c3ob41791c.
(329) Reddy, K. R.; Lubian, E.; Pavan, M. P.; Kim, H. J.; Yang, E.; Holten, D.; Lindsey, J. S. Synthetic Bacteriochlorins with Integral Spiro-Piperidine Motifs. *New J. Chem.* **2013**, *37* (4), 1157–1173. https://doi.org/10.1039/c3nj41161c.
(330) Niu, S. L.; Ulrich, G.; Ziessel, R.; Kiss, A.; Renard, P.-Y.; Romieu, A. Water-Soluble BODIPY Derivatives. *Org. Lett.* **2009**, *11* (10), 2049–2052. https://doi.org/10.1021/ol900302n.
(331) Niu, S. L.; Massif, C.; Ulrich, G.; Ziessel, R.; Renard, P. Y.; Romieu, A. Water-Solubilisation and Bio-Conjugation of a Red-Emitting BODIPY Marker. *Org. Biomol. Chem.* **2011**, *9* (1), 66–69. https://doi.org/10.1039/c0ob00693a.
(332) Niu, S. L.; Massif, C.; Ulrich, G.; Renard, P. Y.; Romieu, A.; Ziessel, R. Water-Soluble Red-Emitting Distyryl-Borondipyrromethene (BODIPY) Dyes for Biolabeling. *Chem. - Eur. J.* **2012**, *18* (23), 7229–7242. https://doi.org/10.1002/chem.201103613.
(333) Massif, C.; Dautrey, S.; Haefele, A.; Ziessel, R.; Renard, P. Y.; Romieu, A. New Insights into the Water-Solubilisation of Fluorophores by Post-Synthetic "Click" and Sonogashira Reactions. *Org. Biomol. Chem.* **2012**, *10* (22), 4330–4336. https://doi.org/10.1039/c2ob25428j.
(334) Romieu, A.; Massif, C.; Rihn, S.; Ulrich, G.; Ziessel, R.; Renard, P. Y. The First Comparative Study of the Ability of Different Hydrophilic Groups to Water-Solubilise Fluorescent BODIPY Dyes. *New J. Chem.* **2013**, *37* (4), 1016–1027. https://doi.org/10.1039/c3nj41093e.
(335) Gao, M.; Yu, F.; Lv, C.; Choo, J.; Chen, L. Fluorescent Chemical Probes for Accurate Tumor Diagnosis and Targeting Therapy. *Chem. Soc. Rev.* **2017**, *46* (8), 2237–2271. https://doi.org/10.1039/C6CS00908E.
(336) Joshi, B. P.; Wang, T. D. Targeted Optical Imaging Agents in Cancer: Focus on Clinical Applications. *Contrast Media Mol. Imaging* **2018**, *2018*, 1–19. https://doi.org/10.1155/2018/2015237.
(337) Haugland, R. P. Antibody Conjugates for Cell Biology. *Curr. Protoc. Cell Biol.* **2000**, *6* (1), 16.5.1-16.5.22. https://doi.org/10.1002/0471143030.cb1605s06.
(338) Davis, S.; Weiss, M. J.; Wong, J. R.; Lampidis, T. J.; Chen, L. B. Mitochondrial and Plasma Membrane Potentials Cause Unusual Accumulation and Retention of Rhodamine 123 by Human Breast Adenocarcinoma-Derived MCF-7 Cells. *J. Biol. Chem.* **1985**, *260* (25), 13844–13850.

(339) Odeh, A. M.; Craik, J. D.; Ezzeddine, R.; Tovmasyan, A.; Batinic-Haberle, I.; Benov, L. T. Targeting Mitochondria by Zn(II)N-Alkylpyridylporphyrins: The Impact of Compound Sub-Mitochondrial Partition on Cell Respiration and Overall Photodynamic Efficacy. *PLoS ONE* **2014**, *9* (9), e108238. https://doi.org/10.1371/journal.pone.0108238.
(340) Lepage, M. L.; Mirloup, A.; Ripoll, M.; Stauffert, F.; Bodlenner, A.; Ziessel, R.; Compain, P. Design, Synthesis and Photochemical Properties of the First Examples of Iminosugar Clusters Based on Fluorescent Cores. *Beilstein J. Org. Chem.* **2015**, *11*, 659–667. https://doi.org/10.3762/bjoc.11.74.
(341) He, H.; Lo, P.-C.; Yeung, S.-L.; Fong, W.-P.; Ng, D. K. P. Synthesis and in Vitro Photodynamic Activities of Pegylated Distyryl Boron Dipyrromethene Derivatives. *J. Med. Chem.* **2011**, *54* (8), 3097–3102. https://doi.org/10.1021/jm101637g.
(342) Atilgan, S.; Ekmekci, Z.; Dogan, A. L.; Guc, D.; Akkaya, E. U. Water Soluble Distyryl-Boradiazaindacenes as Efficient Photosensitizers for Photodynamic Therapy. *Chem. Commun.* **2006**, No. 42, 4398–4400. https://doi.org/10.1039/b612347c.
(343) Zhu, S.; Zhang, J.; Vegesna, G.; Luo, F.-T.; Green, S. A.; Liu, H. Highly Water-Soluble Neutral BODIPY Dyes with Controllable Fluorescence Quantum Yields. *Org. Lett.* **2011**, *13* (3), 438–441. https://doi.org/10.1021/ol102758z.
(344) Atilgan, S.; Ozdemir, T.; Akkaya, E. U. A Sensitive and Selective Ratiometric near IR Fluorescent Probe for Zinc Ions Based on the Distyryl-Bodipy Fluorophore. *Org. Lett.* **2008**, *10* (18), 4065–4067. https://doi.org/10.1021/ol801554t.
(345) Ke, M.-R.; Yeung, S.-L.; Ng, D. K. P.; Fong, W.-P.; Lo, P.-C. Preparation and in Vitro Photodynamic Activities of Folate-Conjugated Distyryl Boron Dipyrromethene Based Photosensitizers. *J. Med. Chem.* **2013**, *56* (21), 8475–8483. https://doi.org/10.1021/jm4009168.
(346) Zhu, S.; Zhang, J.; Janjanam, J.; Bi, J.; Vegesna, G.; Tiwari, A.; Luo, F. T.; Wei, J.; Liu, H. Highly Water-Soluble, near-Infrared Emissive BODIPY Polymeric Dye Bearing RGD Peptide Residues for Cancer Imaging. *Anal. Chim. Acta* **2013**, *758*, 138–144. https://doi.org/10.1016/j.aca.2012.10.026.
(347) Isik, M.; Ozdemir, T.; Turan, I. S.; Kolemen, S.; Akkaya, E. U. Chromogenic and Fluorogenic Sensing of Biological Thiols in Aqueous Solutions Using BODIPY-Based Reagents. *Org. Lett.* **2013**, *15* (1), 216–219. https://doi.org/10.1021/ol303306s.
(348) Sui, B.; Yue, X.; Kim, B.; Belfield, K. D. Near-IR Two-Photon Fluorescent Sensor for K\textlesssup\textgreater+\textless/Sup\textgreater Imaging in Live Cells. *ACS Appl. Mater. Interfaces* **2015**, *7* (32), 17565–17568. https://doi.org/10.1021/acsami.5b04506.
(349) Zhang, N.; Jiang, J.; Liu, M.; Taniguchi, M.; Mandal, A. K.; Evans-Storms, R. B.; Pitner, J. B.; Bocian, D. F.; Holten, D.; Lindsey, J. S. Bioconjugatable, PEGylated Hydroporphyrins for Photochemistry and Photomedicine. Narrow-Band, near-Infrared-Emitting Bacteriochlorins. *New J. Chem.* **2016**, *40* (9), 7750–7767. https://doi.org/10.1039/c6nj01155a.

(350) Liu, M.; Chen, C. Y.; Mandal, A. K.; Chandrashaker, V.; Evans-Storms, R. B.; Pitner, J. B.; Bocian, D. F.; Holten, D.; Lindsey, J. S. Bioconjugatable, PEGylated Hydroporphyrins for Photochemistry and Photomedicine. Narrow-Band, Red-Emitting Chlorins. *New J. Chem.* **2016**, *40* (9), 7721–7740. https://doi.org/10.1039/c6nj01154c.
(351) Mandal, A. K.; Holten, D.; Sahin, T.; Liu, M.; Lindsey, J. S.; Bocian, D. F. Photophysical Comparisons of PEGylated Porphyrins, Chlorins and Bacteriochlorins in Water. *New J. Chem.* **2016**, *40* (11), 9648–9656. https://doi.org/10.1039/C6NJ02091G.
(352) Knop, K.; Hoogenboom, R.; Fischer, D.; Schubert, U. S. Poly(Ethylene Glycol) in Drug Delivery: Pros and Cons as Well as Potential Alternatives. *Angew. Chem. - Int. Ed.* **2010**, *49* (36), 6288–6308. https://doi.org/10.1002/anie.200902672.
(353) Adey, W. R. Tissue Interactions with Nonionizing Electromagnetic Fields. *Physiol. Rev.* **1981**, *61* (2), 435–514. https://doi.org/10.1152/physrev.1981.61.2.435.
(354) Adey, W. R. Biological Effects of Electromagnetic Fields: Biophysics of Electromagnetic Fields. *J. Cell. Biochem.* **1993**, *51* (4), 410–416. https://doi.org/10.1002/jcb.2400510405.
(355) Adams, P. G.; Collins, A. M.; Sahin, T.; Subramanian, V.; Urban, V. S.; Vairaprakash, P.; Tian, Y.; Evans, D. G.; Shreve, A. P.; Montaño, G. A. Diblock Copolymer Micelles and Supported Films with Noncovalently Incorporated Chromophores: A Modular Platform for Efficient Energy Transfer. *Nano Lett.* **2015**, *15* (4), 2422–2428. https://doi.org/10.1021/nl504814x.
(356) Harris, M. A.; Sahin, T.; Jiang, J.; Vairaprakash, P.; Parkes-Loach, P. S.; Niedzwiedzki, D. M.; Kirmaier, C.; Loach, P. A.; Bocian, D. F.; Holten, D.; et al. Enhanced Light-Harvesting Capacity by Micellar Assembly of Free Accessory Chromophores and LH1-like Antennas. *Photochem. Photobiol.* **2014**, *90* (6), 1264–1276. https://doi.org/10.1111/php.12319.
(357) Lundrigan, T.; Crawford, S. M.; Cameron, T. S.; Thompson, A. Cl-BODIPYs: A BODIPY Class Enabling Facile B-Substitution. *Chem Commun* **2012**, *48* (7), 1003–1005. https://doi.org/10.1039/C1CC16351E.
(358) Nguyen, A. L.; Bobadova-Parvanova, P.; Hopfinger, M.; Fronczek, F. R.; Smith, K. M.; Vicente, M. G. H. Synthesis and Reactivity of 4,4-Dialkoxy-BODIPYs: An Experimental and Computational Study. *Inorg. Chem.* **2015**, *54* (7), 3228–3236. https://doi.org/10.1021/ic502821m.
(359) Deniz, E.; Battal, M.; Cusido, J.; Sortino, S.; Raymo, F. M. Insights into the Isomerization of Photochromic Oxazines from the Excitation Dynamics of BODIPY–Oxazine Dyads. *Phys. Chem. Chem. Phys.* **2012**, *14* (29), 10300. https://doi.org/10.1039/c2cp41089c.
(360) Shaban Ragab, S.; Swaminathan, S.; Deniz, E.; Captain, B.; Raymo, F. M. Fluorescence Photoactivation by Ligand Exchange around the Boron Center of a BODIPY Chromophore. *Org. Lett.* **2013**, *15* (12), 3154–3157. https://doi.org/10.1021/ol401380n.
(361) Zhang, G.; Wang, M.; Fronczek, F. R.; Smith, K. M.; Vicente, M. G. H. Lewis-Acid-Catalyzed BODIPY Boron Functionalization Using Trimethylsilyl

Nucleophiles. *Inorg. Chem.* **2018**, *57* (23), 14493–14496. https://doi.org/10.1021/acs.inorgchem.8b02775.
(362) Brizet, B.; Bernhard, C.; Volkova, Y.; Rousselin, Y.; Harvey, P. D.; Goze, C.; Denat, F. Boron Functionalization of BODIPY by Various Alcohols and Phenols. *Org. Biomol. Chem.* **2013**, *11* (44), 7729–7737. https://doi.org/10.1039/c3ob41370e.
(363) Ulrich, G.; Goze, C.; Guardigli, M.; Roda, A.; Ziessel, R. Pyrromethene Dialkynyl Borane Bomplexes for "Cascatelle" Energy Transfer and Protein Labeling. *Angew. Chem. - Int. Ed.* **2005**, *44* (24), 3694–3698. https://doi.org/10.1002/anie.200500808.
(364) Bura, T.; Retailleau, P.; Ziessel, R. Efficient Synthesis of Panchromatic Dyes for Energy Concentration. *Angew. Chem. - Int. Ed.* **2010**, *49* (37), 6659–6663. https://doi.org/10.1002/anie.201003206.
(365) Kobayashi, H.; Ogawa, M.; Alford, R.; Choyke, P. L.; Urano, Y. New Strategies for Fluorescent Probe Design in Medical Diagnostic Imaging. *Chem. Rev.* **2009**, *110* (5), 2620–2640. https://doi.org/10.1021/cr900263j.
(366) Fukuzumi, S.; Ohkubo, K.; Chen, Y.; Pandey, R. K.; Zhan, R.; Shao, J.; Kadish, K. M. Photophysical and Electrochemical Properties of New Bacteriochlorins and Characterization of Radical Cation and Radical Anion Species. *J. Phys. Chem. A* **2002**, *106* (20), 5105–5113. https://doi.org/10.1021/jp025665x.
(367) Chu, M.; Li, H.; Wu, Q.; Wo, F.; Shi, D. Pluronic-Encapsulated Natural Chlorophyll Nanocomposites for in Vivo Cancer Imaging and Photothermal/Photodynamic Therapies. *Biomaterials* **2014**, *35* (29), 8357–8373. https://doi.org/10.1016/j.biomaterials.2014.05.049.
(368) Li, Y.; Zhang, F.; Wang, X. F.; Chen, G.; Fu, X.; Tian, W.; Kitao, O.; Tamiaki, H.; Sasaki, S. Pluronic Micelle-Encapsulated Red-Photoluminescent Chlorophyll Derivative for Biocompatible Cancer Cell Imaging. *Dyes Pigments* **2017**, *136*, 17–23. https://doi.org/10.1016/j.dyepig.2016.08.018.
(369) Ghoroghchian, P. P.; Frail, P. R.; Susumu, K.; Park, T.-H.; Wu, S. P.; Uyeda, H. T.; Hammer, D. A.; Therien, M. J. Broad Spectral Domain Fluorescence Wavelength Modulation of Visible and Near-Infrared Emissive Polymersomes. *J. Am. Chem. Soc.* **2005**, *127* (44), 15388–15390. https://doi.org/10.1021/ja055571b.
(370) Ghoroghchian, P. P.; Frail, P. R.; Susumu, K.; Blessington, D.; Brannan, K.; Bates, F. S.; Chance, B.; Hammer, D. A.; Therien, M. J.; Ghoroghchian, P. P.; et al. Near Infrared-Emissive Polymersomes: Self-Assembled Soft Matter in Vivo Optical Imaging. *Nat. Methods* **2005**, *2* (4), 245. https://doi.org/10.1038/nmeth0405-245.
(371) Ghoroghchian, P. P.; Frail, P. R.; Li, G.; Zupancich, J. A.; Bates, F. S.; Hammer, D. A.; Therien, M. J. Controlling Bulk Optical Properties of Emissive Polymersomes through Intramembranous Polymer-Fluorophore Interactions. *Chem. Mater.* **2007**, *19* (6), 1309–1318. https://doi.org/10.1021/cm062427w.
(372) Taratula, O.; Doddapaneni, B. S.; Schumann, C.; Li, X.; Bracha, S.; Milovancev, M.; Alani, A. W. G.; Taratula, O. Naphthalocyanine-Based Biodegradable Polymeric Nanoparticles for Image-Guided Combinatorial

Phototherapy. *Chem. Mater.* **2015**, *27* (17), 6155–6165. https://doi.org/10.1021/acs.chemmater.5b03128.
(373) Lemon, C. M.; Karnas, E.; Han, X.; Bruns, O. T.; Kempa, T. J.; Fukumura, D.; Bawendi, M. G.; Jain, R. K.; Duda, D. G.; Nocera, D. G. Micelle-Encapsulated Quantum Dot-Porphyrin Assemblies as in Vivo Two-Photon Oxygen Sensors. *J. Am. Chem. Soc.* **2015**, *137* (31), 9832–9842. https://doi.org/10.1021/jacs.5b04765.
(374) Kumar, R.; Ohulchanskyy, T. Y.; Roy, I.; Gupta, S. K.; Borek, C.; Thompson, M. E.; Prasad, P. N. Near-Infrared Phosphorescent Polymeric Nanomicelles: Efficient Optical Probes for Tumor Imaging and Detection. *ACS Appl. Mater. Interfaces* **2009**, *1* (7), 1474–1481. https://doi.org/10.1021/am9001293.
(375) Carter, K. A.; Shao, S.; Hoopes, M. I.; Luo, D.; Ahsan, B.; Grigoryants, V. M.; Song, W.; Huang, H.; Zhang, G.; Pandey, R. K.; et al. Porphyrin-Phospholipid Liposomes Permeabilized by near-Infrared Light. *Nat. Commun.* **2014**, *5*, 1–11. https://doi.org/10.1038/ncomms4546.
(376) Aravindu, K.; Mass, O.; Vairaprakash, P.; Springer, J. W.; Yang, E.; Niedzwiedzki, D. M.; Kirmaier, C.; Bocian, D. F.; Holten, D.; Lindsey, J. S. Amphiphilic Chlorins and Bacteriochlorins in Micellar Environments. Molecular Design, de Novo Synthesis, and Photophysical Properties. *Chem. Sci.* **2013**, *4* (9), 3459–3477. https://doi.org/10.1039/c3sc51335a.
(377) de Silva, A. P.; Gunaratne, H. Q. N.; Gunnlaugsson, T.; Huxley, A. J. M.; McCoy, C. P.; Rademacher, J. T.; Rice, T. E. Signaling Recognition Events with Fluorescent Sensors and Switches. *Chem. Rev.* **1997**, *97* (5), 1515–1566. https://doi.org/10.1021/cr960386p.
(378) Baki, C. N.; Akkaya, E. U. Boradiazaindacene-Appended Calix[4]Arene: Fluorescence Sensing of PH Near Neutrality. *J. Org. Chem.* **2001**, *66* (4), 1512–1513. https://doi.org/10.1021/jo005706q.
(379) Vegesna, G. K.; Sripathi, S. R.; Zhang, J.; Zhu, S.; He, W.; Luo, F. T.; Jahng, W. J.; Frost, M.; Liu, H. Highly Water-Soluble BODIPY-Based Fluorescent Probe for Sensitive and Selective Detection of Nitric Oxide in Living Cells. *ACS Appl. Mater. Interfaces* **2013**, *5* (10), 4107–4112. https://doi.org/10.1021/am303247s.
(380) Li, G.; Bhosale, S. V.; Wang, T.; Hackbarth, S.; Roeder, B.; Siggel, U.; Fuhrhop, J. H. Nanowells on Silica Particles in Water Containing Long-Distance Porphyrin Heterodimers. *J. Am. Chem. Soc.* **2003**, *125* (35), 10693–10702. https://doi.org/10.1021/ja035558w.
(381) Kappe, C. O.; Van der Eycken, E. Click Chemistry under Non-Classical Reaction Conditions. *Chem. Soc. Rev.* **2010**, *39* (4), 1280–1290. https://doi.org/10.1039/b901973c.
(382) Yalagala, R. S.; Mazinani, S. A.; Maddalena, L. A.; Stuart, J. A.; Yan, F.; Yan, H. Microwave-Assisted Syntheses of BODIPY-Sugar Conjugates through Click Chemistry and Conjugate Assembly into Liposomes. *Carbohydr. Res.* **2016**, *424*, 15–20. https://doi.org/10.1016/j.carres.2016.02.003.
(383) Desbois, N.; Pacquelet, S.; Dubois, A.; Michelin, C.; Gros, C. P. Easy Access to Heterobimetallic Complexes for Medical Imaging Applications via

Microwave-Enhanced Cycloaddition. *Beilstein J. Org. Chem.* **2015**, *11*, 2202–2208. https://doi.org/10.3762/bjoc.11.239.
(384) Locos, O. B.; Heindl, C. C.; Corral, A.; Senge, M. O.; Scanlan, E. M. Efficient Synthesis of Glycoporphyrins by Microwave-Mediated "Click" Reactions. *Eur. J. Org. Chem.* **2010**, *2010* (6), 1026–1028. https://doi.org/10.1002/ejoc.200901292.
(385) Garcia, G.; Naud-Martin, D.; Carrez, D.; Croisy, A.; Maillard, P. Microwave-Mediated "click-Chemistry" Synthesis of Glycoporphyrin Derivatives and in Vitro Photocytotoxicity for Application in Photodynamic Therapy. *Tetrahedron* **2011**, *67* (26), 4924–4932. https://doi.org/10.1016/j.tet.2011.04.080.
(386) Bakleh, M. E.; Sol, V.; Estieu-Gionnet, K.; Granet, R.; Déléris, G.; Krausz, P. An Efficient Route to VEGF-like Peptide Porphyrin Conjugates via Microwave-Assisted "Click-Chemistry." *Tetrahedron* **2009**, *65* (36), 7385–7392. https://doi.org/10.1016/j.tet.2009.07.028.
(387) Obondi, C. O.; Lim, G. N.; Karr, P. A.; Nesterov, V. N.; D'Souza, F. Photoinduced Charge Separation in Wide-Band Capturing, Multi-Modular Bis(Donor Styryl)BODIPY–Fullerene Systems. *Phys. Chem. Chem. Phys.* **2016**, *18* (27), 18187–18200. https://doi.org/10.1039/C6CP03479A.
(388) Kondo, M.; Furukawa, S.; Hirai, K.; Kitagawa, S. Coordinatively Immobilized Monolayers on Porous Coordination Polymer Crystals. *Angew. Chem. Int. Ed.* **2010**, *49* (31), 5327–5330. https://doi.org/10.1002/anie.201001063.
(389) Hitosugi, S.; Tanimoto, D.; Nakanishi, W.; Isobe, H. A Facile Chromatographic Method for Purification of Pinacol Boronic Esters. *Chem. Lett.* **2012**, *41* (9), 972–973. https://doi.org/10.1246/cl.2012.972.
(390) Olmsted, John. Calorimetric Determinations of Absolute Fluorescence Quantum Yields. *J. Phys. Chem.* **1979**, *83* (20), 2581–2584. https://doi.org/10.1021/j100483a006.
(391) Kubin, R. F.; Fletcher, A. N. Fluorescence Quantum Yields of Some Rhodamine Dyes. *J. Lumin.* **1982**, *27* (4), 455–462. https://doi.org/10.1016/0022-2313(82)90045-X.
(392) Kunieda, M.; Mizoguchi, T.; Tamiaki, H. Diastereoselective Self-Aggregation of Synthetic 3-(1-Hydroxyethyl)-Bacteriopyrochlophyll-a as a Novel Photosynthetic Antenna Model Absorbing Near the Infrared Region. *Photochem. Photobiol.* **2004**, *79* (1), 55–61. https://doi.org/10.1562/0031-8655(2004)79<55:dsosha>2.0.co;2.
(393) Kunieda, M.; Tamiaki, H. Self-Aggregation of Synthetic Zinc Oxo-Bacteriochlorins Bearing Substituents Characteristic of Chlorosomal Chlorophylls. *J. Org. Chem.* **2005**, *70* (3), 820–828. https://doi.org/10.1021/jo048263p.
(394) Agostiano, A.; Catucci, L.; Colafemmina, G.; Scheer, H. Role of Functional Groups and Surfactant Charge in Regulating Chlorophyll Aggregation in Micellar Solutions. *J. Phys. Chem. B* **2002**, *106* (6), 1446–1454. https://doi.org/10.1021/jp011718j.
(395) Sahin, T.; Harris, M. A.; Vairaprakash, P.; Niedzwiedzki, D. M.; Subramanian, V.; Shreve, A. P.; Bocian, D. F.; Holten, D.; Lindsey, J. S. Self-

Assembled Light-Harvesting System from Chromophores in Lipid Vesicles. *J. Phys. Chem. B* **2015**, *119* (32), 10231–10243. https://doi.org/10.1021/acs.jpcb.5b04841.
(396) Williams, M. P. A.; Ethirajan, M.; Ohkubo, K.; Chen, P.; Pera, P.; Morgan, J.; White, W. H.; Shibata, M.; Fukuzumi, S.; Kadish, K. M.; et al. Synthesis, Photophysical, Electrochemical, Tumor-Imaging, and Phototherapeutic Properties of Purpurinimide-N-Substituted Cyanine Dyes Joined with Variable Lengths of Linkers. *Bioconjug. Chem.* **2011**, *22* (11), 2283–2295. https://doi.org/10.1021/bc200345p.
(397) Patel, N. J.; Chen, Y.; Joshi, P.; Pera, P.; Baumann, H.; Missert, J. R.; Ohkubo, K.; Fukuzumi, S.; Nani, R. R.; Schnermann, M. J.; et al. Effect of Metalation on Porphyrin-Based Bifunctional Agents in Tumor Imaging and Photodynamic Therapy. *Bioconjug. Chem.* **2016**, *27* (3), 667–680. https://doi.org/10.1021/acs.bioconjchem.5b00656.
(398) Grin, M. A.; Toukach, P. V.; Tsvetkov, V. B.; Reshetnikov, R. I.; Kharitonova, O. V.; Kozlov, A. S.; Krasnovsky, A. A.; Mironov, A. F. Bacteriochlorin-Containing Triad: Structure and Photophysical Properties. *Dyes Pigments* **2015**, *121*, 21–29. https://doi.org/10.1016/j.dyepig.2015.04.034.
(399) Weiner, G. J. Building Better Monoclonal Antibody-Based Therapeutics. *Nat. Rev. Cancer* **2015**, *15* (6), 361–370. https://doi.org/10.1038/nrc3930.
(400) Bodio, E.; Goze, C. Investigation of B-F Substitution on BODIPY and Aza-BODIPY Dyes: Development of B-O and B-C BODIPYs. *Dyes Pigments* **2019**, *160*, 700–710. https://doi.org/10.1016/j.dyepig.2018.08.062.
(401) Wang, M.; Vicente, M. G. H.; Mason, D.; Bobadova-Parvanova, P. Stability of a Series of BODIPYs in Acidic Conditions: An Experimental and Computational Study into the Role of the Substituents at Boron. *ACS Omega* **2018**, *3* (5), 5502–5510. https://doi.org/10.1021/acsomega.8b00404.
(402) Tiller, G. E.; Mueller, T. J.; Dockter, M. E.; Struve, W. G. Hydrogenation of Triton X-100 Eliminates Its Fluorescence and Ultraviolet Light Absorption While Preserving Its Detergent Properties. *Anal. Biochem.* **1984**, *141* (1), 262–266. https://doi.org/10.1016/0003-2697(84)90455-X.
(403) Helenius, A.; McCaslin, D. R.; Fries, E.; Tanford, C. [63] Properties of Detergents. In *Methods in Enzymology*; Elsevier, 1979; Vol. 56, pp 734–749. https://doi.org/10.1016/0076-6879(79)56066-2.
(404) Montazeri Aliabadi, H.; Brocks, D. R.; Lavasanifar, A. Polymeric Micelles for the Solubilization and Delivery of Cyclosporine A: Pharmacokinetics and Biodistribution. *Biomaterials* **2005**, *26* (35), 7251–7259. https://doi.org/10.1016/j.biomaterials.2005.05.042.
(405) Warnan, J.; Buchet, F.; Pellegrin, Y.; Blart, E.; Odobel, F. Panchromatic Trichromophoric Sensitizer for Dye-Sensitized Solar Cells Using Antenna Effect. *Org. Lett.* **2011**, *13* (15), 3944–3947. https://doi.org/10.1021/ol2014686.
(406) Dost, Z.; Atilgan, S.; Akkaya, E. U. Distyryl-Boradiazaindacenes: Facile Synthesis of Novel near IR Emitting Fluorophores. *Tetrahedron* **2006**, *62* (36), 8484–8488. https://doi.org/10.1016/j.tet.2006.06.082.
(407) Deniz, E.; Isbasar, G. C.; Bozdemir, Ö. A.; Yildirim, L. T.; Siemiarczuk, A.; Akkaya, E. U. Bidirectional Switching of near IR Emitting Boradiazaindacene

Fluorophores. *Org. Lett.* **2008**, *10* (16), 3401–3403. https://doi.org/10.1021/ol801062h.
(408) Hiruta, Y.; Koiso, H.; Ozawa, H.; Sato, H.; Hamada, K.; Yabushita, S.; Citterio, D.; Suzuki, K. Near IR Emitting Red-Shifting Ratiometric Fluorophores Based on Borondipyrromethene. *Org. Lett.* **2015**, *17* (12), 3022–3025. https://doi.org/10.1021/acs.orglett.5b01299.
(409) Baruah, M.; Qin, W.; Flors, C.; Hofkens, J.; Vallée, R. A. L.; Beljonne, D.; Van der Auweraer, M.; De Borggraeve, W. M.; Boens, N. Solvent and PH Dependent Fluorescent Properties of a Dimethylaminostyryl Borondipyrromethene Dye in Solution. *J. Phys. Chem. A* **2006**, *110* (18), 5998–6009. https://doi.org/10.1021/jp054878u.
(410) Uppal, T.; Bhupathiraju, N. V. S. D. K.; Vicente, M. G. H. Synthesis and Cellular Properties of Near-IR BODIPY-PEG and Carbohydrate Conjugates. *Tetrahedron* **2013**, *69* (23), 4687–4693. https://doi.org/10.1016/j.tet.2013.03.082.
(411) Xiong, H.; Kos, P.; Yan, Y.; Zhou, K.; Miller, J. B.; Elkassih, S.; Siegwart, D. J. Activatable Water-Soluble Probes Enhance Tumor Imaging by Responding to Dysregulated PH and Exhibiting High Tumor-to-Liver Fluorescence Emission Contrast. *Bioconjug. Chem.* **2016**, *27* (7), 1737–1744. https://doi.org/10.1021/acs.bioconjchem.6b00242.
(412) Liu, X.; Wu, M.; Hu, Q.; Bai, H.; Zhang, S.; Shen, Y.; Tang, G.; Ping, Y. Redox-Activated Light-Up Nanomicelle for Precise Imaging-Guided Cancer Therapy and Real-Time Pharmacokinetic Monitoring. *ACS Nano* **2016**, *10* (12), 11385–11396. https://doi.org/10.1021/acsnano.6b06688.
(413) Zhang, X.; Xiao, Y.; Qi, J.; Qu, J.; Kim, B.; Yue, X.; Belfield, K. D. Long-Wavelength, Photostable, Two-Photon Excitable BODIPY Fluorophores Readily Modifiable for Molecular Probes. *J. Org. Chem.* **2013**, *78* (18), 9153–9160. https://doi.org/10.1021/jo401379g.
(414) Zhang, Q.; Cai, Y.; Wang, X. J.; Xu, J. L.; Ye, Z.; Wang, S.; Seeberger, P. H.; Yin, J. Targeted Photodynamic Killing of Breast Cancer Cells Employing Heptamannosylated β-Cyclodextrin-Mediated Nanoparticle Formation of an Adamantane-Functionalized BODIPY Photosensitizer. *ACS Appl. Mater. Interfaces* **2016**, *8* (49), 33405–33411. https://doi.org/10.1021/acsami.6b13612.
(415) Hu, W.; Ma, H.; Hou, B.; Zhao, H.; Ji, Y.; Jiang, R.; Hu, X.; Lu, X.; Zhang, L.; Tang, Y.; et al. Engineering Lysosome-Targeting BODIPY Nanoparticles for Photoacoustic Imaging and Photodynamic Therapy under Near-Infrared Light. *ACS Appl. Mater. Interfaces* **2016**, *8* (19), 12039–12047. https://doi.org/10.1021/acsami.6b02721.
(416) Altan Bozdemir, O.; Erbas-Cakmak, S.; Ekiz, O. O.; Dana, A.; Akkaya, E. U. Towards Unimolecular Luminescent Solar Concentrators: Bodipy-Based Dendritic Energy-Transfer Cascade with Panchromatic Absorption and Monochromatized Emission. *Angew. Chem. Int. Ed.* **2011**, *50* (46), 10907–10912. https://doi.org/10.1002/anie.201104846.
(417) Liu, J. Y.; Yeung, H.-S.; Xu, W.; Li, X.; Ng, D. K. P. Highly Efficient Energy Transfer in Subphthalocyanine-BODIPY Conjugates. *Org. Lett.* **2008**, *10* (23), 5421–5424. https://doi.org/10.1021/ol8023677.

(418) Guliyev, R.; Coskun, A.; Akkaya, E. U. Design Strategies for Ratiometric Chemosensors: Modulation of Excitation Energy Transfer at the Energy Donor Site. *J. Am. Chem. Soc.* **2009**, *131* (25), 9007–9013. https://doi.org/10.1021/ja902584a.
(419) Menting, R.; Liu, J. Y.; Huang, Y. S.; Ng, D. K. P.; Röder, B.; Ermilov, E. A. Photoinduced Energy and Charge Transfer in a P-Phenylene-Linked Dyad of Boron Dipyrromethene and Monostyryl Boron Dipyrromethene. *Phys. Chem. Chem. Phys.* **2013**, *15* (18), 6912–6919. https://doi.org/10.1039/c3cp50576f.
(420) Diring, S.; Puntoriero, F.; Nastasi, F.; Campagna, S.; Ziessel, R. Star-Shaped Multichromophoric Arrays from Bodipy Dyes Grafted on Truxene Core. *J. Am. Chem. Soc.* **2009**, *131* (17), 6108–6110. https://doi.org/10.1021/ja9015364.
(421) Eggenspiller, A.; Takai, A.; El-Khouly, M. E.; Ohkubo, K.; Gros, C. P.; Bernhard, C.; Goze, C.; Denat, F.; Barbe, J.-M.; Fukuzumi, S. Synthesis and Photodynamics of Fluorescent Blue Bodipy-Porphyrin Tweezers Linked by Triazole Rings. *J. Phys. Chem. A* **2012**, *116* (15), 3889–3898. https://doi.org/10.1021/jp300415a.
(422) Huang, L.; Li, Z.; Zhao, Y.; Yang, J.; Yang, Y.; Pendharkar, A. I.; Zhang, Y.; Kelmar, S.; Chen, L.; Wu, W.; et al. Enhancing Photodynamic Therapy through Resonance Energy Transfer Constructed Near-Infrared Photosensitized Nanoparticles. *Adv. Mater.* **2017**, *29* (28), 1604789(1–7). https://doi.org/10.1002/adma.201604789.
(423) Rong, Y.; Wu, C.; Yu, J.; Zhang, X.; Ye, F.; Zeigler, M.; Gallina, M. E.; Wu, I.-C.; Zhang, Y.; Chan, Y.-H.; et al. Multicolor Fluorescent Semiconducting Polymer Dots with Narrow Emissions and High Brightness. *ACS Nano* **2013**, *7* (1), 376–384. https://doi.org/10.1021/nn304376z.
(424) Barin, G.; Yilmaz, M. D.; Akkaya, E. U. Boradiazaindacene (Bodipy)-Based Building Blocks for the Construction of Energy Transfer Cassettes. *Tetrahedron Lett.* **2009**, *50* (15), 1738–1740. https://doi.org/10.1016/j.tetlet.2009.01.141.
(425) Huang, L.; Cui, X.; Therrien, B.; Zhao, J. Energy-Funneling-Based Broadband Visible-Light-Absorbing Bodipy-C 60 Triads and Tetrads as Dual Functional Heavy-Atom-Free Organic Triplet Photosensitizers for Photocatalytic Organic Reactions. *Chem. - Eur. J.* **2013**, *19* (51), 17472–17482. https://doi.org/10.1002/chem.201302492.
(426) Yang, W.; Karatay, A.; Zhao, J.; Song, J.; Zhao, L.; Xing, Y.; Zhang, C.; He, C.; Yaglioglu, H. G.; Hayvali, M.; et al. Near - IR Broadband-Absorbing Trans - Bisphosphine Pt(II) Bisacetylide Complexes: Preparation and Study of the Photophysics. *Inorg. Chem.* **2015**, *54* (15), 7492–7505. https://doi.org/10.1021/acs.inorgchem.5b01107.
(427) Jiao, G.-S.; Thoresen, L. H.; Kim, T. G.; Haaland, W. C.; Gao, F.; Topp, M. R.; Hochstrasser, R. M.; Metzker, M. L.; Burgess, K. Syntheses, Photophysical Properties, and Application of Through-Bond Energy-Transfer Cassettes for Biotechnology. *Chem. - Eur. J.* **2006**, *12* (30), 7816–7826. https://doi.org/10.1002/chem.200600197.
(428) Li, F.; Yang, S. I.; Ciringh, Y.; Seth, J.; Martin III, C. H.; Singh, D. L.; Kim, D.; Birge, R. R.; Bocian, D. F.; Holten, D.; et al. Design, Synthesis, and Photodynamics of Light-Harvesting Arrays Comprised of a Porphyrin and One,

Two, or Eight Boron-Dipyrrin Accessory Pigments. *J. Am. Chem. Soc.* **1998**, *120* (39), 10001–10017. https://doi.org/10.1021/ja9812047.
(429) Zhai, J.; Pan, T.; Zhu, J.; Xu, Y.; Chen, J.; Xie, Y.; Qin, Y. Boronic Acid Functionalized Boron Dipyrromethene Fluorescent Probes: Preparation, Characterization, and Saccharides Sensing Applications. *Anal. Chem.* **2012**, *84* (23), 10214–10220. https://doi.org/10.1021/ac301456s.
(430) Huang, L.; Yu, X.; Wu, W.; Zhao, J. Styryl Bodipy-C60 Dyads as Efficient Heavy-Atom-Free Organic Triplet Photosensitizers. *Org. Lett.* **2012**, *14* (10), 2594–2597. https://doi.org/10.1021/ol3008843.
(431) Turro, N. J. The Role of Intersystem Crossing Steps in Singlet Oxygen Chemistry and Photo-Oxidations. *Tetrahedron* **1985**, *41* (11), 2089–2098. https://doi.org/10.1016/S0040-4020(01)96579-2.
(432) Ng, K. K.; Takada, M.; Jin, C. C. S.; Zheng, G. Self-Sensing Porphysomes for Fluorescence-Guided Photothermal Therapy. *Bioconjug. Chem.* **2015**, *26* (2), 345–351. https://doi.org/10.1021/bc500595d.
(433) Xiong, R.; Andres, J.; Scheffler, K.; Borbas, K. E. Synthesis and Characterisation of Lanthanide-Hydroporphyrin Dyads. *Dalton Trans.* **2015**, *44* (6), 2541–2553. https://doi.org/10.1039/c4dt02448f.
(434) Yang, Z.; Cao, J.; He, Y.; Yang, J. H.; Kim, T.; Peng, X.; Kim, J. S. Macro-/Micro-Environment-Sensitive Chemosensing and Biological Imaging. *Chem. Soc. Rev.* **2014**, *43* (13), 4563–4601. https://doi.org/10.1039/c4cs00051j.
(435) Theillet, F. X.; Binolfi, A.; Frembgen-Kesner, T.; Hingorani, K.; Sarkar, M.; Kyne, C.; Li, C.; Crowley, P. B.; Gierasch, L.; Pielak, G. J.; et al. Physicochemical Properties of Cells and Their Effects on Intrinsically Disordered Proteins (IDPs). *Chem. Rev.* **2014**, *114* (13), 6661–6714. https://doi.org/10.1021/cr400695p.
(436) Signore, G.; Abbandonato, G.; Storti, B.; Stöckl, M.; Subramaniam, V.; Bizzarri, R. Imaging the Static Dielectric Constant in Vitro and in Living Cells by a Bioconjugable GFP Chromophore Analog. *Chem. Commun.* **2013**, *49* (17), 1723–1725. https://doi.org/10.1039/c3cc38071h.
(437) Cuervo, A.; Dans, P. D.; Carrascosa, J. L.; Orozco, M.; Gomila, G.; Fumagalli, L.; Whyte, D.; Bergeron, M.; George, A. PNAS Plus Significance Statements. *Proc. Natl. Acad. Sci.* **2014**, *111* (52), 18411–18413. https://doi.org/10.1073/pnas.ss11152.